Controlling Rheological and Setting Properties of Geopolymers by Optimizing Physical Properties of Particles and Mixing Protocols

Yasemin Keskin Topan

▶ **To cite this version:**

Yasemin Keskin Topan. Controlling Rheological and Setting Properties of Geopolymers by Optimizing Physical Properties of Particles and Mixing Protocols. Civil Engineering. Université Gustave Eiffel, 2022. English. NNT : 2022UEFL2062 . tel-04089427

HAL Id: tel-04089427

https://theses.hal.science/tel-04089427

Submitted on 4 May 2023

HAL is a multi-disciplinary open access archive for the deposit and dissemination of scientific research documents, whether they are published or not. The documents may come from teaching and research institutions in France or abroad, or from public or private research centers.

L'archive ouverte pluridisciplinaire **HAL**, est destinée au dépôt et à la diffusion de documents scientifiques de niveau recherche, publiés ou non, émanant des établissements d'enseignement et de recherche français ou étrangers, des laboratoires publics ou privés.

Controlling Rheological and Setting Properties of Geopolymers by Optimizing Physical Properties of Particles and Mixing Protocols

A thesis presented by

Yasemin KESKIN TOPAN

To

Université Gustave Eiffel

École Doctorale Sciences, Ingénierie et Environnement

For the Degree of Doctor of Philosophy in

Materials Science

Committee members:

M. Arnaud Poulesquen, CEA	Thesis Reviewer
Mme. Marta Palacios, CSIC	Thesis Reviewer
M. Jean Baptiste d'Espinose De Lacaillerie, ESPCI	Thesis Examiner
M. Nhu Cuong Tran, EDF	Thesis Invitee
Mme. Sylvie Rossignol, IRCER	Thesis Co-Supervisor
Mme. Hela Bessaies-Bey, UGE	Thesis Supervisor
M. Nicolas Roussel, UGE	Thesis Director

Champs-sur-Marne, France, 5 July 2022

Acknowledgement

First of all, I would like to thank to my thesis supervisors Hela Bessaies-Bey and Sylvie Rossignol for the support they have given me throughout these three years. Thank you Hela for sharing your scientific knowledge and experience with me, giving me the motivation and for trusting me. Thank you Sylvie for always being available, for all the relevant advises and tutoring. I have never been grateful enough for all you have brought to me.

I also thank to my thesis director Nicolas Roussel. Thank you Nicolas for all your support and encouragement, fruitful discussions, kindness and scientific contribution to this research project.

I would like to thank to Jean Baptiste d'Espinose de Lacallaire for agreeing to chair my jury, for his availability and welcoming me at SIMM and especially sharing his knowledge on the NMR with me.

I would like to thank to Marta Palacios and Arnaud Poulesquen for agreeing to report my work, for their time and relevant remarks that contributed to the improvement of my dissertation. Thank you also for attending and participating in my PhD defense.

I would like to thank to Nhu Cuong Tran and Laurent Petit, my industrial supervisors, for the interest they have shown in this research and for the relevant questions that have helped to bring out enriching perspectives.

I would like to thank the teams of CPDM and Navier laboratories for their contribution to this work: Patrick Belin, Jean-François Bouteloup, Jean-Daniel Simitambe, Issam Nour and Tony Pons.

I would like to thank to my colleagues for all they have brought to me both professionally and humanly. Thank you Janine Deau for your inspiring discussions, positive energy and for all the fun and good memories we had. I am grateful for your effort and support during all the moments when I needed it. Thank you Oumayma Ahmadah for your support and kindness. It was a great pleasure for me to share all the moments of conviviality with you. I also thank to Elie, Robert, Kassem, Anatole, Hicham, Badreddine, Walid and all the PhD students I met in IRCER, ESPCI and Gustave Eiffel University during these three years. I wish them good luck for the future.

I would like to express also my gratitude to all the professors from master SMCD at École Nationale des Ponts et Chaussées Paristech, particularly to Xavier Chateau. Thank you Xavier for always being kind and all your pedagogical support. I have learned a lot from you and I will always be grateful for your patience and the trust in me.

Finally, many thanks to my family and my family-in-law for their support and love. In particular, I thank to my husband, Tayfun Topan, for his endless patience, encouragement and helpful

advises. Thank you for your smiles that have given me the power and motivation I needed. I will never be grateful enough for all you have done for me. Thank you.

This work has specifically received partial funding from the MAI–SN, Materials Ageing Institute, http://themai.org. The Materials Aging Institute is a utility-oriented research center founded by EDF in 2008 and cofinanced by EPRI (US), KEPCO (J), CGNPC (CN), EDF Energy (UK), TEPCO (J), MHI (J), CRIEPI (J), CEA (F) and FRAMATOME (F). The main purpose of this collaborative effort is to bring together scientific skills and research facilities to address aging of material used in electric power plants, and particularly in nuclear power plants.

Abstract

In this thesis, the effect of the packing properties of the constitutive powder on the rheological properties of geopolymers is studied. Moreover, the effects of the applied mixing protocol on rheology, reaction kinetics, and resulting setting time are investigated.

In a first part, the packing density of various powders are optimized using the Compressible Packing Model (CPM) that is developed for the optimization of the particle size distribution of construction materials.

Our results show that optimization of particle packing allows for a decrease in the viscosity of geopolymers. It moreover allows for a control of the fresh properties independently from the mechanical properties. These are shown to be dictated, as known in literature, by the nature of the powder in binary mixture, solid volume fraction of geopolymer sample or molar ratio and viscosity of sodium silicate solution changes.

In a second part, we show that the geopolymer mixing protocol, or more generally its shear history, affects reaction kinetics, rheological behavior and setting time. By studying materials with various shear history using simple penetration tests or advanced oscillation rheometry while varying the temperature of the constitutive liquid, we suggest that the variations in temperature induced by mixing or shearing are the main parameter at the origin of these changes. This suggests, in turn, that, while high speed shearing affects the morphology and localization of hydrates in cement pastes and only slightly their temperatures, temperature variations in the highly viscous typical geopolymer pastes are driving material aging or so-called workability loss.

Keywords: viscosity, packing density, particle size distribution, mixing, temperature, setting time

Résumé

Dans cette thèse, l'effet des propriétés d'empilement de la poudre constitutive sur les propriétés rhéologiques des géopolymères est étudié. De plus, les effets du protocole de malaxage appliqué sur la rhéologie, la cinétique de réaction et le temps de prise sont étudiés.

Dans une première partie, l'empilement de diverses poudres est optimisé à l'aide du modèle d'empilement compressible (MEC) qui est développé pour l'optimisation de la distribution granulométrique des matériaux de construction.

Nos résultats montrent que l'optimisation de l'empilement des particules permet une diminution de la viscosité des géopolymères. Il permet en outre un contrôle des propriétés à l'état frais indépendamment des propriétés mécaniques. Ces changements sont dictés, comme on le sait dans la littérature, par la nature de la poudre dans le mélange binaire, la fraction volumique solide de l'échantillon de géopolymère ou le rapport molaire et la viscosité de la solution de silicate de sodium.

Dans une seconde partie, nous montrons que le protocole de malaxage du géopolymère, ou plus généralement son historique de cisaillement, affecte la cinétique de réaction, le comportement rhéologique et le temps de prise. En étudiant la rhéologie et le temps de prise de matériaux soumis à différents cisaillements, tout en faisant varier la température de la solution de silicate de sodium, nous suggérons que les variations de température induites par le cisaillement sont à l'origine de ces changements. Ceci suggère que, même si le cisaillement à grande vitesse influence la morphologie et la localisation des hydrates dans les pâtes de ciment et seulement légèrement leur température, les variations de température dans les pâtes géopolymères, caractérisées par leur importante viscosité, sont à l'origine de l'accélération de la prise et de la perte d'ouvrabilité.

Mots-clés: viscosité, densité de l'empilement, distribution granulométrique, malaxage, température, temps de prise

Table of contents

Acknowledgement 3
Abstract 7
Résumé 8
Table of contents 10
Introduction 14

Chapter 1: Bibliography 21
1.1. Synthesis of geopolymers 21
1.2. Essential parameters influencing reaction kinetics, fresh and hardened state behaviors of geopolymers 23
1.2.1. Choice of raw material 24
1.2.2. Geopolymer formulation, processing and measurement conditions 25
1.3. Introduction to rheology 29
1.4. Rheological properties of geopolymers 31
1.5. Microscopic origins of rheological behavior of cementitious materials 37
1.5.1. Colloidal interactions 38
1.5.2. Hydrodynamic interactions 39
1.5.3. Contribution of formation of hydration products 41
1.5.4. Contribution of particle inertia 42
1.6. Methods of controlling the rheological behavior of cementitious materials 43
1.6.1. Effect of chemical admixtures on controlling rheological behavior of geopolymers 43
1.6.2. Effect of optimization of particle packing on controlling rheological behavior of geopolymers 46
1.7. Objective of the study 49
1.8. Conclusion 50

Chapter 2: Introduction to mineral powder materials and the characterization of physical properties 62
2.1. Choice of Materials 62
2.2. Materials 63
2.2.1. Metakaolin powders 64
2.2.2. Limestone and Quartz powders 64
2.2.3. Activation solution: sodium silicate (Na2SiO3) 65
2.3. Measurement of material density 65
2.3.1. Measurement protocol of density of powder materials 65
2.3.2. Measurement protocol of density of liquid materials 66
2.4. Maximum packing fraction of powder materials 67
2.4.1. Essential parameters influencing maximum packing fraction 67

2.4.2. Methods of determination of maximum packing density 69
2.4.3. Measurement protocol of maximum particle packing density 70
2.4.4. Maximum packing densities of powder materials 71
2.5. Measurement of particle size distribution 72
2.5.1. Introduction to laser light diffraction 73
2.5.2. Parameters influencing measurement of particle size distribution by laser diffraction granulometry 74
2.5.2.1. Sampling 74
2.5.2.2. Obscuration 75
2.5.2.3. Dispersion 75
2.5.2.4. Optical indexes 75
2.5.2.5. Particle shape 75
2.5.3. Measurement instrument of laser diffraction granulometry: Malvern Mastersizer 3000 76
2.5.4. Determination of measurement protocols for particle size distribution of powders 76
2.5.4.1. Measurement protocols of limestone and quartz powders 76
2.5.4.2. Measurement protocol for metakaolin powders 77
2.5.5. Results of particles size distributions of powder materials 79
2.6. Conclusion 81

Chapter 3: Optimization of particle packing fractions 89
3.1. Introduction to packing models 89
3.2. Compressible Packing Model (CPM) 93
3.2.1. Maximum virtual packing density 93
3.2.2. Maximum real packing density 96
3.3. Methods followed to optimize particle packing 97
3.4. Residual packing density of studied powder materials 99
3.5. Computed maximum packing density of identified powder mixtures 100
3.6. Correlation between computed and measured maximum packing densities 102
3.7. Particle packing optimization 103
3.7.1. Metakaolin couples 103
3.7.2. Metakaolin and limestone couples 104
3.7.3. Metakaolin-quartz couples 106
3.8. Conclusion 106

Chapter 4: Influence of particle packing optimization on rheological and mechanical behaviors of geopolymer suspensions 110
4.1. Influence of particle packing optimization on rheological properties 110
4.1.1. Protocols of rheological measurements 110
4.1.1.1. Preparation of geopolymer suspension 110
4.1.1.2. Shear protocol for rheological measurements of geopolymers 111
4.1.1.3. Shear protocol for rheological measurements of liquid materials 112
4.1.2. Rheological properties of limestone and quartz powders suspended in sodium silicate solution over time 113

4.1.3. Rheological behavior of sodium silicate solutions 115
4.1.4. Rheological behavior of geopolymer suspensions 116
4.1.5. Correlation between rheological measurement results and maximum packing fractions of geopolymers 120
4.2. Influence of particle packing optimization on mechanical properties 122
4.2.1. Protocols of mechanical measurements 122
4.2.2. Evolution of mechanical strength over time 123
4.2.3. Mechanical properties of geopolymers based on mixtures between two metakaolin powders 125
4.2.4. Mechanical properties of geopolymers based on grinded metakaolin powders 129
4.2.5. Mechanical properties of geopolymers based on metakaolin-limestone or metakaolin-quartz mixtures 131
4.3. Conclusion 134
4.3.1. Conclusion for rheological properties 134
4.3.2. Conclusion for mechanical properties 134

Chapter 5: Early reactivity of geopolymers Part I: mechanism of geopolymerisation and the development of mechanical properties of a metakaolin-based geopolymer 138
5.1. Principles of Nuclear Magnetic Resonance (NMR) Measurements 138
5.2. Principles of Oscillation Rheology 140
5.3. Measurement protocols 141
5.3.1. Measurement protocol of NMR 141
5.3.2. Measurement protocol of oscillation rheology 142
5.4. Evolution of Al concentration during early geopolymerisation 143
5.5. Evolution of elastic modulus during early geopolymerisation 145
5.6. Conclusion 146

Chapter 6: Early reactivity of geopolymers Part II: interplay between parameters of mixing process and its impact on rheological and mechanical behavior of a metakaolin-based geopolymer 150
6.1. Measurement protocols 151
6.1.1. Measurement protocol of NMR 151
6.1.2. Measurement protocol of oscillation rheology 152
6.1.3. Measurement protocol of setting time 156
6.1.4. Measurement protocol of mechanical strength 157
6.2. Evolution of Al concentration during early geopolymerisation 158
6.3. Evolution of elastic modulus during early geopolymerisation 159
6.4. Evolution of setting time with respect to temperature 162
6.5. Evolution of mechanical strength with respect to applied mixing protocol 165
6.6. Conclusion 167

Conclusions and Perspectives 171

Appendix A: Technical safety data sheets of materials 174

Appendix B: Flow curves and results of rheological and mechanical measurements of geopolymer suspensions 180

Introduction

Since the development of Portland cement around 200 years ago, it has become the most used binder in construction industry. The total volume of worldwide cement production amounted to an estimated 4.4 billion tons in 2021 [1]. As it is a versatile and durable material with a considerable economic value and relatively low embodied energy in comparison to other binder materials, Portland cement has growing recognition level [2]. However, production of Portland cement results in a non-negligible negative environmental impact that has to be reduced. Today, CO_2 emissions from the worldwide cement industry have increased globally from 0.86 Gt (i.e. 1990) to 2.46 Gt (i.e. in 2019), which makes the cement industry the second largest industrial CO_2 emitter (~25% of global industrial CO_2 emissions) globally [3]. Hence, cement industry is under pressure to reduce the resulting environmental impact and is actively looking for alternative binders for Portland cement [2].

Alternative binders (e.g. calcium sulfoaluminate cements) have been developed to reduce its environmental impact [2, 4, 5, 6, 7, 8]. Alkali activated cement binders (AACB) are one of the alternative binders providing competitive mechanical performance while promising the decrease of environmental impact [9, 10]. Geopolymers are the most recognized alkali activated binders that could decline CO_2 emissions considerably [11]. These materials are commonly formed by alkali activation of industrial aluminosilicate waste materials such as coal ash, blast furnace slag, fly ash etc. and they could exhibit superior chemical and mechanical performance in comparison to ordinary Portland cement-based cementitious materials with a correct mix design and formulation development [11, 12]. Today, industrial applications of geopolymeric materials are composed of low or high strength concretes with good resistance to corrosion or chloride penetration, fire and/or acid resistant coatings, waste immobilization solutions for particularly chemical and nuclear industries etc. [9, 11, 12]. Although several studies have confirmed that these materials could ensure intended mechanical and durability performance [9, 13, 14], they still show some shortcomings, which require to be addressed so that they could compete effectively against Portland cement [9]. The main problem of geopolymeric materials is their elevated viscosity that induces limited workability during industrial applications [15]. Depending on the selected materials as well as the formulation parameters, geopolymeric materials could exhibit 10 to 100 times higher viscosity than cementitious materials based on ordinary Portland cement [16] and their viscosity evolves over time [17]. Moreover, it has been referred recently that geopolymeric materials are sensitive to variation of temperature [18], where the increase of temperature could favor the acceleration of reaction mechanism, thus could result in rapid setting [17, 19]. These characteristic properties could create serious difficulties for several industrial applications such as spraying, pumping or casting. Therefore, controlling especially rheological behavior of geopolymeric materials has crucial importance.

In literature, the use of chemical admixtures has been widely investigated for controlling rheological and mechanical behavior of geopolymeric materials [20, 21, 22, 23, 24]. The majority of the studies reported that the use of chemical agents does not certainly supply

decreased viscosity with improved workability due to potential structural modifications and the competitive adsorption (i.e. with alkaline solution) of these products, thus loss of the effectiveness in the alkaline medium of geopolymeric materials [22, 25]. Moreover, their usage could also have an impact on ultimate mechanical performance or setting time of geopolymers [23, 26]. Only a few studies reported the effectiveness of the use of boron or phosphor-based mineral additives on the decrease of viscosity as well as the prolongation of setting time [27, 28]. However, incorporation of chemical or mineral additives into a geopolymeric material could modify the stability of its chemical formulation, thus final rheological and mechanical performance. In this case, an alternative method that ensures the stability of chemical formulation while improving workability and rapid setting would be better to be used for controlling rheological behavior. The optimization of particle packing could be a useful method since it could supply the decrease of viscosity while keeping good mechanical performance. Its benefits are mentioned widely for cementitious materials based on ordinary Portland cement and alkaline activation by several researchers [29, 30, 31, 32, 33]. In general, packing optimization of particles in cementitious materials provides a better mix design, where porosity in the material structure is filled by finer particles and it is affected mainly by size and shape of particles and the method used for optimization. Therefore, this process requires first, identification of physical parameters of particles (i.e. mainly size and shape) and second, selection of an application method for optimization. In addition to utilization of packing optimization for the decrease of viscosity, variation of mixing protocol could be useful to control setting time of geopolymers. Although the bibliographical background about the effect of mixing on rheological and mechanical properties is very limited, a few studies mentioned that applied mixing protocol could influence development of mechanical properties and could affect setting time of geopolymeric materials [16, 20].

The objective of this thesis is controlling mainly rheological and setting properties of geopolymers using optimization of particle packing and variation of mixing protocol. Since the optimization of particle packing requires initially the identification of physical parameters of particles and choice of a method for optimization, we will study primarily characterization of physical properties of materials used to produce geopolymers. Afterwards, we will study different models developed for packing optimization and choose a suitable model to optimize particle packing. Later, we will study the effect of packing optimization on rheological and mechanical properties of geopolymers. Finally, we will study the effect of applied mixing protocol on rheological, mechanical and setting properties of studied geopolymers.

The first chapter provides a background on geopolymeric materials. We will present the synthesis process and the parameters influencing the characteristic properties of geopolymers. Afterwards, we will introduce basic information about rheology and the rheological properties of geopolymers while mentioning the essential difficulties met in their industrial applications and the factors affecting their rheological performance. Later, we will introduce the microscopic origins of different rheological behaviors that could be observed from various mineral suspensions (i.e. including geopolymers). Finally, we will discuss in details various potential methods for assessing the rheological behavior of geopolymeric materials and mention the selected methods for this thesis.

In the second chapter, we will present the characterization of the physical properties of materials used to produce geopolymers in this thesis. We will first present studied powder materials with alkaline solution and then we will introduce the methods used to identify density, particle size distributions and maximum packing fraction of these materials. Finally, we will present the measured physical properties of the studied materials.

In the third chapter, we will study the optimization of particle packing by developing binary powder mixtures used as solid precursors of geopolymers. We will introduce various packing models from literature developed for packing optimization. Then, we will present the Compressible Packing Model, that is chosen here to optimize packing since its suitability and effectiveness for cementitious materials is reported by various studies. Later, we will present the values of particle packing that are computed by Compressible Packing Model and show a correlation between these values and those measured experimentally. Finally, we will identify high-potential binary powder couples giving the best improvements in packing.

In the fourth chapter, we will study the influence of packing optimization on rheological and on mechanical properties of geopolymers prepared using the promising binary powder couples identified previously. First, we will present its influence on rheological properties by showing the evolution of viscosity as a function of packing optimization. Second, we will present the impact of packing optimization on mechanical properties. We will focus on the evolution of mechanical strength over time and then we will present the evolution of mechanical strength as a function of packing optimization.

In the fifth chapter, we will study the early reactivity of geopolymers using static ^{27}Al Nuclear Magnetic Resonance and oscillation rheology. We will first provide a theoretical background for nuclear magnetic resonance and oscillation rheology. We will then present the evolution of an equivalent aluminum dissolution over time and discuss the kinetics of chemical reaction. Finally, we will present the evolution of elastic modulus over time.

In the sixth chapter, we will study the influence of the mixing process on rheological, mechanical and setting properties using various measurement methods. First, we will discuss the variation in the equivalent aluminum concentration over time induced by various mixing protocols. We will then show the development of mechanical properties as a function of mixing. Finally, we will discuss the setting and mechanical properties with respect to the applied mixing protocol and focus on the role of temperature.

References

[1] M. Garside, "Statista," Statista, 1 April 2022. [Online]. Available: https://www.statista.com/statistics/1087115/global-cement-production-volume/. [Accessed 12 May 2022].

[2] M. C. G. Juenger, F. Winnefeld, J. L. Provis and J. H. Ideker, "Advances in alternative cementitious binders," *Cement and Concrete Research,* vol. 41, pp. 1232-1243, 2011.

[3] C. Chen, R. Xu, D. Tong, X. Qin, J. Cheng, J. Liu, B. Zheng, L. Yan and Q. Zhang, "A striking growth of CO2 emissions from the global cement industry driven by new facilities in emerging countries," *Environmental Research Letter,* vol. 17, no. 4, pp. 1-12, 2022.

[4] A. Nonat, *L'hydratation des ciments. Course notes of master class "Cement Hydration" at Ecole des Ponts Paristech.,* Champs-sur-Marne, 2016.

[5] S. F. Al-Mamoori, A. A. Shubbar, Z. S. Al-Khafaji, M. S. Nasr, A. Alkhayyat, A. Al-Rifaie, R. L. Al-Mufti, M. Sadique and K. Hashim, "Production of Ternary Blend Binder as an Alternative to Portland Cement," *IOP Conference Series: Materials Science and Engineering,* vol. 1090, no. 012069, 2021.

[6] L. Coppola, T. Bellezze, A. Belli and M. C. B. e. al., "Binders alternative to Portland cement and waste management for sustainable construction—part 1," *Journal of Applied Biomaterials and Functional Materials,* vol. 16, no. 3, pp. 186-202, 2018.

[7] L. Coppola, T. Bellezze and A. B. e. al., "Binders alternative to Portland cement and waste management for sustainable construction – Part 2," *Journal of Applied Biomaterials and Functional Materials,* vol. 16, no. 4, pp. 207-221, 2018.

[8] E. Gartner, "Industrially interesting approaches to "low-CO2" cements," *Cement and Concrete Research,* vol. 34, pp. 1489-1498, 2004.

[9] A. Nazari and J. G. Jansayan, Handbook of Low Carbon Concrete, UK: Butterworth-Heinemann, by Elsevier, 2017.

[10] J. Davidovits, D. C. Comrie, J. H. Paterson and D. J. Ritcey, "Geopolymeric Concretes for Environmental Protection," *ACI Concrete International: Design and Construction,* vol. 12, no. 7, pp. 3-40, 1990.

[11] P. Duxson, J. L. Provis, G. C. Lukey and J. S. J. v. Deventer, "The role of inorganic polymer technology in the development of 'green concrete'," *Cement and Concrete Research,* vol. 37, pp. 1590-1597, 2007.

[12] J. L. Provis and J. S. J. v. Deventer, Geopolymers. Structure, processing, properties and industrial applications., Woodhead Publishing Limited, 2009.

[13] J. Davidovits, "Geopolymers. Inorganic polymerie new materials.," *Journal of Thermal Analysis,* vol. 37, pp. 1633-1656, 1991.

[14] R. E. Lyon, P. N. Balaguru, A. Foden, U. Sorathia, J, Davidovits and M. Davidovics, "Fire-resistant Aluminosilicate Composites," *Fire and Materials,* vol. 21, pp. 67-73, 1997.

[15] D. Zheng, J. S. J. v. Deventer and P. Duxson, "The dry mix cement composition methods and systems involving same". Patent WO 2007/109862 A1, 4 October 2007.

[16] A. Favier, "Mécanisme de prise et rhéologie de liants géopolyméres modèles. Materials.," Université Paris-Est, Champs-sur-Marne, 2013.

[17] A. Bourlon, "Physico-chimie et rhéologie de géopolymères frais pour la cimentation des puits pétroliers. Chimie-Physique.," Université Pierre et Marie Curie - Paris VI, Paris, 2010.

[18] J. Aupoil, "Etude des mécanismes de dissolution/polycondensation lors de la géopolymérisation: réactivité du métakaolin et influence de la solution d'activation. Matériaux.," Université Paris sciences et lettres, Paris, 2020.

[19] M. Palacios, M. M. Alonso, C. Varga and F. Puertas, "Influence of the alkaline solution and temperature on the rheology and reactivity of alkali-activated fly ash pastes," *Cement and Concrete Composites,* vol. 95, pp. 277-284, 2019.

[20] M. Palacios, P. F. G. Banfill and F. Puertas, "Rheology and Setting of Alkali-Activated Slag Pastes and Mortars: Effect of Organic Admixture," *ACI Materials Journal,* no. 105-M16, pp. 140-148, 2008.

[21] M. Criado, A. Palomo, A. Fernandez-Jimenez and P. F. G. Banfill, "Alkali activated fly ash: effect of admixtures on paste rheology," *Rheologica acta,* vol. 48, no. 4, pp. 447-455, 2009.

[22] M. Palacios and P. Fuertas, "Effect of superplasticizer and shrinkage-reducing admixtures on alkali-activated slag pastes and mortars," *Cement and Concrete Research ,* vol. 35, p. 1358– 1367, 2005.

[23] F. Puertas, A. Palomo, A. Fernandez-Jimenez, J. D. Izquierdo and M. L. Granizo, "Effect of superplasticisers on the behaviour and properties of alkaline cements," *Advances in Cement Research,* vol. 15, no. 1, pp. 23-28, 2003.

[24] M. Palacios and F. Puertas, "Stability of superplasticizer and shrinkage-reducing admixtures in high basic media," *Materiales De Construcción,* vol. 54, no. 276, pp. 65-86, 2004.

[25] D. Marchon, U. Sulser, A. Eberhardt and R. J. Flatt, "Molecular design of comb-shaped polycarboxylate dispersants for environmentally friendly concrete," *Soft Matter,* vol. 9, pp. 10719-10728, 2013.

[26] T. Bakharev, J. G. Sanjayan and Y. B. Cheng, "Effect of admixtures on properties of alkali-activated slag concrete," *Cement and Concrete Research,* vol. 30, pp. 1367-1374, 2000.

[27] C. Dupuy, A. Gharzouni, I. Sobrados, N. Texier-Mandoki, X. Bourbon and S. Rossignol, "29Si, 27Al, 31P and 11B magic angle spinning nuclear magnetic resonance study of the structural evolutions induced by the use of phosphor- and boron–based additives in geopolymer mixtures," *Journal of Non-Crystalline Solids,* vol. 521, no. 119541, 2019.

[28] C. Dupuy, J. Havette, A. Gharzouni, N. Texier-Mandoki, X. Bourbon and S. Rossignol, "Metakaolin-based geopolymer: Formation of new phases influencing the setting time with the use of additives," *Construction and Building Materials,* vol. 200, pp. 272-281, 2019.

[29] F. d. Larrard, Concrete Mixture Proportioning, London and New York: E & FN Spon, 1999.

[30] A. Aboulayt, R. Jaafri, H. Samouh, A. C. E. Idrissi, E. Roziere, R. Moussa and A. Loukili, "Stability of a new geopolymer grout: Rheological and mechanical performances of metakaolin-fly ash binary mixtures," *Construction and Building Materials,* vol. 181, pp. 420-436, 2018.

[31] M. F. Nuruddin, K. Y. Chang and N. M. Azmee, "Workability and compressive strength of ductile self compacting concrete (DSCC) with various cement replacement materials," *Construction and Building Materials,* vol. 55, pp. 153-157, 2014.

[32] M. Moini, I. Flores-Vivian, A. Amirjanov and K. Sobolev, "The optimization of aggregate blends for sustainable low cement concrete," *Construction and Building Materials,* vol. 93, pp. 627-634, 2015.

[33] P. Perez-Cortes and J. I. Escalante-Garcia, "Design and optimization of alkaline binders of limestone-metakaolin-A comparison of strength, microstructure and sustainability with portland cement and geopolymers," *Journal of Cleaner Production,* vol. 273, no. 123118, 2020.

[34] O. Ahmadah, "Contrôle de la rhéologie des liants à faibles impacts environnementaux," Université Paris-Est and Université Sherbrooke, Champs-sur-Marne, 2021.

[35] T. Sedran, "Rhéologie et Rhéométrie des bétons. Application aux bétons autonivelants," Ecole Nationale des Ponts et Chaussées, Champs-sur-Marne, 1999.

[36] D. Marchon, U. Sulser, A. Eberhardt and R. J. Flatt, "Molecular design of comb-shaped polycarboxylate dispersants for environmentally friendly concrete," *Soft Matter,* vol. 9, pp. 10719-10728, 2013.

Chapter 1: Bibliography

A geopolymer is usually defined as a solid aluminosilicate material that forms by alkali hydroxide or alkali silicate activation of a precursor, which is supplied in general as a solid powder [1]. Geopolymers are originally developed as a fire-resistant alternative materials after series of disastrous fires lived in France [2] and the products developed based on geopolymers are used mainly for fire protection [3, 4]. Later, application domain of geopolymers is shifted to construction since they supply an equivalent performance to traditional cementitious binders but with additional advantage of significantly reduced Greenhouse emissions [5, 6, 7]. Moreover, they can also display variety of properties such as high compressive strength, acid resistance, low shrinkage and thermal conductivity, rapid or slow setting etc., depending globally on the selection of raw material, processing conditions and geopolymeric formulations [8]. In the following sections, first we present synthesis of geopolymers, formulation parameters and processing conditions affecting geopolymer structure. Later, we discuss their current industrial application difficulties and we propose some approaches as a potential solution for understanding the origin of these difficulties as well as the improvement of characteristic properties of geopolymers.

1.1. Synthesis of geopolymers

The principal of geopolymer synthesis is to combine a reactive aluminosilicate powder with an alkaline solution and produce a disordered aluminosilicate gel [1]. In general, Si-Al containing raw materials such as fly ash, metakaolin or blast furnace slag are chosen within the natural sources or industrial by-products to produce geopolymers. Moreover, alkali hydroxide or silicate solutions are used for activation of selected raw material. The most commonly used alkali hydroxides are sodium and/or potassium hydroxide, while sodium silicate or waterglass (i.e. $Na_2O.SiO_2.H_2O$) are used usually as alkaline silicate solutions [8]. Based on the propositions of Davidovits [9], Glukovsky [10] and Xu and van Deventer [11], synthesis procedure of geopolymers are divided globally into three stages as dissolution, reorganization and polycondensation (Figure 1.1). Dissolution starts from the first contact of materials. At this stage, raw material dissolves by alkaline hydrolysis (i.e. water consuming) and this produces aluminate and silicate species. Once these species incorporate into aqueous phase, a complex mixture of silicate, aluminate and aluminosilicate species forms in the medium [8]. This complex mixture is then attributed to a highly reactive intermediate gel and the network of this gel grows with ongoing condensation of the species present in the medium [11]. This process releases water that is primarily consumed during hydrolysis of raw material and the released water stays in the pores of the gel [8]. Reorganization stage starts with increasing network of this intermediate gel. Connectivity of gel network still increases during

this stage, while system becomes more stable [6]. Finally at polycondensation stage, a three-dimensional aluminosilicate network occurs.

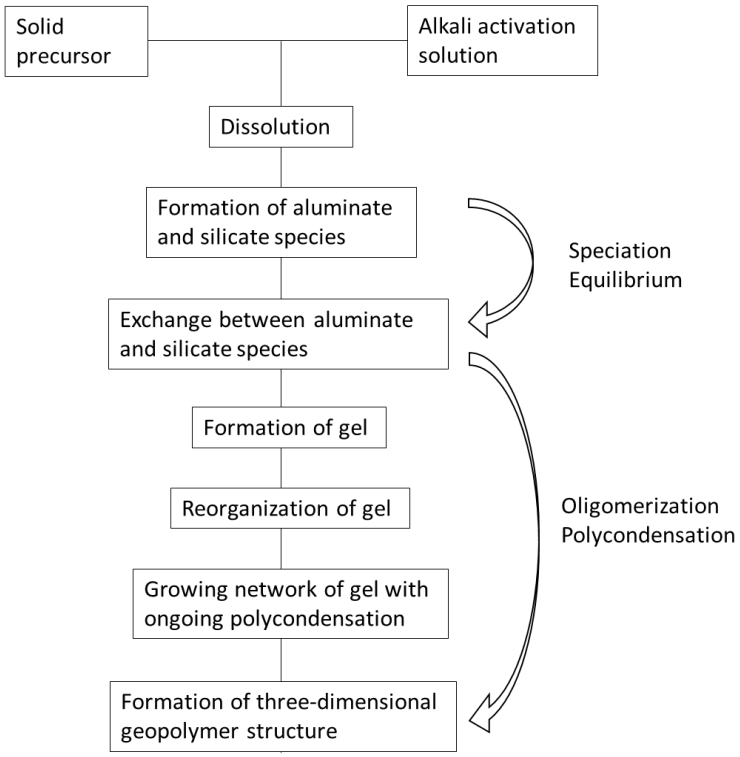

Figure 1.1: Synthesis procedure of geopolymers

Several studies in literature presented potential diagrams of this three-dimensional geopolymer structure [2, 12]. Although showing accurately a complex three-dimensional network in two dimensions is complicated, proposed schematic model by Rowles et al. [13] (Figure 1.2), which is based on the study of Barbosa et al. [14], is probably more reliable model. The fundamental framework of a geopolymer structure is first named as polysialate [2]. However, this nomenclature does not represent anymore full range of possible geopolymeric structures [15]. In general, this framework is a highly connected three-dimensional network of aluminate and silicate tetrahedra, which is linked alternately by sharing oxygen atoms [2, 8]. Alkali metal cations (e.g. Na^{+}, K^{+}, Li^{+} etc.) provided by the activating solution must be present in this framework in order to balance negative charge of Al^{+3} in IV-fold coordination [2, 8]. According to Loewenstein avoidance principle [16], aluminate and silicate species present in the medium form mainly Si-O-Al and Si-O-Si bonds during formation of geopolymer structure, while formation of Al-O-Al bonds is not favored thermodynamically, but still, not impossible [17].

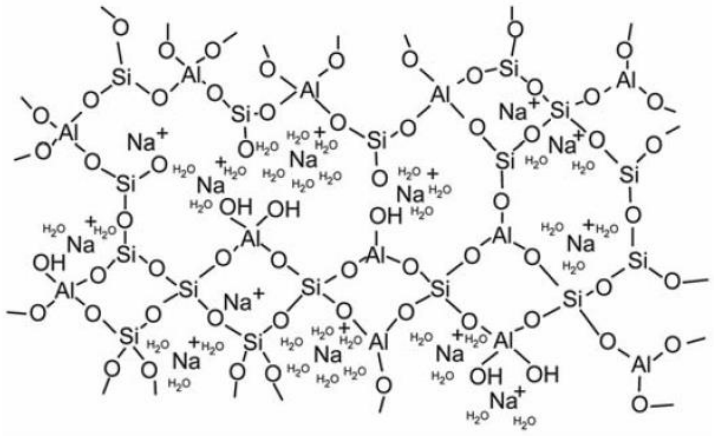

Figure 1.2 : Schematic model of three-dimensional aluminosilicate network proposed by Rowles [13]

Understanding of reaction kinetics of geopolymerisation has crucial importance for improvement and controlling the application properties of geopolymeric materials. Various methods can give insight to synthesis process of a geopolymer structure from different aspects, while any of these methods can be qualified as an observation technic that supplies combined and broad scale information of this process [1]. In fact, the progress of geopolymerisation is generally very rapid due to formulations used to produce these materials. This requires the use of observation methods that could allow to capture almost instantaneously the development of geopolymer structure [1, 6]. In literature, several technics have been used to analyze reaction kinetics as well as the fresh and hardened state properties of geopolymers. The most popular measurement technics are Scanning Electron Microscope (MEB) [18, 19], Nuclear Magnetic Resonance (NMR) [17, 20, 21], rheological measurements performed by rheometer [6, 22], Calorimetry [23, 24], X-Ray Diffraction [25, 26], Fourier Transform Infrared Spectroscopy (FTIR) [27, 28] and modelling [29, 30]. Measurement methods such as NMR, X-Ray Diffraction, FTIR or Calorimetry are used to determine reaction kinetics (e.g. identification and quantification of species formed during geopolymerisation, identification of dissolution enthalpy etc.), while other methods such as MEB or rheometer are used to analyze the evolution of the microstructure or fresh properties (e.g. pore structure, viscosity, elastic modulus etc.) over time [6]. Synthesis of geopolymers could be influenced by several factors (i.e. mainly by formulation and processing conditions). We present essential parameters affecting kinetics of geopolymerisation as well as the fresh and hardened properties of geopolymeric materials in the following section.

1.2. Essential parameters influencing reaction kinetics, fresh and hardened state behaviors of geopolymers

Synthesis of geopolymeric materials is a complex process due to several factors that have impact on reaction kinetics of geopolymerisation and/or final properties of these materials at fresh or hardened state. These factors can be classified mainly as the choice of raw material,

formulation used to produce geopolymers and processing conditions. In following sections, we introduce briefly each of these factors.

1.2.1. Choice of raw material

Choice of raw material is the fundamental step of geopolymer production. The most used geopolymer source materials are preferably fly ash (FA) and blast furnace slag (BFS) due to their low carbon footprint compared to ordinary Portland cement (OPC). Their processing energy involves mainly the post-treatment process (i.e. drying, milling, and separation) [31], which makes researchers use primarily these materials. Fly ash is an industrial byproduct of the coal-burning power plant industry [31], while blast furnace slag is a byproduct of pig-iron manufacture from iron ore [32]. However, in spite of the quality control within individual locations, compositions of FA and BFS vary depending on the ore where they are supplied from, combustion and quenching processes [1]. Other industrial by products are also used as alternative materials. The use of palm oil fuel ash (POFA), which is a waste material of palm industry, is reported widely in palm oil-rich countries such as Malaysia or Thailand [33, 34]. Rice husk ash (RHA), which is a silica rich agriculture by product containing 90–95% by wt. amorphous silica [35], is referred in several studies [36, 37]. Red mud (RM) from alumina refining industry [36], calcined kaolinitic shale residues [38] and copper mine tailings [39] are also suitable raw materials that have considerable use is production of geopolymeric materials. In addition to industrial by products, natural precursors such as volcanic ash (e.g. pumice, scoria) are also very useful [35]. Calcined clays obtained from calcination of naturally occurring clay minerals are one of the most common raw materials for fabrication of geopolymers [1]. Particularly, metakaolin has been the most popular raw material mentioned by several researchers [1, 6, 40].

The type of final product as well as the characteristic properties (e.g. mechanical strength, acid and fire resistance, viscosity etc.) of final geopolymeric material depend considerably on the nature of selected raw material. Fernandez-Jimenez et al. [41] reported main reaction product of an alkali activated fly ash (AAFA) geopolymer system as an X-Ray amorphous aluminosilicate gel, while long reaction times of this system give rise to formation of minor crystalline phases such as herschelite, hydroxysodalite or zeolites. Similarly, Fernandez-Jimenez et al. [40] observed mainly a gel phase and some zeolite crystals of different nature from synthesis of a metakaolin-based geopolymer system, while a geopolymer system composed of 50% of metakaolin and 50% of fly ash exhibit a composite structure made up of gel, zeolites, and unreacted fly ash particles. Zeolites have well-defined crystal structure [15, 40], whereas aluminosilicate gel has a hybrid amorphous nanocrystalline structure [40]. Depending on the included cation in the nature of raw material as well as the alkaline solution, final aluminosilicate structure can be named differently such as N-A-S-H, K-A-S-H, C-A-S-H etc. [42]. Characteristic properties (e.g. compressive strength) of geopolymers evaluate based on this final structure. Fernandez-Jimenez et al. [40] reported higher compressive strength when a geopolymer structure is composed of metakaolin with fly ash then that is composed of only metakaolin. Author mentioned that geopolymer including only metakaolin had a structure that is more porous and its lower compressive strength correlated with the porosity in

microstructure. Actually, it is very difficult to define clearly the impact of raw material alone on the properties of geopolymeric materials. Geopolymerisation itself is very sensitive to any modification such as variation of molar ratios between silicate and aluminate species or temperature during the reaction. Therefore, in literature, majority of fresh state (e.g. viscosity, yield stress etc.) as well as the hardened state (e.g. mechanical strength, acid or corrosion resistances etc.) properties of these materials are discussed especially based on formulations, processing and measurement conditions. Although the same raw material is used, properties such as viscosity (i.e. resistance of a fluid to flow) or compressive strength of obtained geopolymer can change depending on these parameters. For a better understanding, we discuss the impact of formulation, which is basically the variation of molar ratios Si/Al and/or Na/Al, processing and measurement conditions in following section.

1.2.2. Geopolymer formulation, processing and measurement conditions

In addition to choice of raw material discussed above, chemistry of alkaline activator that is required to initiate geopolymerisation reaction is also important [1]. Type of activator affects mainly molar ratios (i.e. Si/Al and Na/Al) of reaction products when it is combined with raw material. Variation of molar ratios could influence the degree of geopolymerisation [30, 43, 44], development of microstructure [45, 46], setting time [17, 47, 48], evolution of elastic modulus over time [6, 49], viscosity [17, 48, 50] and other properties such as acid or thermal resistance, carbonation, corrosion etc.

Komljenovic et al. [51] investigated the use of different fly ash classes as well as the nature and concentration of various activators on mechanical and microstructural properties of a fly ash geopolymer system. Authors used six different fly ash as precursors and aqueous solutions of $Ca(OH)_2$, NaOH, NaOH+Na_2CO_3, KOH and Na_2SiO_3 (waterglass) of various concentrations as alkali activators. Authors reported that nature and concentration of alkali activator is the most dominant factor in the reaction of alkali activation. Depending on the type and concentration of activator, a change in morphology and porosity of alkali activated fly ash was noticed. A fibrous network together with calcium silicate hydrates (C-S-H) and considerable amount of porosity is observed when $Ca(OH)_2$ is used as activator, while geopolymer matrix has a cluster-like morphology with the use of NaOH (Figure 1.3-a and b). Moreover, the highest compressive strength is obtained with Na_2SiO_3, then this is followed by $Ca(OH)_2$, NaOH, NaOH+Na_2CO_3 and KOH. Independent from activator type, compressive strength increased with increased concentration of activator (Figure 1.3-c and d). Rowles et al. [52] studied the influence of the Si/Al and Na/Al ratios on the microstructure of geopolymers prepared by metakaolin and sodium silicate, where sodium silicate is obtained from the dissolution of silica fume in sodium hydroxide. According to microstructural observations coupled with compressive strength measurements, authors observed the highest compressive strength when Si/Al and Na/Al ratios are close to 2.5 and 1.25 respectively (Figure 1.4). The decrease in compressive strength with low Na or high Si content is explained by potentially insufficient OH^- that is necessary for a complete dissolution of Si^{4+} and Al^{3+} ions, which leads to remaining unreacted metakaolin particles in solution, thus weakening the final geopolymer matrix. In case of high Na content, excess of Na ions causes also weakening of geopolymer structure.

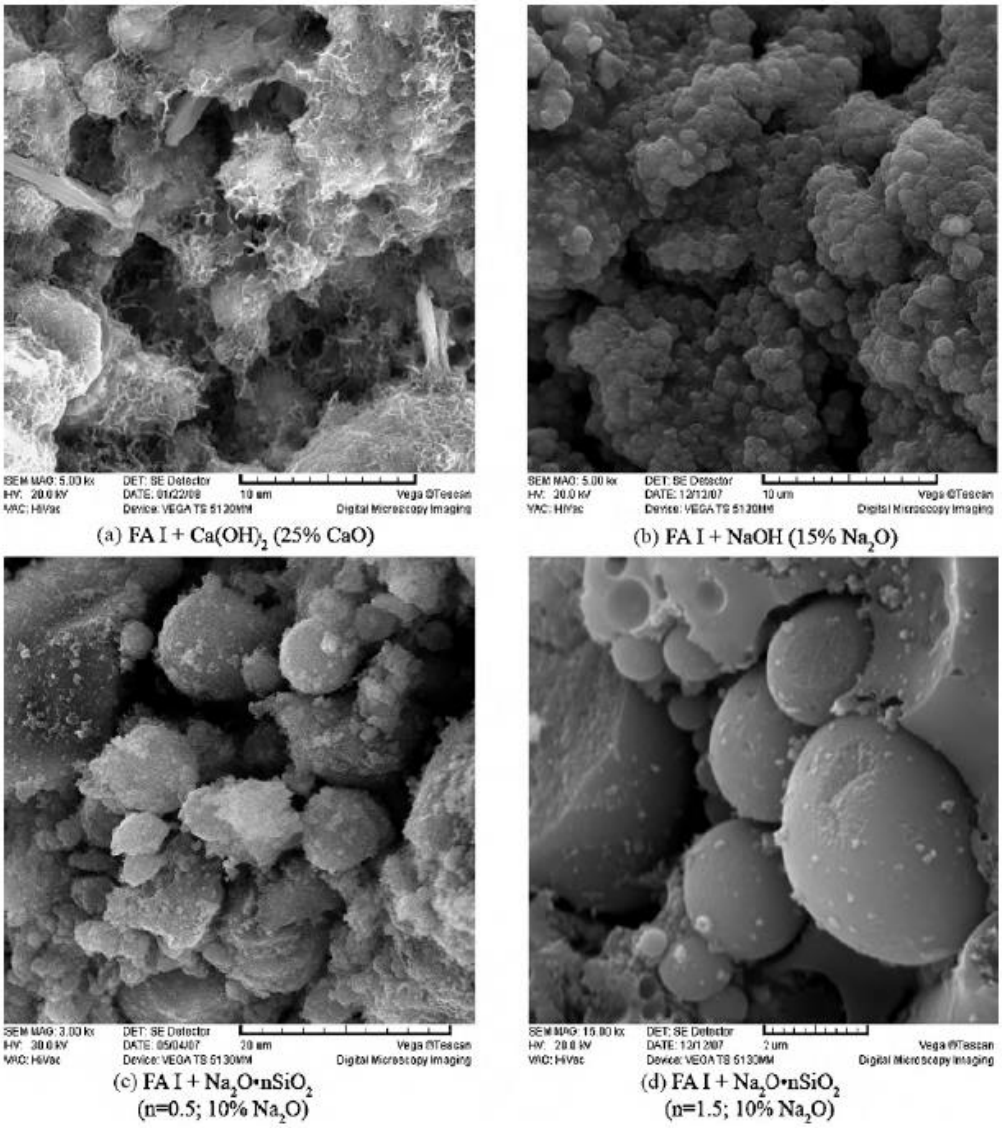

Figure 1.3: Variation of fly ash (FA) morphology according to type (a and b) and concentration (c and d) of alkali activator [51]

Although the impact of molar ratios on development of microstructure or mechanical properties is discussed by many other studies [18, 19], type of alkaline activator as well as the variation of molar ratios are also important for other application properties such as workability or setting time of geopolymeric materials. Provis et al. [1] highlighted that individual viscosity of alkaline hydroxides as well as the composition of sodium silicates used in formulation must be considered for better processing of geopolymeric materials. According to variation of viscosity with concentrations of alkaline hydroxides at 25°C (Figure 1.5-a), a gradual increase of viscosity is observed up to 1M for all types of hydroxides, where increasing trends differ depending on each alkaline hydroxide. Moreover, according to diagram showing composition of sodium silicate solutions (Figure 1.5-b), solution prepared with composition in region D tends to give inconveniently high viscosity, while the use of solutions in region A and C results in partially and highly crystalline mixtures respectively. Compositions of sodium silicate solutions in region B represent commercial sodium silicate solutions.

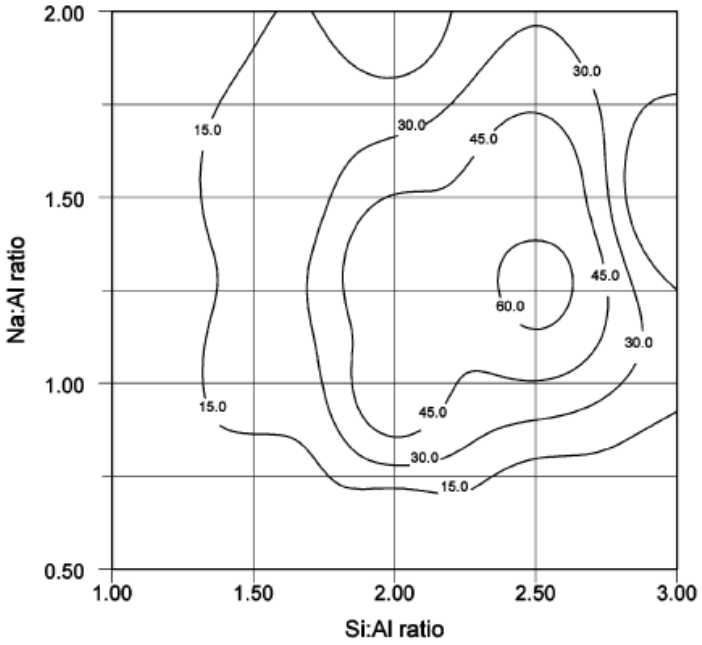

Figure 1.4: Variation of compressive strength according to molar ratios of Si/Al and Na/Al. The compressive strength of Si:Al = 1 and Na:Al = 0.5 is set to zero for contouring purposes [52]

Arnoult et al. [47] investigated controlling the setting time of a geopolymer system using various geopolymer mixtures based on variation of alkaline silicate solutions. Authors reported that setting time decreases with decreasing Si/M (i.e. M = Na or K) ratio. Moreover, when geopolymers are prepared by the same commercial potassium silicate solution with different concentrations, initial viscosities of geopolymers are similar, while setting times become longer with increasing concentrations of potassium silicate solution.

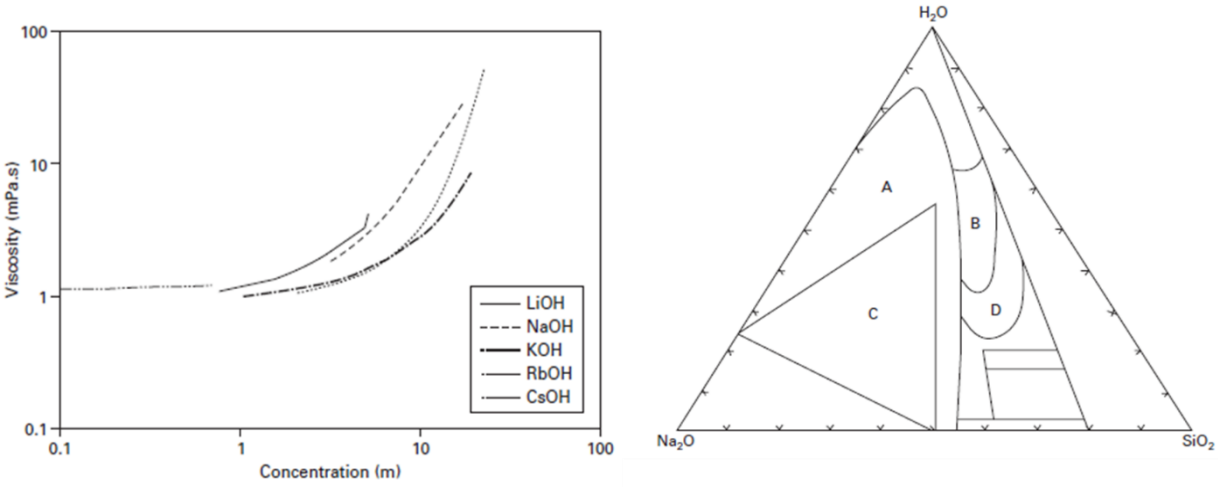

Figure 1.5: Viscosities of alkali hydroxide solutions as a function of molality (a) obtained from data of [53, 54, 55] and compositional regions leading to different types of product in the Na2O-SiO2-H2O system (b) diagram based on [56]

Poulesquen et al. [49] monitored the evolution of elastic and viscous moduli of geopolymers prepared by different silica precursors and alkali activators (i.e. NaOH or KOH) over time. Authors reported faster geopolymerisation kinetics with the use of sodium hydroxide, where weaker interactions between constituents limit formation of oligomers. Although the evolution of elastic modulus of geopolymers prepared by KOH was slower over time, utilization of KOH favors formation of three-dimensional geopolymer structure probably due to a better oligomer connectivity.

In addition to formulation parameters, another important factor having impact on material properties is temperature. In general, temperature plays role depending on processing conditions of raw materials or experimental conditions of geopolymers. Fabbri et al. [57] studied variation of temperature during calcination process of various kaolinite powders. Authors varied calcination temperature between 550°C and 850°C and analyzed modification of physical and chemical properties of resulting metakaolin powders. Authors reported an alteration of kaolinite phase composition by thermal treatment. Aluminum atoms of unfired kaolinite are in six coordination (Al^{VI}), while coordination numbers decrease toward four or five (Al^{IV} or Al^{V}) after calcination. Moreover, small amount of kaolinite is still present after thermal treatment at 550°C, but it disappears completely at 650°C. For a complete decomposition of kaolinite, higher temperatures are required. However, particles tend to agglomerate or sinter completely at higher temperatures starting from 750°C, thus provoke the increase of particle sizes of final metakaolin powders. Modification of phase composition or particle physical parameters could modify reaction kinetics. Diffo et al [58] mentioned that calcination rate (i.e. °C/min) influences compressive strength as well as the setting time of metakaolin-based geopolymers. Authors reported a decrease of compressive strength with a prolongation of setting time of geopolymers at low calcination rates. Several researchers have been also interested in the impact of curing temperature on geopolymer properties in terms of different aspects [59, 60, 61, 62, 63]. Rovnanik [61] studied the effect of curing temperature varied from 10°C to 80°C and curing time on mechanical strength, pore distribution and microstructure of a metakaolin-based geopolymer system activated by sodium silicate solution. Author reported a prolongation of setting time with lower curing temperature. Increasing curing temperature accelerates formation of geopolymer structure but prevents it from being compact and tough. Therefore, early compressive strength of this geopolymer system is higher but then it decreases at later ages. Moreover, higher curing temperature during early hardening process triggers formation of larger pores, which then affects negatively final mechanical properties. Similar observations about pore structure have been reported also with fly ash-based geopolymer systems. Sindhunata et al. [62] studied development of the pore structure of geopolymers synthesized from fly ash and sodium or potassium silicate solutions. Authors mentioned that elevated curing temperature results in the increase of reaction rate, total pore volume and surface area.

Majority of actual research has focused mostly on microstructural analysis as well as the mechanical performance of geopolymeric materials by mainly variation of type or concentration of alkali activator and detailed examinations have been presented by several researchers [8, 35, 64, 65, 66]. In addition to mechanical properties, fresh state properties of

these materials also have crucial importance for industrial applications such as stirring, pumping or spraying. A rapid setting due to increase of alkali activator concentration or temperature or a variation of particle physical properties of raw material due to its fabrication conditions could modify properties such as workability of geopolymeric materials. In this case, application of final geopolymeric material in site would be difficult and less effective. In literature, studying fresh state properties, which are represented especially by rheological investigations, is becoming popular but still, further investigation is needed to understand better the origin of variations of properties at fresh state so that they could be controlled depending on the type of application.

As mentioned, selection of raw material and alkali activator as well as the description of processing and measurement conditions are the key factors affecting the procedure of geopolymer synthesis and final fresh and hardened state properties. There exists a large bibliographical background about the effect of these key factors on hardened state properties, while further rheological investigation is needed in order to understand better and control fresh state properties during in-situ industrial applications. In the following sections, we introduce initially a basic knowledge about rheology and then we present rheological properties of geopolymers, which will be related to different microscopic origins later.

1.3. Introduction to rheology

Rheology is the study of deformation and flow of matter [67]. This definition involves such widely differing materials as asphalt, lubricants, paints, plastics, polymers, suspensions etc. [67]. Here, we introduce principally the rheology of cementitious suspensions. Historically, the basis of rheology dates back to the theory of classical elasticity proposed by Robert Hooke (i.e. English polymath active as a scientist and architect) in 1678. Later, Isaac Newton (i.e. English mathematician, physicist, astronomer, alchemist, theologian, and author) underlined liquids in his book 'Principia' published in 1687 by the hypothesis associated with the simple shear flow [67, 68]. The concept of simple shear flow is based on shearing the material between two infinite parallel planes (Figure 1.6), where these plates are separated by a distance H. Shear occurs only through the relative motion of parallel layers of the material [69]. In order to make material flow with a relative velocity of V, a force F must be applied in the flow direction.

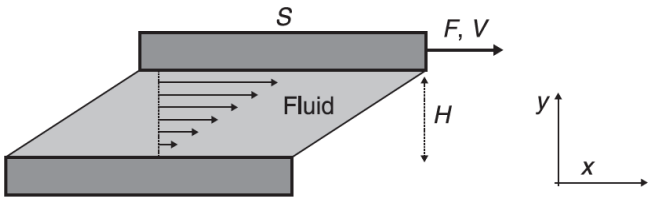

Figure 1.6: Representation of simple shear flow [69]

Noting that x is the direction of flow, y is the direction of the spatial variations of the velocity $V_x(y)$ and S is the surface of plates that supposed to tend to infinity. Applied force F results in a shear stress τ that is proportional to shear rate $\dot{\gamma}$ [69]. Shear stress is the force applied to the

section of a piece of material [70] (Equation 1.1) and shear rate is the ratio of relative velocity to the thickness (Equation 1.2) [70, 71].

$$\tau = \frac{F}{S} \quad (1.1) \quad [69]$$

$$\dot{\gamma} = \frac{V}{H} \quad (1.2) \quad [69]$$

The proportionality between shear stress τ and shear rate $\dot{\gamma}$ is given by the Equation 1.3 below:

$$\tau = \mu\dot{\gamma} \quad (1.3) \; [69]$$

Where μ is the apparent viscosity of material being sheared. In ideal conditions, relation between shear stress τ and shear rate $\dot{\gamma}$ could describe rheological behavior of material. Depending on the considered range of shear rates as well as the mixing proportions, cementitious materials (i.e. including geopolymers) could display Newtonian, Shear-thinning or Shear-thickening behavior [72]. Newtonian behavior represents a constant proportionality between shear stress and shear rate. The flow history does not have any impact on materials showing Newtonian behavior. Hence, these materials initiate flowing immediately at a rate proportional to applied shear stress and their viscosity does not change as a function of applied shear rate [70]. Shear-thinning and shear-thickening behaviors are observed with non-Newtonian materials, where their viscosity changes with variation of shear rate. Apparent viscosity of cementitious materials showing shear-thinning behavior decreases with increasing shear rate, while in case of shear-thickening behavior, apparent viscosity increases with increasing shear rate [72].

Concentrated suspensions of solid particles in Newtonian liquids such as cement suspension show frequently yield stress followed by nearly Newtonian behavior [73]. Yield stress is the critical stress value τ_c under which material behaves like an elastic solid. When the applied stress becomes higher than critical stress τ_c, material behaves like a liquid [70]. Suspensions that need a minimum amount of stress value that is equivalent to critical yield stress in order flow are called yield stress fluids (i.e. also called Bingham plastics) [73]. Several mathematical modellings are developed to represent non-Newtonian rheological behaviors [67, 73, 74, 75]. Bingham [76] and Herschel-Bulkley [77] models are the most used models to describe behavior of yield stress fluids. For traditional cement suspensions, Bingham model given in Equation (1.4) is usually used to express their shear-thinning behavior [72].

$$\tau = \tau_0 + \mu_p\dot{\gamma} \quad \text{with} \quad \tau \geq \tau_0 \quad (1.4) \quad [72, 73]$$

Where τ_0 is the critical yield stress that must be applied to initiate flowing (i.e. $\tau_0 = \tau_c$) and μ_p is the plastic viscosity. Based on a dimensionless empirical number Γ defined in [72] (Equation 1.5), it is possible to determine a critical shear rate value $\dot{\gamma}_0$ (i.e. Γ = 1) above which the effect of yield stress on the flow behavior is ignorable.

$$\Gamma = \frac{\mu_p\dot{\gamma}}{\tau_0} \quad (1.5) \; [72]$$

When applied shear rate is lower than critical shear rate (i.e. $\dot{\gamma} < \dot{\gamma}_0$), fluid has shear-thinning behavior, while a plateau is expected when applied shear rate is greater than critical shear rate (i.e. $\dot{\gamma} >> \dot{\gamma}_0$) (Figure 1. 7) [72].

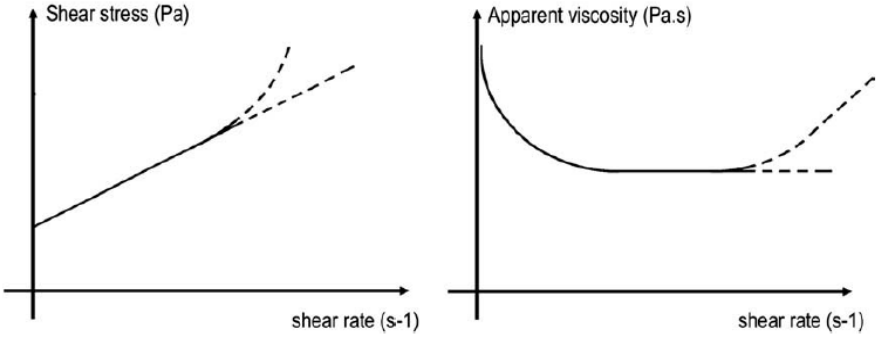

Figure 1.7: Relations between shear stress and shear rate (at left) and apparent viscosity and shear rate (at right) for cement suspensions. Dashed lines represent potential rheological behaviors that could be observed depending on the range of shear rates as well as the mixing proportions [72]

For flow behavior of geopolymer suspensions, different rheological models have been proposed in literature. Several studies reported that NaOH-activated slag (AAS) suspensions behave as Bingham fluid [22, 78], while flow behavior of waterglass activated slag or fly ash suspensions fits well to Herschel-Bulkley model (Equation 1.6) [22, 50, 79].

$$\tau = \tau_0 + K\dot{\gamma}^n \quad (1.6)\ [50]$$

Where K is the consistency coefficient (Pa.s^n) and n is the dimensionless flow index. Suspensions have shear-thinning behavior with n < 1, shear-thickening behavior with n > 1 and Newtonian behavior with n = 1 (i.e. only if τ_0 = 0) (see Figure 1.7). Unlike these studies based on non-Newtonian fluid behaviors, Favier et al. [80] described metakaolin-based geopolymer suspensions activated by alkaline silicate solution as Newtonian fluids with the viscosity controlled mainly by the elevated viscosity of the suspending silicate solution. In the following section, we present rheological properties of geopolymers while mentioning industrial application difficulties.

1.4. Rheological properties of geopolymers

Main difficulty for industrial applications of geopolymeric materials is the constrained maneuverability due to their elevated viscosity. To have an idea about their viscosity, a cement and a geopolymer suspension can be compared. In the absence of chemical additives, main components of a cement suspension are water and cement particles [81]. Viscosity of this suspension depends on several parameters (e.g. presence of admixtures), while viscosity of a geopolymer suspension is controlled primarily by the viscosity of alkaline activator used to produce this suspension [6]. In this case, a comparison between interstitial fluids of these suspensions would reflect the difference between their rheological behaviors. Viscosity of water at 20°C is 0.001 Pa.s, while viscosity of an alkaline activator is 10 to 100 times higher

than that of water [80, 82]. This means, if we neglect other parameters influencing rheological properties, industrial application of a geopolymeric material necessitates 10 to 100 times more energy for its industrial application, thus increased costs and dealing with more application problems. Figure 1.8 presents the difference between casting processes of a geopolymer and an ordinary Portland cement (OPC) concretes.

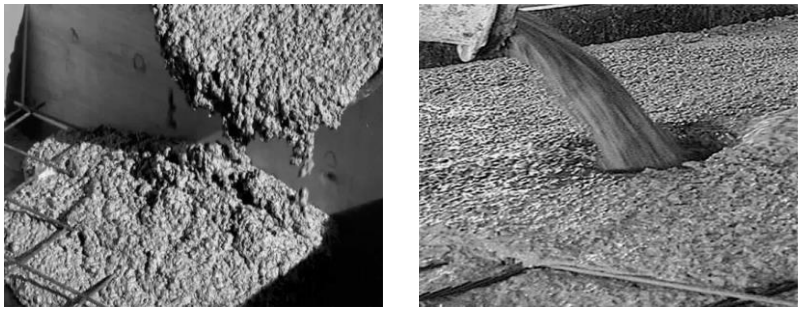

Figure 1.8: Casting of a geopolymer concrete (at left) and OPC concrete (at right) [83, 84]

Moreover, viscosity of a geopolymer suspension rises over time. Bourlon [17] studied the evolution of viscosity of a metakaolin-based geopolymer system over time and reported that viscosity of this system increases consistently (Figure 1.9-a). Author showed that viscosity is influenced by formulation (i.e. mainly by the ratio of Si/Al) and by temperature. Increasing ratio of Si/Al decelerates the increase of viscosity (Figure 1.9-b) and results in longer setting times. Setting time of geopolymer having Si/Al = 1.9 is around 3 hours, while it increases toward 10 hours with Si/Al = 2.2. Moreover, increase of temperature causes the decrease of initial viscosity due to decreasing viscosity of alkaline activator with temperature, while the increment of viscosity over time accelerates owing to a potential modification of reaction kinetics with increased temperature (Figure 1.9-c).

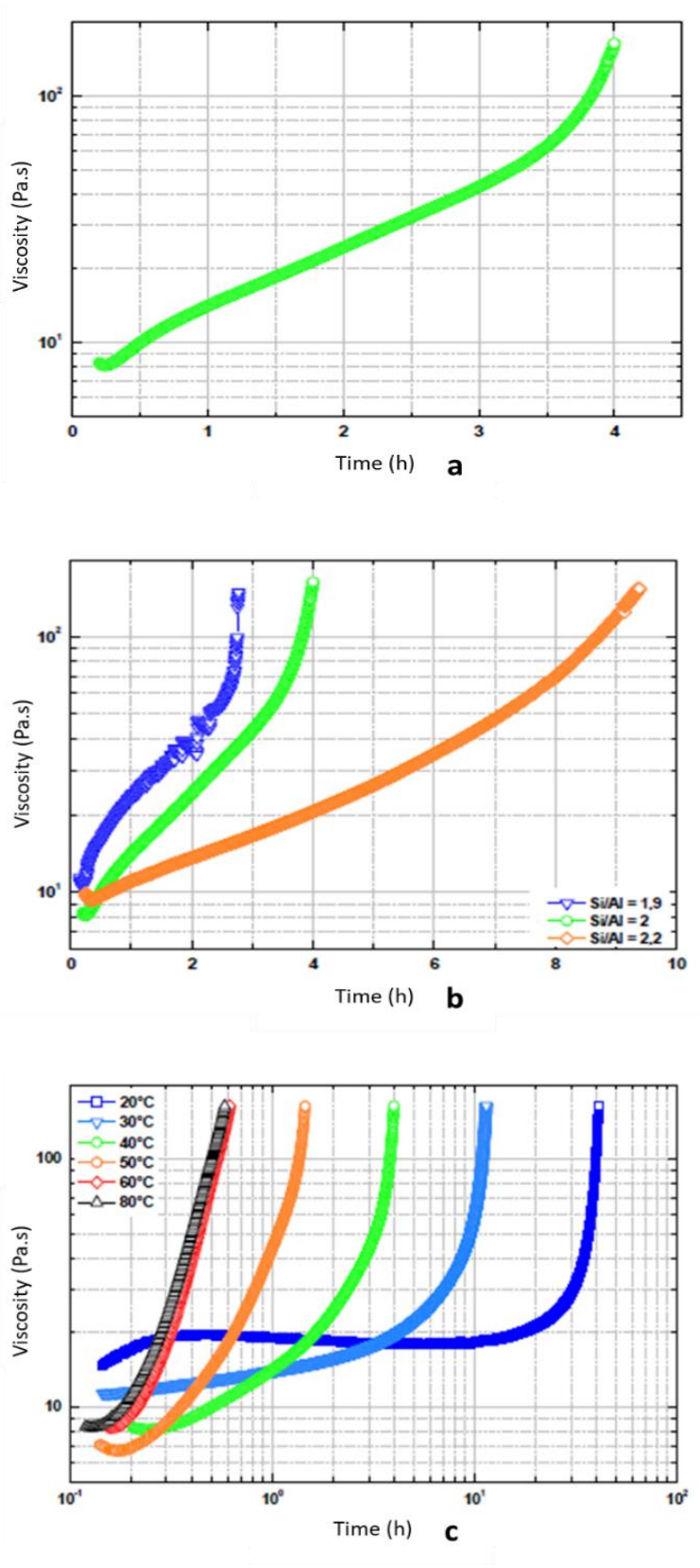

Figure 1.9: Evolution of viscosity of a metakaolin-based geopolymer over time (a), Influence of the Si/Al ratio on the evolution of the viscosity (b), Influence of temperature on the evolution of the viscosity (c). (Si/Al = 2, Na/Al = 1, H2O/Na2O = 15, T= 40°C for a and c. Si/Al = 1.9, 2 or 2.2, Na/Al = 1, H2O/Na2O = 15, T= 40°C for b). Adapted from [17]

Palacios et al. [50] reported similar observations about the increase of viscosity with rising temperature on alkali activated fly ash (AAFA) systems. Authors investigated the effect of nature and concentration of alkaline activator as well as the temperature on the rheological behavior of this system. Commercial sodium silicate solutions, which contain sodium hydroxide pellets at different concentrations, are used as alkali activators. Regardless of the concentration or silica modulus (i.e. mixture percentages between commercial silicate and sodium hydroxide) of activator solutions, authors observed an increase of viscosity with rising temperatures, especially above 65°C (Figure 1.10). Increase of viscosity is related to the onset of physical-chemical interactions and the formation of initial reaction products, where increased temperature favors the reaction (i.e. mainly dissolution of fly ash particles), thus formation of reaction products.

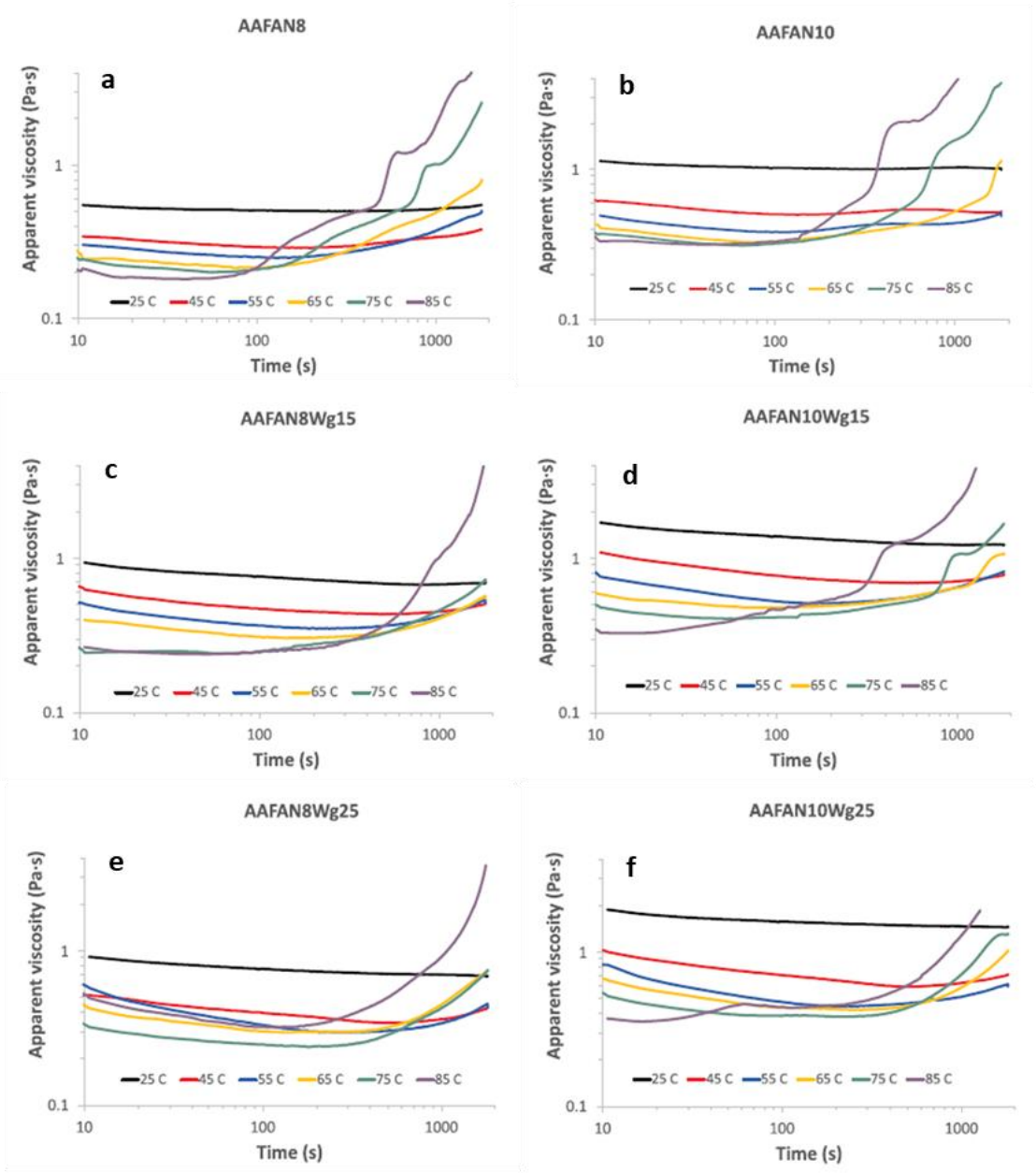

Figure 1.10: Evolution of viscosity (at different temperatures) of AAFA geopolymer systems over time. N8 and N10: 8 or 10 molar NaOH, Wg15 and Wg25: percentage of sodium silicate solution by weight of activating solution. Adapted from [50]

In addition to evolution of viscosity, which is already high initially, over time, another important issue that could create difficulties for industrial applications of geopolymeric materials is the influence of mixing on rheological properties of these materials. Favier [6] mentioned that evolution of elastic modulus of a metakaolin-based geopolymer system modifies by applied mixing protocol, which indicates an alteration of development of mechanical properties depending on mixing process. First, author studied the evolution of elastic and viscous moduli of this system over time by oscillation rheology measurements. Both viscous and elastic moduli increased rapidly during the first several hundreds of seconds and then it was followed by a slow linear increase. After a couple of hours, another sharp increase for elastic and viscous moduli was observed (Figure 1.11).

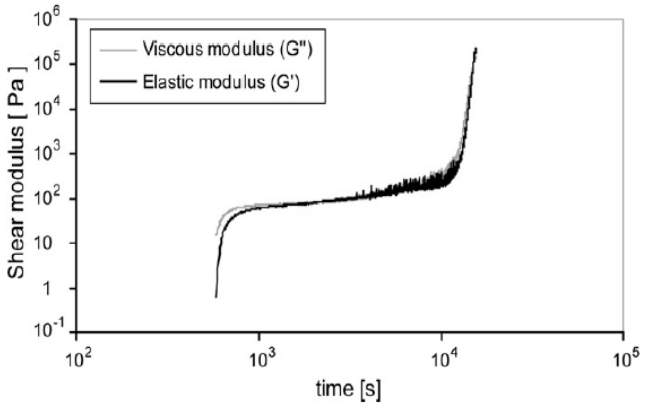

Figure 1.11: Evolution of elastic and viscous moduli of a metakaolin-based geopolymer system over time (T = 26°C, Si/Al < 4.5, H_20/Na_2O = 10) [6, 82]

The origin of initial rapid increase of elastic modulus is attributed to a formation of an Al-rich gel having Si/Al < 4 at the grain boundaries of metakaolin particles. Following slight increase represents that this gel becomes denser by the progressive increase of its network due to condensation. Hence, this period is the transition between the liquid and the solid state [85]. Second sharp increase, which appears after a few hours, is interpreted as a precipitation of a denser gel (i.e. called Si-rich gel) having high Si connectivity with tetrahedral aluminum. Comparison between evolution of elastic modulus with evolutions of equivalent Al and Na concentrations monitored by static ^{27}Al and ^{23}Na NMR measurements over time shows that concentrations of both Al and Na decrease at the moment where second sharp increase of elastic modulus is observed (Figure 1.12), which confirms precipitation.

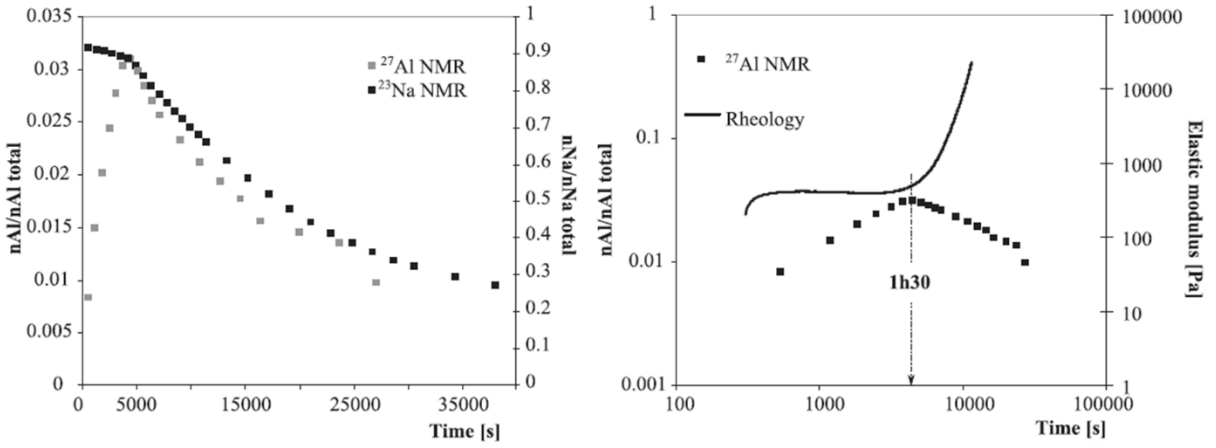

Figure 1.12: Comparison between evolutions of Na and Al concentrations monitored by static ^{27}Al and ^{23}Na static NMR (a); Comparison between evolution of Al concentration followed by NMR and evolution of elastic modulus by oscillation rheology (SiO_2/Na_2O = 1.06, H_2O/Na_2O) [6, 85]

Secondly, author investigated the impact of structural homogenization applied by variation of mixing duration on the evolution of elastic modulus over time. Two formulations are identified with molar ratios SiO_2/Na_2O = 1.06, H_2O/Na_2O = 20, Si/Al = 1.71, Na_2O/Al_2O_3 = 0.67 for first one and with molar ratios SiO_2/Na_2O = 1.6, H_2O/Na_2O = 20, Si/Al = 1.86, Na_2O/Al_2O_3 = 0.63 for second one. Geopolymers are mixed at a constant speed of 200 min^{-1} during 2000 seconds (i.e. for first formulation) or during 2000 seconds and 5000 seconds (i.e. for second formulation). Author observed that homogenized geopolymer systems have lower initial elastic modulus, which represents Al-Rich gel, reduced transition period and sharper increment of second elastic modulus, where this increment accelerates with increased mixing time. Moreover, formation of denser gel (called primarily Si-Rich gel) delays and does not correlate anymore with monitored aluminum concentrations by NMR. Therefore, it was supposed to obtain either a new NMR invisible gel with developing mechanical properties or a transformation of initial Al-Rich gel to an alternative gel.

Actually, all parameters are related to each other. Since the viscosity of a geopolymeric material is controlled primarily by the viscosity of alkaline activator in its composition, any modification that could influence the viscosity of activator could then modify also rheological behavior as well as the reaction kinetics. Mixing process could trigger the increase of temperature, where increase of temperature could then accelerate reaction kinetics and cause rapid setting. Alternatively, mixing process could increase viscosity of geopolymer due to a potential contribution to dissolution, thus formation of reaction kinetics. Formulations used to produce geopolymeric materials could result in the alteration of rheological or mechanical performances as well as the development of microstructure. Whatever the reason of rapid setting, a weaker geopolymer structure could form due to incomplete dissolution of raw material, thus a decrease of mechanical strength or a variation of microstructure could be observed. Moreover, material performance to acid resistance, corrosion, carbonation etc. could decrease. Interconnection between all these parameters implies that the development of rheological properties (i.e. mainly elevated viscosity) of geopolymers is the basic step to

ameliorate material performance at fresh or solid state. It is crucial to improve initially constrained maneuverability, obtain a dense and durable structure and to decrease carbon footprint due to the use of traditional cementitious materials.

As mentioned, geopolymeric materials could behave differently depending on the designed formulations as well as the application conditions. Industrial application difficulties of these materials are initially their elevated viscosity and the evolution of viscosity over time. In addition, application conditions (e.g. applied mixing process) could modify the development of mechanical properties and this could result in undesired outcomes such as rapid setting. In the following section, we discuss microscopic origins of different rheological behaviors, which will constitute the theoretical background of controlling the rheological properties as well as the reaction kinetics of geopolymers.

1.5. Microscopic origins of rheological behavior of cementitious materials

Let us start with the reaction mechanism of a traditional cement suspension. In general, the term "hydration" is used to describe all the reactions that occur during mixing cement with water [86]. Starting from the first contact between materials, a partial dissolution of cement particles takes place and the initial hydration products occur, while interstitial fluid becomes strongly alkaline and saturated in ionic species of calcium Ca^{2+}, potassium K^{+}, sodium Na^{+}, hydroxide OH^{-}, sulphate SO_4^{2-} and silicates [87]. Main hydration products are calcium silicate hydrates (C-S-H) and calcium hydroxide $Ca(OH)_2$ (i.e. also called Portlandite) [81].

Hydration of cement suspensions is a complex process including different types of interactions, which are mainly colloidal interactions, Brownian forces, hydrodynamic interactions, and contact forces between particles [72]. In geopolymer suspensions, interaction forces depend primarily on selected raw material. When industrial by products such as fly ash or slag are used to produce geopolymers, similar hydration products with cement suspensions (e.g. C-A-S-H) can be observed [1, 88]. Similarly, colloidal interactions present in cement suspensions could also occur in geopolymer suspensions [50] since similar ions (e.g. Ca^{2+}, hydroxide OH^{-}, silicates etc.) exist in both systems. When raw materials used to produce geopolymers do not contain Ca^{2+} ions, which is the case for metakaolin-based systems, hydrodynamic interactions (i.e. mainly viscous contributions) start governing the system [6, 80]. Favier et al. [80] report that colloidal interactions between particles in a metakaolin-based geopolymer suspension could be negligible since rheological behavior of this system is controlled primarily by hydrodynamic interactions. Authors show that viscosity of a geopolymer suspension is lower than that of a cement suspension when applied shear rate is low (i.e. below 10 s^{-1}), while it becomes higher at higher shear rates (Figure 1.13). Moreover, viscosity of geopolymer suspension is nearly independent from shear rate, which means that viscous contributions dominate both colloidal interactions and particle inertia over a wide range of shear rate.

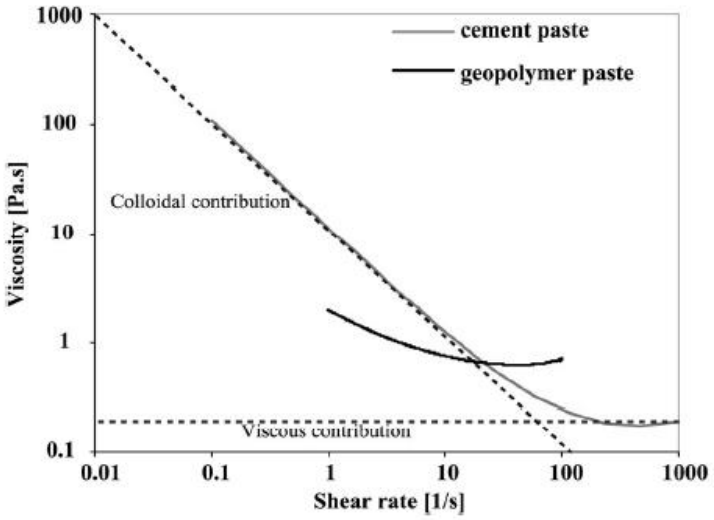

Figure 1.13: Apparent viscosity of a metakaolin-based geopolymer suspension and a cement suspension as a function of shear rate [80]. Dotted lines represent limits of colloidal and viscous contributions to shear-thinning and Newtonian behaviors respectively.

Difference between types of interactions at microscale implies the necessity of alternative methods to control rheological behavior of particularly geopolymer suspensions. In following sections, we introduce interaction forces that are at microscopic origins of different rheological behaviors, which could occur in cement as well as geopolymer suspensions.

1.5.1. Colloidal interactions

Colloidal interactions are governed essentially by van der Waals attractive forces, which have interatomic electromagnetic origin from the dissymmetrical distribution of the electronic cloud around atoms or molecules [89]. When these forces are dominant, they trigger particles to aggregate, thus suspension becomes instable [75]. In order to disperse particles homogeneously in the liquid, adequate repulsive forces must be present between particles. Electrostatic repulsive forces arise from the charged surfaces of neighboring particles can then act to avoid particle aggregation, thus a homogeneous dispersion [75, 90]. The intensity of van der Waals attractive forces can be found by following Equation 1.7.

$$F_{VDW} = \frac{A_h \alpha^*}{12h^2} \quad (1.7)\ [90]$$

Where α^* is the characteristic size of the surface defects of particles, h is the distance of inter-surface separation at contact points of particles (i.e. in the order of a few nanometers [72, 91]) and A_h is the delayed Hamaker constant depending on the value of h [81, 90] (Figure 1.14).

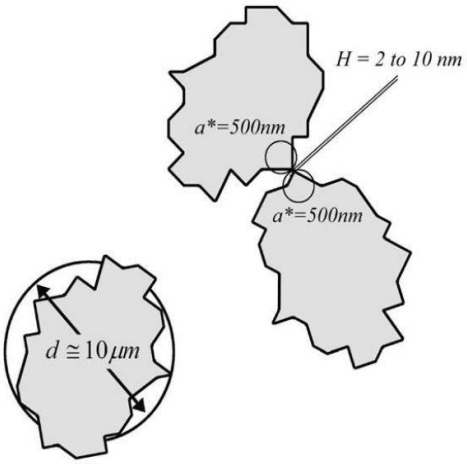

Figure 1.14: Characteristic size of particles (d) (i.e. mean diameter), characteristic size of the surface defects (α^*), distance of inter-surface separation at contact points of particles (h). Schema is based on cement particles [72]

1.5.2. Hydrodynamic interactions

When colloidal particles are exposed to higher shear rates or external gravitational fields (e.g. sedimentation), hydrodynamic effects become essential [92]. In fact, when a particle moves in a fluid, it perturbs the surrounding fluid. This results in a flow field that affects the motion of other particles [92]. Moreover, shearing the particles in such an environment triggers the increase of suspension viscosity compared to that of interstitial fluid [70]. The increase of suspension viscosity depends primarily on the concentration of solid particles in the medium [90]. When concentration of solid particles is low, suspension has a dilute regime, where the movement of each particle during the flow is not influenced by the existence of any of the other particles in the fluid [70, 90]. Hence, particles in suspension are only subjected to the Stokes force (Equation 1.8), which is proportional (i.e. in laminar conditions) to the viscosity of the interstitial fluid (μ_0), mean particle size (d) and the shear rate ($\dot{\gamma}$):

$$F_{Stokes} \approx \mu_0 d^2 \dot{\gamma} \quad (1.8)\ [81, 90]$$

In a dilute regime, viscosity of suspension can be predicted by Einstein's law given in Equation 1.9 below:

$$\mu = \mu_0(1 + 2.5\phi) \quad (1.9)\ [93]$$

Where μ is the viscosity of suspension, μ_0 is the viscosity of interstitial fluid and ϕ is the solid volume fraction (i.e. solid volume divided by total volume). Einstein's law given above is an approximation becoming more accurate when solid volume fraction ϕ becomes smaller [75]. When the concentration of solid particles is higher, which means increasing solid volume fraction ϕ in suspension, flow trajectories of particles are influenced by the movement of other neighboring particles. In this case, viscous dissipation is governed by squeezing force (Equation 1.10), which is proportional to viscosity of interstitial fluid (μ_0), distance of inter-

surface separation at contact points of particles (h), mean particle size (d) and the shear rate ($\dot{\gamma}$) (i.e. in laminar conditions):

$$F_{squeezing} = \mu_0 \frac{d^3 \dot{\gamma}}{h} \quad (1.10) \quad [81, 90]$$

Behavior of a concentrated suspension system depends on how particle network evolves during the flow. Various phenomena could occur such as dilatancy (i.e. volume change of the system with shear deformations), a network of direct interparticle contacts etc. [75]. Viscosity of a concentrated suspension can be predicted by Krieger-Dougherty model given in Equation 1.11 below:

$$\mu = \mu_0 \left(1 - \frac{\phi}{\phi_{max}}\right)^{-q} \quad (1.11) \; [72]$$

Where μ is the viscosity of suspension, μ_0 is the viscosity of interstitial fluid, ϕ is the solid volume fraction, ϕ_{max} is the maximum solid volume fraction that can be reached by particles [70] and q is a constant related to the particle shape [72]. For spherical particles, value of q can be taken as 2, while it is suggested to use a value greater than 2 for non-spherical particles [72]. When solid volume fraction ϕ approaches to maximum packing fraction ϕ_{max}, viscosity tends to infinity (Figure 1. 15). At the compact regime (i.e. $\phi = \phi_{max}$), particles get into contact physically, where this contributes to macroscopic stress and results in jamming [70, 72]. Hence, material is actually solid in compact regime [70].

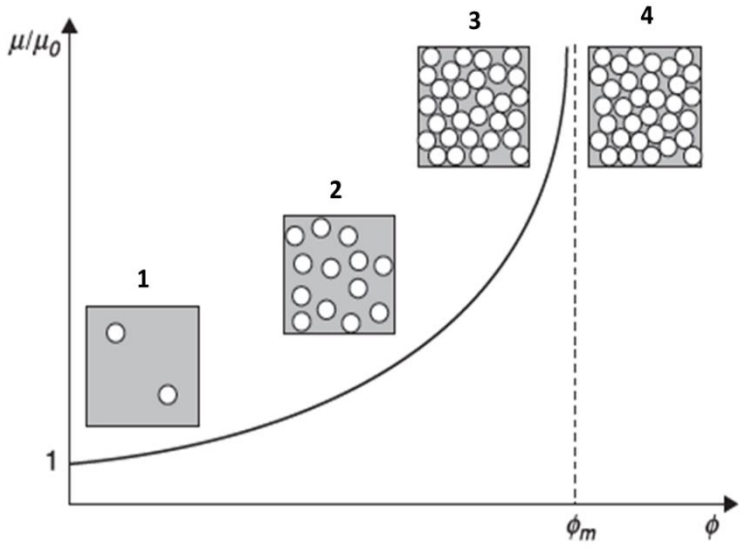

Figure 1.15: Relative viscosity of a suspension composed of spherical particles in a Newtonian fluid as a function of solid volume fraction. Schemes from left to right represent concentrations of dilute (1), semi-dilute (2), concentrated (3) and compact (4) regimes. Adapted from [70]

1.5.3. Contribution of formation of hydration products

It is reported in literature that the nucleation of hydration products (i.e. particularly C-S-H) on the surfaces of cement particles creates local rigid bridges between cement particles and this generates interparticle forces [93, 94]. The size as well as the number of these bridges increase significantly and rapidly (i.e. in few seconds) over time, giving rise to a new interaction network [81]. Contribution of this interaction network to increasing yield stress is presented in Figure 1.16, where the first peak corresponds to the rupture of the percolated network of particles interacting by rigid bridges of hydrates and the second peak is related to the rupture of the percolated network of particles interacting by Van der Waals forces.

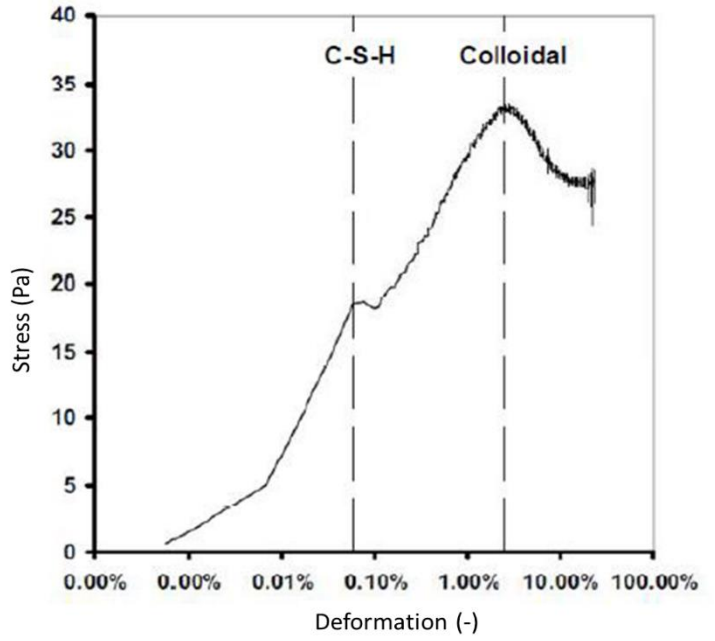

Figure 1.16: Stress as a function of deformation. Measurement is performed at constant frequency and at low deformation rates. Adapted from [94]

In a geopolymer network, C-S-H could occur simultaneously with a geopolymeric gel. Yip et al. [88] studied the coexistence of gel network and C-S-H products at early stage of alkaline activation of metakaolin-granulated blast furnace slag geopolymer system. Authors reported that presence of gel with C-S-H depends on concentration of alkaline activator and metakaolin-slag ratio. When concentration of alkaline activator used to produce geopolymers increases, geopolymeric gel is the predominant phase formed with small C-S-H species within this gel. It is observed that voids and pores within the geopolymeric binder are filled with C-S-H (Figure 1.17) and this helps to create bridges between different hydration products, thus to obtain higher mechanical strength.

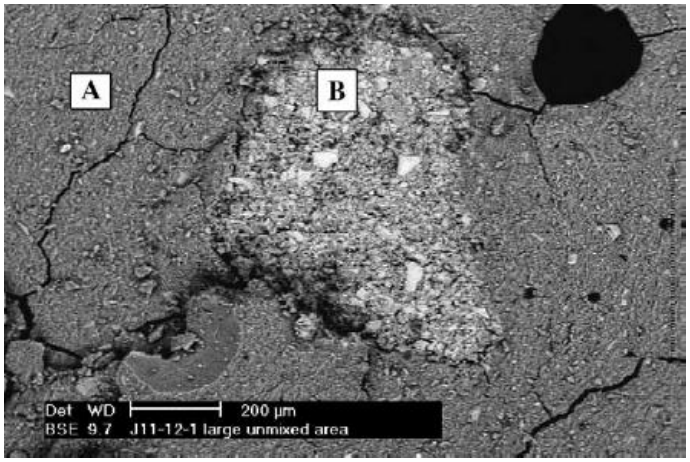

Figure 1.17: SEM micrograph of a metakaolin (MK)-granulated blast furnace (GGBFS) slag geopolymer. A: geopolymeric binder (N-A-S-H) with low calcium content, B: calcium silicate hydrate with small proportion of aluminum ($NaOH+Na_2SiO_3$) / (MK+GGBFS) = 1.45, SiO_2/Na_2O=2 [88]

1.5.4. Contribution of particle inertia

When suspensions are sheared at high shear rates, the effect of particle inertia on rheological behavior becomes visible. In such a situation, hydrodynamic interactions are no longer proportional to applied shear rate or the shear speed of interstitial fluid, but proportional to the kinetic energy of particles in suspension [81]. There is a kind of jamming of the structure beyond a critical shear rate, which is actually the origin of shear-thickening behavior (Figure 1.18-a) [70]. Beyond this critical shear rate, structure under formation by the particles in liquid does not have enough time to relax during macroscopic deformation. Hence, the imposed deformation by shearing pushes particles close to each other, leading to very high energy dissipation that is associated with a diverging apparent viscosity [70] (Figure 1.18-b).

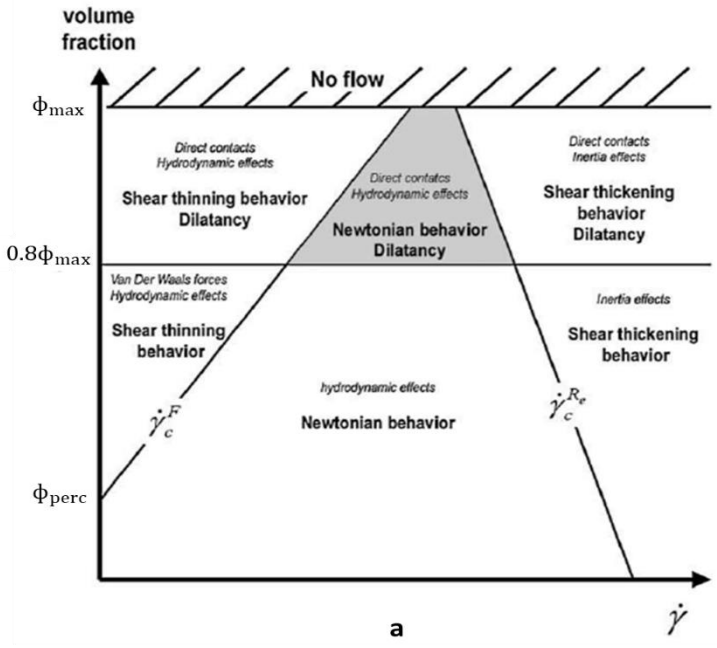

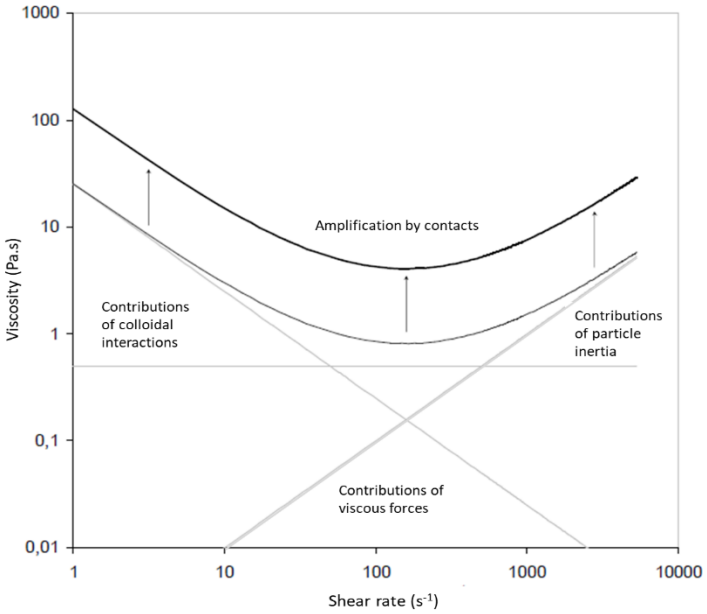

b

Figure 1.18: Rheophysical classification of cement suspensions (a) (ϕ_{perc}: percolation volume fraction above which a network of colloidal interactions appears, ϕ_{max}: maximum packing fraction of particles) [72] and viscosity as a function of shear rate for a traditional cement paste (b) [81]

As mentioned, depending on the design parameters of formulations (e.g. type of alkali cation, solid volume fraction etc.), microscopic origin of rheological behavior of geopolymeric materials could be colloidal or hydrodynamic interactions, contributions of hydration products or particle inertia. Depending on the microscopic origin, method used for controlling the rheological behavior could differ. In the following section, we focus essentially on controlling the rheological properties of geopolymers, which will be then related to the objective of this thesis later.

1.6. Methods of controlling the rheological behavior of cementitious materials

We have introduced in previous sections that rheological behavior of geopolymer suspensions depends on different types of interactions occurring at microscopic scale. Hence, controlling their rheological behavior is then possible depending on the type of interactions present in microscale. In the following sections, we discuss different methods with parameters affecting the process of controlling the rheological behavior of geopolymeric materials.

1.6.1. Effect of chemical admixtures on controlling rheological behavior of geopolymers

Majority of chemical admixtures used for industrial applications of cementitious materials are actually polymers having different structural compositions. Polymers are developed by joining many copies of certain groups of atoms in a long chain, where their basic unit is called

monomer [75]. Scientific background about their synthesis and chemical compositions can be found in literature [81, 75, 91, 95] and it is out of scope of this thesis. Depending on the apparent density of polymers in solution, the nature and intensity of their interactions, new types of structures (e.g. entanglements) may appear and affect the rheological behavior of suspensions having polymers in their formulations [81]. Several categories of polymers exist in literature such as superplasticizers, flocculants, viscosity agents etc. [81]. Superplasticizers are one of the most common type within various polymer families. In literature, several studies mentioned that their use could decrease yield stress and viscosity of cement suspensions [96, 97, 98]. Interaction principle of superplasticizers is based on the fact that a layer of polymer adsorbs onto surfaces of cement particles and creates a steric barrier that increases the interparticle distance [90, 96]. We recall that attractive van der Waals forces are proportional to $1/h^2$ (see Equation 1.7), while hydrodynamic squeezing forces that are responsible for macroscopic viscosity are proportional to 1/h (see Equation 1.10). Consequently, increase of interparticle distance by adsorption of superplasticizers results in the decrease of yield stress and viscosity.

The use of superplasticizers is also a center of interest for geopolymers. Several studies investigated the effect of various types of superplasticizers on rheological, mechanical and setting properties of geopolymers [22, 99, 100, 101, 102, 103]. Palacios et al. [100] studied the impact of five different superplasticizers based on polycarboxylate, melamine, naphthalene and vinyl copolymer and a shrinkage-reducing polymer derived from polypropylenglycol on rheological, mechanical and setting properties of alkaline activated slag pastes and mortars. Authors reported that all studied superplasticizers, except from naphthalene-based polymer, lost their plasticizing properties in mortars activated with sodium hydroxide due to modification of their chemical structure in highly alkaline medium (i.e. pH > 13). Since the chemical structure of naphthalene-based superplasticizer does not change, its use is more beneficial in terms of the improved workability as well as the increase of both mechanical strength and the setting time. Marchon et al. [105] reported later that the loss of fluidity of superplasticizers in highly alkaline medium could be also due to the competitive adsorption of these products with the alkaline activation solution. Puertas et al. [101] studied the influence of superplasticizers based on vinyl copolymers and polycarboxylates on alkaline activated slag or fly ash pastes and mortars. Authors observed that both superplasticizers do not influence the fluidity of slag or fly ash mortar. Moreover, the use of vinyl copolymer-based superplasticizer has a negative impact on the strength development of alkaline activated slag mortars, while the addition of polycarboxylate-based superplasticizer does not have any positive or negative impact on strength development of slag or fly ash based mortars. Bakharev et al. [102] investigated the effect of chemical admixtures belonging to different categories on alkaline activated slag concrete. Authors used a superplasticizer based on modified naphthalene formaldehyde, an air-entraining, a water-reducing and a shrinkage-reducing agent. Authors reported that, although the use of naphthalene formaldehyde-based superplasticizer contributes initially to workability, its contribution is valid only at early age and then setting occurs rapidly. Moreover, increased shrinkage and reduced strength are also observed when naphthalene formaldehyde-based superplasticizer is used in this system. However, the use of air-entraining agent results in the decrease of shrinkage as well as the

improved workability, while compressive strength is not influenced by its presence. Authors concluded by mentioning that the use of an air-entraining agent is more suitable for alkaline activated slag concrete.

As observed by many researchers, utilization of chemical admixtures in geopolymer formulations does not certainly supply improved workability without influencing mechanical strength or setting time, whereas it is important to maintain a good strength for durability and longer setting times for industrial applications within enough time. Dupuy et al. [104, 105] studied the effect of boron and phosphor-based mineral additives on viscosity and setting time of metakaolin-based geopolymers. In the first study [104], authors reported that setting time can be controlled and extended above 24 hours with the addition of 2.8% (i.e. by weight) boric or phosphoric acid or 10% (i.e. by weight) of borax. Moreover, viscosity decreases below these addition amounts. When the amounts of additives used in geopolymer formulations becomes higher than 2.8% for boric or phosphoric acids or 10% for borax, viscosity starts to increase and their use become unbeneficial. In the second study [105], authors observed that contribution of these additives to setting time and viscosity until a certain amount is due to formation of a secondary network during geopolymerisation, where phosphor or boron atoms integrate into geopolymer network, decrease the connectivity between aluminate and silicate species, thus retards setting and triggers decrease of viscosity. Many other studies investigated the role of boron-based additives or borax on microstructural evolution, setting time and mechanical strength of alkali activated fly ash or slag geopolymers [106, 107, 108, 109, 110]. In general, until a certain amount of addition, use of boron-based additives or borax supplies increasing setting time and mechanical strength. Antoni et al. [106] reported that addition of borax in fly ash-based geopolymer system increases slightly compressive strength in comparison to that does not contain borax. However, compressive strength decreases when addition amount of borax is higher than 20% [107].

In addition to use of chemical admixtures, applied mixing protocol of geopolymeric materials could also play role on yield stress and viscosity. Palacios et al. [22] studied the effect of prolonged mixing on rheological behavior of alkali activated slag-based geopolymer systems, where waterglass and NaOH solutions are used as alkali activators. Authors observed that when waterglass activated geopolymer pastes are exposed to a constant shear rate at 200 s^{-1}, shear stress rises rapidly, reaching 160 Pa in 3 minutes. When applied shear breaks the initial floc structures, yield stress decreases gradually (Figure 1.19). Moreover, authors reported that increasing mixing time from 3 minutes to 10 minutes retards initial and final setting times by more than 40 minutes and 4 hours respectively. When mixing is extended to 30 minutes, initial and final setting times delayed by 2 hours and 8 hours respectively.

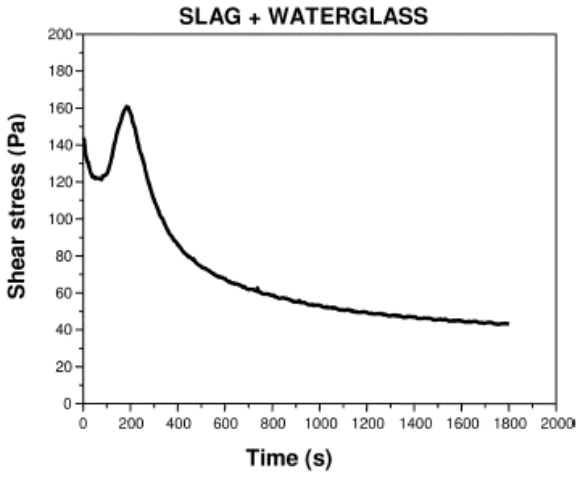

Figure 1.19: Shear stress as a function of mixing time at a constant mixing rate of 200 s^{-1} for a waterglass activated slag geopolymer [22]

Based on studies mentioned in literature, controlling rheological behavior (i.e. particularly yield stress and high viscosity) of geopolymeric materials by the use of chemical additives is a complex procedure due to several reasons. First, certain types of additives that belong to different polymer families could lose their characteristic mechanism of interaction due to variations on their chemical structure or due to their competitive adsorption with activation solution in highly alkaline medium. Second, majority of studied admixtures are developed primarily for cement suspensions, where reaction kinetics as well as the hydration products are clearly different from that of geopolymer pastes. This implies that certain types of polymers may not behave in a geopolymer medium as expected. Moreover, even sufficient workability could be obtained with the use of chemical additives, they may trigger reduced strength or rapid setting. In this case, variation of applied mixing protocol to control rheological behavior of geopolymeric materials seems interesting because it could allow to control yield stress and viscosity without changing formulation parameters. However, other factors induced by mixing could play role on final rheological behavior and this necessitates further investigation.

1.6.2. Effect of optimization of particle packing on controlling rheological behavior of geopolymers

Optimization of particle packing is an alternative method to control rheological behavior of cementitious materials. First, we recall that microscopic interactions present in cementitious suspensions depend also on solid volume fractions of particles. Yield stress and viscosity increase with solid volume fractions and diverge at a compact regime (i.e. $\phi = \phi_{max}$) (see Figure 1.15). Moreover, we mentioned that at a concentrated regime, where hydrodynamic interactions arise from viscous dissipations are dominant (i.e. suspension behaves as a Newtonian fluid), colloidal interactions could be negligible and Krieger-Dougherty model could be used to predict the viscosity. According to this model, suspension viscosity (μ) can be decreased by reducing the viscosity of interstitial fluid (μ_0) or solid volume fractions of particles (ϕ) or by increasing maximum solid volume fraction (ϕ_{max}) in the system (see

Equation 1.11). Reducing the viscosity of interstitial fluid requires modifications of solution parameters especially for geopolymer suspensions. It is possible to decrease viscosity of an alkaline solution by varying its molar ratio of SiO_2/Na_2O. Bourlon [17] reported that viscosity of a sodium silicate solution decreases when the ratio SiO_2/Na_2O of this solution increases until around 2.6 (Figure 1.20). However, as we mentioned previously, changing molar ratios of alkaline solutions used to produce geopolymers could have non-negligible impacts on reaction kinetics of geopolymerisation, which may also affect negatively the development of characteristic properties such as mechanical strength. Hence, reducing viscosity of alkaline solution would not be primarily a good option. Similarly, reducing solid volume fraction of particles in geopolymer suspensions would result in formation of insufficient reaction products, thus a weaker gel network with fewer connections. This could trigger a decrease of mechanical strength. Increasing maximum solid volume fraction (i.e. also called maximum packing fraction) in a geopolymer suspension, while keeping viscosity of interstitial fluid (i.e. alkaline activator) and solid volume fraction constant allows to reduce viscosity without any modification of chemical composition. This means, only optimizing the physical parameters of particles of raw materials used to produce geopolymers could be enough to decrease the viscosity, thus control rheological behaviors of geopolymeric materials while assuring a stable reaction kinetics as well as the good mechanical properties. In this case, the best option to decrease viscosity of a geopolymer suspension would be the augmentation of maximum solid volume fraction at a constant viscosity of interstitial fluid and solid volume.

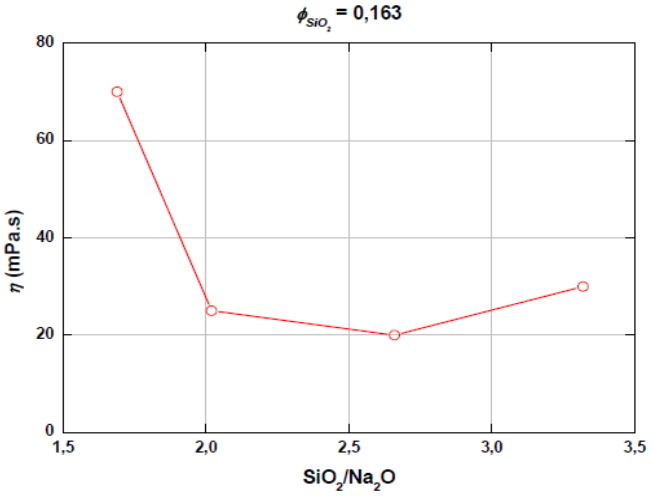

Figure 1.20: Evolution of viscosity of a sodium silicate solution as a function of SiO_2/Na_2O [17]

Maximum packing fraction is an intrinsic geometrical property of a particle system, which depends mainly on shapes and sizes of particles in this system [71]. Basically, maximum packing of a suspension can be increased by enhancing the occupied space by particles. This requires first, an identification of physical properties of particles (i.e. size or shape) and second, a method to apply for amelioration of packing. Majority of industrial powders used for fabrication of cementitious materials have polydispersity, where sizes of particles in their composition could vary from nanometric to micrometric scale. Suspensions prepared by polydispersed powders could supply higher packing density in comparison to those involving only monodispersed particles (Figure 1.21). This is because smaller particles in polydispersed

materials are better at filling the voids in a given volume, thus increases the efficiency of the optimization.

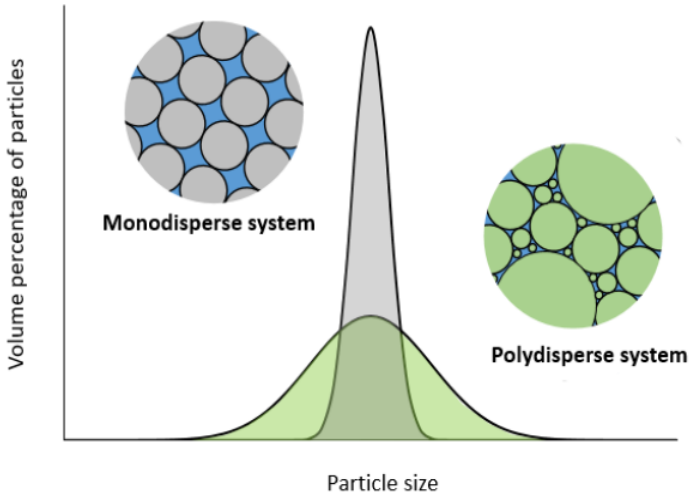

Figure 1.21: Effect of particle size distribution on packing density [71]

However, in case of polydispersity, influence of particle shape on packing optimization depends various factors such as orientation of particles, aspect ratio (i.e. ratio between length and width of particle) or roughness [111]. Packing of spherical particles and packing of rounded particles having the same aspect ratio but different roughness does not necessarily correspond to the same packing fraction (Figure 1.22) [90]. Moreover, application of different methods for optimization of particle packing could also result in different packing values. When particles are gathered into a container gently or by an agitation such as shaking, their final packing values will be different. Here, former method corresponds to the random loose packing, while it is called as random close packing when there is an external agitation such as shaking [111]. Hafid et al. [112] studied the effect of morphological parameters (i.e. mainly aspect ratios) of various sand particles on rheological behavior of their suspensions. Authors showed that random loose and random close packing values of particles decrease with increasing aspect ratios and they suggested a correlation between variations of yield stress and viscosity due to an alteration in the particle morphology. Chindaprasirt et al. [113] reported that shape of fly ash particles used in geopolymers plays an important role on improvement of workability. Authors observed that particles with a spherical shape and a smooth surface contribute to improvement of flow of the subsequent fresh mixes without any need of additional water or water-reducing admixtures. Cassagnabère et al. [114] studied flow properties of cement-metakaolin based mortars having mix proportions of 3:1:0.5 for sand, binder and water respectively. Authors prepared binders either by 100% of ordinary Portland cement or by replacing 12.5% or 25% of cement (i.e. by weight) with a metakaolin powder. Authors reported a strong dependency of slump and viscosity on the morphology of metakaolin particles, where decreasing roundness or increasing ruggedness of these particles cause higher viscosity and lower slump.

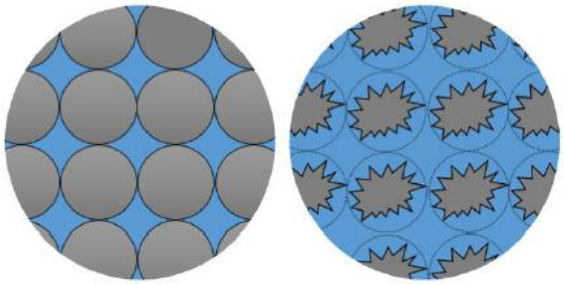

Figure 1.22: Effect of particle shape on packing density [90]

Optimization of particle packing is a common method to improve mix design, thus workability and mechanical strength and to decrease the fabrication costs as well as the carbon footprint of cementitious materials [111, 115, 116]. Based on the literature, initial step of packing optimization is the characterization of physical properties of raw materials that lead to improve packing of particles, while second step is an effective mix design of formulation components. In literature, several models are developed initially to improve mix design of ordinary Portland cement concrete [117, 118, 119], while these models are then also used to develop mix design of mortars or pastes based on ordinary Portland cement [90, 120]. Although, it has a great potential to decrease the elevated viscosity of geopolymeric materials, optimization of particle packing has not been extensively used to control rheological behavior of these materials. Therefore, controlling rheological behaviors of geopolymeric materials by particle packing optimization requires further investigation.

1.7. Objective of the study

As we mentioned primarily, geopolymers are highly viscous materials, where their viscosity can be influenced by several parameters such as choice of raw material or alkaline activator, selected molar ratios, temperature, applied mixing protocol etc. Moreover, their viscosity evolves rapidly, which could trigger a fast setting. A fast setting could result in a weaker geopolymer structure due to incomplete dissolution of raw material, thus a decrease of mechanical strength or a modification of microstructure. Hence, their initial elevated viscosity with its rapid evolution could cause primarily the reduction of time for transportation of these materials and several industrial application difficulties such as instable casting, spraying etc. due to limited workability and it could also affect implicitly the deterioration of mechanical performance and long term properties (e.g. resistance to corrosion, carbonation etc.). Consequently, controlling the rheological behavior (i.e. essentially elevated viscosity and rapid setting time) of geopolymeric materials is a fundamental requirement in order to improve both rheological as well as the mechanical performances of these materials.

The objective of this thesis is controlling the viscosity and setting time of metakaolin-based geopolymers. First, we aim to decrease viscosity while keeping mechanical performance stable. Since the use of chemical additives could be complicated in terms of compatibility of these materials with a highly alkaline medium, we will use the method of particle packing optimization to decrease viscosity. This will allow to maintain chemical formulation while

varying only particle physical properties. We recall that optimization of particle packing requires the identification of physical properties of particles and a packing method. Therefore, in order to decrease viscosity:

- We will identify initially the characteristic physical properties of raw materials,

- We will optimize packing fractions of solid precursors of studied geopolymers by developing binary powder mixtures between different raw materials,

- We will investigate the effect of improved packing on the evolution of viscosity of geopolymers.

Secondly, we aim to prevent rapid setting without modifying chemical formulations of geopolymers. Although some of the boron- or phosphor- based mineral admixtures are efficient to control setting time, variation of applied mixing protocol is a better option because it ensures keeping a stable chemical formulation. However, modifying applied mixing could modify also temperature of geopolymers, thus their viscosity or reaction kinetics of geopolymerisation. Therefore, in order to control rapid setting:

- We will investigate the impact of variations of mixing speed or mixing duration with the impact of temperature on setting properties of geopolymers.

1.8. Conclusion

In this chapter, first we introduced a general perspective about geopolymers including their synthesis and the parameters influencing their rheological and mechanical properties. Afterwards, we introduced a fundamental physical background about the rheology and we highlighted the importance of the development of rheological properties by stressing on the difficulties of industrial applications of geopolymeric materials. Later, we presented microscopic origins of different rheological behaviors and we mentioned that depending on the type of interaction at microscopic scale, rheological behavior could be controlled by either incorporation of chemical additives or by optimization of particle packing. Finally, we introduced the objective of the study by referring the chosen methods to control viscosity and setting properties of geopolymers. Following chapters are dedicated to introduce the details of all the steps given in the objectives of this study.

References

[1] J. L. Provis and J. S. J. v. Deventer, Geopolymers. Structure, processing, properties and industrial applications., Woodhead Publishing Limited, 2009.

[2] J. Davidovits, "Geopolymers. Inorganic polymerie new materials.," *Journal of Thermal Analysis,* vol. 37, pp. 1633-1656, 1991.

[3] R. E. Lyon, P. N. Balaguru, A. Foden, U. Sorathia, J, Davidovits and M. Davidovics, "Fire-resistant Aluminosilicate Composites," *Fire and Materials,* vol. 21, pp. 67-73, 1997.

[4] J. Giancaspro, P. N. Balaguru and R. E. Lyon, "Use of Inorganic Polymer to Improve the Fire Response of Balsa Sandwich Structures," *Journal of Materials in Civil Engineering. ASCE,* vol. 18, no. 3, pp. 390-397, 2006.

[5] E. Gartner, "Industrially interesting approaches to "low-CO2" cements," *Cement and Concrete Research,* vol. 34, pp. 1489-1498, 2004.

[6] A. Favier, "Mécanisme de prise et rhéologie de liants géopolyméres modèles. Materials.," Université Paris-Est, Champs-sur-Marne, 2013.

[7] P. Duxson, J. L. Provis, G. C. Lukey and J. S. J. v. Deventer, "The role of inorganic polymer technology in the development of 'green concrete'," *Cement and Concrete Research,* vol. 37, pp. 1590-1597, 2007.

[8] P. Duxson, A. Fernandez-Jimenez, J. L. Provis, G. C. Lukey, A. Palomo and J. S. J. v. Deventer, "Geopolymer technology: the current state of the art," *Journal of Materials Science,* vol. 42, pp. 2917-2933, 2007.

[9] J. Davidovits and M. Davidovics, "Geopolmer: Room-Temperature Ceramic Matrix for Composites," *Ceramic Engineering and Science Proceedings,* vol. 9, pp. 835-842, 1988.

[10] V. Glukovsky, Soil silicates, Kiev: Gosstroyizdat Publish, 1959.

[11] H. Xu and J. S. J. v. Deventer, "The geopolymerisation of alumino-silicate minerals," *International Journal of Mineral Processing,* vol. 59, pp. 247-266, 2000.

[12] G. Engelhardt, D. Hoebbel, M. Tarmak, A. Samoson and E. Lippmaa, "29Si-NMR-Untersuchungen zur Anionenstruktur von Kristallinen Tetramethylammonium-alumosilicaten und-alumosilicatlösungen," *Zeitschrift für anorganische und allgemeine Chemie,* vol. 484, no. 1, pp. 22-32, 1982.

[13] M. R. Rowles, J. V. Hanna, K. J. Pike, M. E. Smith and B. H. O'Connor, "29Si, 27Al, 1H and 23Na MAS NMR Study of the Bonding Character in Aluminosilicate Inorganic Polymers," *Applied Magnetic Resonance,* vol. 32, pp. 663-689, 2007.

[14] V. F. F. Barbosa, K. J. D. MacKenzie and C. Thaumaturgo, "Synthesis and characterisation of materials based on inorganic polymers of alumina and silica: sodium polysialate polymers," *International Journal of Inorganic Materials ,* vol. 2, pp. 309-317, 2000.

[15] J. L. Provis, G. C. Lukey and J. S. J. v. Deventer, "Do Geopolymers Actually Contain Nanocrystalline Zeolites? A Reexamination of Existing Results," *Chemistry of Materials,* vol. 17, pp. 3075-3085, 2005.

[16] W. Loewenstein, "The distribution of aluminum in the tetrahedra of silicates and aluminates," *American Mineralogist,* vol. 39, pp. 92-96, 1954.

[17] A. Bourlon, "Physico-chimie et rhéologie de géopolymères frais pour la cimentation des puits pétroliers. Chimie-Physique.," Université Pierre et Marie Curie - Paris VI, Paris, 2010.

[18] P. Duxson, J. L. Provis, G. C. Lukey, S. W. Mallicoat, W. M. Kriven and J. S. J. v. Deventer, "Understanding the relationship between geopolymer composition, microstructure and mechanical properties," *Colloids and Surfaces A: Physicochemical Engineering Aspects,* vol. 269, pp. 47-58, 2005.

[19] P. D. Silva, K. Sagoe-Crenstil and V. Sirivivatnanon, "Kinetics of geopolymerization: Role of Al2O3 and SiO2," *Cement and Concrete Research,* vol. 37, pp. 512-518, 2007.

[20] S. G. M. Palacios, M. .. Alonso, J. B. d. d. Lacaillerie, B. Lothenbach, A. Favier, C. Brumaud and F. Puertas, "Early reactivity of sodium silicate-activated slag pastes and its impact on rheological properties," *Cement and Concrete Research,* vol. 140, no. 106302, 2021.

[21] P. Duxson, J. L. Provis, G. C. Lukey, F. Separovic and J. S. J. v. Deventer, "29Si NMR Study of Structural Ordering in Aluminosilicate Geopolymer Gels," *Langmuir,* vol. 21, pp. 3028-3036, 2005.

[22] M. Palacios, P. F. G. Banfill and F. Puertas, "Rheology and Setting of Alkali-Activated Slag Pastes and Mortars: Effect of Organic Admixture," *ACI Materials Journal,* no. 105-M16, pp. 140-148, 2008.

[23] S. Alonso and A. Palomo, "Calorimetric study of alkaline activation of calcium hydroxide±metakaolin solid mixtures," *Cement and Concrete Research,* vol. 31, pp. 25-30, 2001.

[24] Z. Zhang, J. L. Provis, H. Wang, F. Bullen and A. Reid, "Quantitative kinetic and structural analysis of geopolymers. Part 2. Thermodynamics of sodium silicate activation of metakaolin," *Thermochimica Acta,* vol. 565, pp. 163-171, 2013.

[25] J. L. Provis and J. S. J. v. Deventer, "Geopolymerisation kinetics. 1. In situ energy-dispersive X-ray diffractometry," *Chemical Engineering Science,* vol. 62, pp. 2309-2317, 2007.

[26] P. D. Silva and K. Sagoe-Crenstil, "Medium-term phase stability of Na2O–Al2O3–SiO2–H2O geopolymer systems," *Cement and Concrete Research,* vol. 38, pp. 870-876, 2008.

[27] A. Fernandez-Jimenez and A. Palomo, "Composition and microstructure of alkali activated fly ash binder: Effect of the activator," *Cement and Concrete Research ,* vol. 35, pp. 1984-1992, 2005.

[28] C. A. Rees, J. L. Provis, G. C. Lukey and J. S. J. v. Deventer, "Attenuated Total Reflectance Fourier Transform Infrared Analysis of Fly Ash Geopolymer Gel Aging," *Langmuir,* vol. 23, pp. 8170-8179, 2007.

[29] J. L. Provis and J. S. J. v. Deventer, "Geopolymerisation kinetics. 2. Reaction kinetic modelling," *Chemical Engineering Science,* vol. 62, pp. 2318-2329, 2007.

[30] J. L. Provis, P. Duxson, G. C. Lukey, F. Separovic, W. M. Kriven and J. S. J. v. Deventer, "Modeling Speciation in Highly Concentrated Alkaline Silicate Solutions," *Industrial and Engineering Chemistry Research,* vol. 44, pp. 8899-8908, 2005.

[31] A. Nazari and J. G. Jansayan, Handbook of Low Carbon Concrete, UK: Butterworth-Heinemann, by Elsevier, 2017.

[32] S. Aydin and B. Baradan, "Mechanical and microstructural properties of heat cured alkali-activated slag mortars," *Materials and Design,* vol. 35, pp. 374-383, 2012.

[33] M. O. Yusuf, M. A. M. Johari, Z. A. Ahmad and M. Maslehuddin, "Strength and microstructure of alkali-activated binary blended binder containing palm oil fuel ash and ground blast-furnace slag," *Construction and Building Materials,* vol. 52, pp. 504-510, 2014.

[34] M. J. A. M. M. A. M. Johari and Z. A. Ahmad, "Synthesis of geopolymer from large amounts of treated palm oil fuel ash: Application of the Taguchi method in investigating the main parameters affecting compressive strength," *Construction and Building Materials,* vol. 52, pp. 473-481, 2014.

[35] Z. G. Ralli and S. J. Pantazopoulou, "State of the art on geopolymer concrete," *International Journal of Structural Integrity,* vol. 12, no. 4, pp. 511-533, 2020.

[36] J. He, J. Zhang, Y. Yu and G. Zhang, "Synthesis and characterization of red mud and rice husk ash-based geopolymer composites," *Cement & Concrete Composites,* vol. 37, pp. 108-118, 2013.

[37] A. Nazari, A. Bagheri and S. Riahi, "Properties of geopolymer with seeded fly ash and rice husk bark ash," *Materials Science and Engineering A,* vol. 528, pp. 7395-7401, 2011.

[38] O. Bortnovsky, Z. Sobalik, Z. Tvaruzkova, J. Dedecek, P. Roubicek, Z. Prudkova and M. Svoboda, "Structure and stability of geopolymers synthesized from kaolinitic and shale clay," in *Proceedings, World Congress Geopolymer, Institut Geopolymer*, Saint Quentin, 2005.

[39] S. Ahmari and L. Zhang, "Production of eco-friendly bricks from copper mine tailings through geopolymerization," *Construction and Building Materials,* vol. 29, pp. 323-331, 2012.

[40] A. Fernandez-Jimenez, M. Monzo, M. Vicent, A. Barba and A. Palamo, "Alkaline activation of metakaolin–fly ash mixtures: Obtain of Zeoceramics and Zeocements," *Microporous and Mesoporous Materials,* vol. 108, pp. 41-49, 2008.

[41] A. Fernandez-Jimenez, A. Palomo, I. Sobrados and J. Sanz, "The role played by the reactive alumina content in the alkaline activation of fly ashes," *Microporous and Mesoporous Materials,* vol. 91, pp. 111-119, 2006.

[42] P. Suraneni, M. Palacios and R. J. Flatt, "New insights into the hydration of slag in alkaline media using a micro-reactor approach," *Cement and Concrete Research,* vol. 79, pp. 209-216, 2016.

[43] T. W. Swaddle, "Silicate complexes of aluminum (III) in aqueous systems," *Coordination Chemistry Reviews,* Vols. 219-221, pp. 665-686, 2001.

[44] I. L. Svensson, S. Sjoberg and L. O. Ohman, "Polysilicate Equilibria in Concentrated Sodium Silicate Solutions," *Journal of the Chemical Society, Faraday Transactions 1: Physical Chemistry in Condensed Phases,* vol. 82, no. 12, pp. 3635-3646, 1986.

[45] M. Steveson and K. Sagoe-Crentsil, "Relationships between composition, structure and strength of inorganic polymers. Part I Metakaolin-derived inorganic polymers," *Journal of Materials Science,* vol. 40, pp. 2023-2036, 2005.

[46] W. K. W. Lee and L. S. J. v. Deventer, "The effects of inorganic salt contamination on the strength and durability of geopolymer," *Colloids and surfaces. A, Physicochemical and engineering aspects,* vol. 211, pp. 115-126, 2002.

[47] M. Arnoult, M. Perronnet, A. Autef and S. Rossignol, "How to control the geopolymer setting time with the alkaline silicate solution," *Journal of Non-Crystalline Solids,* vol. 495, pp. 59-66, 2018.

[48] M. Arnoult, M. Perronnet, A. Autef and S. Rossignol, "Geopolymer synthetized using reactive or unreactive aluminosilicate. Understanding of reactive mixture," *Materials Chemistry and Physics,* vol. 237, no. 121837, 2019.

[49] A. Poulesquen, F. Frizon and D. Lambertin, "Rheological behavior of alkali-activated metakaolin during geopolymerization," *Journal of Non-Crystalline Solids,* vol. 357, pp. 3565-3571, 2011.

[50] M. Palacios, M. M. Alonso, C. Varga and F. Puertas, "Influence of the alkaline solution and temperature on the rheology and reactivity of alkali-activated fly ash pastes," *Cement and Concrete Composites,* vol. 95, pp. 277-284, 2019.

[51] M. Komljenovic, Z. Bascarevic and V. Bradic, "Mechanical and microstructural properties of alkali-activated fly ash geopolymers," *Journal of Hazardous Materials,* vol. 181, pp. 35-42, 2010.

[52] M. Rowles and B. O'Connor, "Chemical optimisation of the compressive strength of aluminosilicate geopolymers synthesised by sodium silicate activation of metakaolinite," *Journal of Materials Chemistry,* vol. 13, pp. 1161-1165, 2003.

[53] M. Laliberté, "Model for calculating the viscosity of aqueous solutions," *Journal of Chemical and Engineering Data,* vol. 52, pp. 321-335, 2007.

[54] R. Fricke, "Zähigkeit von Rubidiumhydroxydlösungen," *Zeitschrift für Anorganische und Allgemeine Chemie,* vol. 139, pp. 419-420, 1924.

[55] P. M. Sipos, G. Hefter and P. M. May, "Viscosities and densities of highly concentrated aqueous MOH solutions," *Journal of Chemical and Engineering Data,* vol. 45, pp. 613-617, 2000.

[56] J. G. Vail, Soluble Silicates: Their Properties and Uses, New York, Reinhold: Hassell Street Press , 1952.

[57] B. Fabbri, S. Gualtieri and C. Leonardi, "Modifications induced by the thermal treatment of kaolin and determination of reactivity of metakaolin," *Applied Clay Science,* vol. 73, pp. 2-10, 2013.

[58] B. B. K. Diffo, A. Elimbi, M. Cry, J. D. Manga and H. T. Kouamo, "Effect of the rate of calcination of kaolin on the properties of metakaolin-based geopolymers," *Journal of Asian Ceramic Societies,* vol. 3, pp. 130-138, 2015.

[59] G. Gokhan and G. Kurklu, "The influence of the NaOH solution on the properties of the fly ash-based geopolymer mortar cured at different temperatures," *Composites: Part B,* vol. 58, pp. 371-377, 2014.

[60] A. Mishra, D. Choudhary, N. Jain, M. Kumar, N. Sharda and D. Dutt, "Effect of Concentration of Alkaline Liquid and Curing Time on Strength and Water Absorption of Geopolymer Concrete," *ARPN (Asian Research Publishing Network) Journal of Engineering and Applied Sciences,* vol. 3, no. 1, pp. 14-18, 2008.

[61] P. Rovnanik, "Effect of curing temperature on the development of hard structure of metakaolin-based geopolymer," *Construction and Building Materials,* vol. 24, pp. 1176-1183, 2010.

[62] Sindhunata, J. S. J. v. Deventer, G. C. Lukey and H. Xu, "Effect of Curing Temperature and Silicate Concentration on Fly-Ash-Based Geopolymerization," *Industrial & Engineering Chemistry Research,* vol. 45, pp. 3559-3568, 2006.

[63] A. Nazari, A. Maghsoudpour and J. G. Sanjayan, "Boroaluminosilicate geopolymers: role of NaOH concentration and curing temperature," *Royal Society of Chemistry Advances,* vol. 5, pp. 11973-11979, 2015.

[64] H. Castillo, H. Collado, T. Droguett, M. Vesely, P. Garrido and S. Palma, "State of the art of geopolymers: A review," *e-Polymers,* vol. 22, pp. 108-124, 2022.

[65] T. Srividya, P. R. K. Rajkumar, M. Sivasakthi, A. Sujitha and R. Jeyalakshmi, "A state-of-the-art on development of geopolymer concrete and its field applications," *Case Studies in Construction Materials,* vol. 16, no. e00812, 2022.

[66] M. Wasim, T. D. Ngo and D. Law, "A state-of-the-art review on the durability of geopolymer concrete for sustainable structures and infrastructure," *Construction and Building Materials,* vol. 291, no. 123381, 2021.

[67] H. A. Barnes, J. F. Hutton and K. Walters, An Introduction to Rheology, The Netherlands: Elsevier Science Publishers, 1989.

[68] I. Newton, Mathematical Principles of Natural Philosophy, New York: Daniel Adee, 1687.

[69] G. Ovarlez, Introduction to the rheometry of complex suspensions, from the book "Understanding the rheology of concrete" Edited by N. Roussel, Cambridge: Woodhead Publishing Limited, 2012.

[70] P. Coussot, Introduction to the rheology of complex fluids, from the book "Understanding the rheology of concrete" Edited by N. Roussel, Cambridge: Woodhead Publishing Limited, 2012.

[71] J. Deau, "Control of the Rheological Behavior of Chocolate Suspensions by Optimizing the Morphological Properties of the Particles," Université Paris-Est, Champs-sur-Marne, 2021.

[72] N. Roussel, A. Lemaitre, R. J. Flatt and P. Coussot, "Steady state flow of cement suspensions: A micromechanical state of the art," *Cement and Concrete Research,* vol. 40, pp. 77-84, 2010.

[73] C. W. Macosko, Rheology. Principles, Measurements and Applications, USA: Wiley-VCH, 1994.

[74] F. A. Morrison, Understanding Rheology, New York: Oxford University Press Inc. , 2001.

[75] P. Coussot, Rheophysics. Matter in All Its States, Switzerland: Springer International Publishing, 2014.

[76] E. C. Bingham, An Investigation of the Laws of Plastic Flow, U.S. Government Printing Office, 1917.

[77] W. H. Herschel and R. Bulkley, "Konsistenzmessungen von Gummi-Benzollösungen," *Kolloid Zeitschrift,* vol. 39, pp. 291-300, 1926.

[78] F. Puertas, C. Varga and M. M. Alonso, "Rheology of alkali-activated slag pastes. Effect of the nature and concentration of the activating solution," *Cement and Concrete Composites,* vol. 53, pp. 279-288, 2014.

[79] M. Romagnoli, C. Leonelli, E. Kamse and M. L. Gualtieri, "Rheology of geopolymer by DOE approach," *Construction and Building Materials,* vol. 36, pp. 251-258, 2012.

[80] A. Favier, J. Hot, G. Habert, N. Roussel and J. B. d. d. Lacaillerie, "Flow properties of MK-based geopolymer pastes. A comparative study with standard Portland cement pastes," *The Royal Society of Chemistry. Soft Matter,* vol. 10, pp. 1134-1141, 2014.

[81] H. Bessaies-Bey, "Polymères et propriétés rhéologiques d'une pâte de ciment : une approche physique générique. Matériaux composites et construction.," Université Paris-Est, Champs-sur-Marne, 2015.

[82] A. Favier, G. Habert, J. B. d. d. Lacaillerie and N. Roussel, "Mechanical properties and compositional heterogeneities of fresh geopolymer pastes," *Cement and Concrete Research,* vol. 48, pp. 9-16, 2013.

[83] V. Sasalatti, "NBM and CW Infra Construction Magazine," Visvesvaraya Technological University, Belagavi, May 2020. [Online]. Available: https://www.nbmcw.com/product-technology/construction-chemicals-waterproofing/concrete-admixtures/mechanical-properties-of-geopolymer-concrete-with-alternative-materials.html. [Accessed April 2022].

[84] C. Costs, "Indiamart," Clean Costs Limited, [Online]. Available: https://www.indiamart.com/proddetail/superplasticizer-for-concrete-conproof-superplast-r201-m-18585321533.html. [Accessed April 2022].

[85] A. Favier, G. Habert, N. Roussel and J. B. d. d. Lacaillerie, "A multinuclear static NMR study of geopolymerisation," *Cement and Concrete Research,* vol. 75, pp. 104-109, 2015.

[86] A. Nonat, *L'hydratation des ciments. Course notes of master class "Cement Hydration" at Ecole des Ponts Paristech.,* Champs-sur-Marne, 2016.

[87] H. F. W. Taylor, Cement Chemistry, London Academic Press, 1990.

[88] C. K. Yip, G. C. Lukey and J. S. J. v. Deventer, "The coexistence of geopolymeric gel and calcium silicate hydrate at the early stage of alkaline activation," *Cement and Concrete Research,* vol. 35, p. 1688– 1697, 2005.

[89] J. Fusier, "Suspensions floculées modèles : de la caractérisation à la modélisation," Université Paris-Est, Champs-sur-Marne, 2016.

[90] O. Ahmadah, "Contrôle de la rhéologie des liants à faibles impacts environnementaux," Université Paris-Est and Université Sherbrooke, Champs-sur-Marne, 2021.

[91] R. J. Flatt, "Towards a prediction of superplasticized concrete rheology," *Materials and Structures,* vol. 37, pp. 289-300, 2004.

[92] L. Turetta and M. Lattuada, "The role of hydrodynamic interactions on the aggregation kinetics of sedimenting colloidal particles," *Royal Society of Chemistry: Soft Matter,* vol. 18, pp. 1715-1730 , 2022.

[93] C. M. Neubauer, M. Yang and H. M. Jennings, "Interparticle potential and sedimentation behaviour of cement suspensions: effects of admixtures," *Advanced cement based materials,* vol. 8, pp. 17-27, 1998.

[94] N. Roussel, G. Ovarlez, S. Garrault and C. Brumaud, "The origins of thixotropy of fresh cement pastes," *Cement and Concrete Research,* vol. 42, pp. 148-157, 2012.

[95] R. Flatt, "Interparticle forces and superplasticizers in cement suspensions," Ecole Polytechnique Fédérale de Lausanne , Lausanne, 1999.

[96] R. Flatt, Superplasticizers and the rheology of concrete, from the book "Understanding the rheology of concrete" edited by N. Roussel, Woodhead Publishing Limited, 2012.

[97] J. Hot, H. Bessaies-Bey, C. Brumaud, M. Duc, C. Castella and N. Roussel, "Adsorbing polymers and viscosity of cement pastes," *Cement and Concrete Research,* vol. 63, pp. 12-19, 2014.

[98] C. Zhang, X. Kong, J, Yin and X. Fu, "Rheology of fresh cement pastes containing polymer nanoparticles," *Cement and Concrete Research,* vol. 144, no. 106419, 2021.

[99] M. Criado, A. Palomo, A. Fernandez-Jimenez and P. F. G. Banfill, "Alkali activated fly ash: effect of admixtures on paste rheology," *Rheologica acta,* vol. 48, no. 4, pp. 447-455, 2009.

[100] M. Palacios and P. Fuertas, "Effect of superplasticizer and shrinkage-reducing admixtures on alkali-activated slag pastes and mortars," *Cement and Concrete Research ,* vol. 35, p. 1358– 1367, 2005.

[101] F. Puertas, A. Palomo, A. Fernandez-Jimenez, J. D. Izquierdo and M. L. Granizo, "Effect of superplasticisers on the behaviour and properties of alkaline cements," *Advances in Cement Research,* vol. 15, no. 1, pp. 23-28, 2003.

[102] T. Bakharev, J. G. Sanjayan and Y. B. Cheng, "Effect of admixtures on properties of alkali-activated slag concrete," *Cement and Concrete Research,* vol. 30, pp. 1367-1374, 2000.

[103] M. Palacios and F. Puertas, "Stability of superplasticizer and shrinkage-reducing admixtures in high basic media," *Materiales De Construcción,* vol. 54, no. 276, pp. 65-86, 2004.

[104] C. Dupuy, J. Havette, A. Gharzouni, N. Texier-Mandoki, X. Bourbon and S. Rossignol, "Metakaolin-based geopolymer: Formation of new phases influencing the setting time with the use of additives," *Construction and Building Materials,* vol. 200, pp. 272-281, 2019.

[105] C. Dupuy, A. Gharzouni, I. Sobrados, N. Texier-Mandoki, X. Bourbon and S. Rossignol, "29Si, 27Al, 31P and 11B magic angle spinning nuclear magnetic resonance study of the structural evolutions induced by the use of phosphor- and boron–based additives in geopolymer mixtures," *Journal of Non-Crystalline Solids,* vol. 521, no. 119541, 2019.

[106] A. Antoni, S. W. Wijaya, J. Satria, A. Sugiarto and D. Hardjito, "The Use of Borax in Deterring Flash Setting of High Calcium Fly Ash Based Geopolymer," *Materials Science Forum,* vol. 857, pp. 416-420, 2016.

[107] A. Antoni, A. A. T. Purwantoro, W. S. P. D. Suyanto and D. Hardjito, "Fresh and Hardened Properties of High Calcium Fly Ash-Based Geopolymer Matrix with High Dosage of Borax," Iranian Journal of Science and Technology, 2019.

[108] A. Bagheri, A. Nazari, J. G. Sanjayan and P. Rajeev, "Alkali activated materials vs geopolymers: Role of boron as an eco-friendly replacement," *Construction and Building Materials,* vol. 146, p. 297–302, 2017.

[109] H. Liu, J. G. Sanjayan and Y. Bu, "The application of sodium hydroxide and anhydrous borax as composite activator of class F fly ash for extending setting time," *Fuel,* vol. 206, pp. 534-540, 2017.

[110] A. Nazari, A. Maghsoudpour and J. G. Sanjayan, "Characteristics of boroaluminosilicate geopolymers," *Construction and Building Materials,* vol. 70, pp. 262-268, 2014.

[111] X. Chateau, Particle packing and the rheology of concrete from the book "Understanding the rheology of concrete" Edited by N.Roussel, Woodhead Publishing Limited, 2012.

[112] H. Hafid, G. Ovarlez, F. Tousaint, P. H. Jezequel and N. Roussel, "Effect of particle morphological parameters on sand grains packing properties and rheology of model mortars," *Cement and Concrete Research,* vol. 80, pp. 44-51, 2016.

[113] P. Chindaprasirt, C. Chareerat, S. Hatanaka and T. Cao, "High-Strength Geopolymer Using Fine High-Calcium Fly Ash," *Journal of Materials in Civil Engineering,* vol. 23, no. 3, pp. 264-270, 2011.

[114] F. Cassagnabère, P. Diederich, M. Mouret, G. Escadeillas and M. Lachemi, "Impact of metakaolin characteristics on the rheological properties of mortar in the fresh state," *Cement and Concrete Composites,* vol. 37, pp. 95-107, 2013.

[115] V. Wong, K. W. Chan and A. K. H. Kwan, "Applying Theories of Particle Packing and Rheology to Concrete for Sustainable Development," *Organization Technology and Management in Construction. An International Journal,* vol. 5, no. 2, pp. 844-851, 2013.

[116] S. A. A. M. Fennis, "Design of Ecological Concrete by Particle Packing Optimization," Delft University of Technology, Delft, Netherlands, 2011.

[117] F. d. Larrard, Concrete Mixture Proportioning, London and New York: E & FN Spon, 1999.

[118] A. K. H. Kwan, K. W. Chan and V. Wong, "A 3-parameter particle packing model incorporating the wedging effect," *Powder Technology,* vol. 237, pp. 172-179, 2013.

[119] G. Roquier, "The 4-parameter Compressible Packing Model (CPM) including a critical cavity size ratio," in *EPJ Web of Conferences, Powders and Grains*, 2017.

[120] J. Juhart, G. A. David, M. R. M. Saade, C. Baldermann, A. Passer and F. Mittermayr, "Functional and environmental performance optimization of Portland cement-based materials by combined mineral filler," *Cement and Concrete Research,* vol. 122, pp. 157-178, 2019.

Chapter 2: Introduction to mineral powder materials and the characterization of physical properties

In this chapter, we will present mainly characterization of density, maximum packing fraction, and particle size distribution of studied materials. First, we will introduce the identification of relevant powder materials to be studied and then we will present materials used in this thesis. Afterwards, we will introduce selected and developed measurement protocols for determination of density, maximum packing fraction and particle size distribution with the obtained characteristic properties of materials.

2.1. Choice of Materials

In the previous chapter, we mentioned that geopolymers could be produced from variety of raw materials, whereas slag, fly ash, and metakaolin are common raw materials for their production [1, 2]. When slag is used for geopolymer synthesis, a geopolymeric structure including mainly Al^{3+}, Si^{4+}, Ca^{2+}, and Mg^{2+} cations forms, while depending on the concentration of alkaline activator, this structure could also contain CSH products [1, 3]. This means, in order to control rheological behavior of a geopolymer suspension based on slag, colloidal and hydrodynamic interactions must be taken into account with the contribution of CSH products, which corresponds to a complex process. Moreover, slag composition varies depending on the furnace or ore from where it is obtained. This could induce formation of specific products during geopolymerisation. Hence, certain types of specific gel networks could remain undiscovered and may influence material performance [4]. Based on the literature, synthesis of geopolymers using slag seems disadvantageous. In case of fly ash, similar disadvantages may occur. The most used fly ashes are called Class F and Class C fly ashes. In comparison to slag, Class F fly ash has the lowest content of Ca^{2+}, while Class C fly ash stays between Class F fly ash and slag in terms of Ca^{2+} content [1]. Unlike the more homogeneous glassy phases in slag, fly ash involves different phases with interparticle and intraparticle inhomogeneity [5]. Dependence on the production sources, presence of inhomogeneity, variation of phases during geopolymerisation and involving Ca^{2+} in its composition makes also utilization of fly ash disadvantageous. Metakaolin is another common source that has a quasi amorphous matrix consisting predominantly reactive alumina and silica due to calcination of kaolinite clay at temperatures ranging from 500-800°C [1, 6]. Structure of metakaolin composes of alternating buckled silicate and aluminate layers, with the silicon in 4-coordination and the aluminum in a mixture of 4-, 5- and 6-coordination [1], which makes this structure rich in aluminum. Since the amount of available aluminum and the rate of its release throughout reaction control extensively properties of geopolymers (e.g. setting, microstructure, strength etc.) [2, 7],

utilization of metakaolin is more advantageous due to its structure rich in aluminum. Moreover, absence of Ca^{2+} cations prevents formation of CSH or $Ca(OH)_2$ during geopolymerisation, which engenders a simple system for analysis of reaction kinetics and for controlling the rheological behavior of geopolymers. Consequently, we selected metakaolin as a precursor to produce geopolymers.

We recall that second step of particle packing optimization leading to decrease viscosity of geopolymers is improving the mix design of formulation components. For cementitious materials based on ordinary Portland cement, substitution of a part of clinker with alternative mineral additives (e.g. limestone, fly ash etc.) has been widely studied and has become a very common method to improve mix design, thus viscosity and mechanical strength [8, 9, 10, 11]. Similarly, for metakaolin-based geopolymers, several researchers studied the effect of metakaolin substitution by fly ash [12, 13, 14], slag [15], limestone [16] or rice husk ash [17] and reported the improvement of workability, compressive strength, thermal performance and microstructure. Since it is beneficial to decrease viscosity, we decided to optimize particle packing by developing different two-part blends (i.e. binary powder mixtures) as a powder precursor of geopolymers. When reactive materials such as fly ash or slag are used for substitution, they could participate to chemical reaction and affect the reaction mechanism, thus final reaction products. As we aim to decrease viscosity of geopolymers while maintaining a chemical stability, substitution of metakaolin by reactive materials is not suitable. In case when limestone is used for substitution of metakaolin, some of the studies in literature mentioned that limestone acts as filler [16, 18], while others observed carboaluminate phases due to its participation to geopolymerisation [19, 20, 21]. Although different observations have been reported about limestone reactivity in an alkaline medium, its use contributes to increase of fluidity and mechanical strength. Hence, it could be suitable for packing optimization. In addition to limestone, quartz could be an alternative inert material for metakaolin substitution. In general, its presence in a geopolymer medium does not influence visibly the reaction mechanism of geopolymerisation and provides supplementary nucleation sites for reaction products, which then leads to improvement of mechanical strength [22, 23, 24]. In this case, substitution a part of metakaolin by quartz could be suitable for packing optimization as well. Consequently, we decided to use limestone and quartz with metakaolin in order to develop two-part blends of solid precursors of geopolymers. We will introduce the details about packing optimization and the development of two-part blends in Chapter 3. Here, we will introduce only physical properties of materials.

Furthermore, we recall that alkali hydroxides (e.g. NaOH) or alkaline silicate solutions (i.e. $Na_2O.SiO_2.H_2O$) are generally used as activators. In this thesis, we used waterglass alkaline solution to produce geopolymers. We introduce all powder and liquid materials in following section.

2.2. Materials

In this section, we present selected powder materials and alkaline solution. First, we introduce metakaolin powders that are used primarily as solid precursors. Second, we present limestone and quartz powders that are used for the development of particle packing optimization of

geopolymers. At last, we present commercial sodium silicate solution that is used to produce waterglass alkaline activator. In addition to information given in following sections, technical safety data sheets of materials are also given in Appendix A, while some of the materials cannot be presented due to confidentiality restrictions. These materials will be communicated in corresponding sections.

2.2.1. Metakaolin powders

We used four commercial, two laboratory-based metakaolin powders that are presented in Table 2.1. In addition to these powders, we also grinded commercial metakaolin Argical 1200S along different durations and we used each of these metakaolins for the study. We performed grinding using an industrial ball mill instrument (i.e. Faure Equipment SA, France). The principle of ball milling is the grinding powder particles between various balls having different sizes during a rotation at a given speed. Ball mill instrument used for grinding in this study is equipped with around 250 balls, where their diameters vary between 1 cm and 3 cm and it rotates at a speed of 39 revolutions per minute. In order to obtain grinded metakaolins, each time we introduced 5 kg of Argical 1200S and the instrument grinded powder samples during 3, 6 or 15 hours.

Table 2.1: Studied metakaolin powders

Argical 1200S	Imerys Refractory Minerals, France (commercial)
Argical 1000	Imerys Refractory Minerals, France (commercial)
Metamax	BASF, USA (commercial)
Metastar	Imerys, USA (commercial)
Metakaolin D1	The Institute of Research for Ceramics (IRCER), University of Limoges (laboratory-produced)
Metakaolin D2	The Institute of Research for Ceramics (IRCER), University of Limoges (laboratory-produced)

We presented technical safety data sheets of Argical 1200S and Argical 1000 in Appendix A, while data of Metamax, Metastar, Metakaolin D1 and Metakaolin D2 cannot be presented due to confidentiality restrictions.

2.2.2. Limestone and Quartz powders

Commercial limestone and quartz powders used in this study are presented in Table 2.2.

Table 2.2: Studied limestone and quartz powders

Durcal 5	Omya, France
Durcal 65	Omya, France
Quartz C800	Sibelco, France

We presented technical safety data sheets of Durcal 5, Durcal 65 and Quartz C800 powders in Appendix A.

2.2.3. Activation solution: sodium silicate (Na_2SiO_3)

In order to prepare sodium silicate solution that is used to produce geopolymers, we mixed commercial sodium silicate solution together with the commercial granulated sodium hydroxide (NaOH) pellets supplied from VWR, France. Purity of sodium hydroxide is 99%. Table 2.3 presents molar ratios of commercial sodium silicate solution.

Table 2.3: Molar ratios of commercial sodium silicate solution

	SiO_2	**Na_2O**	**H_2O**
Sodium silicate solution (VWR, France)	25.9	7.9	66.2

We mixed sodium hydroxide pellets and sodium silicate solution using magnetic stirrer during 1 day. Concentration of sodium hydroxide in final sodium silicate solution (i.e. also called waterglass) is 9,8% wt. The heat of waterglass solution increases rapidly after the initial contact between commercial sodium silicate and NaOH pellets. Hence, it needs to cool down before being used in a geopolymer suspension. Therefore, we use this final waterglass solution a day after its production in order to be sure that its temperature becomes equivalent to a room temperature.

2.3. Measurement of material density

2.3.1. Measurement protocol of density of powder materials

We use a gas pycnometer Micromeritics AccuPyc II 1345 to determine density of powder materials. Before starting each measurement, we place 4 grams of powder in a cell having 10 cm^3 volume and we put this cell into a sample chamber. Afterwards, instrument injects inert Helium gas inside this chamber, where Helium gas flows along the sample and fills its porosity until it reaches the target pressure of 1.5 bars. Once system becomes stable inside chamber, instrument discharges Helium gas toward an expansion chamber, while it pursues pressures to compute volume of sample.

In order to compute solid phase volume, instrument records pressure values of filling the sample chamber (P_1) and the expansion chamber (P_2), then uses them to compute solid volume by following the equation below:

$$V_{sample} = V_{sample\ cell} - \frac{V_{expansion\ chamber}}{\frac{P_1}{P_2} - 1} \quad (2.1)\ [25]$$

Where V_{sample} is volume of powder, $V_{sample\ cell}$ is volume of sample cell (V_{cell} = 10 cm^3) and $V_{expansion\ chamber}$ is volume of expansion chamber. As the mass introduced to instrument is known (i.e. M_{sample} = 4 g), density of powder can be obtained by dividing its mass to volume computed by gas pycnometer as below:

$$\rho_{sample} = \frac{M_{sample}}{V_{sample}} \quad (2.2)$$

Where ρ_{sample} is density of powder. Table 2.4 presents obtained density values of studied powder materials.

Table 2.4: Density values of powder materials

Powder	Density (g/cm^3)
Argical 1200S	2.55
Argical 1000	2.64
Metamax	2.7
Metastar	2.64
Metakaolin D	2.55
Durcal 5	2.74
Durcal 65	2.74
Quartz C800	2.6

2.3.2. Measurement protocol of density of liquid materials

We measured density values of liquid materials using 10 ml glass flask (i.e. also called water pycnometer) supplied from VWR, France. In order to measure density, we follow two stages. At first stage, we weigh empty pycnometer with its cap and find its vacant mass (m_1). Afterwards, we fill it by distilled water having a density of 1 g/cm^3 and weigh again to find its filled mass (m_2). We divide the difference of both mass to density of water and find the total internal volume of pycnometer ($V_{Pycnometer}$) using the formula below.

$$V_{Pycnometer} = \frac{m_2 - m_1}{\rho_{water}} \quad (2.3)$$

At second stage, we fill again pycnometer by liquid sample and weigh its filled mass (m_3). We divide the difference of mass between empty and filled pycnometer to total volume of pycnometer by using equation below. Table 2.5 presents obtained density values of studied liquid materials.

$$\rho_{sample} = \frac{m_3 - m_1}{V_{pycnometer}} \quad (2.4)$$

Table 2.5: Density values of liquid materials

Liquid	Density (g/cm^3)
Commercial Sodium silicate	1.35
Final Sodium silicate	1.46

We presented density of powder and liquid materials used in this thesis. In the following section, we will present maximum packing fraction of powder materials.

2.4. Maximum packing fraction of powder materials

2.4.1. Essential parameters influencing maximum packing fraction

In previous chapter, we discussed briefly maximum particle packing by mentioning that size and shape of particles are main parameters influencing maximum packing of the system. For a better understanding of particle packing, let us start from the basic definitions. The packing fraction (also called packing density) of a medium is the ratio of total solid volume V_S (i.e. total volume of particles present in the medium) to total volume V_T, while porosity of this medium is ratio of the volume of voids V_V to total volume [26]. When particles are placed in a medium, depending on their size distribution (i.e. mono- or poly- dispersity), shape or the way that they are placed in this medium, packing value would be different. If we place gently mono-dispersed spherical particles in a medium while assuming their diameter size is large enough to neglect colloidal interactions, packing density of this medium would be 0.60, which corresponds to random loose packing. Now if we place the same particles in the same medium by shaking the system during a few seconds, packing density would become 0.64, which corresponds to random close (or random dense) packing. If we assume ideal conditions, where all particles are placed in this medium one by one at the right position to minimize porosity, packing would be higher than 0.64, which would correspond to ordered dense packing [26]. In case where particles placed in the medium are non-spherical, packing value would be still different depending on the shape parameters of these particles. We present some of the random close packing values of particles having different shapes in Table 2.6.

Table 2.6: Random close packing density values for particles of different shapes. L/D: size ratio, D: Diameter, L: Length [26]

Particle Shape	Random close packing
Spheres	0.60-0.64
Cubes	0.76
Parallelepiped (4 < L/D < 8)	0.51-0.67
Disks (L/D = 1)	0.63
Spheroids (0.6 < L/D < 1.3)	0.58-0.61
Rounded aggregates	0.59-0.63
Crushed aggregates	0.50-0.57
Fibers (L/D = 10)	0.48
Fibers (L/D = 167)	0.03

Philipse [27] reported that packing density of different rod/wire systems decreases drastically with increasing aspect ratios. According to simulation of a three-dimensional sediment with a random packing of wooden rods (Figure 2.1-a) and copper wires (Figure 2.1-b), author observed that rods with smaller aspect ratios (i.e. L/D < 30) flow more or less like a liquid when the vessel in which they are placed is shaken erratically. However, with an increasing aspect ratio, rods have an increasing tendency to form solid like stiff structures with shaking. Consequently, at higher aspect ratios, volume fractions decrease considerably and packing density becomes close to the random close packing of mono-dispersed spherical particles when aspect ratio is equal to 1 (Figure 2.1-c).

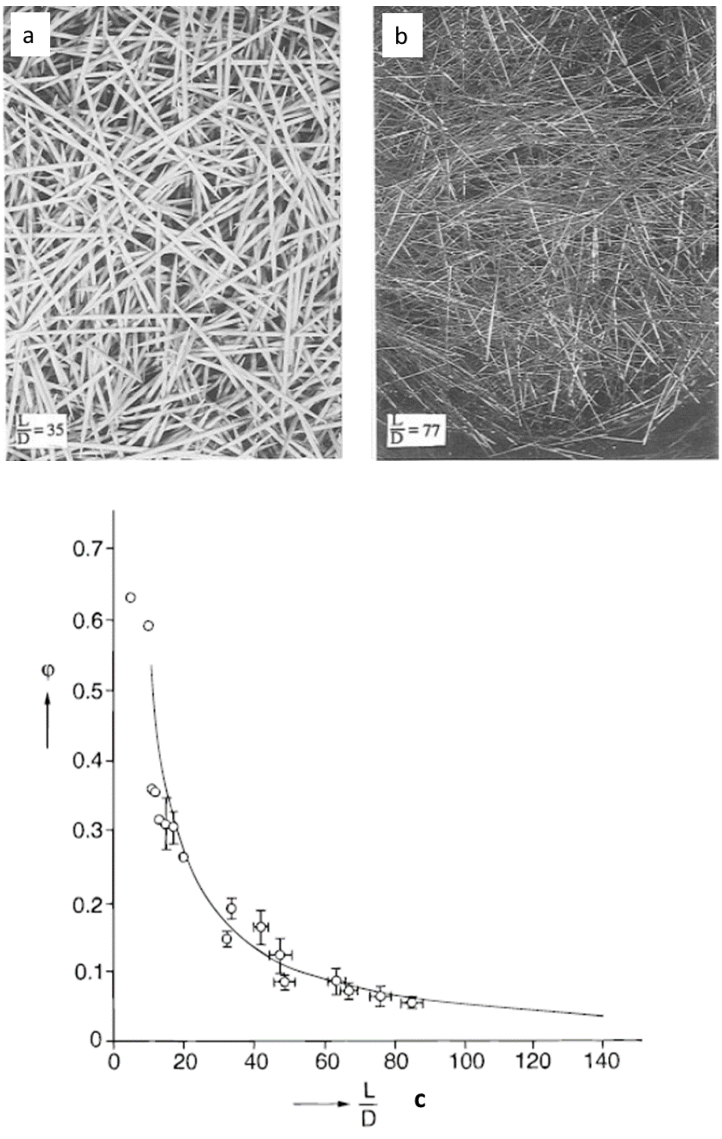

Figure 2.1: Simulation of with a random packing of wooden rods (a) and copper wires (b) and evolution of packing density as a function of aspect ratio (c) [27]

Moreover, it must be recognized that considering only simple shape parameters such as size ratio cannot be enough to involve all the effects playing role in particle packing density [26]. In practice, two or more than two part blends could exist as binders of cementitious materials. In this case, geometrical interactions between particles belonging to different size classes

could exist and affect the resulting packing value. Hence, their impact on packing density is non-negligible. The origin of these interactions dates back to Appolonian packing that is based on packing of spherical particles and developed by Apollonius of Perga (i.e. Ancient Greek geometer and astronomer). According to Appolonian packing, each void in a packing of spheres is filled with a sphere having the exact volume of the void so that it could touch all the neighboring particles (Figure 2.2) [26]. In order fill all the voids, where packing density tends towards one, the size of the inserted particles must become smaller and smaller while the number of added particles must increase continuously [26].

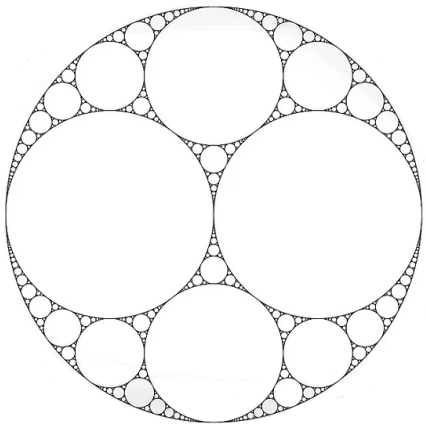

Figure 2.2: Diagram of Appolonian packing [28]

However, in real life, it is not possible to choose ideal particles one by one as in case of Appolonian packing. In general, either morphological properties of particles are given or must be chosen from a limited set of values due to practical constraints such as price, allowance etc. [26]. Therefore, several packing models have been developed to enhance packing density of systems in which different particle size classes, shapes or geometrical interactions could exist. We will give further information about different packing models in Chapter 3. Here, we will introduce mainly determination methods of maximum packing density.

2.4.2. Methods of determination of maximum packing density

Maximum packing density can be measured by several methods such as pressure filtration, centrifugation or water demand, where basic principle is generally filling the porosity of particles by water [8, 29]. Pressure filtration method consists of filtering the excess water of a suspension by applying a constant pressure using a filter press [8]. Filter must have smaller sizes than particles in suspension so that it can retain particles while draining excess water. At the end of a pressure filtration cycle, the entire consolidated body is subjected to a uniform uniaxial compressive stress that could be used to predict uniform volume fraction [30]. Moreover, in case of cementitious suspensions in which attractive interactions dominate the colloidal interactions, superplasticizers must be added to deflocculate the suspension. In this case, a size separation occurs and affects the measurement. Centrifugation method (i.e. also called centrifugal consolidation) comprise of consolidating powder suspension by centrifugation in order to remove excess water in suspension [8]. This method allows to

control the protocol of preparation of suspension and it is independent from the operator performing measurement. However, in presence of superplasticizers, homogenization of suspension is required to avoid separation of particles according to their sizes and densities during measurement [8]. Water demand method focuses on finding the minimum water dosage that produces a paste of studied powder [29, 31] (Figure 2.3). Here, determination of paste transition is repeatable and depends on the operator performing measurement. Water demand is a quick method with a simple application procedure. It supplies repeatable results, thus can be assumed as reliable. Therefore, we will use water demand method for measurement of maximum particle packing density of powder materials. We introduce measurement protocol of this method in following section.

2.4.3. Measurement protocol of maximum particle packing density

In order to define maximum particle packing density of powder materials by water demand method, we apply following measurement protocol:

- We start by mixing 350 g of metakaolin, limestone or quartz powder (i.e. powder mass M_p = 350 g) with a small amount of tap water by means of a mortar mixer in compliance with the norm NF EN 196-1. Mixer has low and high speed stages. Measuring starts with low speed.

Here, we remark that when some of the cementitious powders (i.e. particularly limestone in this study) are present in water, colloidal interactions could occur, which could then induce flocculation of particles, thus packing density. Ahmadah [8] studied the effect of particle flocculation on different cementitious powders including limestone and observed that the use of superplasticizers with concentrations between 1% and 2% of total mass of powder leads to avoid particle flocculation and improves the increase of maximum packing density. Hence, in order to suppress potential colloidal interactions during the measurement of limestone powder, we added a superplasticizer Tempo 12 (Sika, France) with a concentration of 1% of total initial mass into the initial amount of water.

- While mixing continues, we increase gradually quantity of water until particles of metakaolin, limestone or quartz powders create groups of pellets. Appearance of pellets means that powder becomes humid. At this moment, we rise mixing speed and continue to add water gradually (Figure 2.3, number 2).

- At a certain moment, only a small droplet of water is enough to cover total porosity. The minimum amount of water covering porosity transforms humid powder to a paste (Figure 2.3, number 3), which means the achievement of maximum packing density. When this transformation occurs, we calculate maximum packing fraction (ϕ_{max}) using the equation below:

$$\phi_{max} = \frac{1000}{1000+\rho_p \frac{M_w}{M_p}} \quad (2.5)\ [31]$$

Where ρ_p is the density of metakaolin, limestone or quartz powder, M_w is the mass of total water quantity that is added during measurements to cover the porosity and M_p is the total mass of metakaolin, limestone or quartz powder.

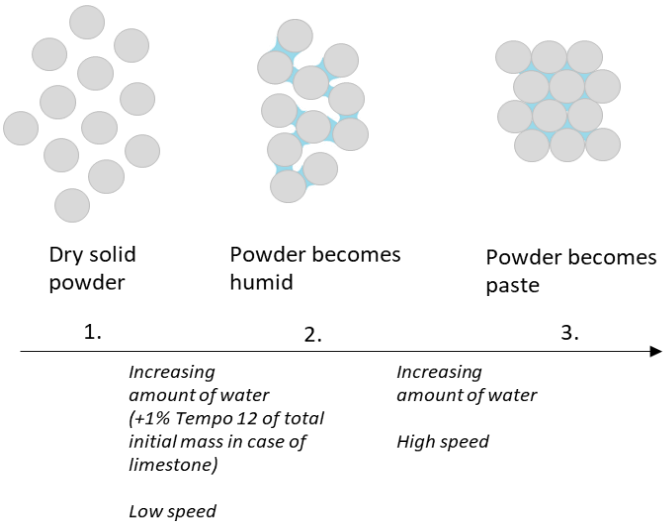

Figure 2.3: Diagram of Water Demand Method

2.4.4. Maximum packing densities of powder materials

We observed that maximum packing fractions of commercial metakaolin powders Argical 1200S, Metastar and Metamax are around 30%, while commercial metakaolin Argical 1000 and laboratory-based Metakaolin D1 and Metakaolin D2 have maximum packing values around 40%. Moreover, grinding of Argical 1200S improves its packing density. We obtained increasing packing density of Argical 1200S from 30% toward 40% with increasing grinding duration. Maximum packing of Quartz C800 powder is around 47%, while Limestone powders Durcal 5 and Durcal 65 have packing fractions around 66%. We present maximum packing density of each powder in Figure 2.4, while the exact numerical values are given in Table 2.7.

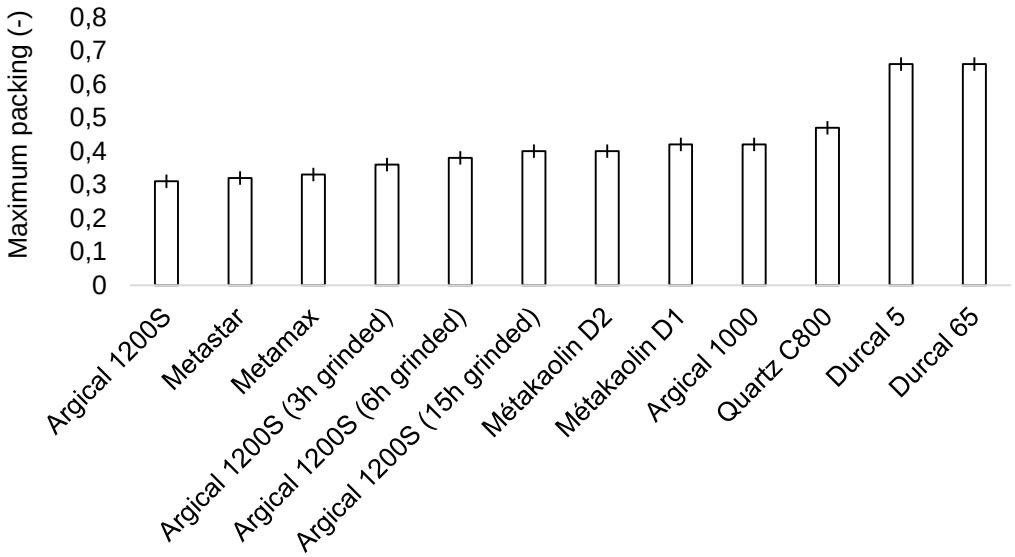

Figure 2.4: Maximum packing fractions of powders

Table 2.7: Maximum packing densities of studied powders

Powder	Maximum packing fraction (%)
Argical 1200S	0.31 ± 0.016
Metastar	0.32 ± 0.005
Metamax	0.33 ± 0.005
Argical 1200S (3h grinded)	0.36 ± 0.016
Argical 1200S (6h grinded)	0.38 ± 0.016
Argical 1200S (15h grinded)	0.40 ± 0.016
Metakaolin D2	0.40 ± 0.010
Metakaolin D1	0.42 ± 0.010
Argical 1000	0.42 ± 0.007
Quartz	0.47 ± 0.010
Durcal 5	0.66 ± 0.013
Durcal 65	0.66 ± 0.002

We presented in detail the effect of size and shape of particles and the method of packing on the maximum packing fraction. We introduced briefly different measurement methods to obtain maximum packing density and we showed the maximum packing values of powder materials obtained by Water Demand method. In the following section, we will present measurement of particle size distribution.

2.5. Measurement of particle size distribution

In this thesis, description of "particle" is limited in the range of solid (e.g. powders) or liquid (e.g. suspensions) particles or gas bubbles (e.g. aerosols), which have variations of sizes from nanometer to micrometer [32]. Particles are three-dimensional (3D) objects. It is not possible to measure size of a particle without considering its 3D characteristics. In reality, size cannot be totally described by a unique number, except the case where particle is ideally spherical [32, 33, 34]. For irregular shaped particles (e.g. plate-like), description of size with two or more dimensions could make measurement procedure complicated. In order to simplify measurement procedure, size of an irregular-shaped particle is defined by an equivalent spherical diameter, where it is assumed that sphere has the same property (e.g. volume) as the actual particle [32, 33, 35]. Theoretical approach is explained rigorously in [35] as well as the equations developed for equivalent spherical diameter (ESD) model and its details are out of context of this thesis. Several measurement techniques use different equivalent sphere model (Figure 2.5). This means, results obtained from different measurement method would not necessarily give the same particle size value [32, 33, 34].

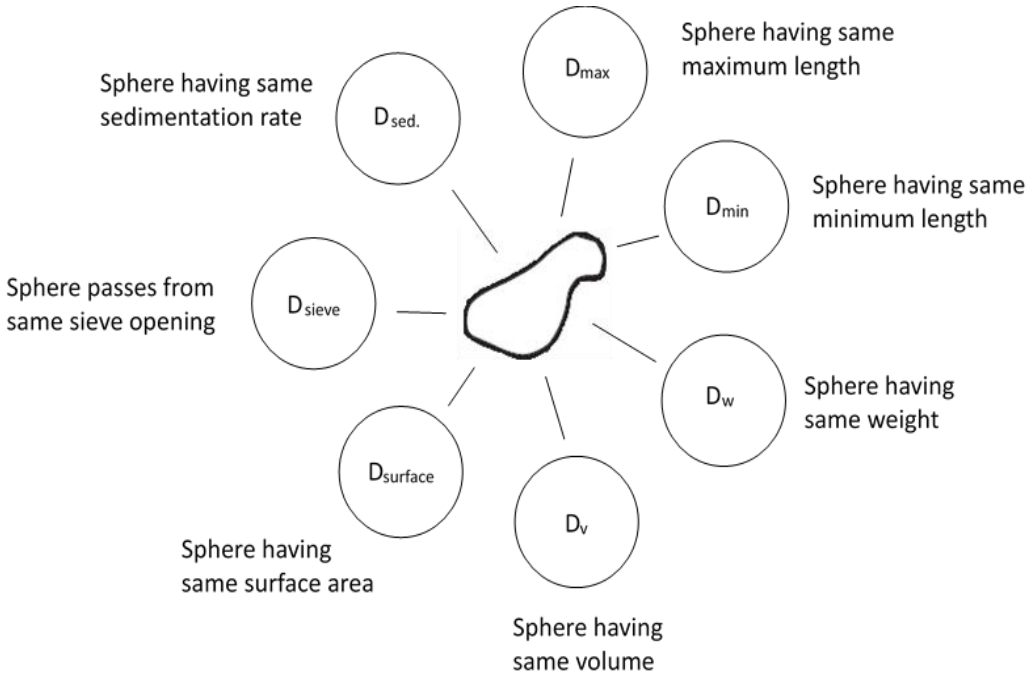

Figure 2.5: Variation of equivalent spherical diameter

We recall that in most of the cases, industrial materials comprise of poly-dispersed particles. Poly-dispersed materials have actually a statistical distribution of varied particle sizes [32]. Particle size distribution (PSD) can be measured by various methods based on different physical principles (e.g. sedimentation, sieving, particle counting, light scattering etc.) [36]. Available amount of sample, cost of measurement instrument, degree of automation or operator skill are some of the parameters affecting choice of method [36]. Ferraris [37] referred that measurement procedure on laser granulometer is the most common method among several laboratories. It is fast, which leads to a rapid analysis of data. It provides reproducible, wide range of size distribution from hundreds of nanometers to several millimeters [32]. Therefore, we use method of laser diffraction granulometry in order to study particle size distribution of powder materials in this thesis.

2.5.1. Introduction to laser light diffraction

Fundamental principle of laser light diffraction is observing the interaction of light while light passes through a particle [38]. When light meets particle, it could be reflected, adsorbed, refracted, diffracted or these incidents could happen at the same time (Figure 2.6). All phenomena, which happen on illuminated particle, are called light scattering [39]. Light scattering pattern (i.e. spatial distribution of scattered light) depends on the ratios of particle diameter (D) and the wavelength (λ) of incident light [39].

Laser light diffraction method assumes volume equivalent sphere model. Fraunhofer, Mie or Rayleigh scattering models could be used to obtain particle size distribution from light scattering pattern. Fraunhofer model is used when $D >> \lambda$. Rayleigh model is used when $D << \lambda$. Mie scattering model is used when D/λ ratio is around one [36, 39].

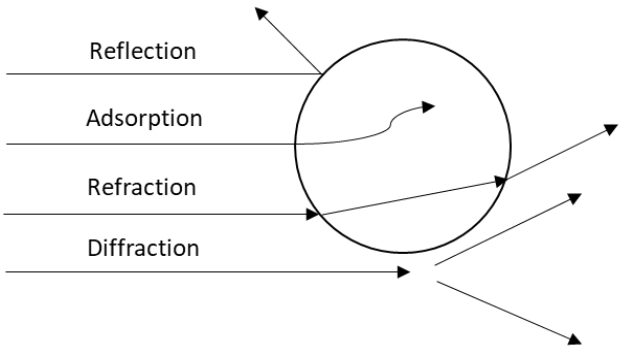

Figure 2.6: Light scattering phenomena

Laser granulometer instruments use vigorously Mie scattering model. This model works with a refractive index consisting of a complex number (Equation 2.6) since it solves problems of light scattering (e.g. emission of light in all directions).

$$n = A + iB \quad (2.6)\ [40]$$

Where n is the complex number, A and B are real and the imaginary parts of refractive index respectively. Modern instruments propose upgraded database where refractive index of several fluids as well as powders can be chosen directly for PSD measurement.

2.5.2. Parameters influencing measurement of particle size distribution by laser diffraction granulometry

2.5.2.1. Sampling

The purpose of sampling is to compile a small amount of powder from bulk quantity where it represents best the physical and chemical properties of entire quantity of powder. Incorrect of non-representative sampling could result in poor characterization, system or process failure, customer dissatisfaction etc. [36]. However, sampling is not as simple as it is supposed to be. Actually, a pile of powder material cannot be perfectly homogeneous, which makes selection of small powder amount from a heterogeneous pile a random process. Therefore, any sampling procedure from a heterogeneous pile would create different sampling errors [41, 42, 43]. Only Fundamental Sampling Error (FSE) is defined as predictable among others. FSE is inversely proportional to the required mass of sample so that it decreases by increased powder mass. Variance associated with FSE or convenient sample mass can be calculated by using the equation below.

$$\sigma_{FSE}^2 = \frac{Kd^3}{M_s} \quad (2.7)\ [41, 42, 43]$$

Where σ_{FSE}^2 is the variance associated with FSE, K is a constant which represents characteristic properties of material, d is the maximum particle size and M_s is the required sample mass. Since characteristic properties of material play role, appropriate mass could change according to material used. Some sampling methods (e.g. large container sampling, bag sampling) are

detailed in [36]. In this thesis, we first mix each powder material before sampling and then we take small amount of this powder from the middle using a spoon.

2.5.2.2. Obscuration

Obscuration is the measurement of percentage of emitted laser light, which is lost by scattering or adsorption during size measurement process [44]. Particle concentration in sample cell should be sufficiently high to reach an acceptable signal-to-noise ratio but still sufficiently low to avoid multiple scattering.

2.5.2.3. Dispersion

Powders may segregate or aggregate in case of wide size distribution depending on the surface characteristics of particles. Therefore, ensuring a good dispersion, where individual particles are separated spatially, is necessary in order to acquire reliable and reproducible size analysis. Laser diffraction granulometer proposes two methods: dry and wet dispersion. In dry dispersion, a flow of gas (e.g. dry air) disperses particles and delivers them to the detection zone. In wet dispersion, particles suspend in a liquid solvent (i.e. also called dispersant), where solvent should not dissolve particles and should favor stable dispersion. Its refractive index should also be different from the refractive index of particles [44]. Wet dispersion is more favorable since it is possible to vary type of solvent, modify solution conditions by controlling pH, introduce chemical agents or break agglomerated particles by using ultrason or agitation [36, 45]. Moreover, ultrason is the most frequent tool for dispersion of particles, where mainly duration or power of ultrason device plays role on dispersion [46]. Suitable ultrason duration or energy for powder dispersion can be determined from the moment, where particle size of material becomes stable. However, particles can re-agglomerate after dispersion. To ensure long-standing dispersion, addition of chemical additives could be useful [47]. Several studies mentioned the improvement of particle dispersion in presence of additives having different interaction mechanisms (e.g. steric repulsion) [8, 39, 47, 48] but care must be taken about the quantity introduced to solvent. Over addition may lead to appearance of side effects such as bubbles.

2.5.2.4. Optical indexes

Optical indexes are both real and imaginary parts of refractive index (i.e. introduced in section 2.5.1). Real part (A) of several materials can be found from different database as well as the studies propose applicable values [40, 47]. Imaginary part (B) is related to absorption coefficient (i.e. fraction of light absorbed per unit thickness of the material that it passes through) of material itself. Non-absorbing particles (i.e. transparent) such as water have coefficient of absorption (B) that is zero [45], while value increases with particles become darker.

2.5.2.5. Particle shape

Particle shape can also have impact on particle flow, especially during dispersion. Irregular-shaped anisotropic particles could have different orientations. Literature mentions that

under/over estimations of PSD are observed for anisotropic particles [47, 49, 50]. Therefore, shape must also be considered for particle size measurement.

2.5.3. Measurement instrument of laser diffraction granulometry: Malvern Mastersizer 3000

A standard laser diffraction instrument has four main components: a laser source, a cell for sample, optical equipment (mainly optical bench, high and low angle detectors) and a computer system in order to analyze the data and find PSD of sample. Laser source is generally chosen as Helium-Neon in the region of 632 nm wavelength. Sample dispersion units are designed to make measurements of samples that are either wet or dry. They are also equipped with agitators to assure dispersion of sample, thus avoiding possible agglomerations during measurement. Optical equipment process incident light after it interacts with sample. High and low angle detectors convert scattered light intensity into electrical signals. Computer system, having a special software, processes these signals and gives particle size distribution of sample. In this study, we used Malvern Mastersizer 3000 Laser Granulometer that can measure particle size range from 100 nm to 1 mm. Instrument is equipped with red right He-Ne laser source having 632.8 nm wavelength. We used Hydro SV cell having volume range between 5.6 ml and 7 ml to disperse sample, where this cell applies wet dispersion. A software controlled magnetic stirrer disperses sample in liquid at 1200 rpm during measurements.

2.5.4. Determination of measurement protocols for particle size distribution of powders

As mentioned, characterization of industrial materials could be complicated due to their polydispersity, heterogeneity etc. Hence, choice of measurement parameters before determination of final protocol is an important issue. The most important parameters are sampling, dispersion method and choice of optical index. Sampling affects also obscuration and it relates to dispersion method. In this section, we will introduce steps followed to define measurement protocols for particle size distribution of powder materials studied in this thesis.

2.5.4.1. Measurement protocols of limestone and quartz powders

The most commonly used solvent is deionized water for insoluble materials [51]. Nevertheless, it is not coherent for every powder due to poor wetting or dissolution of particles. Moreover, we recall that particularly in presence of limestone particles in water, potential colloidal interactions could provoke flocculation of particles. In order to prevent flocculation, organic liquids (e.g. alcohols) could be used as solvent for measurement of particle size dispersion of limestone powder. In addition to limestone, quartz could also be dispersed in organic solvents. Ahmadah [8] studied dispersion of different cementitious powders (e.g. cement, quartz, limestone etc.) in isopropyl alcohol (i.e. also called isopropanol) and observed that dispersion of a powder quantity between 1 mg and 20 mg represents well size distributions of these powders. Based on the literature, we decided to use isopropanol as a solvent and we defined a powder quantity of 5 mg for dispersion of both limestone and quartz powders. In order to avoid elevated concentrations, some of the studies propose

obscuration intervals between 11% and 13% [8], while others mention that interval can enlarge up to 20% for polydispersed materials [48]. We chose an obscuration level of 14% for our measurements. We recall that using an ultrason instrument is the most frequent method to ensure separation of particles during dispersion. Therefore, we used ultrason as a dispersion method. Optimum ultrason duration can change from 1 minute [46] to 20 minutes [8, 47, 52, 53]. We chose a duration of 15 minutes for dispersion of limestone and quartz powders since it is sufficient for the majority of cementitious materials [8, 47]. We define optical indexes of materials using a calibration method proposed by laser granulometer. Instrument supplies a calculation of the difference between measured and theoretical intensities. An optical index value, which supplies the least difference, can be chosen for corresponding material. Refractive index values that we defined for isopropanol solution, limestone and quartz powders are presented in Table 2.8 with the values proposed in literature.

Table 2.8: Refractive indexes used in thesis and in literature for isopropanol, limestone and quartz powders

	Isopropanol	**Durcal 5**	**Durcal 65**	**Quartz C800**
Real part (A)	1.38 1.39-1.40 [47] 1.377-1.378 [40]	1.65 1.596 [47] 1.68 [40]	1.65 1.596 [47] 1.68 [40]	1.543 1.529 [47] 1.543 [8]
Imaginary part (B)	0 (transparent)	0.001 0.001 [8] 0.001 [47]	0.001 0.001 [8] 0.001 [47]	0.01 0.01 [8] 0.001 [47]

Consequently, the measurement protocol of particle size distribution for limestone and quartz powders is as follow:

- We disperse 5 mg of limestone or quartz powder in 10 ml isopropanol using ultrason Branson 200 (VWR, France) during 15 minutes,

- We transfer 20% of suspension dropwise by a pipette to measurement cell until reaching an obscuration value 14%,

- We perform measurement. Each measurement cycle consists of 5 test and we repeat each measurement cycle 3 times.

2.5.4.2. Measurement protocol for metakaolin powders

We selected deionized water for dispersion of metakaolin powders. In literature, some of the studies mentioned that metakaolin particles tend to agglomerate when they dispersed in water [54]. In order to avoid the effect of potential particle agglomerations of metakaolin particles during measurements, we used the dispersion method of ultrason with a prolonged duration of 30 minutes. Moreover, we also tested the use of chemical additives Darvan (i.e. ammonium salt of polymethacrylic acid, in aqueous form) and Sodium Hexametaphosphate (NaHMP) (i.e. salt of composition $Na_6[(PO_3)_6]$, in crystalline form) to observe whether they

improve the dispersion of metakaolin particles in water. The principle of their deflocculation mechanism is the modification of electrical charges on the surface of metakaolin particles [55, 56]. We decided their concentrations based on the common addition amounts of chemical additives used for ordinary Portland cement [57]. In case of their presence, before dispersing metakaolin powder, first we dispersed 0.01% or 0.05% of Darvan (Vanderbilt Minerals LLC, USA) by weight of water or we dispersed 0.1% or 0.6% of NaHMP (Sigma Aldrich, France) by total weight in water. Afterwards, we added metakaolin in water that already involves Darvan or NaHMP and then we performed measurements. We defined a coherent obscuration interval between 10% and 20%. Refractive index values that we defined for deionized water and metakaolin powders are presented in Table 2.9 with proposed values in literature. In order to determine a measurement protocol that is relatively simple and applicable for all metakaolin powders, we chose commercial and 15 hours grinded Argical 1200S and performed the trials of protocol development with these metakaolin powders. In fact, we assume that a prolonged grinding duration of 15 hours could decrease particle size. By taking the size of commercial Argical 1200S as a reference and using the same protocol on both metakaolin, showing a decrease of particle size by grinding duration means the achievement of a representative measurement protocol. Before determining a definitive protocol that is valid for all metakaolin powders, we compared particle size distributions of commercial and grinded Argical 1200S obtained from the trial measurements of prolongation of ultrason duration and the use of Darvan or NaHMP at different concentrations in Figure 2.7.

Table 2.9: Refractive indexes used in thesis and in literature for deionized water and metakaolin powders

	Deionized water	**Metakaolin**
Real part (A)	1.33 1.33 [47] 1.33 [40]	1.56 1.529 [47] 1.533-1.577 [40]
Imaginary part (B)	0 (transparent)	0.1 0.01 [47]

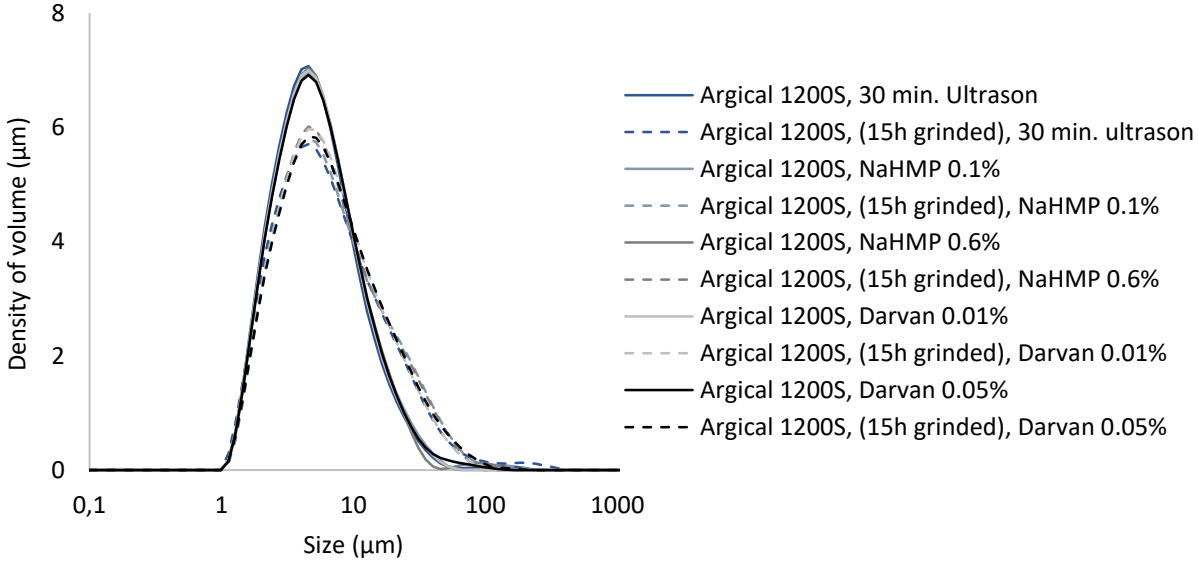

Figure 2.7: PSD of commercial (continuous lines) and 15h grinded (dashed lines) Argical 1200S obtained from different measurement protocols

Figure 2.7 presents particle size distribution as a function of volume proportions for commercial and grinded Argical 1200S. According to figure, prolonged ultrason duration or the use of chemical additives does not influence size distributions of both metakaolins since their PSD give similar results for different protocols applied. We obtained mean particle sizes around 5 µm and 6 µm for commercial and grinded metakaolin respectively. Moreover, all PSD of grinded Argical 1200S have a bulge throughout 100 µm, which is not obtained in case of commercial Argical 1200S. Since this bulge does not disappear with different dispersion methods, it seems that a morphological alteration of particles arises after prolonged grinding. Consequently, we did not observe a decrease of particle size as a function of grinding. We will discuss obtained results in following section. Since a prolonged ultrason duration or incorporation of chemical additives into water does not influence size distributions, we chose prolonged ultrason as a final dispersion method due to simplicity of its application. Hence, definitive measurement protocol that is determined for dispersion of metakaolin powders is as follow:

- We disperse 0.1 g of metakaolin powder in 10 ml deionized water using ultrason TUC (Jeken, China) during 30 minutes,

- We transfer 20% of suspension dropwise by a pipette to measurement cell until reaching an obscuration value between 10% and 20%,

- We perform measurement. Each measurement cycle consists of 5 test and we repeat each measurement cycle 3 times.

2.5.5. Results of particles size distributions of powder materials

We present particle size distributions of all studied powder materials in Figure 2.8.

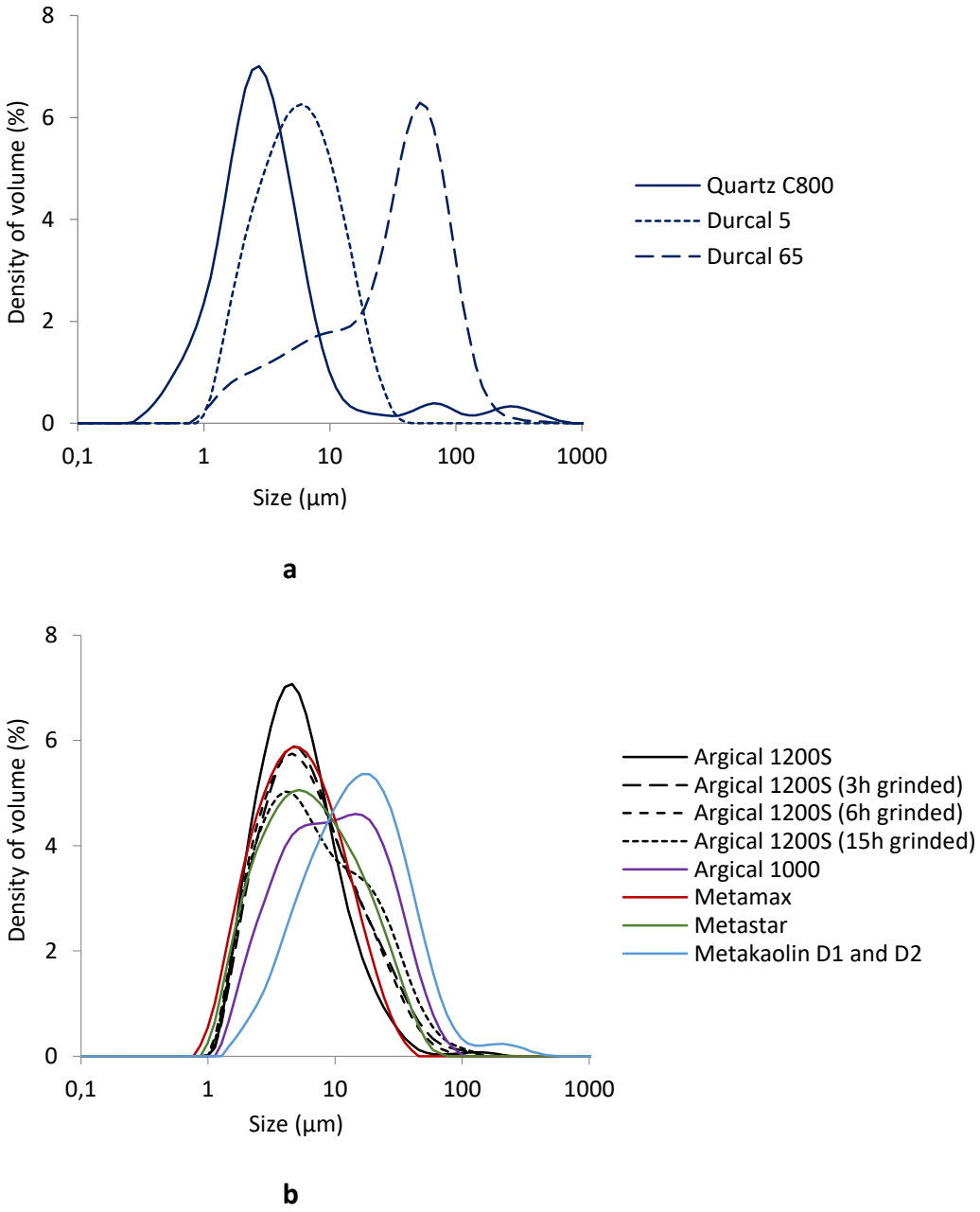

Figure 2.8: Particle size distributions of limestone (a), quartz (a) and metakaolin (b) powders

Figure 2.8 represents density of volume as a function of particle sizes of studied limestone, quartz and metakaolin powders. According to (Figure 2.8-a), Quartz C800 has smaller mean particle size (around 3 µm) than limestone powders, where we obtained mean particle sizes around 5 µm and 40 µm for Durcal 5 and Durcal 65 respectively. Moreover, mean particle sizes of commercial and grinded Argical 1200S powders are around 5 µm and 6 µm respectively. Particle size distributions of 3, 6 and 15 hours grinded Argical 1200S have bulge throughout 100 µm as observed previously, while PSD of commercial Argical 1200S does not present this bulge (Figure 2.8-b). PSD of 3 and 6 hours grinded Argical 1200S fit into one another, while PSD of 15 grinded Argical 1200S is smoothly different with increased bulge size, indicating growing particle size. As we mentioned, this suggests that prolonged grinding duration may alter morphological properties of particles. In fact, increasing grinding duration could supply

the energy that is necessary to collapse particles and result in irreversible sintering. In case of sintering, laser granulometer cannot distinguish between a single large particle and a group of sintered particles. Hence, appearance of bulge indicating increasing particle size may represent not only single particles but also groups of sintered particles formed after 15 hours grinding. As sintering is irreversible, any method would not work for particle dispersion. This could explain why PSD of grinded metakaolin powders are stable and do not change depending on the dispersion method. Therefore, we assume that particles of Argical 1200S are sintered during grinding and increasing grinding duration makes the effect of sintering more visible. Furthermore, commercial Metamax, Metastar and Argical 1000 powders have mean particle sizes around 5.5 µm, 6.5 µm and 10 µm respectively, while laboratory-based Metakaolin D1 and Metakaolin D2 have mean sizes around 16 µm. We presented characteristic diameters D_{10}, D_{50} and D_{90} (i.e. volume based diameters below which 10%, 50% and 90% of particles are undersized) of all studied powder materials in Table 2.10.

Table 2.10: Characteristic diameters D_{10}, D_{50} and D_{90} of studied powders

Powder	D_{10}	D_{50}	D_{90}
Quartz	1.1 ± 0.10	2.9 ± 0.10	3.6 ± 0.10
Durcal 5	2.2 ± 0.01	5.9 ± 0.07	15.5 ± 0.20
Durcal 65	4.4 ± 0.10	40.1 ± 0.10	100.6 ± 0.10
Argical 1200S	2.2 ± 0.04	5.2 ± 0.31	15.0 ± 3.00
Argical 1200S (3h grinded)	2.3 ± 0.07	6.2 ± 0.12	23.3 ± 0.16
Argical 1200S (6h grinded)	2.3 ± 0.05	6.3 ± 0.70	24.8 ± 6.62
Argical 1200S (15h grinded)	2.3 ± 0.02	6.8 ± 0.17	29.2 ± 1.00
Argical 1000	2.9 ± 0.04	10.3 ± 0.18	34.3 ± 1.20
Metamax	1.9 ± 0.04	5.4 ± 0.05	15.7 ± 0.04
Metastar	2.2 ± 0.01	6.6 ± 0.02	23.4 ± 0.38
Metakaolin D1 and D2	4.6 ± 0.04	15.8 ± 0.30	48.4 ± 1.82

2.6. Conclusion

In this chapter, we presented initially selected raw materials and then the methods used for characterization of their density, maximum packing density and particle size distributions. We determined density of powder and liquid materials using a gas pycnometer and a glass flask respectively. For measurement of maximum packing density of materials, we presented in detail essential parameters affecting packing of particles, different measurement methods to obtain maximum packing density and we showed maximum packing values of powder materials obtained by Water Demand method. We observed that studied metakaolin powders had lower packing densities than the studied quartz and limestone powders. In addition, maximum packing value of a commercial metakaolin increased with increasing grinding duration. We measured particle size distribution (PSD) of powder materials using laser diffraction granulometry. We introduced parameters influencing measurement of PSD, selected and developed measurement protocols and we showed PSD of studied powder

materials. We observed that PSD of grinded metakaolin powders exhibited a bulge that does not exist on PSD of commercial metakaolin and increasing grinding duration makes this bulge more visible. We assumed that grinding results in irreversible sintering, thus different dispersion methods could not influence PSD of grinded metakaolin.

References

[1] J. L. Provis and J. S. J. v. Deventer, Geopolymers. Structure, procesing, properties and industrial applications, CRC Press, Woodhead Publishing Limited, 2009.

[2] P. Duxson, A. Fernandez-Jimenez, J. L. Provis, G. C. Lukey, A. Palomo and J. S. J. v. Deventer, "Geopolymer technology: the current state of the art," *Journal of Materials Science,* vol. 42, p. 2917–2933, 2007.

[3] C. K. Yip, G. C. Lukey and J. S. J. v. Deventer, "The coexistence of geopolymeric gel and calcium silicate hydrate at the early stage of alkaline activation," *Cement and Concrete Research,* vol. 35, pp. 1688-1697, 2005.

[4] K. Shimoda, Y. Tobu, K. Kanehashi, T. Nemoto and K. Saito, "Total understanding of the local structures of an amorphous slag: Perspective from multi-nuclear (29Si, 27Al, 17O, 25Mg, 43Ca) solid-state NMR," *Journal of Non-Crystalline Solids,* vol. 354, p. 1036–1043, 2008.

[5] R. T. Hemmings and E. E. Berry, "On the Glass in Coal Fly Ashes: Recent Advances," *MRS Online Proceedings Library,* vol. 113, pp. 3-38, 1987.

[6] M. Bohac, R. Novotny, F. Frajkorova, R. S. Yadav, T. Opravil and M. Palou, "Properties of Cement Pastes with Different Particle Size Fractions of Metakaolin," *International Journal of Materials and Metallurgical Engineering,* vol. 9, no. 14, pp. 301-305, 2015.

[7] L. Weng, K. Sagoe-Crentsil, T. Brown and S. Song, "Effects of aluminates on the formation of geopolymers," *Materials Science and Engineering B,* vol. 117, pp. 163-168, 2005.

[8] O. Ahmadah, "Contrôle de la rhéologie des liants à faibles impacts environnementaux," Université Paris-Est, Université Shebrooke, Champs-sur-Marne, 2021.

[9] A. Nonat, *L'hydratation des ciments, course note of master class "Cement hydration" at Ecole des Ponts Paristech,* Champs-sur-Marne, 2016.

[10] N. Kabay, M. M. Tufekci, A. B. Kizilkanat and D. Oktay, "Properties of concrete with pumice powder and fly ash as cement replacement materials," *Construction and Building Materials,* vol. 85, pp. 1-8, 2015.

[11] M. F. Nuruddin, K. Y. Chang and N. M. Azmee, "Workability and compressive strength of ductile self compacting concrete (DSCC) with various cement replacement materials," *Construction and Building Materials,* vol. 55, pp. 153-157, 2014.

[12] J. Wu, Z. Zhang, Y. Zhang and D. li, "Preparation and characterization of ultra-lightweight foamed geopolymer (UFG) based on fly ash-metakaolin blends," *Construction and Building Materials,* vol. 168, pp. 771-779, 2018.

[13] E. Papa, V. Medri, E. Landi, B. Ballarin and F. Miccio, "Production and characterization of geopolymers based on mixed compositions of metakaolin and coal ashes," *Materials and Design ,* vol. 56, p. 409–415, 2014.

[14] A. Aboulayt, R. Jaafri, H. Samouh, A. C. E. Idrissi, E. Roziere, R. Moussa and A. Loukili, "Stability of a new geopolymer grout: Rheological and mechanical performances of metakaolin-fly ash binary mixtures," *Construction and Building Materials,* vol. 181, pp. 420-436, 2018.

[15] J. Xiang, L. Liu, Y. He, N. Zhang and X. Cui, "Early mechanical properties and microstructural evolution of slag/metakaolin-based geopolymers exposed to karst water," *Cement and Concrete Composites ,* vol. 99, pp. 140-150, 2019.

[16] A. Aboulayt, M. Riahi, M. O. Touhami, H. Hannache, M. Gomina and R. Moussa, "Properties of metakaolin based geopolymer incorporating calcium carbonate," *Advanced Powder Technology ,* vol. 28, p. 2393–2401, 2017.

[17] H. Zhu, G. Liang, Z. Zhang, Q. Wu and J. Du, "Partial replacement of metakaolin with thermally treated rice husk ash in metakaolin-based geopolymer," *Construction and Building Materials ,* vol. 221, pp. 527-538, 2019.

[18] Q. Jiang and S. Mu, "Study on influence of limestone powder on the fresh and hardened properties of early-aged metakaolin-based geopolymer," in *International Conference on Calcined Clays for Sustainable Concrete*, Lausanne, Switzerland, 2015.

[19] R. Firdous, T. Hirsch, D. Klimm, B. Lothenbach and D. Stephan, "Reaction of calcium carbonate minerals in sodium silicate solution and its role in alkali-activated systems," *Minerals Engineering,* vol. 165, no. 106849, 2021.

[20] M. Antoni, J. Rossen, F. Martirena and K. Scrivener, "Cement substitution by a combination of metakaolin and limestone," *Cement and Concrete Research,* vol. 42, p. 1579–1589, 2012.

[21] D. Damidot, B. Lothenbach, D. Herfort and F. P. Glasser, "Thermodynamics and cement science," *Cement and Concrete Research ,* vol. 41, pp. 679-695, 2011.

[22] Q. Wan, Y. Zhang and R. Zhang, "Using mechanical activation of quartz to enhance the compressive strength of metakaolin based geopolymers," *Cement and Concrete Composites,* vol. 111, no. 103635, 2020.

[23] Q. Wan, F. Rao, S. Song, D. F. Cholico-Gonzalez and N. L. Ortiz, "Combination formation in the reinforcement of metakaolin geopolymers with quartz sand," *Cement and Concrete Composites,* vol. 80, pp. 115-122, 2017.

[24] L. M. Costa, N. G. S. Almeida, M. Houmard, P. R. Getlin, G. J. B. Silva and M. T. P. Aguilar, "Influence of the addition of amorphous and crystalline silica on the structural properties of metakaolin-based geopolymers," *Applied Clay Science ,* vol. 215, no. 106312, 2021.

[25] J. Deou, "Control of the rheological behaviour of chocolate suspensions by optimizing the morphological properties of the particles. Materials science," Université Paris-Est, Champs-sur-Marne, 2021.

[26] X. Chateau, Understanding the Rheology of Concrete, Edited by Nicolas Roussel, Woodhead Publishing Limited, 2012.

[27] A. P. Philipse, "The Random Contact Equation and Its Implications for (Colloidal) Rods in Packings, Suspensions, and Anisotropic Powders," *Langmuir,* vol. 12, pp. 1127-1133, 1006.

[28] Wikihow, "Wikihow," 6 May 2021. [Online]. Available: https://www.wikihow.com/Create-an-Apollonian-Gasket. [Accessed 2 May 2022].

[29] S. Fennis, "Delft University of Technology," 08 March 2011. [Online]. Available: https://citeseerx.ist.psu.edu/viewdoc/download?doi=10.1.1.621.2695&rep=rep1&type=pdf. [Accessed 09 March 2022].

[30] K. T. Miller, R. M. Melant and C. F. Zukovski, "Comparison of the Compressive Yield Response of Aggregated Suspensions: Pressure Filtration, Centrifugation and Osmotic consolidation," *Journal of American Ceramic Society,* vol. 79, no. 10, pp. 2545-2556, 1996.

[31] T. Sedran, "Rhéologie et rhéometrie des bétons. Application aux bétons autonivelants.," Ecole Nationale des Ponts et Chaussées, Champs-sur-Marne, 1999.

[32] Malvern, "Malvern Instruments Limited," 20 June 2012. [Online]. Available: https://www.malvernpanalytical.com/en/learn/knowledge-center/whitepapers/WP120620BasicGuidePartChar. [Accessed 24 February 2022].

[33] H. G. Brittain, "Particle size distribution, Part I. Representations of particle shape, size and distribution," *Pharmaceutical Technology,* 2001.

[34] Malvern, "Atascientific," February 2017. [Online]. Available: https://www.atascientific.com.au/wp-content/uploads/2017/02/AN020710-Basic-Principles-Particle-Size-Analysis.pdf. [Accessed 24 February 2022].

[35] B. Jennings and K. Parslow, "Particle size measurement: the equivalent spherical diameter," *Proceedings of the Royal Society,* vol. 419, pp. 137-149, 1988.

[36] A. Jillavenkatesa, S. J. Dapkunas and L. H. Lum, "Particle size characterization," National Institute of Standards and Technology, 2001.

[37] C. F. Ferraris, V. A. Hackley, A. I. Aviles and C. E. B. Jr, "Analysis of the ASTM Round-Robin Test on Particle Size DIstribution of Portland Cement: Phase II," National Institute of Standards and Technology , 2002.

[38] Innopharma, "Innopharma Technology," September 2019. [Online]. Available: https://www.innopharmatechnology.com/docs/default-source/eyecon2-whitepapers/methods-of-particle-size-determination.pdf. [Accessed 24 February 2022].

[39] Z. Stojanovic and S. Markovic, "Determinations of particle size distributions by laser diffractrion," *Technics-New Materials,* vol. 21, pp. 11-20, 2012.

[40] Malvern, *User manual of laser granulometer supplied by Malvern Instruments,* Malvern Instruments Limited.

[41] L. Petersen, P. Minkkinen and K. H. Esbensen, "Representative sampling for reliable data analysis: Theory of Sampling," *Chemometrics and Intelligent Laboratory Systems,* vol. 77, pp. 261-277, 2005.

[42] P. M. Gy, "The sampling of particulate materials, a general theory," *International Journal of Mineral Processing,* vol. 3, pp. 289-312, 1976.

[43] R. C. A. Minnintt, P. M. Rice and C. Spangenbergs, "Part 1: Understanding the components of the fundamental sampling error: a key to good sampling practice," *The Journal of The Southern African Institute of Mining and Metallurgy,* vol. 107, pp. 505-511, 2007.

[44] A. Virden, "Method Development for Laser-Diffraction Particle-Size Analysis," *Pharmaceutical Technology,* Vols. 34, Issue 11, November 2010.

[45] C. Ferrraris, M. Peltz and B. Toman, "Certification of standard reference material at 46h: fineness of cement - addition of blaine and particle size distribution," *National Institute of Standards and Technology, Special Publication 260-190,* 2018.

[46] C. F. Ferraris, J. W. Bullard and V. Hackley, "Particle size distribution by laser diffraction spectrometry: application to cementitious powders," *National Institute of Standard and Technology,* 2006.

[47] K. Scrivener, R. Snellings and B. Lothenbach, A practical guide to microstructural analysis of cementitious materials, CRC Press, 2016.

[48] Malvern, "Malvern Panalytical," 22 February 2013. [Online]. Available: https://www.malvernpanalytical.com/en/learn/knowledge-center/technical-notes/TN130222WetLiquidDispersionMethodDevelopment. [Accessed 26 February 2022].

[49] A. Califice, F. Michel, G. Dislaire and E. Pirard, "Influence of particle shape on size distribution measurements by 3D and 2D image analyses and laser diffraction," *Powder technology,* vol. 237, pp. 67-75, 2013.

[50] G. Gouesbet and G. Grehan, Opticle particle sizing, 1988.

[51] H. Zhang, J. Baeyens and Q. Kang, "Measuring suspended particle size with high accuracy," *International Journal of Petrochemical Science and Engineering,* Vols. 2, Issue 6, pp. 201-206, 2017.

[52] S. Erdogan, X. Nie, P. E. Stutzman and E. J. Garboczi, "Micrometer-scale 3-D shape characterization of eight cements: Particle shape and cement chemistry, and the effect of particle shape on laser diffraction particle size measurement," *Cement and Concrete Research,* vol. 40, pp. 731-739, 2010.

[53] M. Bittelli, S. Pellegrini, R. Olmi, M. C. Andrenelli, G. Simonetti, E. Borrelli and F. Morari, "Experimental evidence of laser diffraction accuracy for particle size analysis," *Geoderma,* vol. 409, p. 115627, 2022.

[54] H. Paiva, A. Velosa, P. Cachim and V. M. Ferreira, "Effect of metakaolin dispersion on the fresh and hardened state properties of concrete," *Cement and Concrete Research,* vol. 42, pp. 607-612, 2012.

[55] F. Andreola, E. Castellini, J. M. F. Ferreira, S. Olhero and M. Romagnoli, "Effect of sodium hexametaphosphate and ageing on the rheological behaviour of kaolin dispersions," *Applied Clay Science,* vol. 31, pp. 56-64, 2006.

[56] B. P. Singh, S. Bhattacharjee, L. Besra and D. K. Sengupta, "Evaluation of dispersibility of aqueous alumina suspension in presence of Darvan C," *Ceramics International,* vol. 30, pp. 939-946, 2004.

[57] A. Favier, "Mécanisme de prise et rhéologie de liants géopolymères modèles. Materials.," Université Paris-Est, 2013.

[58] G. Frigione and S. Marra, "Relationship between Particle Size Distribution and Compressive Strength in Portland Cement," *Cement and Concrete Research,* vol. 6, pp. 113-128, 1976.

[59] D. Bondar, S. Nanukuttan, J. L. Provis and M. Soutsos, "Efficient mix design of alkali activated slag concretes based on packing fraction of ingredients and paste thickness," *Journal of Cleaner Production,* vol. 218, pp. 438-449, 2019.

[60] F. Skvara, K. Kolar, J. Novotny and Z. Zadak, "The Effect of Cement Particle Size Distribution upon Properties of Pastes and Mortars with Low Water-to-Cement Ratio," *Cement and Concrete Research,* vol. 11, pp. 247-255, 1981.

[61] K. J. D. MacKenzie, D. R. M. Brew, R. A. Fletcher and R. Vagana, "Formation of aluminosilicate geopolymers from 1:1 layer-lattice minerals pre-treated by various methods: A comparative study," *Journal of Materials Science,* vol. 42, p. 4667–4674, 2007.

[62] K. J. D. MacKenzie, I. W. M. Brown, R. H. Meinhold and M. E. Bowden, "Outstanding problems in the kaolinite-mullite reaction sequence investigated by 29Si and 27Al solid-state nuclear magnetic resonance: I Metakaolinite," *Journal of the American Ceramic Society,* vol. 68, pp. 293-297, 1985.

[63] J. Rocha and J. Klinowski, "Solid-state NMR studies of the structure and reactivity of metakaolinite," *Angewandte Chemie (International ed.) ,* vol. 29, no. 5, pp. 553-554, 1990.

[64] M. L. Granizo, M. T. Blanco-Varela and S. Martinez-Ramirez, "Alkali activation of metakaolins: parameters affecting mechanical, structural and microstructural properties," *Journal of Materials Science ,* vol. 42, p. 2934–2943, 2007.

Chapter 3: Optimization of particle packing fractions

In this chapter, we will introduce the development of packing density with improved mixture proportions of solid precursors of geopolymers using Compressible Packing Model (CPM). We recall that limestone and quartz powders will be used together with different metakaolin powders in order to define the best two-part blends (i.e. binary powder mixtures) leading to increase of maximum particle packing. Initially, we will refer several packing models that are developed for improvement of mix design. Afterwards, we will introduce Compressible Packing Model (CPM) by mentioning a brief mathematical background of this model and then we will present the process followed for packing optimization. Starting from the determination of best two-part blends between different powder couples, we will present that maximum packing density increases by mixing metakaolin powders with other metakaolin, limestone or quartz powders and CPM predicts well the change in maximum packing density of studied powder mixtures.

3.1. Introduction to packing models

The objective of packing optimization is to fill the voids of bulk volume (Figure 3.1), which exist between larger particles in a system. Packing models are based on selecting favorable particle size and proportion of smaller particles that allow to fill voids of larger particles as much as possible [1].

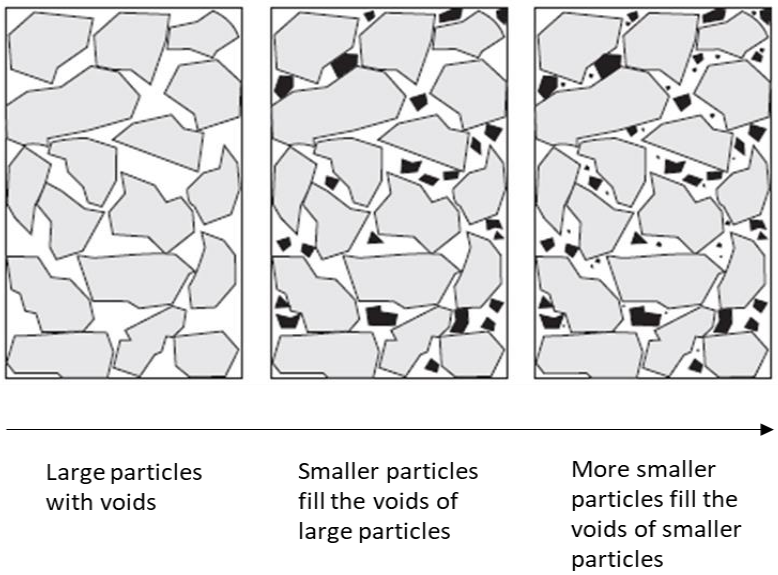

Figure 3.1 : Diagram of packing optimization (adapted from [1])

In 1931, Clifford Cook Furnas (American author, Olympic athlete and scientist, 1900-1969) published the first performable mathematical relations behind packing of binary mixture [2]. In his model, the idea is to introduce infinitely small particles (d_2) into the cavity of large particles (d_1) so that there is no geometric interaction between these two particle size classes since $d_2 << d_1$ [2]. This means, it is possible for fine particles to fill the voids without displacing coarse ones and it is also possible to insert coarse particles just by removing the fine particles that are situated in the domain to be occupied by coarse particles [3]. Packing density of the binary mixture could be found by considering two cases: either coarse grains are embedded within the fine particles (Figure 3.2, a) or fine grains locate in the voids of coarse particles (Figure 3.2, b). Fine particles are dominant in the first situation, while coarse ones become dominant in the later situation [1, 3, 4].

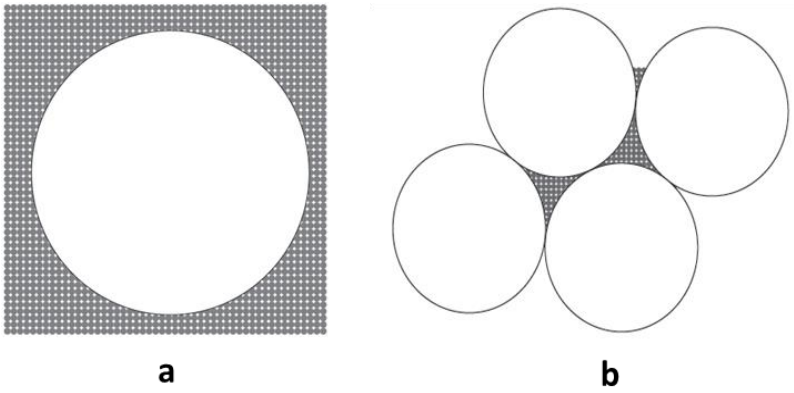

Figure 3.2 : Coarse grains are embedded in fine grains (a), fine grains fill the voids of coarse grains (b) [3]

Furnas Model is valid when the ratio between coarse and fine particle sizes tends toward to infinity ($d_2 << d_1$). However, when size ratio is not large enough (e.g. lower than ten [3] or $d_1 \approx d_2$ [1]), interactions between particles of different size classes cannot be ignorable. After Furnas, preliminary models tried to improve calculations of packing density by considering particle interactions, which result mainly in wall and loosening effects (Figure 3.3-a and Figure 3.3-b). Wall effect occurs when coarse grains insert into a matrix of fine grains. Insertion of coarse grains in this matrix disturbs local packing of fine grains. Thus, results in the decrease of packing density [1, 4, 5]. Contrarily, loosening effect occurs when fine grains insert into a matrix of coarse grains. Basically, it is expected that fine particles fill easily the voids if they are small enough. However, if fine particles have larger sizes than expected to fit into empty space between coarse particles, their insertion will also induce the decrease of packing density [1, 3]. Several preliminary models based on binary mixing systems [6, 7, 8] as well as the others based on ternary mixing systems [9, 10] mention wall and loosening effects.

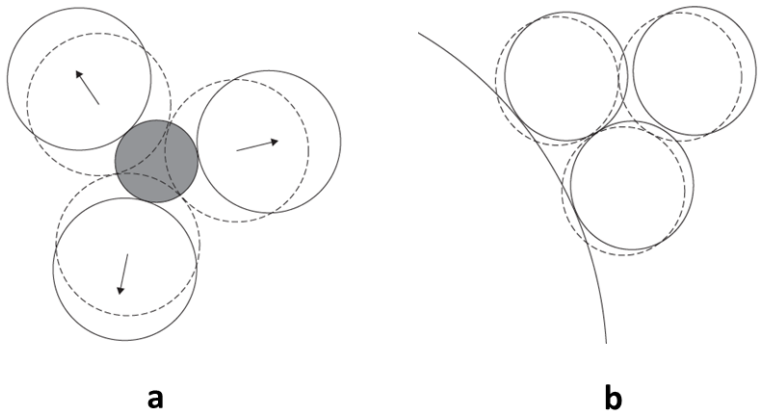

Figure 3.3 : Loosening (a) and wall (b) effects [3]

Preliminary models are valid within the limited set of particle size classes and they become inappropriate for the study of multi-component mixtures (i.e. mixtures that have unlimited particle size classes) [11]. Series of new generation packing models comprising multi-component mixtures are proposed in literature essentially by de Larrard [12, 13, 14]. Linear Packing Density Model (LPDM, [13]) is the basis of these second-generation models. LPDM show that it could predict well the optimal proportions of cementitious materials [4, 11, 14]. Nevertheless, it still needs to be improved due to its linear nature. De Larrard [14] mentioned the inadequacy of this model by explaining that the curves giving relationship between packing density and mixing proportions present angular points around optimal values but such a property does not exist in practice. Moreover, packing values obtained practically are lower than expected theoretical values. In the Solid Suspension Model (SSM), de Larrard and Sedran [14] improved LPDM model mainly by separating virtual (i.e. maximum attainable packing density [12, 15], corresponds to ordered dense packing mentioned in Chapter 2) and real (i.e. corresponds to random close packing, mentioned in Chapter 2) packing densities. Afterwards, de Larrard mentioned that the method used for packing is also important and should be considered for calculations [12]. In the final Compressible Packing Model (CPM), de Larrard improved SSM by introducing this time the compaction index (K), which represents how packing is processed [12]. As CPM considers both wall and loosening effects, it is also called 2-parameters model.

Kwan, Chan and Wong [16] introduced a new particle interaction effect called wedging effect. According to their study, wedging effect occurs when coarse particles are wedged apart by one or two isolated fine particles locate in the gap (Figure 3.4-a) or when isolated fine particles are trapped between coarse particles instead of filling voids (Figure 3.4-b). As this model considers wall, loosening and wedging effects, it is also called 3-parameters CPM. Roquier [17] have recently developed 4-parameters CPM. This model considers a new parameter, called critical cavity size ratio, together with wall and loosening effects and also compaction index. Below critical cavity size ratio, fine particles can insert into small cavities arise from touching coarser particles, while local volume of coarse class decreases beyond this ratio.

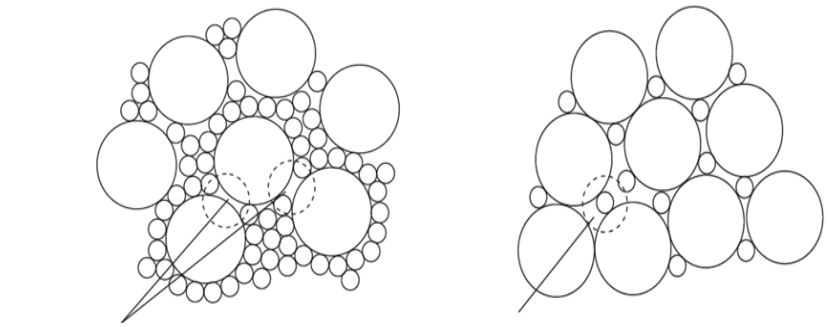

Figure 3.4 : Wedging effect when coarse particles wedged apart by fine particles (a) and when fine particles are trapped between coarse particles (b) [16]

Models existing in literature are categorized mainly as discrete and continuous models. Discrete models involve two or more separate particle size classes, while continues models assume that all possible sizes are already present in the system [1]. Figure 3.5 presents the classification of fundamental models with respect to mixing concepts they are based on.

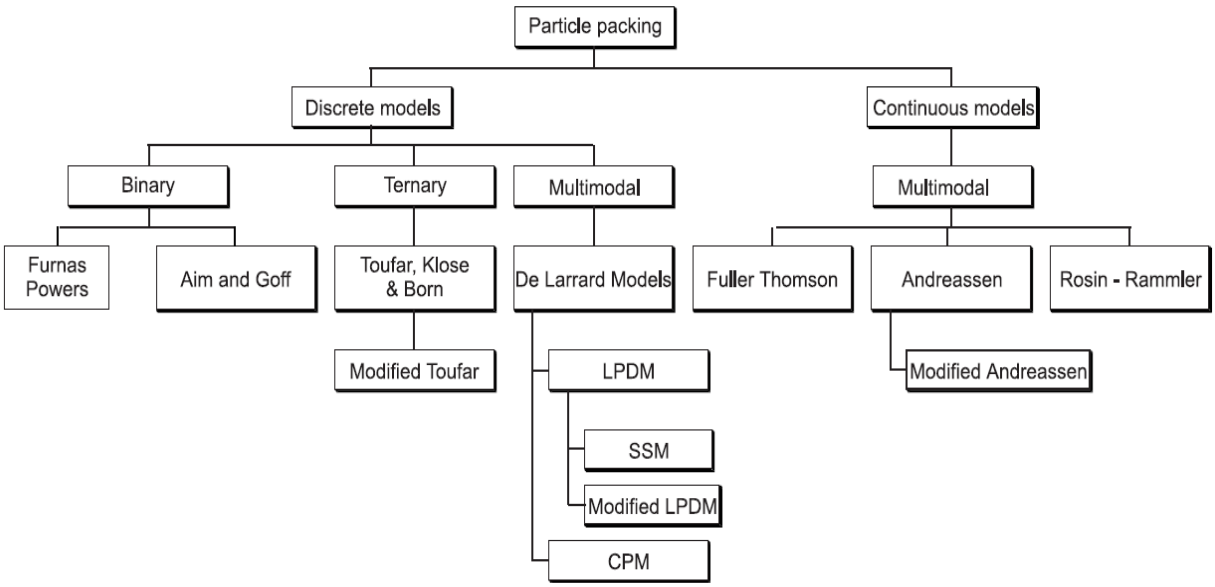

Figure 3.5 : Classification of fundamental packing models

Compressible Packing Model (CPM) developed by de Larrard allows to predict a representative real packing density of material by virtue of compaction index (K) mentioned above. Moreover, it considers interactions between particles and could be used for the study of multi-component mixtures. Several studies have validated utilization of CPM for cementitious materials [11, 18] as well as the cacao powders [19]. It is practical and it supplies repeatable results of the prediction of packing density. Therefore, we used CPM in order to optimize particle packing of powder mixtures of geopolymer suspensions in this thesis.

3.2. Compressible Packing Model (CPM)

CPM is a semi-empirical multi-component model, where it assumes that all particle size classes interact each other, thus influence the total packing. Moreover, model considers particle size distribution (PSD) as well as the individual maximum packing density of material. It is supposed that shape of the same material does not change according to different size classes and shape coefficient is computed based on PSD and maximum packing density of material [19]. CPM computes first the maximum virtual packing density (i.e. corresponds to ordered dense packing, mentioned in Chapter 2) and then the maximum real packing density (i.e. corresponds to random close packing, mentioned in Chapter 2) from the virtual one using compaction index (K), where this index represents the method used for packing of particles. In order to compute virtual and real packing values, CPM takes into account wall and loosening effects, which occur due to partial interactions between different size classes. In following sections, we present initially binary and polydisperse mixtures, where particles in mixtures interact partially and then we introduce computation details of virtual and real packing densities. CPM shows predicted packing density as a function of mixing proportions, where the optimal mixing proportion could be defined. For simplicity, a nomenclature of parameters used for computation is given in Table 3.1.

Table 3.1 : Computation parameters of CPM [18]

n	Number of size class
d_1,d_2, d_3, d_i	Diameter sizes of class 1, class 2 , class 3 and class i
β_1,β_2, β_3, β_i	Residual packing densities of class 1, class 2, class 3 and class i
ϕ_1,ϕ_2, ϕ_3, ϕ_i	Partial volumes of class 1, class 2, class 3 and class i
γ_1,γ_2, γ_3, γ_i	Virtual packing densities when class 1, class 2, class 3 or class i is dominant
y_1, y_2, y_3, y_i	Volume fractions of class 1, class 2, class 3 and class i
α, b	Loosening and wall effects respectively

3.2.1. Maximum virtual packing density

First, let us consider a binary mixing system consisting of size class 1 (d_1) and size class 2 (d_2) with $d_1 \geq d_2$. System has partial interaction between particles. Each size class has its own residual packing value, partial volume and volume fraction (Table 3.1). Partial volumes are the volumes occupied by each size class in a unit bulk volume [12, 15]. From this information, volume fraction of each size class can be defined as:

$$y_1 = \frac{\phi_1}{\phi_1 + \phi_2}$$

$$y_2 = \frac{\phi_2}{\phi_1 + \phi_2}$$

Where:

$$y_1 + y_2 = 1$$

CPM assumes that at least one size class must be dominant in order to define packing density. When size class 2 inserts in the porosity of size class 1 (i.e. class 1 is dominant), it fills the porosity until the moment that particles do not fit into voids anymore. At this moment, there will be a local volume decrease of class 1 (loosening effect, Figure 3.3-a). CPM mentions that if particles are sufficiently far from each other, this effect could be considered as a linear function of the volume of class 2. In this case, virtual maximum packing can be found by the equations below (mainly by equation 3.1):

$$\gamma = \phi_1 + \phi_2 = \beta_1(1 - \alpha_{1,2}\phi_2) + \phi_2$$

$$\gamma = \beta_1 + (\phi_1 + \phi_2)(1 - \beta_1\alpha_{1,2})y_2$$

$$\gamma = \gamma_1 = \frac{\beta_1}{1-(1-\alpha_{1,2}\beta_1/\beta_2)y_2} \quad (3.1)$$

Where $\alpha_{1,2}$ represents loosening effect exerted by size class 2 into size class 1. When size class 1 submerges into size class 2 (i.e. class 2 is dominant), voids in the packing of class 2 will increase in the interface vicinity (wall effect, Figure 3.3, b). CPM considers that if submerged particles of class 1 are sufficiently far from each other, this loss of solid volume is proportional to:

$$\frac{\phi_1}{(1 - \phi_1)}$$

In this case, virtual maximum packing becomes:

$$\gamma = \phi_1 + \phi_2 = \phi_1 + \beta_2\left(1 - \frac{\phi_1}{1-\phi_1} b_{2,1}\right)(1 - \phi_1)$$

$$\gamma = \gamma_2 = \frac{\beta_2}{1-[1-\beta_2+b_{2,1}\beta_2(1-1/\beta_1)]y_1} \quad (3.2)$$

Where $b_{2,1}$ represents wall effect exerted by size class 1 into size class 2. Whatever the dominant size class is, impenetrability between particles must be satisfied by:

$$\gamma \leq \gamma_1 \text{ and } \gamma \leq \gamma_2$$

Then, impenetrability constraints become:

$$\phi_1 \leq \beta_1$$

$$\phi_2 \leq \beta_2(1 - \phi_1)$$

It is concluded that maximum virtual packing density must be:

$$\gamma = \text{Min}(\gamma_1, \gamma_2)$$

Otherwise, impenetrability constrains are violated and it results in a non-physical situation [13]. Boundary conditions for loosening ($\alpha_{1,2}$) and wall ($b_{2,1}$) effects are:

$$\alpha_{1,2} = b_{2,1} = 0 \text{ when } d_1 \gg d_2 \quad \text{(i.e. there is no interaction)}$$

$$\alpha_{1,2} = b_{2,1} = 1 \text{ when } d_1 = d_2 \quad \text{(i.e. total interaction)}$$

Figure 3.6 presents the evolution of maximum virtual packing density as a function of volume fractions of small particles (introduced as size class 2). When the size ratio between two size class increases (i.e. from total interaction toward no interaction), virtual packing density increases until optimal mixing proportion (peak values of the curves in Figure 3.6) and then decreases. However, this does not mean that there is always an optimal mixing proportion for every mixed classes.

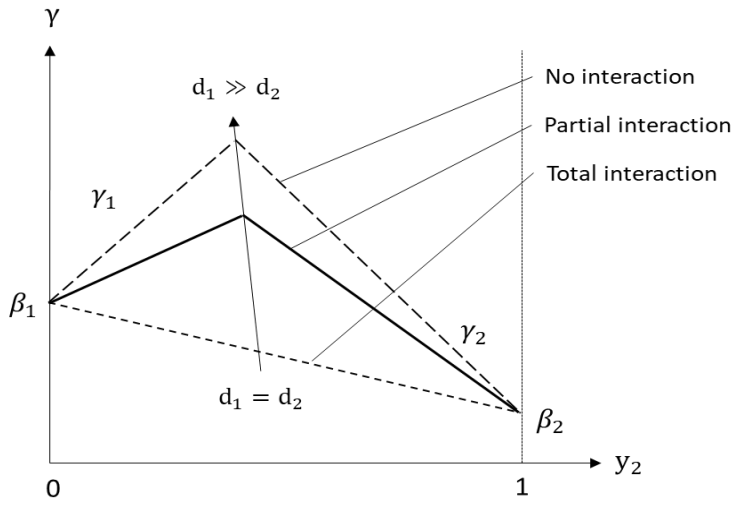

Figure 3.6 : Virtual maximum packing density of a binary mixing as a function of volume fraction of small size class [12]

Now let us consider a ternary mixing system with $d_1 \geq d_2 \geq d_3$ and class size 2 is dominant. Let us assume that class size 3 exerts loosening effect while class size 1 exerts wall effect on class size 2 (Figure 3.7).

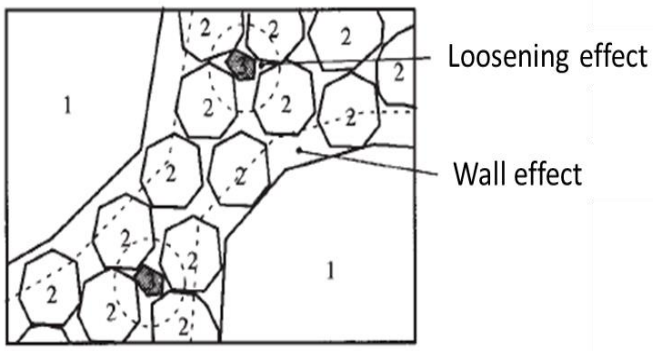

Figure 3.7 : Wall and loosening effects exerted on class size 2 [12]

In this case, virtual maximum packing density can be found mainly by the equation 3.3:

$$\gamma = \phi_1 + \phi_2 + \phi_3$$

$$\gamma = \gamma_2 = \frac{\beta_2}{1-[1-\beta_2+b_{1,2}\beta_2(1-1/\beta_1)]y_1-(1-\alpha_{1,2}\beta_2/\beta_3)y_3} \quad (3.3)$$

In case of "n" classes of grains (i.e. polydisperse mixing system), it is verified in [12] that the assumption of "at least one size class is dominant" is still valid. Thanks to the linearity of the formulation, virtual maximum packing given above (equation 3.3) can be generalized when size class i is dominant in a mixture. In this case, maximum virtual packing becomes:

$$\gamma_i = \frac{\beta_i}{1-\sum_{j=1}^{i-1}[1-\beta_i+b_{i,j}\beta_i(1-1/\beta_j)]y_i-\sum_{j=i+1}^{n}[1-\alpha_{i,j}\beta_i/\beta_j]y_i} \quad (3.4)$$

With impenetrability constraint:

$$\gamma = \underset{1\le i\le n}{\text{Min}}\ \gamma_i$$

And with loosening and wall effects:

$$\alpha_{i,j} = \sqrt{1-(1-d_j/d_i)^{1,02}}$$

$$b_{i,j} = \sqrt{1-(1-d_i/d_j)^{1,5}}$$

Details of mathematical background of all equations can be found in [12, 13, 14, 15].

3.2.2. Maximum real packing density

As mentioned above, CPM computes maximum real packing density from the maximum virtual packing density using a compaction index K. Calculation of K is based on the assumption where its value depends only on the process of packing. It is assumed that:

$$K = \sum_{i=1}^{n} K_i$$

After detailed calculations given in [12], K becomes for a binary mixture:

$$K = \frac{y_1/\beta_1}{1/\phi_{\text{computed real packing}}-1_{\gamma 1}} + \frac{y_2/\beta_2}{1/\phi_{\text{computed real packing}}-1_{\gamma 2}} \quad (3.5)$$

In case of polydisperse mixture, where there is n classes of particle size, K becomes:

$$K = \sum_{i=1}^{n} K_i = \sum_{i=1}^{n} \frac{y_i/\beta_i}{1/\phi_{\text{computed real packing}}-1/\gamma_i} \quad (3.6)$$

Actually, K is an increasing function of ϕ, meaning that there is only one value of ϕ that satisfies equations for any positive value of K (Figure 3.8) [12, 15]. For a monodisperse packing, K can be found by the equation below:

$$K = \frac{1}{\beta/\phi_{\text{computed real packing}}{}^{-1}} \quad (3.7)$$

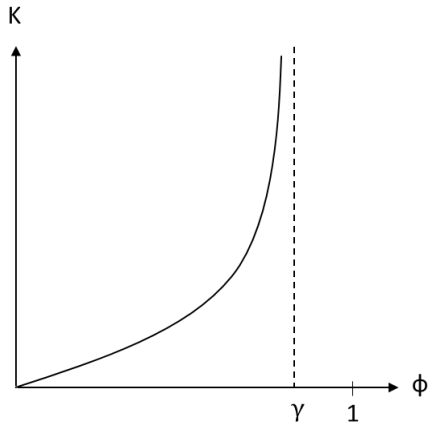

Figure 3.8 : Relation between K and ϕ

Some of the compaction index (K) values depending on different packing processes are summarized in Table 3.2.

Table 3.2 : Summary of K values depending on the method used for packing [12, 15]

Packing method	Pouring	Sticking with a rod	Vibration	Vibration+ Compression (10 kPa)	Water demand (Smooth, thick paste)	Virtual
K	4.1	4.5	4.75	9	6.7	∞

3.3. Methods followed to optimize particle packing

We remind that the goal of packing optimization is to fill the voids of bulk volume. Therefore, methods that we followed to do packing optimization are based mainly on filling the porosity of bulk volume. In order to enhance particle packing density, we mix metakaolin powders with other metakaolin, limestone or quartz powders that have different PSD, maximum packing density and shape coefficients. Hence, we identified three different types of binary mixing systems: mixtures between two metakaolin powders, mixtures between a metakaolin and a limestone powder, mixtures between a metakaolin and a quartz powder. The objective is that each time we mix a powder that has fine grains with another powder that has coarse grains.

For mixtures of two different metakaolin powders, Metakaolin D1 (or Metakaolin D2) has the highest mean particle size (see Table 2.10 in Chapter 2). Therefore, coarse-grain powder will be Metakaolin D1 and whatever the second metakaolin will be fine-grain powder. In case where we mix a metakaolin with a limestone, we have two possibilities: either we mix a fine-

grain metakaolin with a coarse-grain limestone or we mix a coarse-grain metakaolin with a fine-grain limestone. For the first possibility, coarse-grain limestone will be Durcal 65 and any metakaolin will be fine-grain. For the second possibility, fine-grain limestone will be Durcal 5 and any metakaolin will be coarse-grain. In case that we mix a metakaolin with a quartz, quartz will be fine-grain powder and whatever the metakaolin will be coarse-grain since quartz powder has the smallest particle size (Table 2.10, Chapter 2). We present studied powder couples of identified mixture types in Table 3.4.

We remark that from now on, maximum real packing density obtained from the maximum virtual packing density by CPM will correspond to the **computed maximum packing density**, while the term **measured maximum packing density** will correspond to the packing values obtained from the measurements of Water Demand method introduced in previous chapter. Subsequently, we will focus on the improvement of measured maximum packing density of identified powder mixtures. The steps followed to optimize packing density of each binary mixture are as follow:

- First, we determine density, particle size distribution (PSD) and individual maximum packing density of each powder using the protocols presented in Chapter 2,

- We **compute** maximum packing densities of powder mixtures using the individual values of density, PSD and maximum packing density of each powder in the mixture. Computation allows to identify promising powder couples that give the highest maximum packing density. We use combinations given in Table 3.3 and a value of 6.7 for compaction index K in order to compute maximum packing density and to compare the obtained values with those that are measured.

- We **measure** maximum packing density of powder mixtures by Water Demand method,

- We compare computed and measured maximum packing values to verify whether CPM predicts well maximum packing densities of mixtures.

Table 3.3 : Combinations of powder mixtures

	Volume fraction % (by total volume of solid particles)		**Total volume fraction**
	Component 1	Component 2	
Combination 1	0	1	1
Combination 2	0.1	0.9	1
Combination 3	0.2	0.8	1
Combination 4	0.3	0.7	1
Combination 5	0.4	0.6	1
Combination 6	0.5	0.5	1
Combination 7	0.6	0.4	1
Combination 8	0.7	0.3	1
Combination 9	0.8	0.2	1
Combination 10	0.9	0.1	1
Combination 11	1	0	1

Table 3.4 : Studied powder couples of different mixing types

	Component 1	Component 2
Mixtures between two metakaolin powders	Metakaolin D1 (D_{50} =15.8 ± 0.30)	Argical 1200S (D_{50} = 5.2 ± 0.31)
	Metakaolin D1 (D_{50} =15.8 ± 0.30)	Argical 1000 (D_{50} = 10.3 ± 0.18)
	Metakaolin D1 (D_{50} =15.8 ± 0.30)	Metamax (D_{50} = 5.4 ± 0.05)
	Metakaolin D1 (D_{50} =15.8 ± 0.30)	Metastar (D_{50} = 6.6 ± 0.02)
Mixtures between a small metakaolin and a large limestone powder	Durcal 65 (D_{50} = 40.1 ± 0.10)	Argical 1200S (D_{50} = 5.2 ± 0.31)
	Durcal 65 (D_{50} = 40.1 ± 0.10)	Argical 1000 (D_{50} = 10.3 ± 0.18)
	Durcal 65 (D_{50} = 40.1 ± 0.10)	Metamax (D_{50} = 5.4 ± 0.05)
	Durcal 65 (D_{50} = 40.1 ± 0.10)	Metastar (D_{50} = 6.6 ± 0.02)
	Durcal 65 (D_{50} = 40.1 ± 0.10)	Metakaolin D1 (D_{50} =15.8 ± 0.30)
Mixtures between a large metakaolin and a small limestone powder	Durcal 5 (D_{50} = 5.9 ± 0.07)	Argical 1200S (D_{50} = 5.2 ± 0.31)
	Durcal 5 (D_{50} = 5.9 ± 0.07)	Argical 1000 (D_{50} = 10.3 ± 0.18)
	Durcal 5 (D_{50} = 5.9 ± 0.07)	Metamax (D_{50} = 5.4 ± 0.05)
	Durcal 5 (D_{50} = 5.9 ± 0.07)	Metastar (D_{50} = 6.6 ± 0.02)
	Durcal 5 (D_{50} = 5.9 ± 0.07)	Metakaolin D1 (D_{50} =15.8 ± 0.30)
Mixtures between a metakaolin and a quartz powder	Quartz C800 (D_{50} = 2.9 ± 0.10)	Argical 1200S (D_{50} = 5.2 ± 0.31)
	Quartz C800 (D_{50} = 2.9 ± 0.10)	Argical 1000 (D_{50} = 10.3 ± 0.18)
	Quartz C800 (D_{50} = 2.9 ± 0.10)	Metamax (D_{50} = 5.4 ± 0.05)
	Quartz C800 (D_{50} = 2.9 ± 0.10)	Metastar (D_{50} = 6.6 ± 0.02)
	Quartz C800 (D_{50} = 2.9 ± 0.10)	Metakaolin D1 (D_{50} =15.8 ± 0.30)

3.4. Residual packing density of studied powder materials

When particles in a system are spherical, investigation of packing improvement is simpler due to regularity of particle shape. In case where non-spherical particles exist in this system, shape parameters such as aspect ratio (i.e. length/diameter), roundness or sphericity could be chosen to describe the effect of particle morphology (i.e. mainly shape) on packing improvement [5, 11]. In this study, shape of particles of different powder materials is represented by residual packing density, where it is computed based on PSD and maximum packing density of corresponding powder material. We present residual packing density (β) of each studied powder in Figure 3.9.

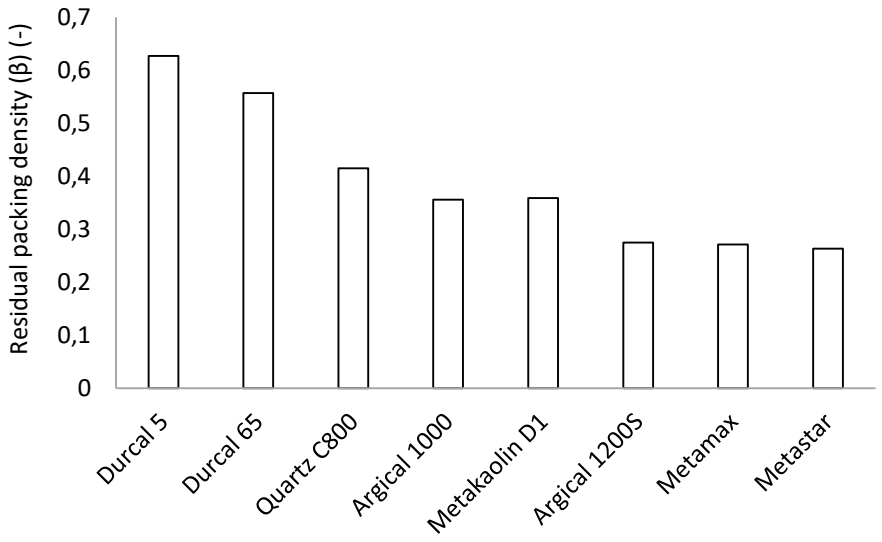

Figure 3.9 : Residual packing density of studied powders

Figure 3.9 shows decreasing values of residual packing densities from limestone to metakaolin powders. We note that the shape of limestone particles approaches to sphericity, while the shape of quartz and metakaolin particles are more quadrangular shapes with variable elongations [11]. In this case, the difference between residual packing density values and their decreasing trend could be explained by the shape of particles, which becomes more elongated from limestone to metakaolin powders. We recall that the increase of elongation results in the increase of aspect ratio, which then results in the decreasing packing density (see Figure 2.1, Chapter 2). This suggests that the use of limestone would be beneficial in terms of the improvement of maximum packing density. Its use could optimize better the maximum packing density than the use of metakaolin alone.

3.5. Computed maximum packing density of identified powder mixtures

We present computed maximum packing density of different powder mixtures as a function of volume fractions of Metakaolin D1, Durcal 5, Durcal 65 or Quartz C800 in Figure 3.10.

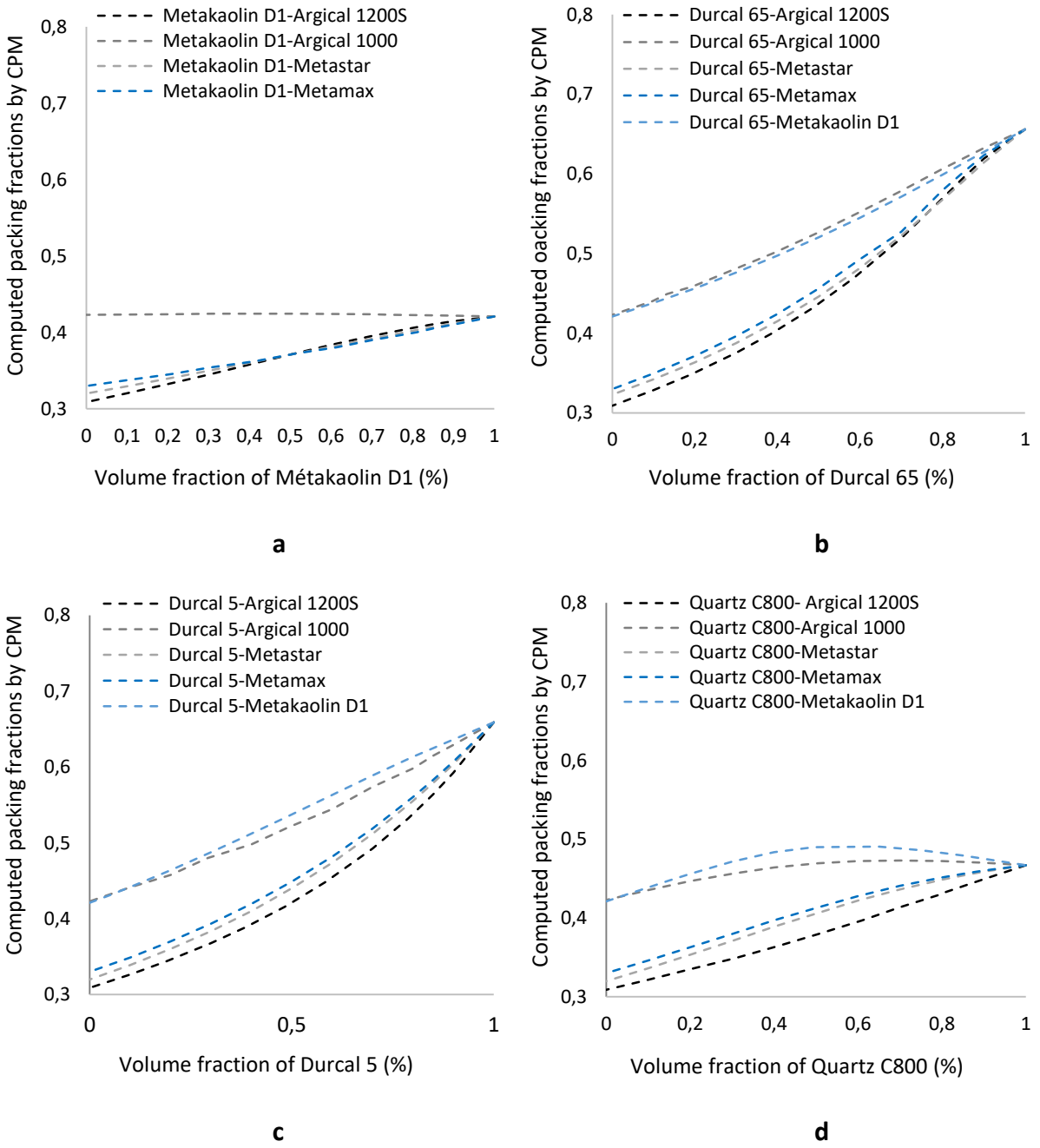

Figure 3.10 : Computed maximum packing densities of couples between two metakaolin (a), a metakaolin and a large limestone (b), a metakaolin and a small limestone (c) a metakaolin and a quartz (d) based on CPM

According to Figure 3.10-a, Figure 3.10-b and Figure 3.10-c, computed maximum packing density of metakaolin-metakaolin and metakaolin-small or large limestone powder mixtures increase throughout their highest values with increasing volume fractions of Metakaolin D1, Durcal 5 or Durcal 65. In case of powder mixtures between metakaolin and quartz (Figure 3.10-d), we observed optimum mixing proportions around 50% of Quartz C800. We identified couples given in Table 3.6 as promising binary mixtures since they give the best computation results of maximum packing. In the following section, we study the validation of CPM by comparing computed and measured maximum packing densities of these promising couples.

Table 3.5 : Identified promising powder couples of different mixture types giving the best maximum packing density values

	Component 1	Component 2
Mixtures between two metakaolin powders	Metakaolin D1 (D_{50} =15.8 ± 0.30)	Argical 1200S (D_{50} = 5.2 ± 0.31)
	Metakaolin D1 (D_{50} =15.8 ± 0.30)	Argical 1000 (D_{50} = 10.3 ± 0.18)
	Metakaolin D1 (D_{50} =15.8 ± 0.30)	Metamax (D_{50} = 5.4 ± 0.05)
	Metakaolin D1 (D_{50} =15.8 ± 0.30)	Metastar (D_{50} = 6.6 ± 0.02)
Mixtures between a small metakaolin and a large limestone powder	Durcal 65 (D_{50} = 40.1 ± 0.10)	Argical 1200S (D_{50} = 5.2 ± 0.31)
	Durcal 65 (D_{50} = 40.1 ± 0.10)	Argical 1000 (D_{50} = 10.3 ± 0.18)
Mixtures between a large metakaolin and a small limestone powder	Durcal 5 (D_{50} = 5.9 ± 0.07)	Argical 1000 (D_{50} = 10.3 ± 0.18)
	Durcal 5 (D_{50} = 5.9 ± 0.07)	Metakaolin D1 (D_{50} =15.8 ± 0.30)
Mixtures between a metakaolin and a quartz powder	Quartz C800 (D_{50} = 2.9 ± 0.10)	Argical 1000 (D_{50} = 10.3 ± 0.18)
	Quartz C800 (D_{50} = 2.9 ± 0.10)	Metakaolin D1 (D_{50} =15.8 ± 0.30)

3.6. Correlation between computed and measured maximum packing densities

In order to validate CPM, first we measure maximum packing densities of promising couples that gave the best computation results in previous section (see Table 3.6) using Water Demand method. Afterwards, we compare these measured values with computed values presented in previous section. We present correlation between both packing values in Figure 3.11.

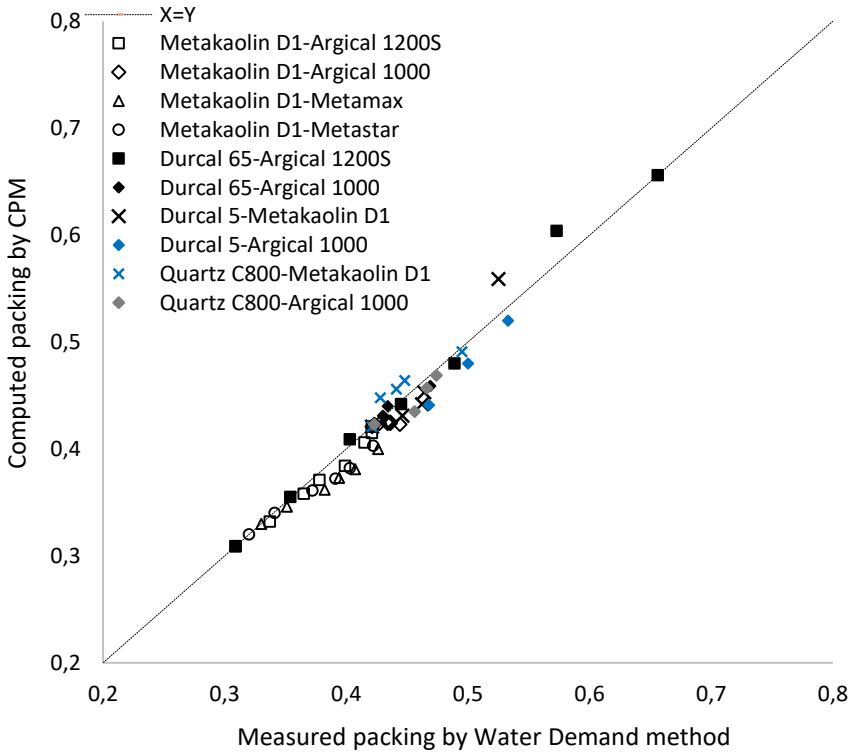

Figure 3.11 : Comparison between computed and measured packing density of all powder couples belonging to different mixture types

Figure 3.11 shows that computed and measured maximum packing densities of studied powder couples correlate well since their values align throughout the equality line (i.e. X=Y). According to figure, we can deduce that CPM predicts well the maximum packing density regardless of the mixture type of powder couple. In order to present detailed analysis of correlations for each studied powder couple, we classified results of correlations according to mixture type and presented in following sections.

3.7. Particle packing optimization

3.7.1. Metakaolin couples

Figure 3.12 presents computed and measured maximum packing values of metakaolin powder mixtures as a function of volume fraction of Metakaolin D1.

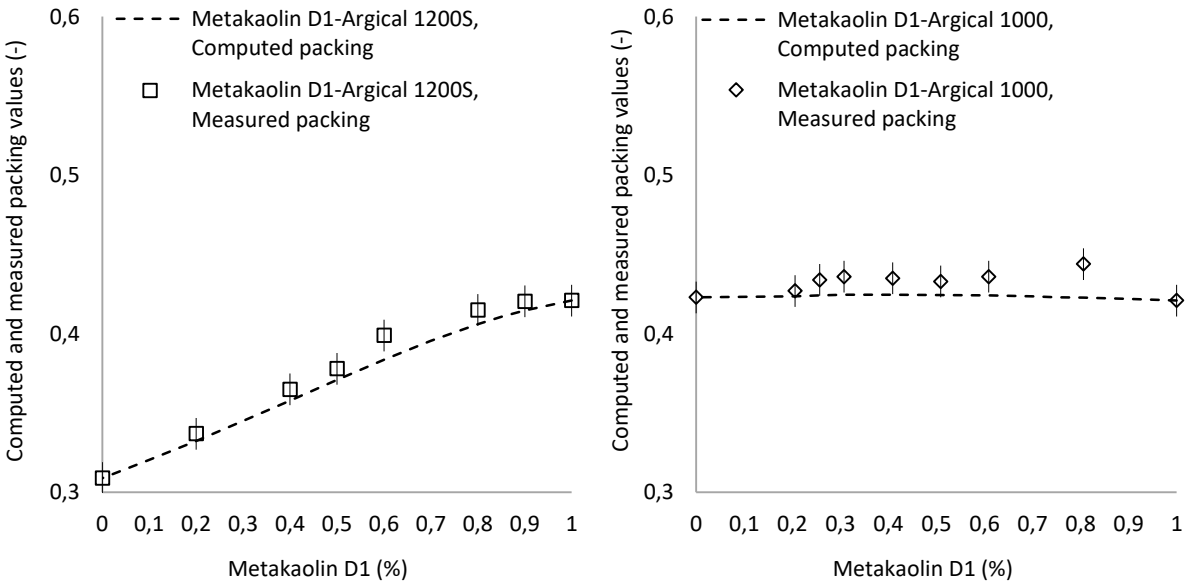

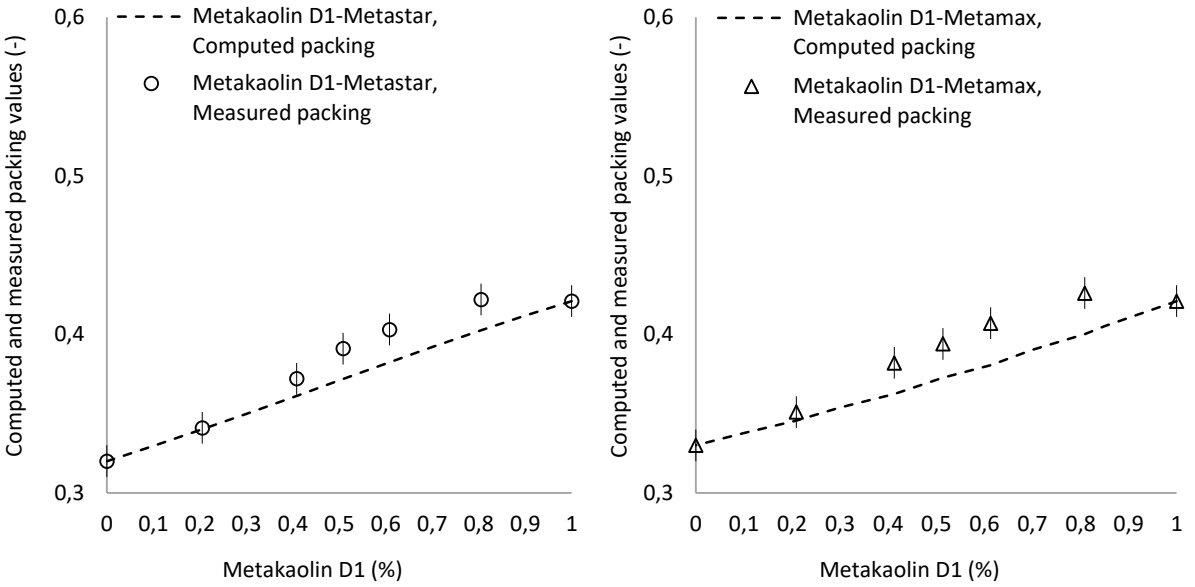

c **d**

Figure 3.12 : Comparison between computed and measured packing density of identified metakaolin powder couples

According to Figure 3.12-a and Figure 3.12-b, computed and measured maximum packing densities of couples Metakaolin D1-Argical 1200S and Metakaolin D1-Argical 1000 correlate well since their values are very close. For other two couples where Metakaolin D1 is mixed with Metastar or Metamax (Figure 3.12-c and Figure 3.12-d), we observed that measured packing densities are slightly higher. However, computed and measured values are still close. Moreover, we note that maximum packing values increase with increasing volume fraction of Metakaolin D1 for each couple. Although, correlations do not present remarkable optimum mixing proportions, mixing proportion 80% of Metakaolin D1 seems to be optimal for all couples.

3.7.2. Metakaolin and limestone couples

Figure 3.13 presents computed and measured maximum packing values of metakaolin-limestone powder mixtures as a function of volume fractions of Durcal 5 or Durcal 65.

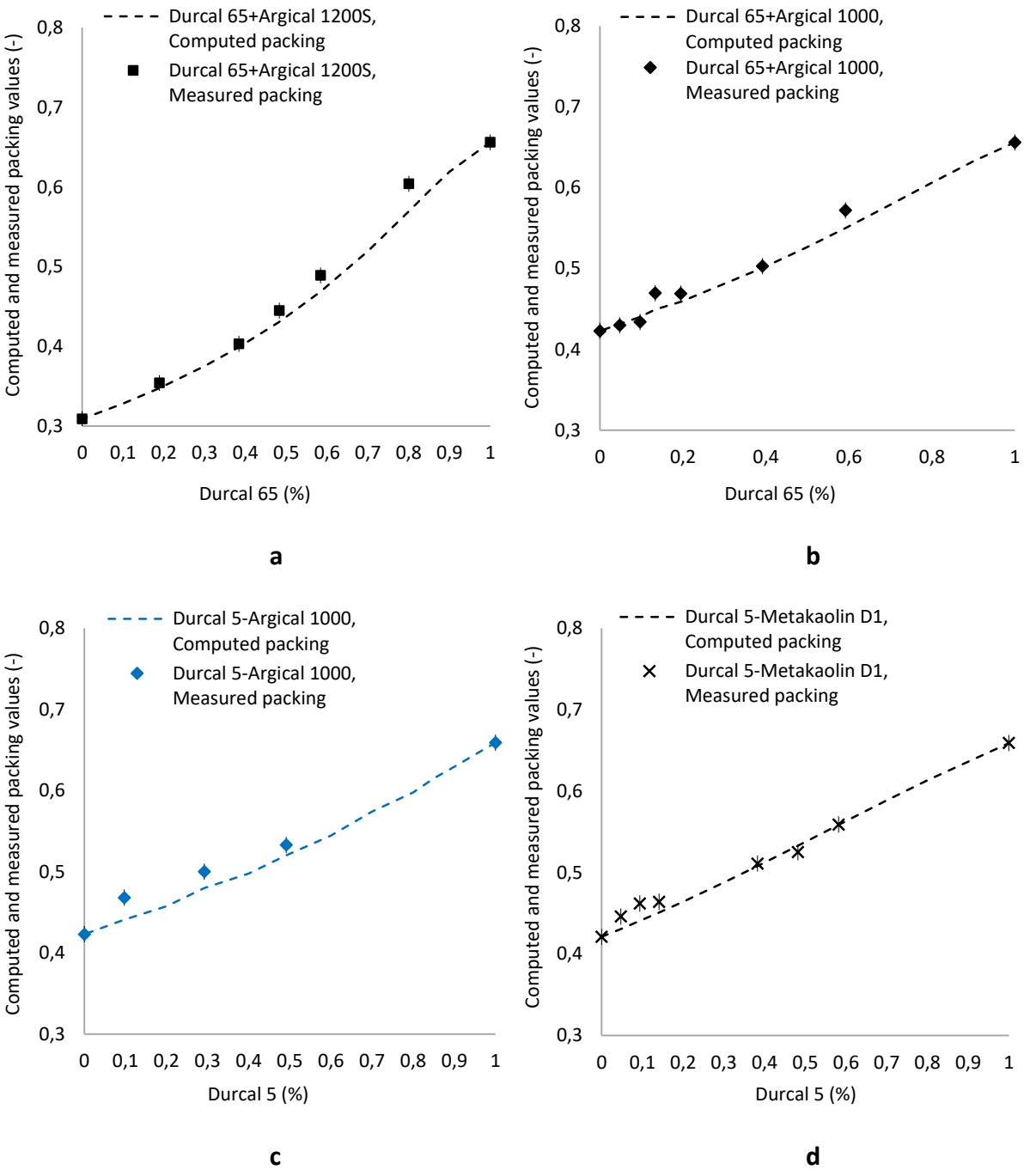

Figure 3.13 : Comparison between computed and measured packing density of identified powder couples for mixtures between small metakaolin-large limestone (a and b) and large metakaolin-small limestone (c and d)

According to Figure 3.13, maximum packing density of studied couples increases with increasing volume fractions of Durcal 5 or Durcal 65. Moreover, computed and measured maximum packing values of all couples correlate well, which means, CPM predicts well the maximum packing density of metakaolin-limestone powder mixtures.

3.7.3. Metakaolin-quartz couples

Figure 3.14 presents computed and measured maximum packing values of metakaolin-quartz powder mixtures as a function of volume fraction of Quartz C800.

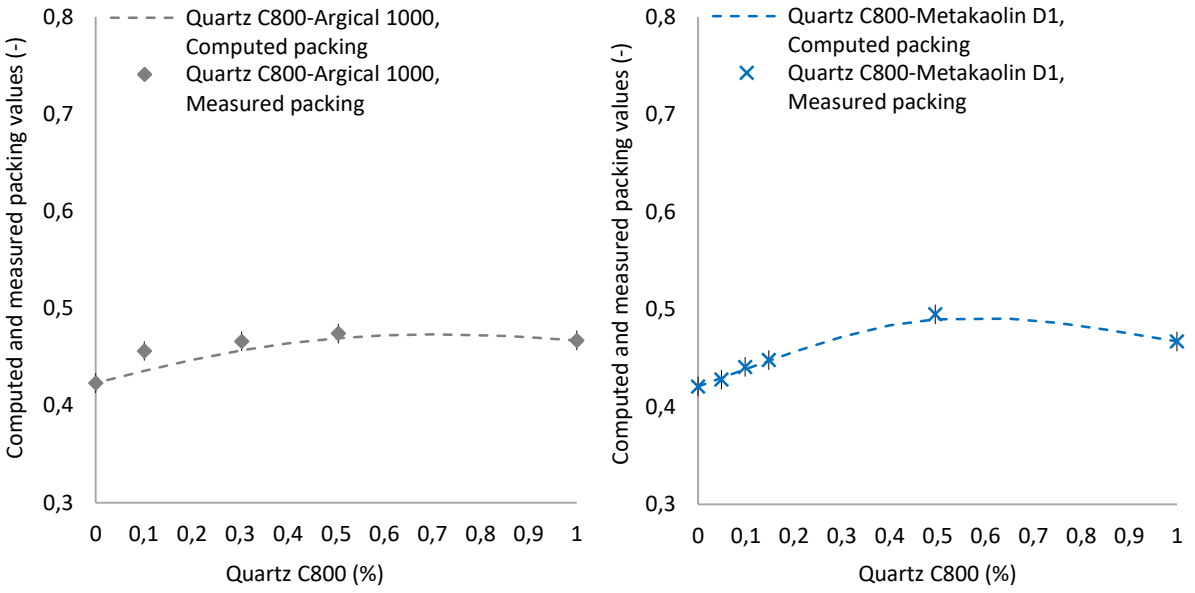

a **b**

Figure 3.14 : Comparison between computed and measured packing density of identified powder couples for metakaolin-quartz mixtures

According to Figure 3.14, maximum packing density of studied couples increases until around 50% of Quartz C800 and then starts to decrease beyond this volume fraction. According to these results, we can deduce the mixing proportion, where volume fraction of Quartz C800 is 50%, is optimal beyond which maximum packing decreases. Decease of maximum packing is more remarkable for couple Metakaolin D1-Quartz C800 (Figure 3.14-b).

3.8. Conclusion

In this chapter, we introduced initially different packing models existing in literature, which are used to develop mix design of formulation components of cementitious materials. We mentioned that we selected Compressible Packing Model (CPM) for the rest of the study due to its practical use that provides repeatable results, meaning reliable predictions of packing density. Afterwards, we introduced Compressible Packing Model with a brief mathematical background. We explained how this model computes maximum packing density using the virtual packing values. In the following, we presented the procedure of packing optimization. First, we identified different types of binary powder mixtures, where a metakaolin powder is mixed with another metakaolin, limestone or quartz powder. Second, we computed packing values of these powder mixtures using different mixing combinations by CPM. We observed that maximum packing values of powder couples improves with the increasing amounts of a metakaolin having large particle size, limestone or quartz. Based on these computed packing

values by CPM, we identified the best couples giving the highest values of maximum packing. Finally, we measured maximum packing values of these couples using Water Demand method and showed a correlation between obtained values and those that are computed primarily by CPM. According to correlations, we observed that Compressible Packing Model predicts well the improvement of maximum packing density of a powder mixture regardless of the type of this mixture.

References

[1] S. Kumar and M. Santhanam, "Particle packing theories and their application in concrete mixture proportioning: A review," *The Indian Concrete Journal,* vol. 77 (9), pp. 1324-1331, 2003.

[2] C. C. Furnas, "Grading aggregates I. Mathematical relations for Beds of Broken Solids of Maximum Density," *INDUSTRIAL AND ENGINEERING CHEMISTRY,* vol. 23, no. 9, pp. 1052-1058, 1931.

[3] X. Chateau, Particle packing and the rheology of concrete. Chapter 6 of the book: Understanding the rheology of concrete. Edited by Nicolas Roussel, Woodhead Publishing, 2012.

[4] M. N. Mangulkar and S. S. Jamkar, "Review of Particle Packing Theories Used For Concrete Mix Proportioning," *International Journal Of Scientific & Engineering Research,* Vols. 4, Issue 5, pp. 143-148, 2013.

[5] I. Mehdipour and K. H. Khayat, "Understanding the role of particle packing characteristics in rheo-physical properties of cementitious suspensions: A literature review," *Construction and Building Materials,* vol. 161, pp. 340-353, 2018.

[6] T. C. Powers, Properties of Fresh Concrete, New York: John Wiley and Sons. Inc. , 1968.

[7] R. B. Aim and P. L. Goff, "Effet de paroi dans les empilements désordonnés de sphères et application à la porosité de mélanges binaires," *Powder Technology,* vol. 1, pp. 281-290, 1968.

[8] J. Dewar, Computer Modelling of Concrete Mixtures, London: CRC Press, 1999.

[9] W. Toufar, M. Born and E. Klose, ""“Contribution of optimisation of components of different density in polydispersed particle systems," *Freiberger Booklet A 558 (VEB Deutscher Verlag ftir Grundstoflindustrie, in German),* pp. 29-44, 1976.

[10] P. Goltermann, V. Johansen and L. Palbol, "Packing of aggregates: an alternative tool to determine the optimal aggregate mix," *ACI Material Journal,* vol. 94, no. 5, pp. 435-443, 1997.

[11] O. Ahmadah, "Contrôle de la rhéologie des liants à faibles impacts environnementaux," Université Gustave Eiffel and Université Sherbrooke, Paris, 2021.

[12] F. d. Larrard, Concrete Mixture Proportioning. A Scientific Approach, London and New York: E & FN SPON, An Imprint of Routledge, 1999.

[13] T. Stovall, F. d. Larrard and M. Buil, "Linear Packing Density Model of Grain Mixtures," *Powder Technology,* vol. 48, pp. 1-12, 1986.

[14] F. d. Larrard and T. Sedran, "Optimization of Ultra-High-Performance Concrete By The Use Of a Model," *Cement and Concrete Research,* vol. 24, no. 6, pp. 997-1009, 1994.

[15] F. d. Larrard, Structures granulaires et formulation des bétons, Paris: Laboratoire Central des Ponts et Chaussées, 2000.

[16] A. K. H. Kwan, K. W. Chan and V. Wong, "A 3-parameter particle packing model incorporating the wedging effect," *Powder Technology,* no. 237, pp. 172-179, 2013.

[17] G. Roquier, "The 4-parameter Compressible Packing Model (CPM) including a critical cavity size ratio," in *EPJ Web of Conferences, Powders and Grains*, 2017.

[18] T. Sedran, "Rhéologie et Rhéometrie des bétons. Applications aux bétons autonivelants.," Ecole Nationale des Ponts et Chaussées, Paris, 1999.

[19] J. Deou, "Control of the rheological behaviour of chocolate suspensions by optimizing the morphological properties of the particles," Université Paris-Est, Champs-sur-Marne, 2021.

Chapter 4: Influence of particle packing optimization on rheological and mechanical behaviors of geopolymer suspensions

In the previous chapter, we observed that maximum packing density of a metakaolin powder used to produce geopolymers increases by substituting a part of this metakaolin by another metakaolin, limestone or quartz powder. Our objective for this chapter is to present the effect of particle packing optimization on the rheological and mechanical properties of geopolymer suspensions. In the first part, we will present the influence of packing optimization on rheological properties. As the objective is to decrease viscosity while modifying primarily physical parameters of particles, we checked that both limestone and quartz powders remain inert within the time when geopolymers are studied at fresh state. Hence, we will show the effect of packing optimization on rheological properties by assuming only the contribution of physical properties of particles. In the second part of this chapter, we will present the impact of packing optimization as well as the variation of chemical formulation on mechanical properties of geopolymers. We will introduce protocols of rheological and mechanical measurements at the beginning of corresponding sections and then we will present evolutions of rheological and mechanical performances of geopolymers as a function of packing optimization or modification of chemical formulation.

4.1. Influence of particle packing optimization on rheological properties

4.1.1. Protocols of rheological measurements

4.1.1.1. Preparation of geopolymer suspension

In order to prepare a geopolymer suspension, first we prepare powder mixture that is used as a precursor with respect to volume fractions. Afterwards, we mix this mixture with a sodium silicate solution, which is prepared using commercial sodium silicate solution and sodium hydroxide pellets (see section 2.2.3, Chapter 2), using a Turbo-Test Rayneri VMI mixer. Mixing protocol of Rayneri is as follow: we mix powder mixture and sodium silicate solution during 1 minute at 1400 revolutions per minute (rpm), we make 30 seconds break and we continue to mix during 1 more minute at 1400 rpm.

4.1.1.2. Shear protocol for rheological measurements of geopolymers

We perform rheological measurements of geopolymer suspensions using a Bohlin C-Vor Instrument equipped with a vane geometry (Figure 4.1). In this geometry, material is placed between a vane tool, which consists of 4 thin blades centered on a thin shaft, and an outer cylinder that is fixed [1]. The inner radius (i.e. length of a blade) is R_i = 12.5 mm, while the outer radius (i.e. radius of the outer cylinder) is R_o = 25 mm. Height of the outer cylinder is 60 mm.

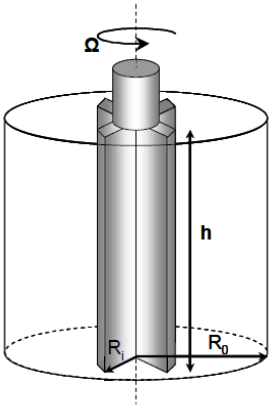

Figure 4.1: Vane geometry [2]

We use vane geometry because it has mainly two advantageous. First, there is minimum material disturbance during the insertion of the tool. Second, material that is in the gap of the vane geometry is sheared by the same material entrapped between blades [1]. As outer cylinder is fixed, shear is imposed by rotating blades around the symmetry axis at a velocity Ω, thus resulting in a torque T. In cylindrical coordinates, shear stress τ(r) can be found by Equation 4.1 at the stress equilibrium:

$$\tau(r) = \frac{T}{2\pi h r^2} \quad \text{with} \quad R_i < r < R_o \qquad (4.1)$$

Assuming that material is sheared all around an air gap at a constant shear rate with a no-slip boundary condition at the surface of the cylinder, shear rate $\dot{\gamma}$ and shear stress τ(r) can be defined in the middle of this air gap as follow:

$$\dot{\gamma} = \Omega \frac{R_i^2 R_0^2}{\bar{R}\,(R_0 - R_i)} \qquad (4.2)$$

Where:

$$\bar{R} = \frac{R_i + R_0}{2} \qquad (4.3)$$

As soon as we prepare geopolymer suspension, we perform rheological measurements by applying following steps:

- First, we apply a pre-shearing at a shear rate 100 s^{-1} during 2 minutes in order to eliminate mechanical mixing history of Rayneri mixer,

- Following to pre-shearing, we let material rest during 30 seconds,

- We apply an ascending shear rate from 1 s^{-1} to 100 s^{-1} during 500 seconds and then we apply a descending shear rate from 100 s^{-1} to 1 s^{-1} during 500 seconds. Actually, applying increasing and decreasing shear rate allows to verify thixotropic behavior of material. At the end of measurement, we obtain a flow curve where viscosity of sheared geopolymer suspension is presented with respect to applied shear rate (Figure 4.2). If the flow curves of ascending and descending shear rates are identical, thixotropic nature of geopolymer suspension is ignorable within the range of applied shear rate. We present flow curves in logarithmic scale as it provides advantage of studying large shear rate interval.

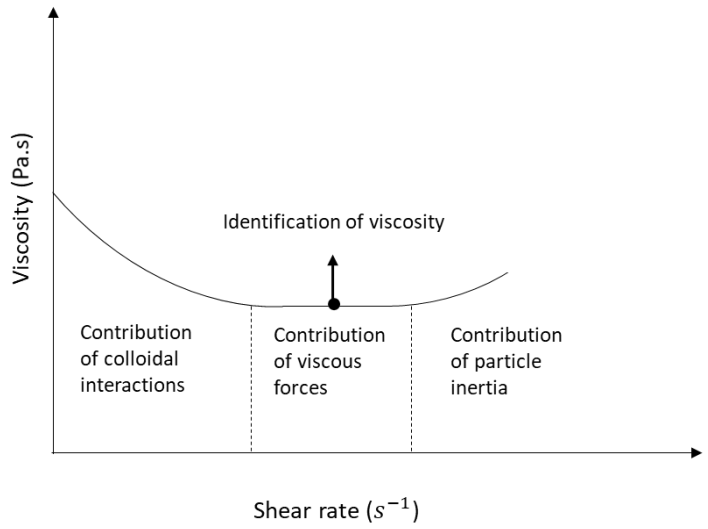

Figure 4.2: Diagram of a flow curve

- We define viscosity of geopolymer suspensions at the plateau of flow curve, where these suspensions behave as a Newtonian fluid (i.e. viscosity does not depend on the shear rate), thus both colloidal interactions and contribution of particle inertia could be neglected. Plateaus of flow curves obtained from rheological measurements correspond to shear rates between 10 s^{-1} and 30 s^{-1}.

4.1.1.3. Shear protocol for rheological measurements of liquid materials

We perform rheological measurements of liquid materials using a Bohlin C-Vor Instrument equipped with a plane-plane geometry (Figure 4.3). In this geometry, material is placed between two disks (i.e. parallel planes) having the same symmetry axis of the same radius R = 2 cm, that is separated by a distance H = 500 µm.

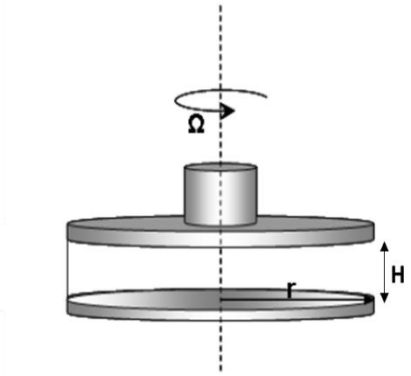

Figure 4.3: Plane – plane geometry (adapted from [2])

Bottom plate is fixed and material is sheared by rotating upper plate around the symmetry axis at a velocity Ω, thus resulting in a Torque T. In cylindrical coordinates, relations between rotational velocity and shear rate (Equation 4.4) and between torque and shear stress (Equation 4.5) are as follow:

$$\dot{\gamma} = \frac{3}{4}\frac{\Omega R}{H} \quad (4.4)$$

$$\tau = \frac{3}{2}\frac{T}{\pi R^3} \quad (4.5)$$

We perform following steps for rheological measurements:

- We drop a small amount of liquid material on bottom plate,

- We lift upper plate down until the distance between both plates becomes 500 µm,

- Since the liquid materials (i.e. mainly sodium silicate solution) used in this thesis behave as Newtonian fluids, verification of thixotropic behavior could be neglected. Therefore, we apply only a descending shear rate from 100 s^{-1} to 10 s^{-1} during 500 seconds without any pre-shearing before measurement.

- Similarly, we obtain flow curves of sheared materials in the end of measurements and we define viscosity from the calculation of mean value of all measured viscosity values.

4.1.2. Rheological properties of limestone and quartz powders suspended in sodium silicate solution over time

The objective of this section is to verify whether limestone or quartz powders stay inert within the duration of rheological measurements. For verifications, we prepare initially limestone and quartz suspensions by mixing Durcal 5 or Quartz C800 powder with sodium silicate solution using the preparation protocol introduced in previous section. Solid volume fraction of Quartz C800 suspension is 22%, while for limestone, we prepare two suspensions with solid volume fractions of 19% and 41%. After preparation, we perform rheological measurements with respect to shear protocol introduced in section 4.1.1.2 as soon as after mixing (t = 0h), 1

hour (t = 1h), 2 hours (t = 2h) and 24 hours after mixing (t = 24) for quartz and limestone suspensions having solid volume fractions of 22% and 19% respectively. For limestone suspension at a solid volume fraction of 41%, we perform measurements immediately after mixing and 2 hours after mixing. This last suspension became solid after the measurement at t = 2 hours, thus measurement at t = 24 hours was not performable (see image given in Figure 4.5-b). We present flow curves of quartz and limestone suspensions in Figure 4.4 and Figure 4.5 respectively.

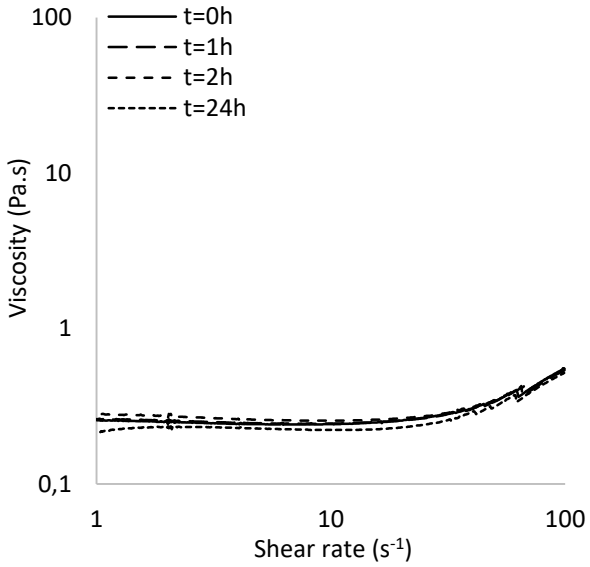

Figure 4.4: Flow curves of Quartz C800 suspensions. Measurements are performed at t = 0h, 1h, 2h, 24h after preparation, ϕ = 22%

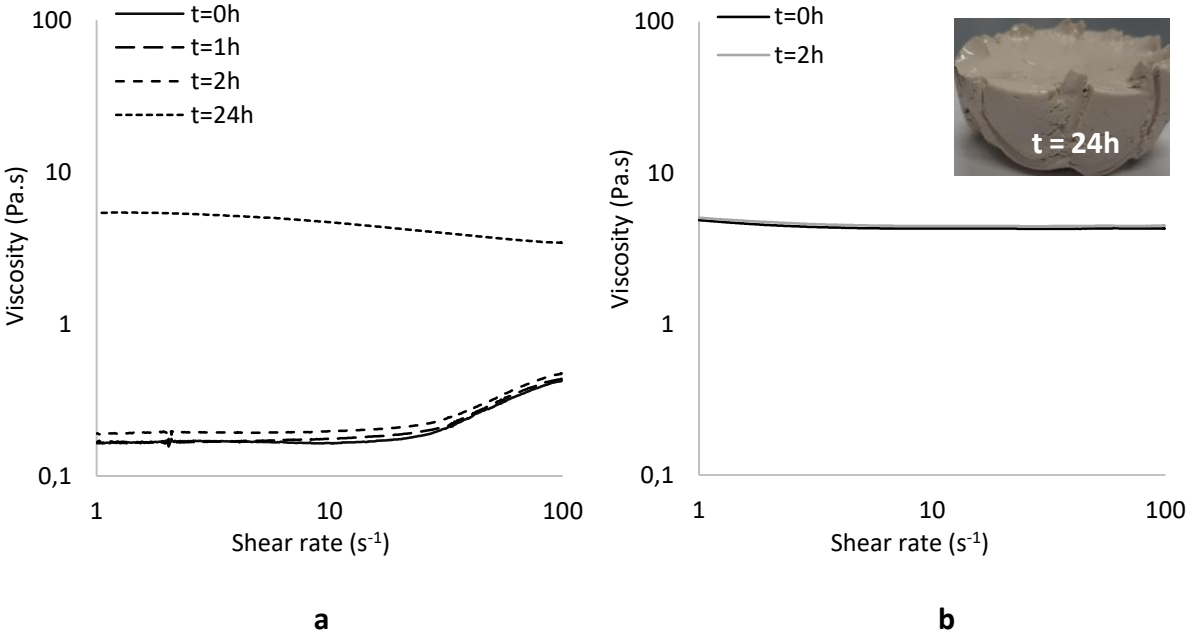

Figure 4.5: Flow curves of Durcal 5 powder suspensions. Measurements are performed at t = 0h, 1h, 2h, 24h for ϕ = 19% (a) and at t = 0h and 2h for ϕ = 41% (b) after preparation

Figure 4.4 shows that all flow curves of quartz suspensions obtained at different measurement times are superimposed. Since we do not observe a modification on flow curves, where viscosity stays stable around 0.2 Pa.s, these results suggest that quartz behaves as an inert filler material in sodium silicate solution within the duration of rheological studies. Moreover, Figure 4.5 shows that viscosities of limestone suspensions having solid volume fractions of 19% and 41% stay constant around 0.2 Pa.s and 4.5 Pa.s respectively until 2 hours after preparation, while values start to increase beyond this time. We observed a remarkable increase of viscosity with a solid volume fraction of 19% at the measurement time t =24 hours (Figure 4.5-a), while viscosity diverges after 2 hours and suspension becomes solid when solid volume fraction is 41% (Figure 4.5-b). In addition, since this second suspension has higher solid volume fraction, viscosity values obtained at t = 0h and t = 2h are higher in comparison to the same measurement times of first suspension having solid volume fraction of 19%. Although there may be a potential contribution of limestone to geopolymerisation reaction beyond 2 hours, these results suggest that limestone stays inert within the duration of rheological measurements. Therefore, we will consider only the contribution of physical properties of both limestone and quartz powders to rheological behavior of geopolymers involving these powders in their compositions.

4.1.3. Rheological behavior of sodium silicate solutions

We studied two laboratory-based sodium silicate solutions that have different reactivity levels. In order to vary reactivity levels, we prepare initially sodium silicate solutions using commercial sodium silicate solution and sodium hydroxide pellets (introduced in section 2.2.3, Chapter 2) and then we vary reactivity level of this solution by adding water and varying slightly the concentration of NaOH. Solution that has additional water will be called less reactive sodium silicate solution. We present molar ratios of both solutions in Table 4.1.

Table 4.1: Molar ratios Si/Na of sodium silicate solutions

	Si / Na
Sodium silicate solution (S_1), μ_{0_1}	0.83
Less reactive sodium silicate solution (S_2), μ_{0_2}	0.88

We obtained viscosities of sodium silicate (μ_{0_1}) and less reactive sodium silicate (μ_{0_2}) solutions around 0.055 Pa.s and 0.013 Pa.s respectively with measurement errors of 2% and 8%. Since we prepare solutions always in the same way, where they exhibit Newtonian behavior, we assume that their viscosities are stable and do not change in time.

4.1.4. Rheological behavior of geopolymer suspensions

In this section, we will present flow curves as well as the viscosity of geopolymer suspensions. First, we recall that we identified several promising binary powder couples showing the improvement of packing optimization in previous chapter. We remark that we observed similar rheological behaviors for these couples, thus presentation of each couple would be redundant. Therefore, we selected mainly two binary couples between different metakaolin powders (i.e. Argical 1200S-Metakaolin D1 and Argical 1000-Metakaolin D1) and geopolymers of grinded metakaolin powders to be presented here. We will refer to rheological behaviors of all powder couples based on different mixture types (i.e. metakaolin-metakaolin, metakaolin-limestone, metakaolin-quartz), while their individual rheological and mechanical measurement results will be presented in Appendix B. We note that geopolymer suspensions of couple Argical 1200S-Metakaolin D1 are prepared using less reactive sodium silicate solution (S_2, μ_{0_2}) at solid volume fractions of 26% and 32% and using sodium silicate solution (S_1, μ_{0_1}) at a solid volume fraction of 29%, while suspensions of all other couples are prepared using sodium silicate solution (S_1, μ_{0_1}) at different solid volume fractions. We present initially flow curves of couple Argical 1200S-Metakaolin D1 (ϕ = 26%) in Figure 4.6, while viscosity values that are identified at a shear rate of 10 s^{-1} of different mixing proportions are given in Table 4.2. The solid volume fraction of Metakaolin D1 increases in the direction of arrow given in figure.

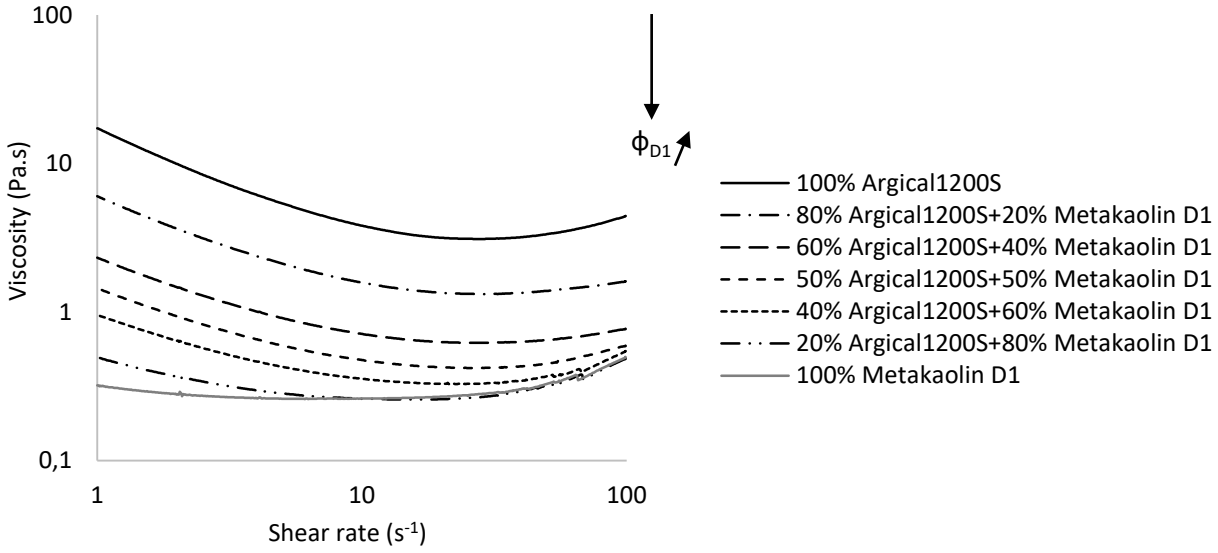

Figure 4.6: Flow curves of couple Argical 1200S-Metakaolin D1 (geopolymers are prepared using less reactive sodium silicate solution S_2 at ϕ = 26%)

Table 4.2: Viscosity and maximum packing values of all mixing proportions of couple Argical 1200S-Metakaolin D1 (ϕ = 26%)

Mixing couple	Viscosity (Pa.s)	Maximum packing fraction (ϕ_{max})
100% Argical 1200S	2.25	0.31
80% Argical 1200S+20% Metakaolin D1	1.07	0.34
60% Argical 1200S+40% Metakaolin D1	0.52	0.37
50% Argical 1200S+50% Metakaolin D1	0.36	0.38
40% Argical 1200S+60% Metakaolin D1	0.28	0.40
20% Argical 1200S+80% Metakaolin D1	0.23	0.42
100% Metakaolin D1	0.24	0.42

Figure 4.6 shows first, decreasing viscosity values of geopolymer suspensions that are identified at the plateau of flow curves when solid volume fraction of Metakaolin D1 rises in suspensions. According to the values presented in Table 4.2, we observe a decrease of viscosity around 10 times from the suspension of 100% Argical 1200S to that of 100% Metakaolin D1. Secondly, flow curves show that contribution of colloidal interactions declines also with increasing solid volume fraction of Metakaolin D1, while there is not a visible contribution of particle inertia.

Moreover, we present flow curves of couple Argical 1000-Metakaolin D1 (ϕ = 28%) in Figure 4.7, while viscosity values identified at a shear rate of 10 s^{-1} of different mixing proportions are given in Table 4.3. Solid volume fraction of Metakaolin D1 increases in the direction of arrow given in figure.

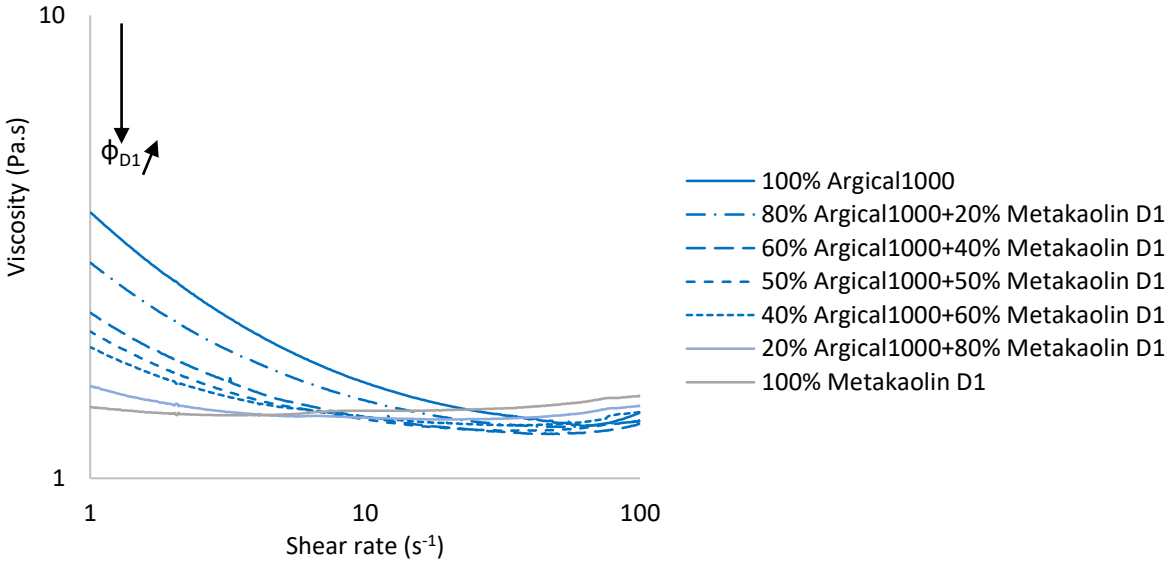

Figure 4.7: Flow curves of couple Argical 1000-Metakaolin D1 (geopolymers are prepared using sodium silicate solution S_1 at ϕ = 28%)

Table 4.3: Viscosity and maximum packing values of all mixing proportions of couple Argical 1200S-Metakaolin D1 (ϕ = 28%)

Mixing couple	Viscosity (Pa.s)	Maximum packing fraction (ϕ_{max})
100% Argical 1000	1.60	0.42
80% Argical 1000+20% Metakaolin D1	1.52	0.43
60% Argical 1000+40% Metakaolin D1	1.37	0.44
50% Argical 1000+50% Metakaolin D1	1.35	0.44
40% Argical 1000+60% Metakaolin D1	1.33	0.44
20% Argical 1000+80% Metakaolin D1	1.31	0.44
100% Metakaolin D1	1.40	0.42

Figure 4.7 shows initially a decrease of viscosity as a function of increasing solid volume fraction of Metakaolin D1, although the decrease of viscosity is less remarkable in comparison to previous metakaolin couple (see Table 4.3). We note that when solid volume fraction of Metakaolin D1 increases from 80% to 100%, viscosity starts somehow to increase smoothly. We observe a similar behavior with the couple Metamax-Metakaolin D1 (see flow curves and measurement results given in Appendix B), where viscosity increases beyond the mixing proportion of 80% Metakaolin D1. This suggests that the mixing proportion of 80% Metakaolin D1 seems optimum to achieve a minimum viscosity for both couples. Moreover, we observe from the figure that contribution of colloidal interactions declines similarly with increased solid volume fractions of Metakaolin D1 and the contribution of particle inertia in not remarkable on flow curves.

Furthermore, we present flow curves of geopolymers prepared using grinded Argical1200S (ϕ = 26%) in Figure 4.8, while viscosity values identified at a shear rate of 10 s^{-1} are given in Table 4.4. Grinding duration increases in the direction of arrow given in figure.

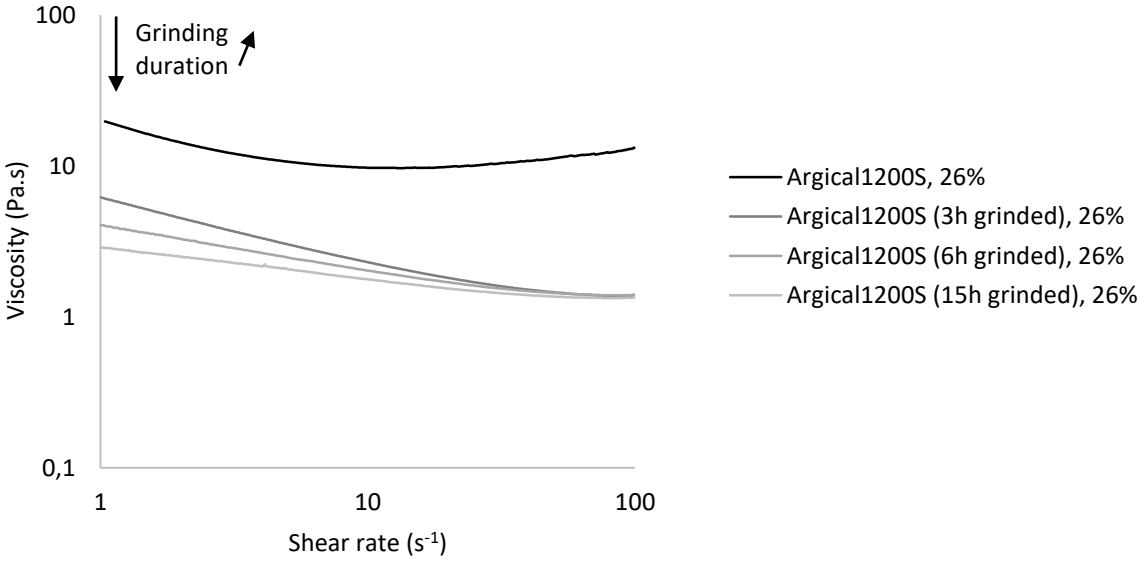

Figure 4.8: Flow curves of geopolymers prepared using grinded metakaolin (geopolymers are prepared using sodium silicate solution S_1 at ϕ = 26%)

Table 4.4: Viscosity and maximum packing values geopolymers prepared by grinded metakaolin (ϕ = 26%)

Mixing couple	Viscosity (Pa.s)	Maximum packing fraction (ϕ_{max})
Argical 1200S, without grinding	8.5	0.31
Argical 1200S, 3 hours grinding	3	0.36
Argical 1200S, 6 hours grinding	2.6	0.38
Argical 1200S, 15 hours grinding	2.3	0.40

Figure 4.8 shows initially a considerable decrease of viscosity as a function of grinding duration. We observe that viscosity declines around 4 times from geopolymer suspension of non-grinded metakaolin toward that of 15 hours grinded metakaolin (see Table 4.4). Secondly, flow curves show that contribution of colloidal interactions declines also with increasing grinding duration, while there is not a visible contribution of particle inertia.

In addition to presented metakaolin couples as well as the grinded metakaolin, we present viscosities of geopolymer suspensions based on powder couples of different mixture types as a function of their solid volume fractions in Figure 4.9. Solid volume fractions of Metakaolin D1, Metakaolin D2, Durcal 5, Durcal 65 and Quartz C800 powders increase in powder composition of corresponding geopolymer suspension in the direction of arrow given in figure. For geopolymer suspensions prepared by grinded Argical 1200S, arrow direction represents the increasing grinding duration.

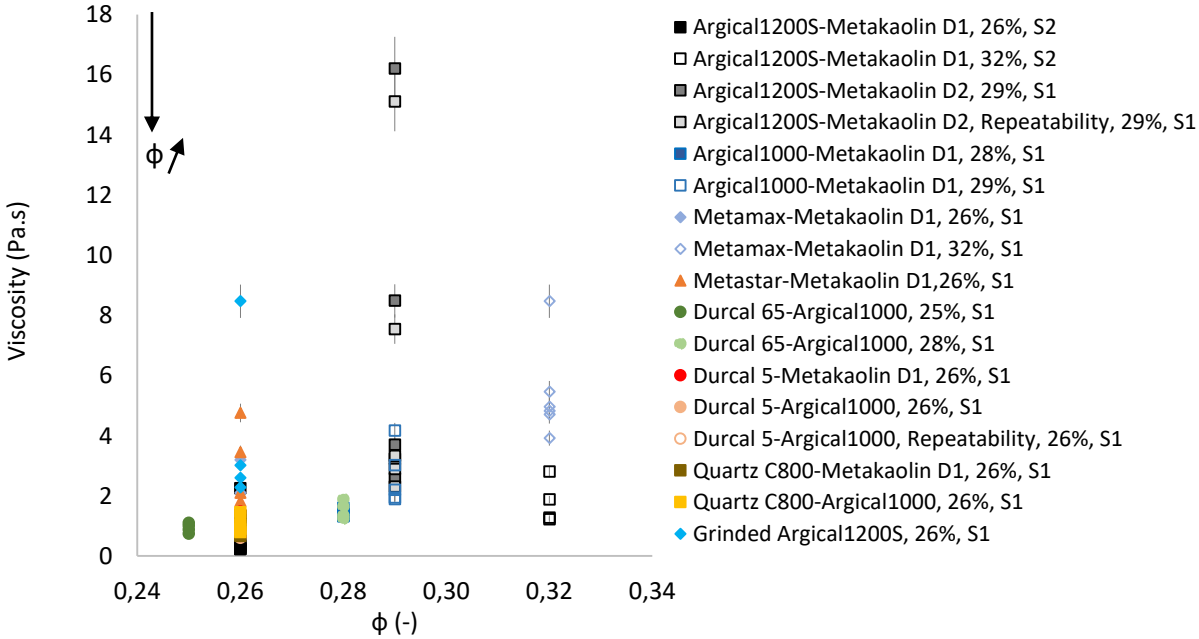

Figure 4.9: Viscosity as a function of solid volume fraction (exact values of solid volume fractions and the sodium silicate solutions used for preparations are given in legend)

Figure 4.9 shows first, at a constant solid volume fraction, viscosity of a geopolymer suspension decreases when the amount of Metakaolin D1/D2, Durcal 5/65 or Quartz C800 powders increases in the composition of this suspension. Exceptionally, for metakaolin couples Argical 1000-Metakaolin D1 and Metamax-Metakaolin D1, viscosity decreases until 80% of Metakaolin D1 since this proportions seems optimal. We recall that beyond this mixing proportion, viscosity starts to increase slightly. Moreover, whatever the value of solid volume fraction of the same powder couple, as soon as this value is constant, viscosity decreases with increasing amount of Metakaolin D1/D2, limestone or quartz in this couple. We note that rheological measurements of all studied geopolymer suspensions are repeatable and the viscosity values presented here have a standard error around 6.5%. According to these results, we observe that viscosity changes remarkably. In the following section, we will present effect of the maximum packing improvement on the variation of viscosity.

4.1.5. Correlation between rheological measurement results and maximum packing fractions of geopolymers

Before we show a correlation between rheological behaviors and maximum packing fractions of studied geopolymer suspensions, we present primarily the rheological results obtained for couples Argical 1200S-Metakaolin D1 (26%) and Argical 1000-Metakaolin D1 (28%) as well as the grinded metakaolin in previous section as a function of their maximum packing fractions in Figure 4.10. Solid volume fraction of Metakaolin D1 or grinding duration increases in the direction of arrow given in figure.

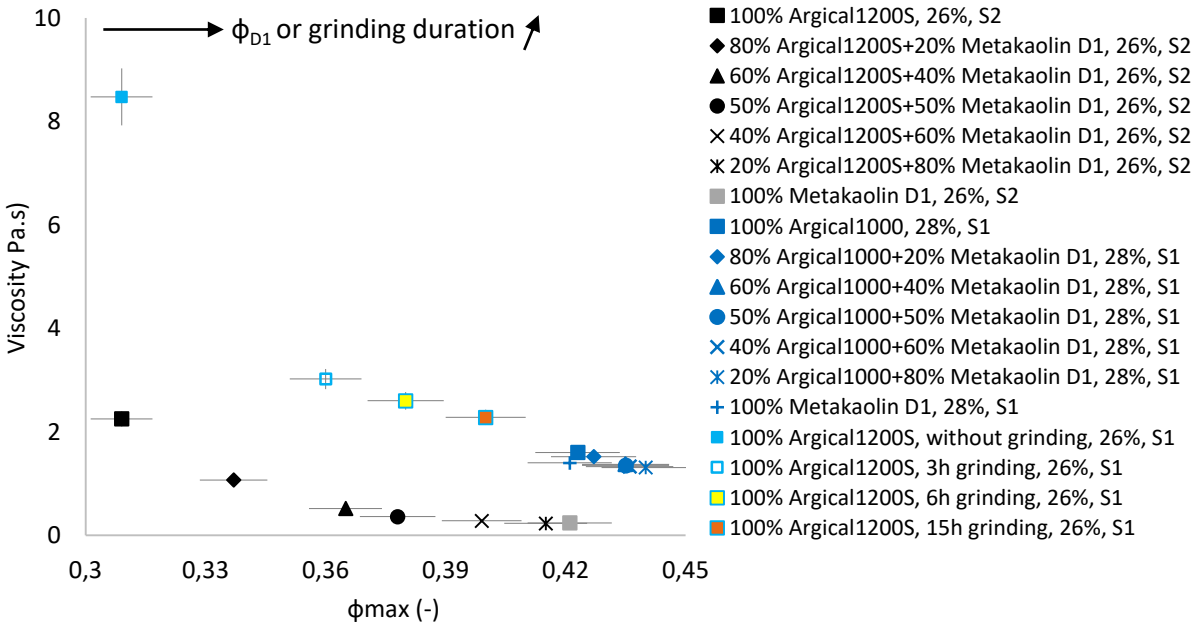

Figure 4.10: Viscosity as a function of maximum packing density (solid volume fractions and the sodium silicate solutions used for preparation of geopolymers are given in legend)

Figure 4.10 shows that viscosity of geopolymer suspensions prepared based on binary metakaolin couples or grinded metakaolin powders decreases as a function of increasing maximum packing fractions. Decrease of viscosity is more remarkable for couple Argical 1200S-Metakaolin D1 (26%) than the couple Argical 1000-Metakaolin D1 (28%). Moreover,

the optimum mixing proportion of the latter couple is captured by the maximum packing density.

In addition to these metakaolin couples and grinded metakaolin powders, we also observed decreasing viscosity values with rising maximum packing fractions of geopolymer suspensions that are produced using different types of powder mixtures (see Appendix B). These results suggest that the improved packing fractions could be the main responsible for observed viscosity decrease. Since Krieger-Dougherty model describes a rheological behavior, where viscosity of concentrated suspensions (μ) decreases with increasing maximum packing fractions (ϕ_{max}) at a constant solid volume fraction (ϕ), our results suggest that rheological behavior of studied geopolymer suspensions could be captured well by Krieger-Dougherty model. In order to show whether this model is suitable to represent rheological behavior of studied geopolymers, we present relative viscosity values as a function of relative solid volume fractions of studied geopolymer suspensions in Figure 4.11. Here, relative viscosity is the ratio between viscosity of geopolymer suspension and sodium silicate solution that is used to prepare this suspension, while relative solid volume fraction is the ratio between solid volume fraction of geopolymer suspension that is fixed and maximum packing fraction of corresponding mixing proportion.

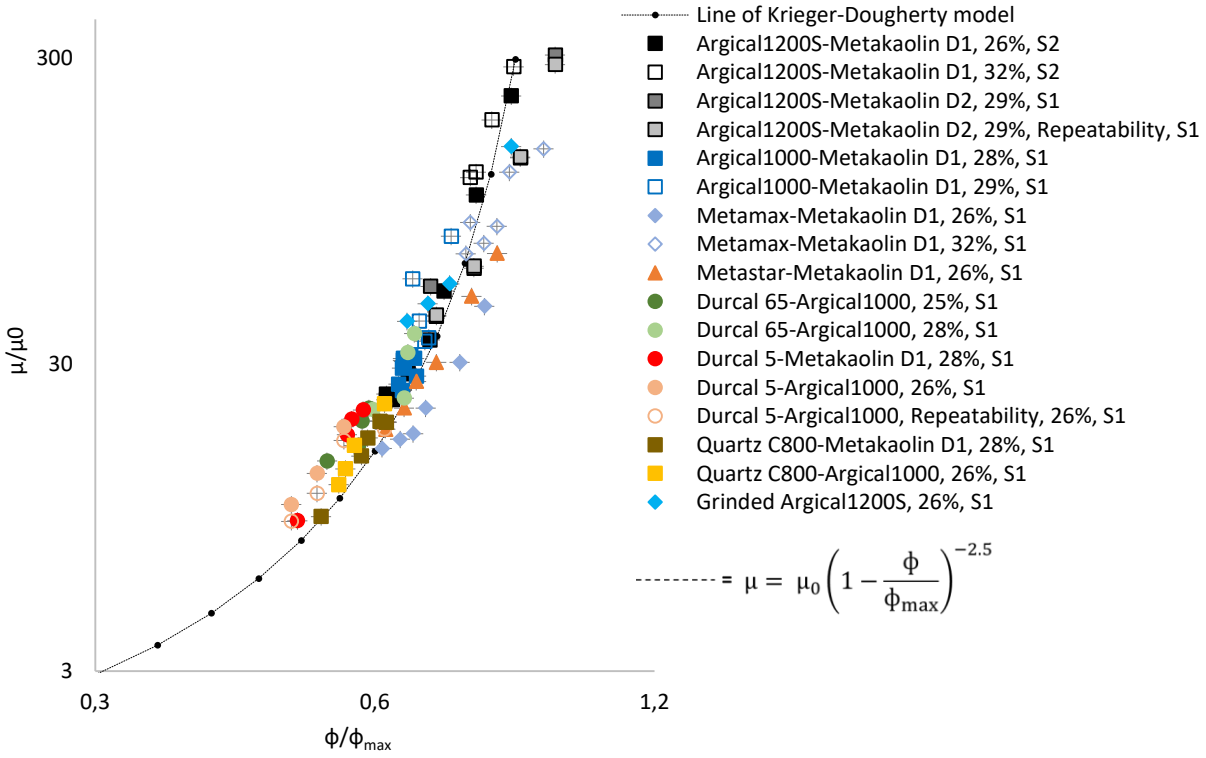

Figure 4.11: Relative viscosity as a function of relative solid volume fraction (solid volume fractions and the sodium silicate solutions used for preparation of geopolymers are given in legend)

Figure 4.11 shows that rheological measurement results of studied geopolymer suspensions align throughout the curve of Krieger-Dougherty model. We note that Krieger-Dougherty is an empirical model, where the value of q depends on the shape of solid particles that are present

in concentrated suspensions. This value is found as 2.5 for the materials used in this thesis. As we observe that rheological measurement results fit well with Krieger-Dougherty model, we can conclude that this model predicts well the evolution of relative viscosity of studied geopolymers as a function of their relative solid volume fractions. We recall that we vary type of binary mixtures, where the nature of powders change, viscosity of sodium silicate solution and solid volume fractions of geopolymer suspensions. In this case, capturing all rheological results with Krieger-Dougherty model means that this model actually works well to predict the evolution of viscosity with the improvement of maximum packing fractions in all conditions where viscosity of alkaline solution, solid volume fractions or the modification of nature of solid materials used to produce geopolymers change. Therefore, we can conclude that our results are in correlation with Krieger-Dougherty model and this model allows to control viscosity of geopolymers only by developing their packing fractions, while keeping a stable chemical formulation. However, decreasing the viscosity would not always be enough to control final behavior of geopolymers. Maintaining a good mechanical performance is also necessary while reducing viscosity.

We presented that viscosity of geopolymers decreases with increasing maximum packing density and the model Krieger-Dougherty predicts well the rheological behavior of geopolymers. In the following section, we will present the effect of optimization of maximum packing fractions as well as the effect of modifying molar ratios and viscosity of sodium silicate solution on mechanical strength of geopolymers.

4.2. Influence of particle packing optimization on mechanical properties

In this section, we will introduce initially protocols that are used for mechanical measurements and then we will present the evolution of flexural and compressive strength of geopolymers over time. Afterwards, we will show the effect of improvement of maximum packing density as well as the modification of molar ratios on flexural and compressive strength of geopolymer suspensions, which are prepared based on metakaolin-metakaolin, metakaolin-limestone and metakaolin-quartz mixtures.

4.2.1. Protocols of mechanical measurements

For mechanical measurements, we prepare initially geopolymer suspensions using the preparation protocol introduced in the beginning of this chapter (see section 4.1.1). After preparation, we fill each geopolymer suspension into a rectangular mold having dimensions 4 cm x 4 cm x 16 cm and we cover the upper surface of sample in order to avoid evaporation. A day after casting geopolymer samples, we demold samples, place them into a plastic bag and keep this bag closed until 7 days or 28 days. In the end of these durations, we perform mechanical flexion and compression tests with respect to the EN196-1 norm using Controls Pilot 4 Automatic Instrument. For flexion tests, we produce three samples for each geopolymer suspension and we perform 3-point flexion tests, where the distance between supports is 10 cm and the displacement rate of press is 50 N/s. For compression tests, we use

the same samples that are broken into two pieces after flexion tests. Hence, for each sample, we perform six compressive strength measurements, where displacement rate of press is 2400 N/s.

4.2.2. Evolution of mechanical strength over time

We present mechanical strength of geopolymers over time in Figure 4.12. Figure represents the evolution of compressive and flexural strength of geopolymer samples prepared by powder couples between Metakaolin D1-Durcal 5 (26%) and Argical 1000-Durcal 65 (25%) as a function of solid volume fractions of Durcal 5/65. We recall that samples of both couples are prepared using sodium silicate solution (S_1, μ_{0_1}) and we note that compressive and flexural strength measurements of both couples are repeatable with a standard error values around 10% and 20% respectively.

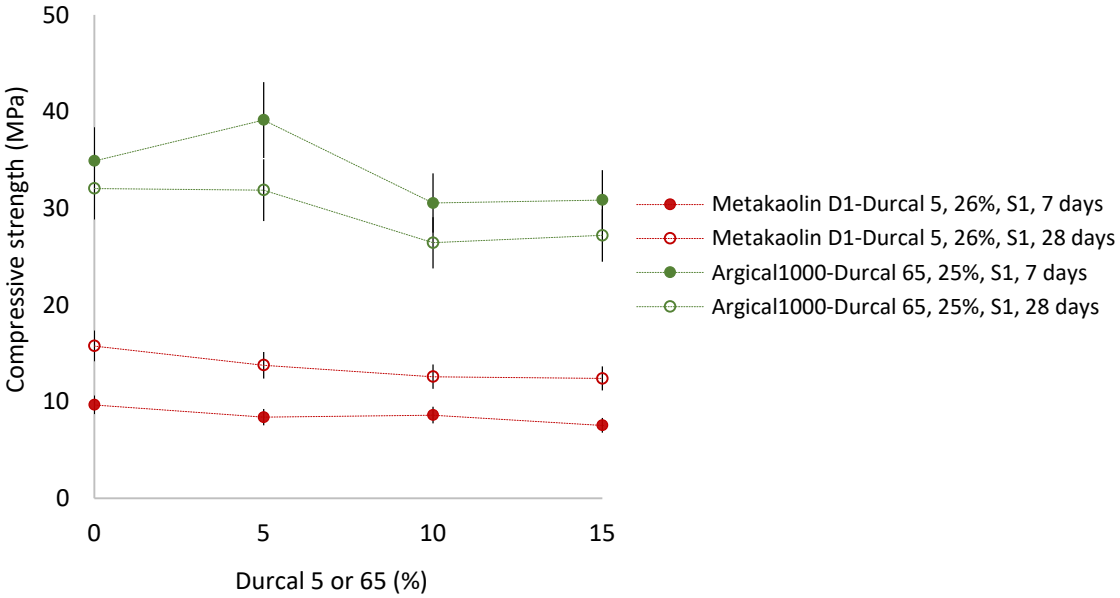

a

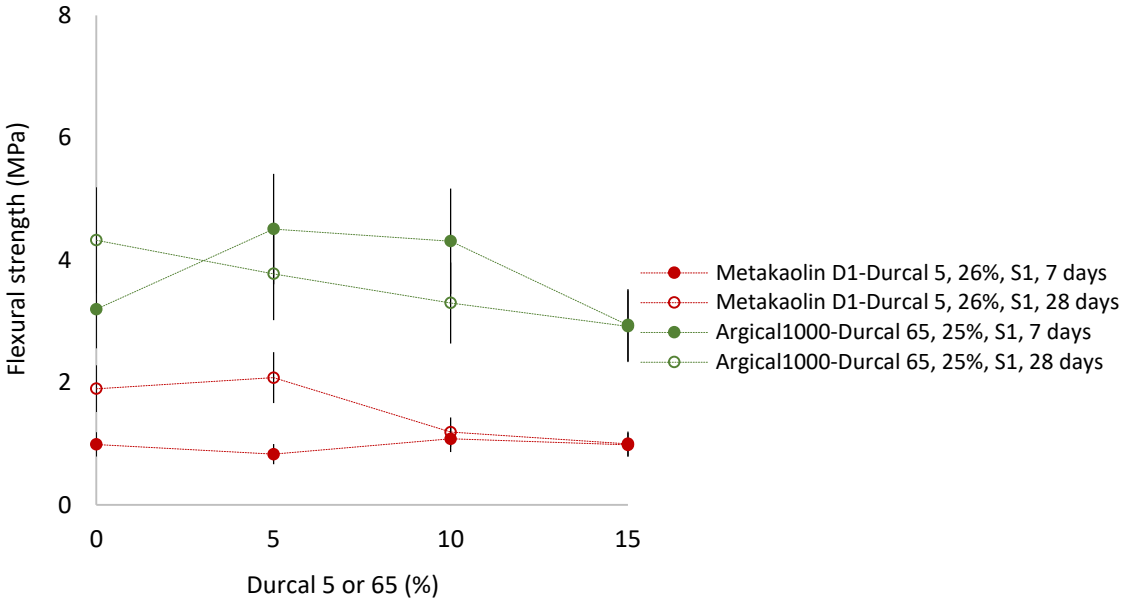

b

Figure 4.12: Compressive (a) and flexural strength (b) of geopolymer suspensions over time (solid volume fractions and the sodium silicate solutions used for preparation of geopolymers are given in legend)

Figure 4.12 shows first, similar compressive and flexural strength values for geopolymer sample of 100% Argical 1000 over time, while these values seem increasing slightly (i.e. from 10 MPa to around 15 MPa) for geopolymer sample of 100% Metakaolin D1 from 7 to 28 days after preparation. However, variations are within the range of standard error, thus we can deduce that compressive and flexural strength of a metakaolin-based geopolymer does not evolve considerably over time, which is coherent with what is observed in literature [3]. Secondly, compressive and flexural strength of geopolymers involving different amounts of Durcal 65 limestone powder in their compositions have decreasing trends over time. Moreover, compressive strength of geopolymers prepared with different mixture proportions of Durcal 5 limestone powder tend to increase over time, while flexural strength of these geopolymers have both increasing and decreasing trends from 7 to 28 days after preparation. Although mechanical strength values of geopolymers including limestone powders vary slightly over time, these variations follow the same trends as a function of limestone proportions. Therefore, we decided to perform mechanical strength measurements after 7 days of preparation for the rest of geopolymer couples. In the following sections, we present mechanical properties of geopolymers that are prepared based on different mixture types, where we will also discuss observed mechanical behaviors in detail in terms of improvement of packing optimization and variation of sodium silicate solution.

4.2.3. Mechanical properties of geopolymers based on mixtures between two metakaolin powders

We present initially compressive and flexural strength of geopolymers based on mixtures between two different metakaolin powders as a function of the solid volume fraction of Metakaolin D1/D2 in Figure 4.13, while the obtained values are presented in Table 4.5.

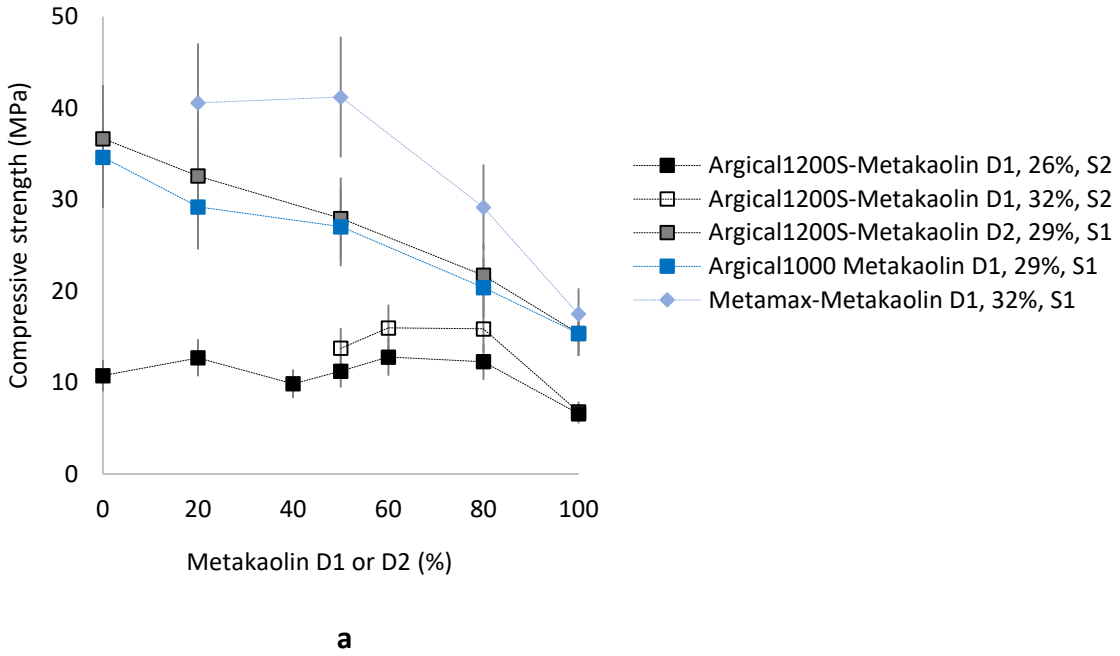

a

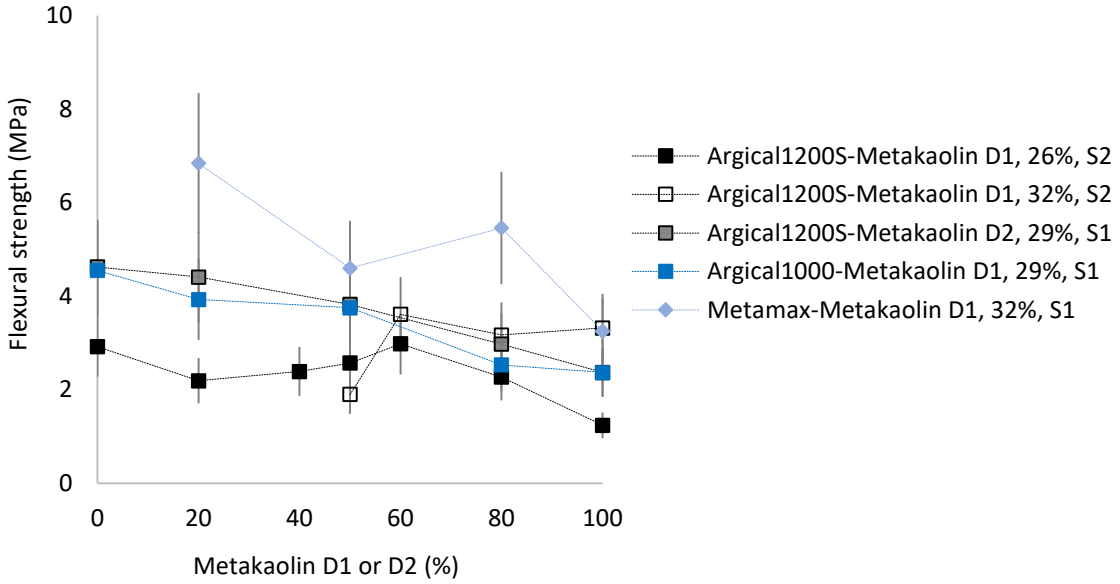

b

Figure 4.13: Compressive (a) and flexural strength (b) of geopolymer suspensions over time (solid volume fractions and the sodium silicate solutions used for preparation of geopolymers

are given in legend, standard error values for compressive and flexural strength are 16% and 22% respectively)

Table 4.5: Mechanical strength and maximum packing values of geopolymers based on binary metakaolin mixtures (solid volume fractions and the sodium silicate solutions used for preparation of geopolymers are given in legend)

Powder couple	**Maximum packing density Φ_{max}**	**Compressive strength (MPa)**	**Flexural strength (MPa)**
100% Argical 1200S, 26%, S2	0.31	10.77	2.92
80% Argical 1200S+20% Metakaolin D1, 26%, S2	0.34	12.71	2.19
60% Argical 1200S+40% Metakaolin D1, 26%, S2	0.37	9.88	2.39
50% Argical 1200S+50% Metakaolin D1, 26%, S2	0.38	11.26	2.57
40% Argical 1200S+60% Metakaolin D1, 26%, S2	0.40	12.80	2.98
20% Argical 1200S+80% Metakaolin D1, 26%, S2	0.42	12.28	2.27
100% Metakaolin D1, 26%, S2	0.42	6.61	1.24
50% Argical 1200S+50% Metakaolin D1, 32%, S2	0.38	13.77	1.90
40% Argical 1200S+60% Metakaolin D1, 32%, S2	0.40	15.98	3.61
20% Argical 1200S+80% Metakaolin D1, 32%, S2	0.42	15.87	3.17
100% Metakaolin D1, 32%, S2	0.42	6.82	3.32
100% Argical 1200S, 29%, S1	0.31	36.66	4.62
80% Argical 1200S+20% Metakaolin D2, 29%, S1	0.34	32.58	4.41
50% Argical 1200S+50% Metakaolin D2, 29%, S1	0.38	27.95	3.82
20% Argical 1200S+80% Metakaolin D2, 29%, S1	0.42	21.74	2.97
100% Metakaolin D2, 29%, S1	0.42	15.39	2.37
100% Argical 1000, 29%, S1	0.42	34.63	4.55
80% Argical 1000+20% Metakaolin D1, 29%, S1	0.43	29.21	3.93
50% Argical 1000+50% Metakaolin D1, 29%, S1	0.44	27.04	3.75
20% Argical 1000+80% Metakaolin D1, 29%, S1	0.44	20.39	2.53
100% Metakaolin D1, 29%, S1	0.42	15.39	2.37
80% Metamax+20% Metakaolin D1, 32%, S1	0.35	40.57	6.84
50% Metamax+50% Metakaolin D1, 32%, S1	0.39	41.21	4.60
20% Metamax+80% Metakaolin D1, 32%, S1	0.43	29.18	5.46
100% Metakaolin D1, 32%, S1	0.42	17.50	3.25

Figure 4.13 shows first, a stable compressive strength until a certain mixing proportion of Metakaolin D1 (i.e. aroud 80%) when geopolymers are prepared using less reactive sodium silicate solution (S_2). We observe that compressive and flexural strength of couple Argical1200S-Metakaolin D1 (26% and 32%) stay stable around 15 MPa and 3 MPa respectively

although solid volume fraction of suspensions and solid volume fraction of Metakaolin D1 in the composition of suspensions vary. However, when mixing proportion of Metakaolin D1 becomes greater than 80%, compressive strength starts to decline. Secondly, mechanical strength of geopolymers prepared using sodium silicate solution (S_1) and different metakaolin powder couples have decreasing tendancies as a function of Metakaolin D1/D2. We observe that compressive strength of couples prepared by sodium silicate solution (S_1) decline remarkably (i.e. from 40 MPa to 15 MPa) with increasing amount of Metakaolin D1/D2 in geopolymer composition, while flextural strenth of these geopolymer decreases slightly.

Moreover, we present compressive and flexural strength of geopolymers based on mixtures between two different metakaolin powders as a function of their molar ratios Si/Al and Na/Al in Figure 4.14. We note that solid volume fraction of Metakaolin D1/D2 increases in the direction of arrow given in figure.

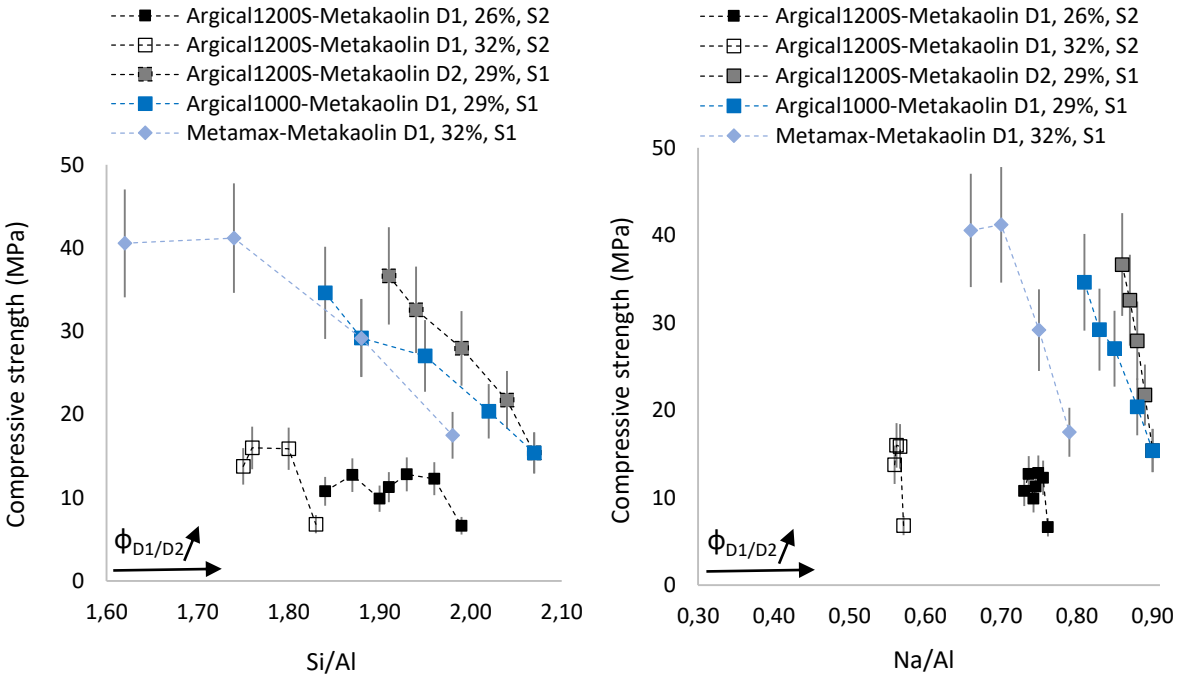

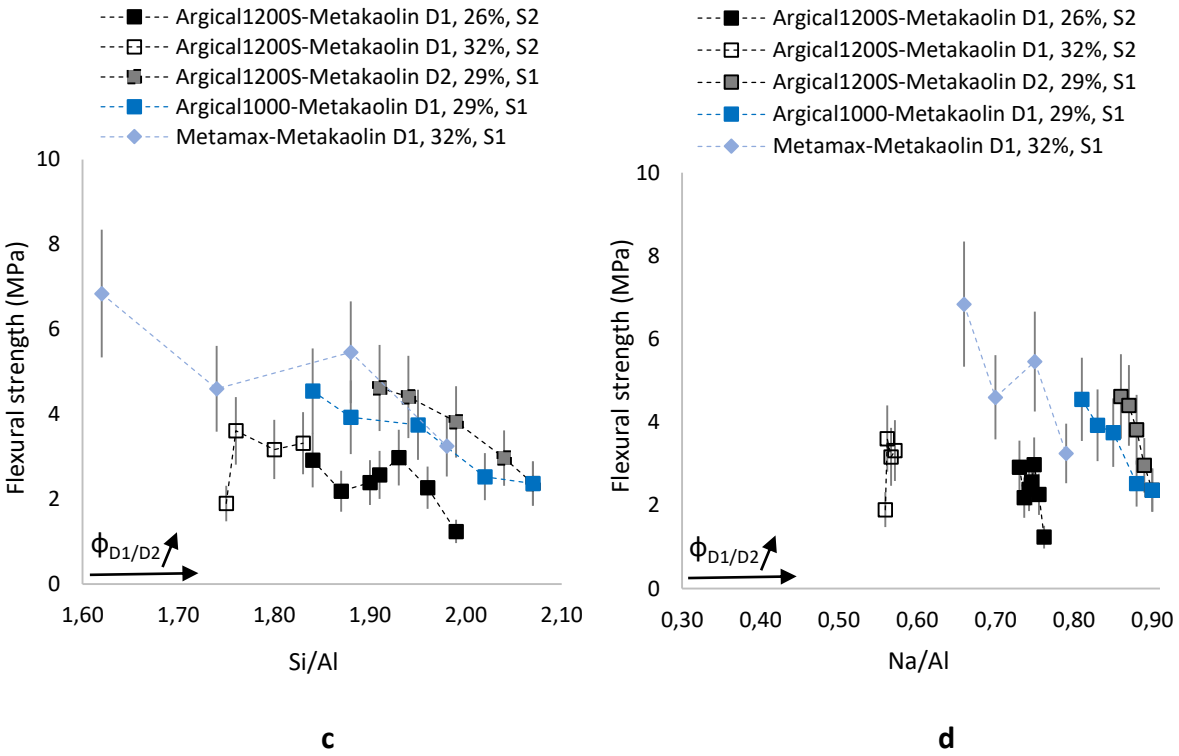

Figure 4.14: Compressive (a and b) and flexural (c and d) strength of geopolymer suspensions of metakaolin powder couples after 7 days (solid volume fractions and the sodium silicate solutions used for preparation of geopolymers are given in legend, standard error values for compressive and flexural strength are 16% and 22% respectively)

Figure 4.14 shows first, a stable mechanical strength as a function of Si/Al molar ratio when binary mixture of metakaolin-based geopolymer suspensions are prepared using less reactive sodium silicate solution (S_2). We observe that compressive and flexural strength of couple Argical1200S-Metakaolin D1 (26% and 32%) stay around 15 MPa and 3 MPa respectively, although the molar ratios of suspension vary. Secondly, mechanical strength of geopolymers prepared using sodium silicate solution (S_1) and different metakaolin powder couples decreases with increasing molar ratios of Si/Al and Na/Al. We observe that compressive and flexural strength of couples prepared by sodium silicate solution (S_1) decline remarkably beyond the value of Si/Al = 1.9. These results are in correlation with what is observed in literature [4], where a deterioration of mechanical strength is reported after Si/Al = 1.9. In addition to molar ratios, mechanical strength of these geopolymers decreases also with increasing solid volume fraction of Metakaolin D1/D2 in their compositions, thus with increasing maximum packing fractions (see values given in Appendix B).

Theoretically, improvement of maximum packing density must lead to decrease of porosity and a formation of a dense and robust structure. Several studies in literature mentioned the improvement of mechanical performance of cementitious materials due to optimization of their packing density [5, 6]. In this case, these results suggest that obtained mechanical behavior of geopolymers could be due to a combined impact of simultaneous variations of molar ratios and maximum packing fractions. Therefore, individual influence of packing optimization on mechanical perfomance of geopolymers cannot be inferred from these

results. However, presentation of mechanical properties of geopolymers based on grinded metakaolin powders could represent well the individual effect of packing optimization on mechanical performance. Since these geopolymers are prepared using the same metakaolin powder and sodium silicate solution, the only variable is the changing maximum packing fractions, thus its impact could be captured alone. Consequently, we present mechanical properties of geopolymers produced using grinded Argical 1200S powder in following section.

4.2.4. Mechanical properties of geopolymers based on grinded metakaolin powders

We present compressive and flexural strength of geopolymers prepared using grinded metakaolin powders as a function of their maximum packing fractions in Figure 4.15. As mentioned, these geopolymers are prepared with the same metakaolin (i.e. Argical 1200S) and sodium silicate solution (S_1). Therefore, their molar ratios are constant, where Si/Al = 2.05 and Na/Al = 1.03. We confirm the repeatability of measurements with standard error values around 13% and 8.5% for compressive and flexural strengths respectively.

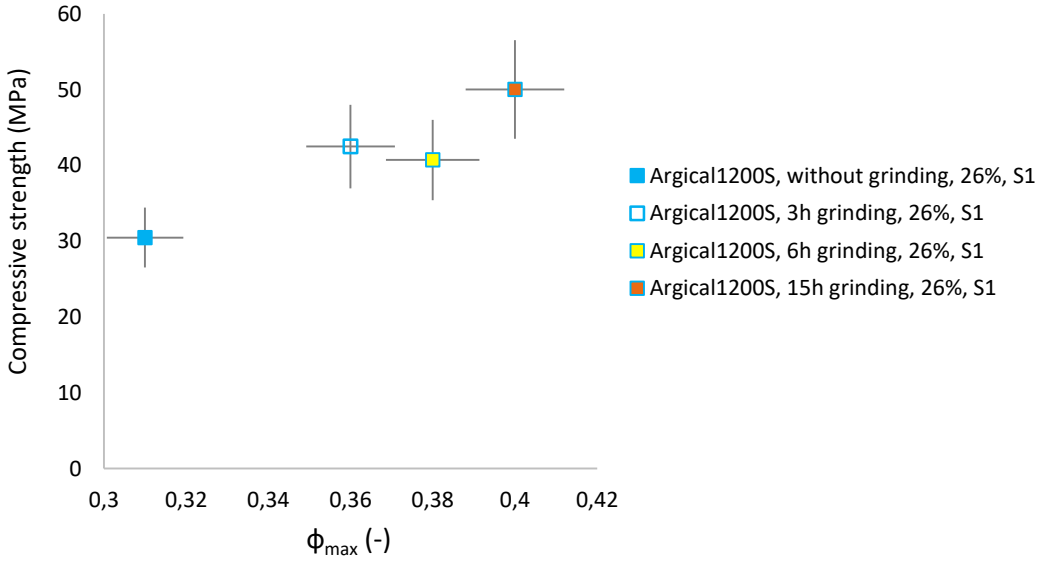

a

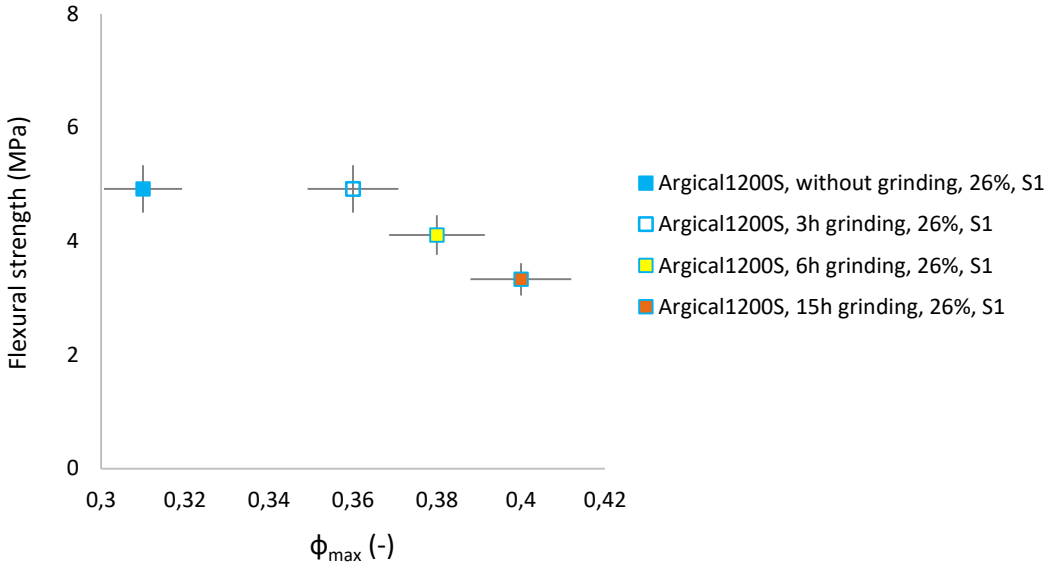

b

Figure 4.15: Compressive (a) and flexural (b) strength of geopolymers based on grinded metakaolin after 7 days (samples prepared by sodium silicate solution S_1 at ϕ=26%)

Figure 4.15 shows first, an increasing compressive strength of a geopolymer based on grinded metakaolin with increasing maximum packing fraction, while maximum packing fraction itself increases with prolonged grinding duration. Secondly, flexural strength of this geopolymer tends to decrease when the value of its maximum packing density extends to 36%. The improvement of compressive strength could have both physical and chemical origins. First, grinding a solid precursor could lead to enlargement of its specific surface, where increased specific surface could serve as expanded nucleation sites for reaction products, thus could contribute to formation of reaction products and enhancement of mechanical performance [7, 8]. Second, grinding could lead to improved packing density, thus formation of a denser structure and the development of mechanical performance [8, 9]. In addition to physical origins, several studies have reported that dissolution degree of solid precursors used to produce geopolymers (i.e. particularly aluminates) becomes higher when they are grinded [10, 11]. Depending on the instrument used for grinding, sufficient amount of energy transferred to solid material during grinding could result in the transformation of crystalline phases in its composition to X-Ray amorphous phases so that leaching of the aluminum would be simpler [12, 13]. Formation of amorphous phases could also explain the decrease of flexural strength of geopolymers when their precursors are grinded [14]. Observed mechanical behavior of geopolymers based on grinded metakaolin powders suggest that when the effect of maximum packing density on mechanical properties is captured alone with increasing grinding durations at a stable chemical composition, compressive strength of geopolymers increases. Hence, results obtained in previous section could be related more on the variation of molar ratios of geopolymers. According to mechanical results obtained from the geopolymers of grinded metakaolin powders, we can conclude that grinding is an alternative method for optimization of maximum packing density, thus the amelioration of mechanical performance of geopolymeric materials while maintaining their chemical formulations stable. In the following

section, we will present mechanical properties of geopolymers based on metakaolin-limestone or metakaolin-quartz powder mixures.

4.2.5. Mechanical properties of geopolymers based on metakaolin-limestone or metakaolin-quartz mixtures

We present initially compressive and flexural strength of geopolymers based on mixtures between metakaolin and limestone or metakaolin and quartz powders as a function of the solid volume fraction of Durcal 5/65 or Quartz C800 in Figure 4.16, while the obtained values are presented in Table 4.6.

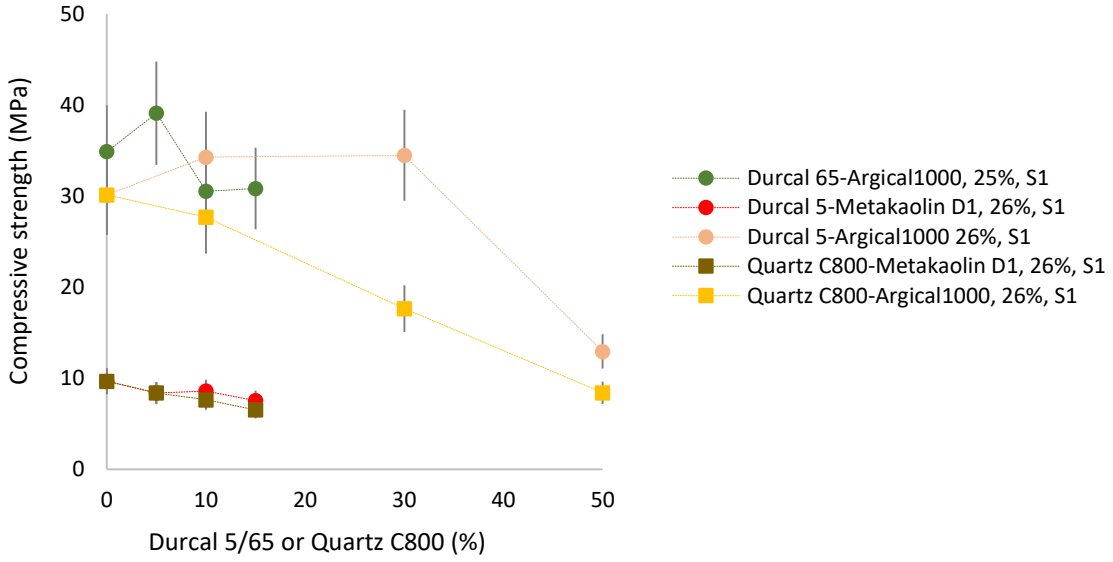

a

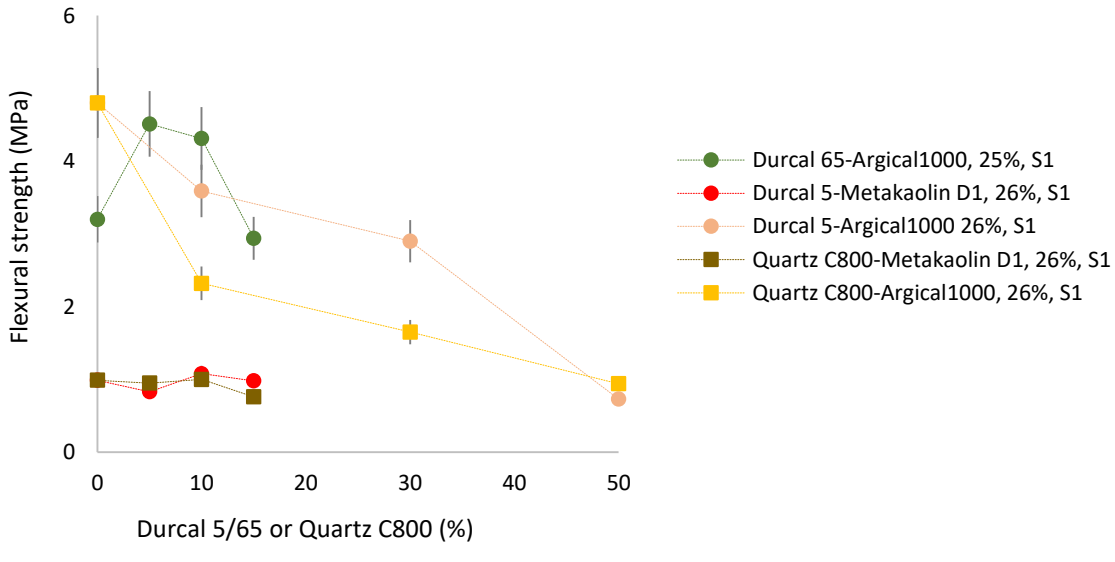

b

Figure 4.16: Compressive (a) and flexural strength (b) of geopolymer suspensions over time (solid volume fractions and the sodium silicate solutions used for preparation of geopolymers are given in legend, standard error values for compressive and flexural strength are 14.5% and 10% respectively)

Table 4.6: Mechanical strength and maximum packing values of geopolymers based on metakaolin-limestone and metakaolin-quartz mixtures (solid volume fractions and the sodium silicate solutions used for preparation of geopolymers are given in legend)

Powder couple	**Maximum packing density Φ_{max}**	**Compressive strength (MPa)**	**Flexural strength (MPa)**
100% Argical 1000, 25%, S1	0.42	34.90	3.20
95% Argical 1000+5% Durcal 65, 25%, S1	0.43	39.12	4.51
90% Argical 1000+10% Durcal 65, 25%, S1	0.43	30.54	4.31
85% Argical 1000+15% Durcal 65, 25%, S1	0.47	30.85	2.94
100% Metakaolin D1, 26%, S1	0.42	9.67	0.99
95% Metakaolin D1+5% Durcal 5, 26%, S1	0.44	8.40	0.83
90% Metakaolin D1+10% Durcal 5, 26%, S1	0.46	8.61	1.08
85% Metakaolin D1+15% Durcal 5, 26%, S1	0.46	7.55	0.98
100% Argical 1000, 26%, S1	0.42	30.13	4.80
90% Argical 1000+10% Durcal 5, 26%, S1	0.43	39.12	4.51
70% Argical 1000+30% Durcal 5, 26%, S1	0.43	30.54	4.31
50% Argical 1000+50% Durcal 5, 26%, S1	0.47	30.85	2.94
100% Metakaolin D1, 26%, S1	0.42	9.67	0.99
95% Metakaolin D1+5% Quartz C800, 26%, S1	0.43	8.39	0.95
90% Metakaolin D1+10% Quartz C800, 26%, S1	0.44	7.63	1.00
85% Metakaolin D1+15% Quartz C800, 26%, S1	0.45	6.54	0.76
100% Argical1000, 26%, S1	0.42	30.13	4.80
90% Argical1000+10% Quartz C800, 26%, S1	0.46	27.70	2.32
70% Argical1000+30% Quartz C800, 26%, S1	0.47	17.65	1.65
50% Argical1000+50% Quartz C800, 26%, S1	0.47	8.41	0.94

Figure 4.16 shows first, decreasing compressive strength values for couples of Metakaolin D1, while flexural strength of these couples are stable as a function of solid volume fraction of Durcal 5 or Quartz C800 powders. Secondly, these couples have lower mechanical strength than the couples prepared using Argical1000. Moreover, compressive strength values of geopolymers based on Argical1000 and a limestone powder are stable until a certain amount of limestone addition, where these couples provide the highest strength values. We observe that beyond 30% of limestone addition, compressive strength of geopolymers decrease.

Incorporation of quartz powder into a geopolymer composition supplies also good compressive strength when the addition amount of quartz is lower (i.e. below 30%). However, compressive strength decreases with increasing amount of quartz powder. Flexural strength of geopolymers prepared using Argical1000 have increasing and decreasing trends as a function of Durcal 5/65 or Quartz C800 mixing proportions. Decreasing mechanical strength could be explained by the decreasing aluminum quantity while a part of metakaolin is substitutued by a limestone or a quartz powder. Hence, decreasing aluminum amount triggers probably formation of a weaker gel network, thus less mechanical strength. We presented the values of compressive and flexural strength of geopolymers based on metakaolin-limestone or metakaolin-quartz mixtures with their molar ratios Si/Al and Na/Al and with the improvement of maximum packing density in Appendix B. Since we assume that limestone and quartz powders behave more like filler materials in an alkaline geopolymer medium, we do not consider their presence for calculations of molar ratios.

In addition to these results, we recall that compressive strength of a geopolymer involving limestone in its composition could tend to increase or decrease over time depending on the type of limestone used for its production (see Figure 4.12 in section 4.2.2). In this case, although a limestone or a quartz powder does not show an evident participation to chemical reaction during early geopolymerisation, observed mechanical behaviors from metakaolin-limestone couples suggest that limestone powders participate probably to geopolymerisation reaction and result in different mechanical properties. In case when a decrease of compressive strength is observed in presence of limestone powder, this decrease could be explained by the structural modification of reaction products. Firdous et al. [15] observed that chemical structure of some reaction products of limestone (e.g. thermonatrite) in an alkaline medium varies over time and applies inner crystallization pressure, thus results in the weakening of geopolymer structure. In case where compressive strength of a geopolymer containing limestone increases over time, the increase of strength could be due to the increase of nucleation sites for reaction products supplied by unreacted limestone particles in the system [16]. We remark that maximum packing fractions of geopolymer couples improve with increasing mixing proportions of limestone or quartz powder (see Table 4.6). As discussed previously, improvement of maximum packing density must provide amelioration of mechanical performance. Although these results do not show a remarkable enhancement of mechanical performance with improved maximum packing density, they show that mechanical performance of geopolymers could be maintained or increased while decreasing their viscosities with mainly the addition of limestone into their compositions. Moreover, as the aluminum quantity decreases with increasing mixing proportions of limestone or quartz powders, observed results could not be dedicated to influence of improvement of maximum packing density alone. There may be possibly a combined impact of simultaneous variations of molar ratios and maximum packing fractions.

4.3. Conclusion

4.3.1. Conclusion for rheological properties

In order to show the effect of packing optimization on rheological properties of geopolymers, we presented initially measurement protocols for sodium silicate solutions and geopolymer suspensions. Afterwards, we checked that limestone and quartz powders behave as inert filler materials within the duration of rheological measurements. Therefore, we assumed only the physical contribution of these powders to optimization of maximum packing density, thus to decrease of viscosity. Later, we showed that viscosity of geopolymer suspensions that are produced using two different metakaolin powders decreases with increasing maximum packing fractions and we observed similar rheological behaviors for all studied binary powder couples with improvement of maximum packing density. We showed that our results correlate well with Krieger-Dougherty model under all the conditions where type of binary mixture, nature of powder in binary mixture, solid volume fraction of geopolymer suspension or molar ratio and viscosity of sodium silicate solution changes. Consequently, a decrease of viscosity of geopolymers by optimization of their particle packing while maintaining a stable chemical formulation is possible.

4.3.2. Conclusion for mechanical properties

We presented mechanical properties of geopolymers based on different types of binary mixtures and grinded metakaolin powders. Results showed that when geopolymers are prepared using binary mixtures between metakaolin powders, compressive strength decreases with increasing molar ratios of Si/Al, Na/Al and maximum packing density, while compressive strength of geopolymers based on metakaolin-limestone or metakaolin-quartz powders could supply maintaining or improvement of a good mechanical performance until a certain amount of mixing proportions. However, the expected enhancement of mechanical performance by packing optimization could not be captured alone due to probably a combined influence of packing optimization with variation of molar ratios. Moreover, mechanical measurement results of geopolymers prepared using grinded metakaolin powders showed well the enhancement of compressive strength with increasing maximum packing density at constant molar ratios of Si/Al and Na/Al of these geopolymers. According to these results, grinding is the most efficient method to decrease viscosity of geopolymers while keeping a good mechanical strength and a stable chemical composition. In addition, incorporation of limestone into a geopolymer composition is also a promising method to decrease viscosity while maintaining or improving mechanical strength.

References

[1] G. Ovarlez, Introduction to the rheometry of complex suspensions, Chapter 2 of the book "Understanding the rheology of concrete" Edited by N. Roussel, Woofhead Publishing Limited, 2012.

[2] H. Bessaies-Bey, "Polymères propriétés rhéologiques d'une pâte de ciment: une approche physique générique," Université Paris-Est, Champs-sur-Marne, 2015.

[3] D. Hardjito, S. E. Wallah, D. M. J. Sumajouw and B. V. Rangan, "Factors Influencing Compressive Strength of Fly-ash based Geopolymer Concrete," *Civil Engineering Dimension,* vol. 6, no. 2, pp. 88-93, 2004.

[4] P. Duxson, J. L. Provis, G. C. Lukey, S. W. Mallicoat, W. M. Kriven and J. S. J. v. Deventer, "Understanding the relationship between geopolymer composition microstructure and mechanical properties," *Colloids and Surfaces A,* vol. 269, pp. 47-58, 2005.

[5] S. A. A. M. Fennis, "Design of Ecological Concrete by Particle Packing Optimization," Delft University of Technology, Delft, Netherlands, 2011.

[6] M. Moini, I. Flores-Vivian, A. Amirjanov and K. Sobolev, "The optimization of aggregate blends for sustainable low cement concrete," *Construction and Building Materials,* vol. 93, pp. 627-634, 2015.

[7] S. Aydin, C. Karatay and B. Baradan, "The effect of grinding process on mechanical properties and alkali–silica reaction resistance of fly ash incorporated cement mortars," *Powder Technology,* vol. 197, pp. 68-72, 2010.

[8] G. Mucsi, S. Kumar, B. Csoke, R. Kumar, Z. Molnar, A. Racz, F. Madai and A. Debreczeni, "Control of Geopolymer Properties by Grinding of Land Filled Fly Ash," *International Journal of Mineral Porcessing,* vol. 143, pp. 50-58, 2015.

[9] X. Chateau, Particle packing and the rheology of concrete, from the book "Understanding the rheology of concrete" Edted by Nicolas Roussle, Woodhead Publishing Limited, 2012.

[10] H. J. H. Brouwers and R. J. V. Eijk, "Fly ash reactivity: extension and application of a shrinking core model and thermodynamic approach," *Journal of Materials Science,* vol. 37, pp. 2129-2141, 2002.

[11] X. Fu, Q. Li, J. Sheng and F. Li, "The physical–chemical characterization of mechanically-treated CFBC fly ash," *Cement and Concrete Composites,* vol. 30, pp. 220-226, 2008.

[12] J. Temuujin, K. Okada, T. S. Jadambaa, K. J. D. MacKenzie and J. Amarsanaa, "Effect of grinding on the leaching behaviour of pyrophyllite," *Journal of European Ceramic Society,* vol. 23, pp. 1277-1282, 2003.

[13] J. L. Provis and J. S. J. v. Deventer, Geopolymers. Structure, Processing, Properties and Industrial Applications, Woodhead Publishing Limited, 2009.

[14] V. I. Ivashchenko, P. E. A. Turchi, S. Veprek, V. I. Shevchenko and J. Leszczynski, "First-principles study of crystalline and amorphous AlMgB14-based materials," *Journal of Applied Physics,* vol. 119, no. 205105, 2016.

[15] R. Firdous, T. Hirsch, D. Klimm, B. Lothenbach and D. Stephan, "Reaction of calcium carbonate minerals in sodium silicate solution and its role in alkali-activated systems," *Minerals Engineering,* vol. 165, p. 106849, 2021.

[16] A. Cwirzen, J. L. Provis, V. Penttala and K. Habermehl-Cwirzen, "The effect of limestone on sodium hydroxide-activated metakaolin-based geopolymers," *Construction and Building Materials,* vol. 66, pp. 53-62, 2014.

[17] Q. Wan, Y. Zhang and R. Zhang, "Using mechanical activation of quartz to enhance the compressive strength of metakaolin based geopolymers," *Cement and Concrete Composites,* vol. 111, p. 103635, 2020.

[18] M. R. Rowles and B. O'Connor, "Chemical optimisation of the compressive strength of aluminosilicate geopolymers synthesised by sodium silicate activation of metakaolinite," *Journal of Materials Chemistry,* vol. 13, pp. 1161-1165, 2003.

[19] M. Antoni, J. Rossen, F. Martirena and K. Scrivener, "Cement substitution by a combination of metakaolin and limestone," *Cement and Concrete Research,* vol. 42, pp. 1579-1589, 2012.

[20] D. Damidot, B. Lothenbach, D. Herfort and F. P. Glasser, "Thermodynamics and cement science," *Cement and Concrete Research,* vol. 41, pp. 679-695, 2011.

[21] I. Mehdipour and K. H. Khayat, "Understanding the role of particle packing characteristics in rheo-physical properties of cementitious suspensions: A literature review," *Construction and Building Materials,* vol. 161, pp. 340-353, 2018.

[22] P. Nanthagopalan, M. Haist, M. Santhanam and H. S. Muller, "Investigation on the influence of granular packing on the flow properties of cementitious suspensions," *Cement & Concrete Composites,* vol. 30, pp. 763-768, 2008.

[23] T. Proske, S. Hainer, M. Rezvani and C. A. Graubner, "Eco-friendly concretes with reduced water and cement contents - Mix design principles and laboratory tests," *Cement and Concrete Research,* vol. 51, pp. 38-46, 2013.

[24] F. V. Mueller, O. H. Wallevik and K. H. Khayat, "Linking solid particle packing of Eco-SCC to material performance," *Cement & Concrete Composites,* vol. 54, pp. 117-125, 2014.

[25] A. Nazari and J. G. Sanjayan, Handbook of Low Carbon Concrete, Butterworth-Heinemann, Elsevier, 2017.

Chapter 5: Early reactivity of geopolymers Part I: mechanism of geopolymerisation and the development of mechanical properties of a metakaolin-based geopolymer

In this chapter, we will focus on the second objective of this thesis that is controlling the rapid setting time of geopolymers. We recall that several studies in literature investigated the use of chemical additives on setting properties of geopolymers and reported that the majority of traditional additives, which work well in the presence of ordinary Portland cement, cannot work efficiently in an alkaline medium due to primarily the variation of their chemical structure [1, 2]. Some of the studies mentioned that the use of boron or phosphor-based mineral additives could lead to prolongation of setting time due to formation of a secondary gel network, thus could be beneficial [3, 4]. In addition to use of chemical additives, controlling setting time could also be possible by modification of mixing protocol [5]. However, modifying the applied mixing protocol could induce undesirable consequences such as the increase of temperature. Today, there is not an extensive bibliographical source about the influence of mixing protocol on setting properties of geopolymers, where further investigation is needed to shed light on this phenomenon. Since we aim to prevent rapid setting without modifying chemical formulations of geopolymers, we decided to do further investigation about the impact of structural homogenization applied by the variation of mixing protocol on rheological, setting and mechanical properties of geopolymers. We divide the study into two parts, where we present first part in this chapter and the second part in the following chapter. In this chapter, we will present mainly the reaction mechanism of geopolymerisation and the development of mechanical properties of a metakaolin-based geopolymer studied by measurements of ^{27}Al Nuclear Magnetic Resonance (NMR) and oscillation rheology respectively. First, we will introduce principles of nuclear magnetic resonance and oscillation rheology and then we will present protocols of both measurements. Afterwards, we will show the evolution of reaction kinetics of a metakaolin-based geopolymer over time. At last, we will present the development of mechanical properties by showing the evolution of elastic modulus over short-term periods.

5.1. Principles of Nuclear Magnetic Resonance (NMR) Measurements

Nuclear Magnetic Resonance (NMR) is a non-destructive, spectroscopic measurement technique that is used for chemical and structural analysis [6]. It is one of the most versatile method that can be performed on the three main states of matter (i.e. liquid, solid, and gas)

under a wide range of sample conditions (e.g. temperature, pressure, concentration, morphology) [7]. Several studies in literature used NMR in order to define chemical species form during geopolymerisation [8] or to follow evolution of microstructure during geopolymerisation [6, 9, 10]. NMR spectroscopy is based on the magnetic properties of the atomic nuclei, where nuclei are positively charged and they spin in circular orbits locate around axis. Hence, they create magnetic field [11, 12]. All atomic nuclei can be characterized by a nuclear spin quantum number I, where $I \geq 0$ (i.e. $I = 0$ is NMR inactive [12]). Since $I \neq 0$, the nuclei possess an angular momentum P resulting in a magnetic moment μ (Equation 5.1) [13].

$$\mu = \gamma P \quad (5.1)$$

where γ is the gyromagnetic ratio. Spin orientations are quantified with respect to the quantum number m, which can only take a discrete number of values as:

$$m = -I, -I+1, -I+2, \ldots, I-2, I-1, I \quad [6]$$

In the ground state, all nuclear magnetic moments are randomly oriented. When an external magnetic field B_0 is applied, nuclear magnetic moments align either with or against to B_0 [12, 14]. Moreover, nuclear magnetic moment precesses about the axis of B_0 at a frequency proportional to its strength, where this precession is called Larmor Precession [6, 13]. Equation 5.2 gives the speed of Larmor Precession.

$$\omega\ (\mathrm{rad/s}) = \gamma B_0 \quad (5.2)\ [13]$$

Now let us suppose that we apply another external magnetic field B_1 perpendicular to B_0 that precesses in the x-y plane, oscillating at exactly the same frequency of ω (i.e. resonance condition). In this case, this second magnetic field B_1 will tilt the nuclear magnetization towards the transverse plain that is out of balance and the return to macroscopic balance is characterized by two relaxation times T_1 and T_2 [6]. T_1 is the spin-lattice or longitudinal relaxation time (i.e. origin is the parallel component to B_0) that indicates the return to Boltzmann equilibrium distribution [6]. The value of T_1 depends on the type of nucleus within a molecule, the dynamics of the molecule, physical state of the sample (e.g. solid or liquid) and the temperature [14]. T_2 is the spin-spin or transverse (i.e. origin is the perpendicular component to B_0) relaxation time that represents the return to a random arrangement around z axis of individual nuclear magnetic moments, which begin to lose the phase coherence acquired when B_1 is applied [14].

NMR spectrometers consist of four main sections: a magnet containing a highly homogeneous magnetic field, radio frequency transmitters and receivers and a controlling computer [11]. Radiofrequency (RF) pulses at specific frequencies and durations are pulsed at high energy into the sample, which sits inside a probe that is in the magnet. Then the receiver coil collects small currents by magnetic induction that are proportional to the sample under magnetization, amplify and digitize them into a signal that becomes ready for post-collection processing [15]. This signal is called Free Induction Decay (FID) and is transformed to the final

spectra using Fourier Transform [15]. Consequently, an NMR measurement composes of an excitation phase, where RF pulses are pulsed toward sample, and a detection phase including signal treatment [6].

Different isotopes (e.g. ^{29}Si, ^{27}Al, ^{23}Na) could be used for microstructural analysis of geopolymer suspensions. However, structural characterization by ^{27}Al NMR spectroscopy, either in liquid or solid state is the most popular since the recent progresses make the acquisition and interpretation of the corresponding NMR spectra much easier. Furthermore, ^{27}Al is an abundant (i.e. 100%) isotope with a good stability. It is also a good element to follow the incorporation of metakaolin into geopolymers since it is initially absent from the activation solution (by contrast to Na and Si). Therefore, we use ^{27}Al NMR spectroscopy to study the evolution of geopolymerisation over time.

5.2. Principles of Oscillation Rheology

Characterization of soft materials (e.g. colloidal suspensions, polymer systems) could be complicated due to their viscoelastic behavior, where their mechanical properties stand between that of purely elastic solid and purely viscous liquid [16]. Utilization of oscillatory rheology could quantify viscoelastic behavior of material [17] by quantifying both viscous-like and elastic-like properties at different time scales [16]. Therefore, it is a useful measurement technique to determine structural and dynamic properties of viscoelastic as well as the geopolymer systems. Basic principle of oscillation rheology is to apply a continuous sinusoidal excitation of either a deformation or a shear stress [18] to a viscoelastic material and measure its final response. Hence, final response of material depends on the type of applied excitation, where it responds with a stress when excitation is applied by deformation or with a deformation when excitation is applied by shear stress [18]. Depending on the material, a phase shift (i.e. delta δ, $0 < \delta < \pi/2$ [16]) occurs between applied sinusoidal signal and the response signal [18]. Phase shift of 0° means that material is purely elastic solid, while it becomes purely viscous liquid with a phase shift of 90° [17]. Viscoelastic behavior is represented by a complex shear modulus G^* (Pa) given in Equation 5.3.

$$G^* = \tau_A/\gamma_A \quad (5.3)\ [19]$$

where τ_A (Pa) is shear-stress amplitude and γ_A is strain amplitude (dimensionless, or expressed in %). The storage (or elastic) modulus G^i (Pa) represents the elastic part of complex shear modulus, while loss (or viscous) modulus G^{ii} (Pa) characterizes its viscous part. In fact, a part of deformation energy is stored in the material by stretching or extending the internal structure without destruction, while another part of this energy is used for internal friction of particles or molecules, thus transforms into heat and dissipates. This is why we call storage or loss moduli to represent elastic and viscous behaviors. Viscoelastic solids have higher elastic modulus than viscous modulus (i.e. $G^i > G^{ii}$), while viscoelastic liquids have higher viscous modulus than elastic modulus (i.e. $G^{ii} > G^i$) [19]. In order to define the transition between solid and liquid states, a loss factor (Equation 5.4) is used.

$$\tan\delta = G^{ii}/G^i \quad (5.4)\ [19]$$

where δ is the angle of phase shift. If there is phase transition during measurement, this means that the character of material changes from liquid to solid or vice versa. Therefore, it is important to determine linear elastic regime (LER) of material before measurements. LER is the regime, where applied deformation is sufficiently small so that elastic or viscous properties of material are not influenced [16, 17], thus there is no phase transition. In order to determine LER, mainly oscillatory amplitude sweeps are used, where the frequency of sinusoidal excitation signal is maintained constant but the amplitude increases gradually until the microstructure breaks down [18]. Moreover, in order to determine behavior of material in LER, oscillatory frequency sweep is used, where this time the amplitude of sinusoidal excitation signal is kept constant while the frequency increases or decreases gradually [18].

In literature, critical strain (or deformation) γ_c value (i.e. value of applied deformation below which system is in LER) is found around 0.1% for a typical metakaolin-based geopolymer suspension [6], which is slightly higher than the critical strain of a conventional Portland cement paste that is found around 0.03% [20, 21].

5.3. Measurement protocols

5.3.1. Measurement protocol of NMR

We performed static ^{27}Al NMR measurements using a Bruker Avance 500 spectrometer equipped with a commercial static broadband Bruker probe with B_0 = 11.7 T. It is mentioned in [6] that nuclear spin interactions (e.g. chemical shift, dipolar or quadrupole couplings) are anisotropic and the oscillation frequency depends on the orientations of molecules in magnetic field. When measurements are performed with liquid materials, Brownian motion (i.e. random motion of particles suspended in a fluid medium) averages this anisotropy to zero [10]. However, when measurements are performed with solid materials, anisotropy does exist and causes large broadening of spectra [10]. As we perform NMR measurements with geopolymer suspensions that are solid/liquid complex systems, we monitor especially mobile chemical species (i.e. ions, small gel) during measurement. Moreover, ^{27}Al is a quadrupolar nucleus with a spin number I = 5/2, which means that it interacts not only with B_0, but also with the electric field gradient generated by its surroundings [22]. However, this quadrupolar interaction can be neglected in liquid [10].

We prepare geopolymer suspension by mixing commercial Argical 1200S with sodium silicate solution (S_1, μ_{0_1}) at a solid volume fraction of 26% using a Dispermat LC55 mixer and the preparation protocol given in section 4.1.1.1 in previous chapter. As soon as after preparation, we place this suspension into a PTFE NMR tube having 5 mm diameter and start measurements. For measurements, we apply one pulse excitation of $\pi/2$ sequence having a recycle delay of 1 s. Pulse duration and number of scans are 3.5 µs and 80 respectively. We weight sample before and after measurements and we calibrate integrated intensities that are obtained from spectra, with respect to the integrated intensity of reference 0.1M $Al(NO_3)_3$ solution. This calibration allows to present intensity of spectra in terms of a number of moles of aluminum. In other words, we present the evolution of a representative equivalent quantity

of aluminum over time, which serves to determine dissolution and precipitation processes of geopolymerisation reaction.

5.3.2. Measurement protocol of oscillation rheology

We performed rheological measurements using a Bohlin C-Vor rheometer equipped with a vane geometry (see Figure 4.1 in previous chapter). First, we determine critical deformation γ_c in order to apply a lower deformation value to keep geopolymer sample always in linear elastic regime (LER) during measurements. In order to determine γ_c, we prepare a geopolymer suspension by mixing Argical 1200S with sodium silicate solution (S_1, μ_{0_1}) at a solid volume fraction of 26% using the same preparation protocol given in previous chapter with Turbo-Test Rayneri VMI mixer. After preparation, we transfer this suspension to rheometer. Transferring the sample to measurement cell could generate residual stresses that must be relaxed before each measurement [23]. Therefore, we apply a pre-shearing at 100 s^{-1} during 2 minutes and a period of 2 minutes resting time before measurements. Afterwards, we perform oscillatory amplitude sweeps with constant frequency of 1 Hz. According to repeatable measurement results, we determine critical deformation value as 0.001%. This value is close to what is observed in literature [23]. In order to keep samples in LER, we chose a deformation value of 0.0002% to be applied for the rest of the rheological measurements.

Secondly, we perform oscillatory rheology measurements to observe the evolution of elastic modulus over time. Preparation of geopolymer sample is the same as mentioned above. Measurement protocol consists of two stages. At first stage, we verify whether the sample is in LER after preparation using the same protocol of oscillatory amplitude sweeps (i.e. Sweep 1) introduced above. At second stage, we perform oscillation measurement and verify again whether sample is still in LER in the end of measurements (i.e. Sweep 2). We present a diagram showing the stages of oscillation measurement in Figure 5.1.

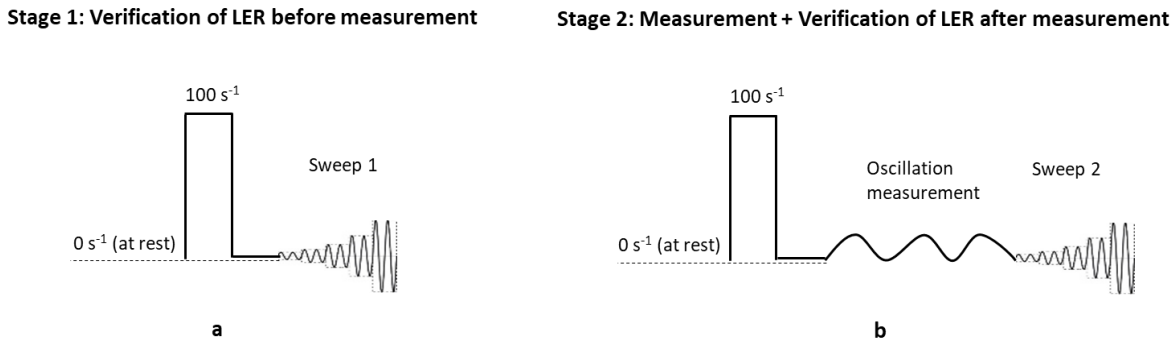

Figure 5.1: Diagram of first (a) and second (b) stage of measurement protocol

In order to perform oscillation measurement, we prepare initially geopolymer suspension and we apply 2 minutes of pre-shearing at 100 s^{-1} with 2 minutes resting time in the end. After resting time, we perform the initial oscillatory amplitude sweeps (Sweep 1, Figure 5.1-a) with constant frequency of 1 Hz to verify whether sample is in LER. After verification, we prepare a new geopolymer suspension for second stage and we perform exactly the same procedure

until the end of resting time. At the end of resting time, we perform oscillation measurement using continuous sinusoidal excitation of deformation that is defined primarily as 0.0002% during 1 hour. As soon as oscillation ends, we apply again the same oscillatory amplitude sweeps to verify state of sample (Sweep 2, Figure 5.1-b). We present storage moduli of both geopolymer suspensions prepared at first and second stages of measurement in Figure 5.2. Dashed line given in figure represents critical deformation γ_c.

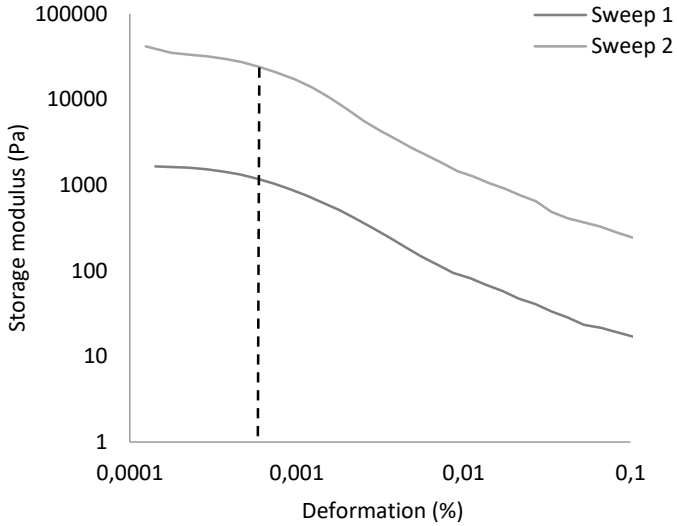

Figure 5.2: Storage modulus of a metakaolin-based geopolymer

Figure 5.2 shows that storage moduli of metakaolin-based geopolymers used during first and second stages of oscillation measurement have plateaus below critical deformation, which indicates that applied deformation value of 0.0002% does not cause a phase transition, thus geopolymer samples are in LER.

5.4. Evolution of Al concentration during early geopolymerisation

We present the evolution of an equivalent Al concentration monitored by static ^{27}Al NMR measurement over time in Figure 5.3.

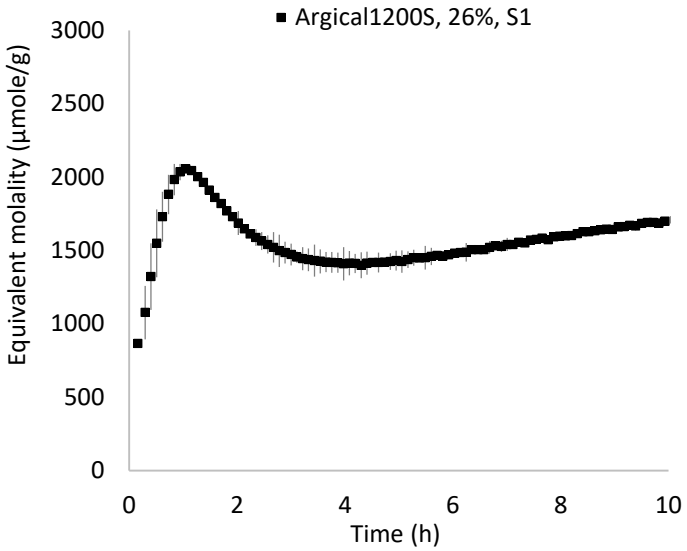

Figure 5.3: Evolution of an equivalent Al concentration over time. Time starts from the first contact of materials (standard error of measurement is 15%)

At first, the amount of Al signal (i.e. presented as equivalent molality) increases linearly as the metakaolin dissolves and releases aluminates into solution [6, 10] and reaches a maximum around 1 hour. After this moment, amount of signal decreases until 3 hours due to the polycondensation of aluminosilicates that consumes the solubilized aluminates from the dissolution of metakaolin [24]. Similar results are obtained in literature [6, 9, 10, 24]. Favier [6] refers that decrease of the equivalent Al concentration obtained from static ^{27}Al NMR measurements of a metakaolin-based geopolymer system correlates with the decrease in Na concentration due to incorporation of Na atoms into aluminosilicates reaction products. Results of Favier [6] are in correlation with the results of Aupoil [24], where an equivalent aluminum concentration of metakaolin-quartz geopolymer system is monitored using static ^{27}Al NMR. Aupoil [24] mentions that condensation of reaction products starts at the same time of dissolution and maximum amount of Al signal represents the moment when polycondensation consumes more aluminates than dissolution brings into solution. Hence, dissolution of metakaolin dominates the reaction below maximum amount of signal, while polycondensation becomes dominant beyond this moment. According to Figure 5.3, we observe that time to reach maximum amount of Al signal is around 1 hour, where the equivalent aluminum concentration is around 2000 µmole/g. This suggests that a certain concentration of aluminum is required for a geopolymer suspension to turn dominant phase from dissolution to polycondensation [24]. Moreover, Al signal obtained from measurement stays constant between 3 and 6 hours and starts to increase slightly from 6 hours over time. In fact, polycondensation provokes a drop of Al mobility that limits the dissolution [24, 25]. Consequently, reaction speed decreases. The stability between 3 and 6 hours could be associated to decrease of reaction speed, while contributions of dissolution and polycondensation neutralize each other [24]. Aluminum atoms of metakaolin have three coordination IV, V and VI, while aluminum atoms of geopolymer matrix have only a coordination IV [25]. Increase of signal from 6 hours could be related to a better excitation of aluminum atoms having IV coordination due to the cubic symmetry of the tetrahedral

environment in the geopolymer matrix [24]. Aupoil [24] has mentioned similar observations and divided the complete geopolymerisation process into 5 periods. Author mentions that dissolution of metakaolin is dominant until 2 – 3 hours (1st period), while polycondensation accelerates between 3 - 6 hours (2nd period). Later, reaction speed decreases between 6 – 8 hours (3rd period) but still contributes to structuration until 20 hours (4th period). Since this moment, author assumes that a certain stabilization of reaction occurs and geopolymer solidifies (5th period). However, geopolymer system mentioned in this study has different molar ratios (SiO_2/Al_2O_3 = 3.6; Na_2O/Al_2O_3 = 1; H_2O/Na_2O = 11.5) than our study (SiO_2/Al_2O_3 = 1.84; Na_2O/Al_2O_3 = 0.77; H_2O/Na_2O = 19.4), which could explain differences between durations of different periods of whole reaction process. In the following section, we present the evolution of elastic modulus during early geopolymerisation.

5.5. Evolution of elastic modulus during early geopolymerisation

We present the evolution of elastic modulus of a metakaolin-based geopolymer suspension over time in Figure 5.4. We note that obtained results are repeatable with a standard error value of 13% and presented in logarithmic scale.

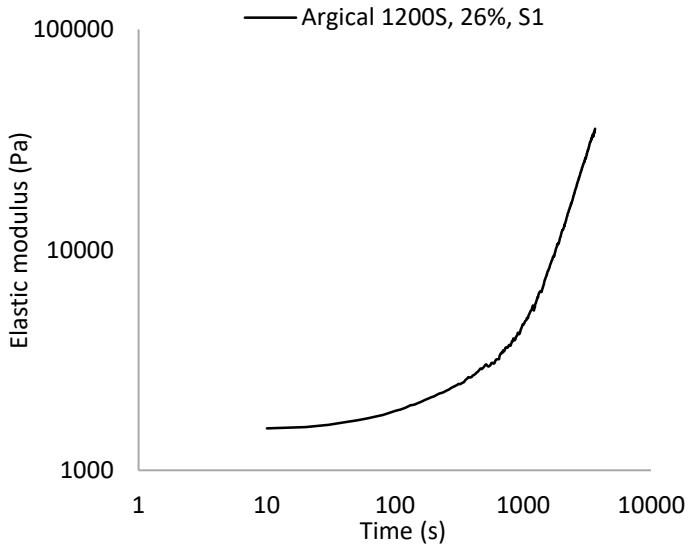

Figure 5.4: Evolution of elastic modulus over time

We can deduce two stages for evolution of elastic modulus over time. At first stage (i.e. ≈ initial 10 minutes), elastic modulus of geopolymer suspension increases slightly but this increase is not remarkable. At second stage (i.e. from around 10 minutes until the end of measurement), elastic modulus rises more remarkably and the increment has a linear trend. According to evolutions of equivalent Al and Na concentrations monitored by static ^{27}Al and ^{23}Na NMR measurements over time during the evolution of elastic modulus by Favier [6], sharp increase at second stage corresponds to the precipitation due to simultaneous decrease of both Al and Na concentrations at this stage (see Figure 1.12 in Chapter 1).

Similar observations are reported in literature for different geopolymer systems [23, 25]. Although geopolymer systems that are composed of different solid precursors or alkaline

solutions present similar evolutions for development of elastic modulus over time, obtained behaviors could vary depending on the modifications of experimental conditions. Favier [6] investigated the effect of structural homogenization applied by mixing at different durations on the development of early mechanical properties and reported different mechanical behaviors depending on the mixing durations. Author observed that elastic modulus decreases with increasing mixing duration at first stage, while at second stage, increasing mixing duration results in the acceleration of elastic modulus. Moreover, Aupoil [24] highlighted the thermo-sensibility of geopolymer systems by referring that temperature must be controlled during measurements in order to obtain reliable results. These observations indicate that development of mechanical properties, thus reaction kinetics, setting time, rheological and mechanical strength of geopolymers could change depending on the applied fabrication process, where mainly applied mixing protocol and temperature of materials vary. Therefore, fabrication and industrial application processes of geopolymeric materials must be under control in order to ensure the stability of their desired properties. In the second part of this study, which will be presented in following chapter, we will discuss the impact of modification of fabrication parameters (i.e. mainly mixing process and temperature) on the evolution of reaction kinetics and elastic modulus over time as well as the setting and mechanical properties of metakaolin- based geopolymers.

5.6. Conclusion

In this chapter, we introduced initially principles of nuclear magnetic resonance and oscillation rheology and then we presented protocols of static ^{27}Al NMR and oscillation rheology measurements. Afterwards, we presented the evolution of an equivalent aluminum concentration observed from the NMR measurements of a metakaolin-based geopolymer. Results showed successive dissolution and polycondensation stages during geopolymerisation. Following to reaction kinetics, we presented the development of mechanical properties by showing the evolution of elastic modulus over time. Results showed that the development of elastic modulus of a metakaolin-based geopolymer composed of two stages. At first stage, elastic modulus increases smoothly and the increment is not remarkable. At second stage, elastic modulus rises considerably with a linear trend of increment. We mentioned that some of the studies in literature highlighted the impact of experimental conditions on development of mechanical properties, where the parameters of these conditions could also have impact on industrial applications at macroscopic scale. We will present second part of the study in the following chapter, where we study primarily the influence of applied mixing protocol and temperature on reaction kinetics, setting time, development of short and long-term mechanical properties.

Chapter 5

References

[1] M. Palacios and F. Puertas, "Effect of superplasticizer and shrinkage-reducing admixtures on alkali-activated slag pastes and mortars," *Cement and Concrete Research,* vol. 35, pp. 1358-1367, 2005.

[2] M. Palacios and F. Puertas, "Stability of superplasticizer and shrinkage-reducing admixtures Stability of superplasticizer and shrinkage-reducing admixtures in high basic media," *Materiales de Construcción,* vol. 54, no. 276, pp. 65-86, 2004.

[3] C. Dupuy, A. Gharzouni, I. Sobrados, N. Texier-Mandoki, X. Bourbon and S. Rossignol, "29Si, 27Al, 31P and 11B magic angle spinning nuclear magnetic resonance study of the structural evolutions induced by the use of phosphor- and boron–based additives in geopolymer mixtures," *Journal of Non-Crystalline Solids,* vol. 521, no. 119541, 2019.

[4] C. Dupuy, J. Havette, A. Gharzouni, N. Texier-Mandoki, X. Bourbon and S. Rossignol, "Metakaolin-based geopolymer: Formation of new phases influencing the setting time with the use of additives," *Construction and Building Materials,* vol. 200, pp. 272-281, 2019.

[5] M. Palacios, P. F. G. Banfill and F. Puertas, "Rheology and Setting of Alkali-Activated Slag Pastes and Mortars: Effect of Organic Admixture," *ACI Materials Journal,* vol. 105, no. 2, pp. 140-148, 2006.

[6] A. Favier, "Mécanisme de prise et rhéologie de liants géopolymères modèles. Materials," Université Paris-Est, Champs-sur-Marne, 2013.

[7] T. Polenova, R. Gupta and A. Goldbourd, "Magic Angle Spinning NMR Spectroscopy: A Versatile Technique for Structural and Dynamic Analysis of Solid-Phase Systems," *Analytical Chemistry by American Chemical Society,* vol. 87, pp. 5458-5469, 2015.

[8] P. Duxson, J. L. Provis, G. C. Lukey, F. Separovic and J. S. J. v. Deventer, "29Si NMR Study of Structural Ordering in Aluminosilicate Geopolymer Gels," *Langmuir,* vol. 21, pp. 3028-3036, 2005.

[9] M. Palacios, S. Gismera, M. M. Alonso, J. d. d. Lacaillerie, B. Lothenbach, A. Favier, C. Brumaud and F. Puertas, "Early reactivity of sodium silicate-activated slag pastes and its impact on rheological properties," *Cement and Concrete Research,* vol. 140, no. 106302, 2021.

[10] A. Favier, G. Habert, N. Roussel and J. B. d. d. Lacallaire, "A multinuclear static NMR study of geopolymerisation," *Cement and Concrete Research,* vol. 75, pp. 104-109, 2015.

[11] Y. Parlak and N. Guzeler, "Nuclear Magnetic Resonance Spectroscopy Applications in Foods," in *Nutraceuticals and Functional Foods Current Research in Nutrition and Food Science*, 2016.

[12] V. University, "Vanderbilt University Chemistry course notes," [Online]. Available: https://www.vanderbilt.edu/AnS/Chemistry/Rizzo/chem220a/Ch13slides.pdf. [Accessed 21 March 2022].

[13] B. University, "Brown University course notes," [Online]. Available: https://www.brown.edu/academics/chemistry/sites/academics-chemistry/files/NMR_Introductory_Lecture.pdf. [Accessed 21 March 2022].

[14] R. S. Macomber, A Complete Introduction to Modern NMR Spectroscopy, John Wiley & Sons Inc, 1997.

[15] M. Maciejewski, "UConn Health," 29 November 2016. [Online]. Available: https://health.uconn.edu/bioinformatics/wp-content/uploads/sites/162/2017/11/NMRBasics_2016.pdf. [Accessed 21 March 2022].

[16] D. Weitz, H. Wyss and R. Larsen, "Oscillatory Rheology, Measuring the Viscoelastic Behaviour of Soft Materials," *G.I.T. Laboratory Journal,* pp. 68-70, 2007.

[17] T. Miri, Viscosity and Oscillatory Rheology, Chapter 2 of the book: Practical Food Rheology, An Interpretive Approach Edited by I. T. Norton, F. Spyropoulos, P. Cox, Birmingham: Wiley-Blackwell, A John Wiley & Sons, Ltd., Publication, 2011.

[18] F. Meyer, "Thermo Fisher," December 2014. [Online]. Available: https://assets.thermofisher.com/TFS-Assets/CAD/Application-Notes/V279-e-Performing-rheological-tests-in-oscillation-with-the-HAAKE-Viscotester-iQ.pdf. [Accessed 21 March 2022].

[19] A. Paar, "Oscillation tests and viscoelasticity," Anton Paar, [Online]. Available: https://wiki.anton-paar.com/en/basics-of-rheology/#approaches-to-measuring-viscoelastic-behavior. [Accessed 21 March 2022].

[20] L. Nachbaur, J. C. Mutin, A. Nobat and L. Choplin, "Dynamic mode rheology of cement and tricalcium silicate pastes from mixing to setting," *Cement and Concrete Research,* vol. 31, pp. 183-192, 2001.

[21] P. Bénard, S. Garrault, A. Nonat and C. Cau-Dit-Coumes, "Hydration process and rheological properties of cement pastes modified by orthophosphate addition," *Journal of the European Ceramic Society,* vol. 25, pp. 1877-1883, 2005.

[22] M. Haouas, F. Taulelle and C. Martineau, "Recent advances in application of 27Al NMR spectroscopy to materials science," *Progress in Nuclear Magnetic Resonance Spectroscopy,* Vols. 94-95, pp. 11-36, 2016.

[23] A. Poulesquen, F. Frizon and D. Lambertin, "Rheological behavior of alkali-activated metakaolin during geopolymerization," *Journal of Non-Crystalline Solids,* vol. 357, pp. 3565-3571, 2011.

[24] J. Aupoil, "Etude des mécanismes de dissolution/polycondensation lors de la géopolymérisation: réactivité du métakaolin et influence de la solution d'activation. Matériaux.," Université Paris sciences et lettres, Paris, 2019.

[25] A. Bourlon, "Physico-chimie et rhéologie de géopolymères frais pour la cimentation des puits pétroliers. Chimie-Physique.," Université Pierre et Marie Curie - Paris VI, Paris, 2010.

Chapter 6: Early reactivity of geopolymers Part II: interplay between parameters of mixing process and its impact on rheological and mechanical behavior of a metakaolin-based geopolymer

We mentioned in bibliography that in addition to chemical formulations, processing and measurement conditions of cementitious materials based on alkaline activation could also influence reaction kinetics, fresh and hardened state behaviors of geopolymers. In literature, the impact of temperature under different conditions (e.g. curing temperature) has been discussed widely from various aspects such as modification the structure of reaction products [1], leaching [2], changing setting time [3, 4], viscosity [3, 5], or alteration of reaction kinetics [6, 7]. In general, studies reported that the increase of temperature could influence particularly dissolution rate of solid precursor, thus the degree of formation of reaction products and implicitly, final characteristic properties of geopolymers. Moreover, some of the studies reported also the influence of applied mixing protocol on setting time [8] and the development of mechanical properties [9]. Modification of mixing protocol could induce variation of viscosity of alkaline solution, thus viscosity of final geopolymeric material. It could also modify yield stress affecting colloidal interactions between particles at microscopic scale [8]. In addition, development of mechanical properties could change with the variation of mixing duration. We recall that Favier [9] observed an acceleration the development of elastic modulus with prolongation of mixing duration. Based on literature, after formulation parameters, mixing protocol and temperature are the most important parameters playing role on rheological and mechanical performance of geopolymers. Therefore, mastering their impacts could supply several advantageous for controlling rheological, setting and mechanical properties.

The objective of this chapter is studying essentially the interplay between parameters of mixing process (i.e. mainly mixing speed, mixing time and temperature) and its influence on reaction kinetics, rheological as well as the mechanical properties and setting time of metakaolin-based geopolymers. It is important to note that temperature could increase during mixing due to chemical and/or mechanical origins that could appear simultaneously. Strong mechanical mixing could induce heating of solid particles as well as the fluid in suspension. For a clear analysis of reaction kinetics, rheological and mechanical behavior or variations of setting time due to mixing process, the impact of the temperature increase must be considered. In this chapter, first we define a reference mixing protocol, where we mix materials by hand. We assume that mixing by hand does not induce a remarkable temperature

variation as in case of mixing by a mixer. Later, either we vary initially the temperature of sodium silicate solution used to prepare geopolymers (i.e. by heating or cooling) before mixing, or we apply different mixing protocols by a mixer to the samples that are mixed already by hand. This is to demonstrate whether a pure temperature variation applied by heating or cooling sodium silicate solution would modify the system in the same way as a temperature variation applied by mixing protocol. We will introduce initially measurement protocols and then we will present the evolution of an equivalent aluminum concentration and elastic modulus over time, variations of setting time and mechanical strength of geopolymers respectively.

6.1. Measurement protocols

We prepare geopolymer suspensions using commercial Argical1200S with sodium silicate solution (S_1, μ_{0_1}) at a constant solid volume fraction of 26%. After several trials to fix a reference protocol, we obtained homogeneous geopolymer samples having repeatable setting times when we mix materials by hand during 4 minutes. Therefore, we determine 4 minutes of hand mixing as a reference mixing protocol. The idea for the rest of measurements is either heating or cooling sodium silicate solution before reference mixing, or applying a supplementary mixing protocol by a mechanical mixer after reference mixing. Formulation and reference mixing is the same for all measurements, while variation of temperature by heating or cooling sodium silicate solution or by mixing protocol depends on the method of measurement. We determine 3 groups to present studied geopolymers. Group 1 represents samples prepared by heated or cooled sodium silicate solutions. Group 2 and Group 3 represent samples prepared by additional mixing protocol following to reference mixing, where mixing speed or duration changes respectively. We introduce details for each measurement method in the following sections.

6.1.1. Measurement protocol of NMR

We perform static ^{27}Al NMR measurements to monitor the evolution of an equivalent aluminum quantity using the same measurement parameters introduced in previous chapter. Measurements involve Group 1 and Group 2 mentioned above. Group 1 includes two geopolymer samples that are prepared by sodium silicate solutions at room temperature (i.e. taken as 22°C) and at 50°C, while Group 2 is composed of samples that are mixed by Dispermat LC55 mixer during 2 minutes at 2800 rpm and at 4000 rpm respectively in addition to reference mixing. We measure temperatures of samples at the end of preparation by an external thermometer and we present these values with the temperature values of sodium silicate solutions before mixing in Table 6.1.

Table 6.1: Temperature values of sodium silicate solutions before preparation and geopolymer samples after preparation

		Temperature of sodium silicate solution before preparation (°C)	Temperature of geopolymer after preparation (°C)
Group 1	Reference mixing only	22°C	22
	Reference mixing only	50°C	39
Group 2	Reference mixing + 2 min. mixing at 2800 rpm	22	27
	Reference mixing + 2 min. mixing at 4000 rpm	22	29

In order to represent truly the effect of temperature variation on reaction kinetics, it is important to minimize heat loss after preparation, which requires controlling the temperature during measurements. However, controlling the temperature during an NMR measurement is complicated due to measurement environment. In fact, we cannot introduce a device into a geopolymer sample to measure its temperature without disturbing magnetic field of NMR instrument [7]. In order to control temperature during measurement, we apply airflow having regulated temperature at 25°C through the NMR probe, thus the vicinity of sample (Figure 6.1).

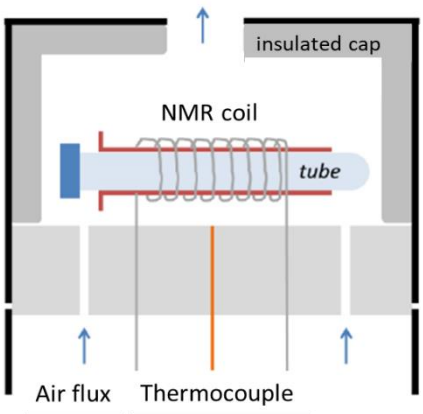

Figure 6.1: Diagram of controlling temperature during NMR measurements (adapted from [7])

Aupoil [7] mentions that temperature in NMR probe differs slightly between 24.4°C and 25.2°C during measurements even it is regulated to 25°C, thus results in a mean temperature value of 24.8°C for a complete measurement. We assume that temperature stays constant at 25°C for our measurements.

6.1.2. Measurement protocol of oscillation rheology

We perform rheological measurements using a Bohlin C-Vor rheometer. First, we confirm that critical deformation values of geopolymer suspensions stay constant at 0.001%. Oscillatory

rheology measurements involve three groups mentioned primarily. For Group 1, we vary temperature of sodium silicate solution from 15°C to 43°C. For Group 2, we apply shear rates of 20 s^{-1} and 100 s^{-1} at a constant duration of 20 minutes after reference mixing, while we apply constant shear rate of 100 s^{-1} during 20 minutes or 60 minutes following to reference mixing for samples of Group 3. In order to control temperature during measurements, first we determine temperature values of samples using a PicoLog TC-08 Temperature Logger (i.e. called thermocouple). Thermocouple is a temperature sensor consisting of two wires of dissimilar metals, which are joined at one end called the measuring junction. When this junction is heated or cooled, a temperature gradient generates a thermoelectric voltage along the wires. Instrument then transfers this voltage to an actual temperature value [10]. For Group 1, we determine temperature of each sample after its preparation, while we determine temperature values of samples belonging to Group 2 and Group 3 after applied shear protocol (Figure 6.2). Afterwards, we impose obtained temperature value of corresponding sample to rheometer using Haake K20 water bath during whole measurement. Principle of water bath is similar to that of airflow. We circulate water at a given temperature value near the sample. There is a 0.2°C difference between actual and imposed temperature values. Therefore, we impose temperature values that are 0.2°C higher than measured values during measurements. We present variations of temperatures before and after applied preparation or shear protocols together with imposed values in Table 6.2.

Table 6.2: Temperature values of sodium silicate solutions before measurements, temperature values of geopolymer samples after applied shear protocols and imposed temperature values during measurements. *: Protocol belongs to both Group 2 and Group 3.

		Temperature of solution before preparation (°C)	**Temperature of geopolymer after preparation (°C)**	**Imposed temperature (°C)**
Group 1	Reference mixing only	15	20	20.2
		22	22.3	22.5
		30	28.6	28.8
		40	34.1	34.3
		43	37.4	37.6
Group 2	Reference mixing + 20min. shear at 20 s^{-1}	22*	21.8*	22*
	Reference mixing + 20min. shear at 100 s^{-1}	22	25.2	25.4
Group 3	Reference mixing + 60min. shear at 100 s^{-1}	22	27.8	28

Measurement protocols consist of two stages. At first stage, we verify whether geopolymer samples are in linear elastic regime (LER) after applied preparation or shear protocols using oscillatory amplitude sweep (Sweep 1). At second stage, we perform measurements on new samples and verify again LER in the end of measurement (Sweep 2). We present a diagram of measurement protocols in Figure 6.2.

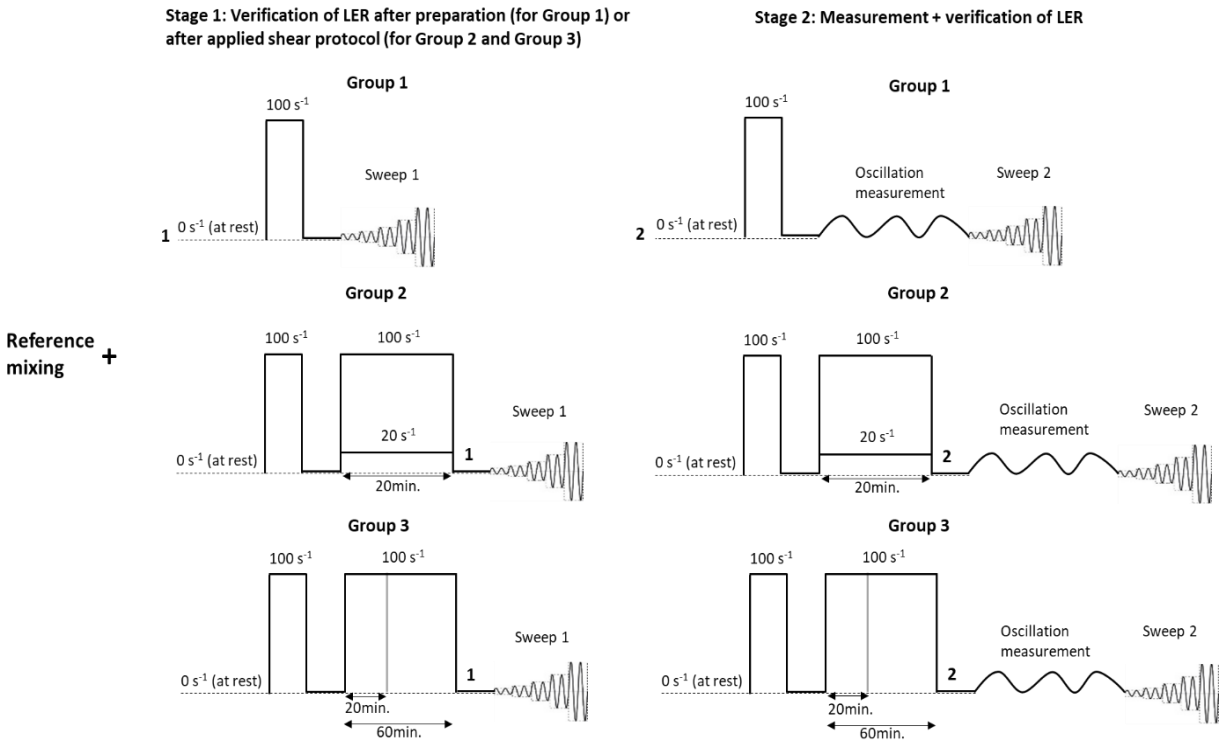

Figure 6.2: Diagram of measurement protocols applied for different groups. Temperature of sample is measured at 1 and measured temperature value is imposed at 2.

In order to perform measurements, at first stage, we apply initially 2 minutes of pre-shearing at 100 s^{-1} and 2 minutes of resting time after preparation for all samples. For Group 1, we verify LER directly after resting time, while we apply 20 minutes of constant shearing at 20 s^{-1} or at 100 s^{-1} for Group 2 or a constant shearing at 100 s^{-1} during 20 or 60 minutes for Group 3 after first resting time and then we verify LER following to 2 minutes of second resting time. We determine temperatures of sheared samples during this second resting time. At second stage, we prepare new geopolymer samples and we follow the same steps of measurements until the end of first (i.e. for Group 1) or second resting time (i.e. for Group 2 and Group 3). At the end of these resting times, we impose temperature values measured from the first stage and we start applying oscillation using a continuous sinusoidal excitation of deformation that is defined primarily as 0.0002% in previous chapter. We note that elevated temperature values that are imposed during measurements (i.e. particularly for samples belonging to Group 1) could trigger a rapid setting, which must be avoided to obtain successful results. In order to prevent a rapid setting during measurements, we vary oscillation durations for Group 1 from 10 minutes to 120 minutes depending on the temperature of corresponding sample (see Table 6.3), while for the samples of Group 2 and Group 3, we apply 1 hour of oscillation.

Table 6.3: Oscillation durations of samples of Group 1

		Temperature of solution before preparation (°C)	Oscillation duration (min)
Group 1	Reference mixing only	15	120
		22	60
		30	45
		40	30
		43	10

We present storage moduli of all geopolymer samples in Figure 6.3. Dashed line given in figure represents critical deformation γ_c value. We present samples with respect to applied shear protocols and imposed temperature values.

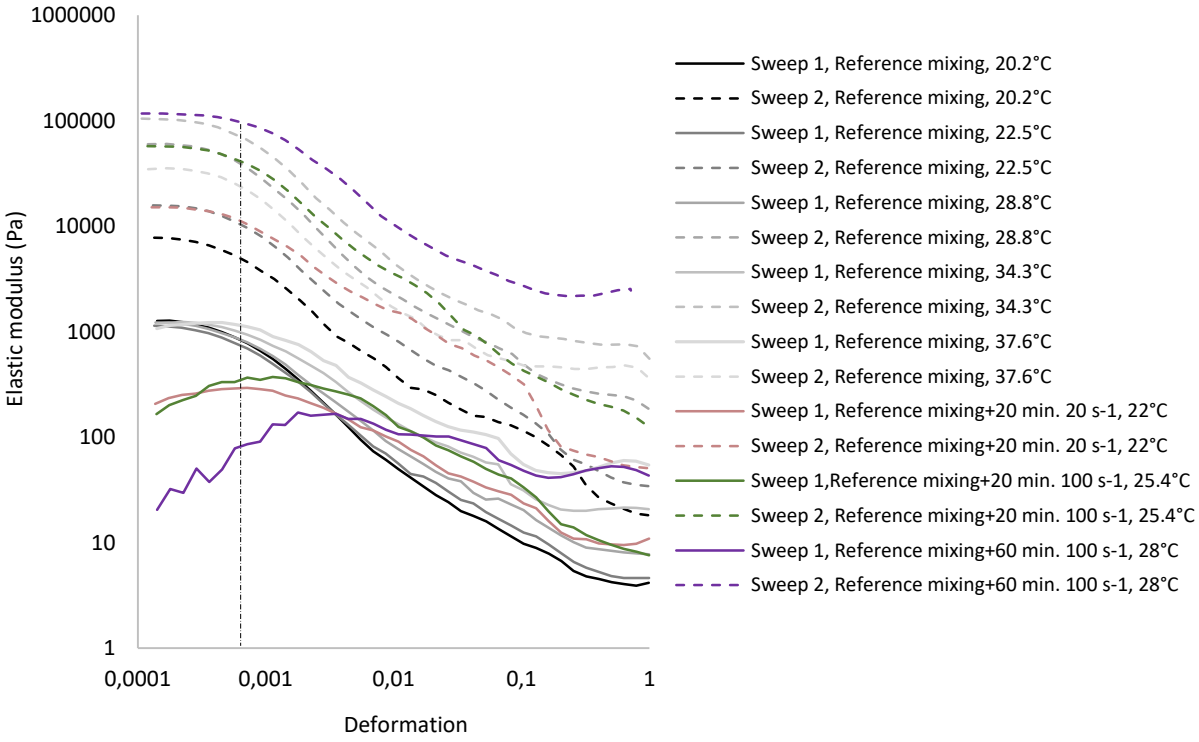

Figure 6.3: Storage moduli of geopolymer samples

Figure 6.3 shows that all samples stay in LER with applied deformation value of 0.0002% except the first sweeping result of sample having imposed temperature value of 28°C. Development of elastic modulus of this sample was disturbed during determination of temperature, thus its storage modulus does not represent a plateau. Since second sweeping of this sample confirms that it is in LER, we assume that sample is always in LER. Moreover, we remark that although shear rate, shear duration or temperature of a geopolymer sample changes, critical deformation value stays constant at 0.001%.

6.1.3. Measurement protocol of setting time

We perform measurement of setting time using Controlab Vicat Instrument. Vicat measurement is a standard technique that is based on the resistance of a paste (i.e. dough-like sample) to a dynamic penetration by Vicat needle (i.e. rod having 1.13 mm diameter and 300 g weight). Instrument measures the penetration depth of the Vicat needle falling down under gravity with respect to EN 196-3 norm. Total setting time of a geopolymer suspension is the time passes from the first contact of materials until the hardening of final geopolymer suspension. For measurements, sample is placed in a circular mold having dimensions of 80 mm and 40 mm for diameter and height respectively. We consider initial setting time from the needle penetration of 40 mm (i.e. needle penetrates completely since geopolymer sample is actually a paste in the beginning). We define final setting time starting from the penetration of 30 mm ± 0.5 mm.

Measurement of setting time includes three groups as well. For Group 1, we vary temperature values of sodium silicate solution from 15°C to 60°C. For Group 2, we mix samples during 2 minutes at mixing speed of 700 rpm, 1400 rpm or 2800 rpm using Rayneri mixer after initial reference mixing, while we mix samples of Group 3 at a constant speed of 2800 rpm during 2 minutes, 4 minutes or 8 minutes after reference mixing. Moreover, in order to observe evolution of temperature after applied protocol, we measure temperatures of samples using PicoLog TC-08 thermocouple over 1 day starting from the end of mixing. According to monitored temperature data, we observed a variation of ± 2.5 °C depending on the laboratory conditions. This variation may manipulate analysis of results due to thermo-sensibility of a geopolymer system. Therefore, we present temperature value of each geopolymer sample as a function of a mean value that is calculated from the data monitored until its final setting time. We present initial temperature values of sodium silicate solutions with the mean temperature values of final geopolymer samples in Table 6.4.

Table 6.4: Initial temperature values of sodium silicate solutions and mean temperature values of geopolymer samples after applied mixing protocol. *: Protocol belongs to both Group 2 and Group 3

		Initial temperature value of sodium silicate solutions before preparation (°C)	Mean temperature value of geopolymer after preparation (°C)
Group 1	Reference mixing only	15	25.4
		22	25.4
		30	30.1
		43	35.6
		50	41.5
		60	47.6
Group 2	Reference mixing + 2min. 700 rpm	22	26.8
	*Reference mixing + 2min. 1400 rpm	22*	27.7*
	Reference mixing + 2min. 2800 rpm	22	28.9
Group 3	Reference mixing + 4min. 2800 rpm	22	30.8
	Reference mixing + 8min. 2800 rpm	22	33.9

6.1.4. Measurement protocol of mechanical strength

We perform mechanical measurements using Controls Pilot 4 Automatic instrument with the same measurement parameters introduced in Chapter 4. Unlike the previous protocols, preparation and mixing protocols of geopolymer samples are slightly different for measurements of mechanical strength. First, we identify two systems to represent two different chemical formulations of geopolymers. For the first system (S^1), we prepare geopolymers using Argical1200S and sodium silicate solution (S_1, μ_{0_1}) at a constant solid volume fraction of 26% with molar ratios of SiO_2/Al_2O_3 = 1.84; Na_2O/Al_2O_3 = 0.77; H_2O/Na_2O = 19.4, while these ratios are SiO_2/Al_2O_3 = 2.05; Na_2O/Al_2O_3 = 1.03; H_2O/Na_2O = 14.4 for the second system (S^2). Secondly, we mix samples directly using Turbo-Test Rayneri VMI mixer, without reference mixing. As soon as we prepare geopolymer samples, we fill each of these samples into a rectangular mold having dimensions 4 cm x 4 cm x 16 cm and we cover the upper surface of sample in order to avoid evaporation. We demold samples one day after and keep closed in a plastic bag until 7 days. We produce 3 geopolymer samples for each studied mixing protocol. Hence, we perform 3 flexion and 6 compression tests after 7 days.

Mechanical measurements involve Group 2 and Group 3. For Group 2, we apply mixing speeds at 1400 rpm, 2240 rpm or 2800 rpm at a constant duration of 2.5 minutes, while we apply a constant mixing speed at 1400 rpm during 2.5 minutes or 20 minutes for Group 3. Each group has the samples belonging to first and second system, where the applied mixing protocols are

the same but the chemical formulations are different. We present studied sample groups with their protocols in Table 6.5.

Table 6.5: Mixing protocols of mechanical measurements. Protocol 1* belongs to both groups

	Group 2			Group 3
	Protocol 1*	Protocol 2	Protocol 3	Protocol 1
Stage 1	1 min. mixing at 1400 rpm	1 min. mixing at 2240 rpm	1 min. mixing at 2800 rpm	1 min. mixing at 1400 rpm
30 s resting time				
Stage 2	1 min. mixing at 1400 rpm	1 min. mixing at 2240 rpm	1 min. mixing at 2800 rpm	18.5 min. mixing at 1400 rpm
Total mixing duration (min)	2.5 min.	2.5 min.	2.5 min.	20 min.
Fixed parameter	Mixing duration: 2.5 minutes			Mixing speed: 1400 rpm

6.2. Evolution of Al concentration during early geopolymerisation

We present the evolution of an equivalent Al concentration monitored by static ^{27}Al NMR measurements over time (i.e. as well as the first three hours by an additional index) in Figure 6.4. Results represent geopolymer suspensions having different temperature values after applied preparation protocols (see Table 6.1). We present samples with respect to their final temperature values at end of preparation.

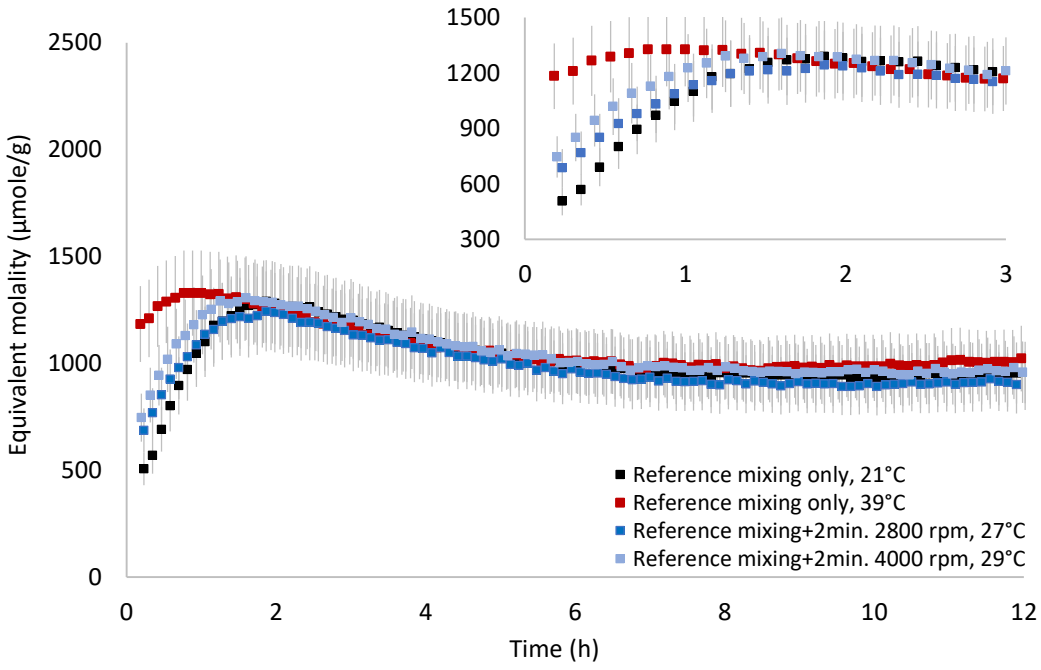

Figure 6.4: Evolution of an equivalent Al concentration over time. Time starts from the first contact of materials (samples prepared using (S_1, μ_{0_1}), ϕ=26%, standard error ≈ 15%)

Figure 6.4 shows initially an increase of equivalent aluminum concentration with increasing time due to dissolution. Moreover, dissolved quantity of aluminum increases and the dissolution accelerates with increasing temperature value of geopolymer sample. Samples with temperatures less than 30°C have similar durations to reach peak value that are around 90 minutes, while for sample that has 39°C in the end of preparation, the duration to reach peak value is around 45 minutes. After reaching peak values, equivalent concentration of aluminum decreases until around 6 hours due to polycondensation and then stays constant for the rest of measurement. Evolution of aluminum concentration starting from polycondensation over time is similar for all samples, which implies similar mechanism of polycondensation independent from the temperature values in the end of preparation. In literature, Bourlon [3] reports that variation of setting temperature of metakaolin-based geopolymers between 20°C and 80°C influences mainly dissolution kinetics of metakaolin. Author observed that geopolymer sample having setting temperature of 80°C consumes 90% of metakaolin in 10 hours, while the same amount of metakaolin is consumed in 2 weeks by the sample having setting temperature of 20°C. Besides, once 90% of metakaolin dissolves, all samples have similar evolutions of the aluminum speciation during setting, indicating that slowing the dissolution kinetics is related mostly to decreased mobility of formed species due to increased viscosity of medium and not the setting temperature.

Based on our results and the observations reported in literature, we can deduce that increasing the temperature of a geopolymer sample could accelerate dissolution of aluminum, while it does not have a visible impact on polycondensation reaction. In the following section, we present evolution of elastic modulus during early geopolymerisation.

6.3. Evolution of elastic modulus during early geopolymerisation

We present evolution of elastic moduli over time in Figure 6.5. Results represent geopolymer samples having different temperature values after applied preparation or shear protocols (see Table 6.2). We present samples with respect to applied shear protocols and imposed temperature values during rheological measurements.

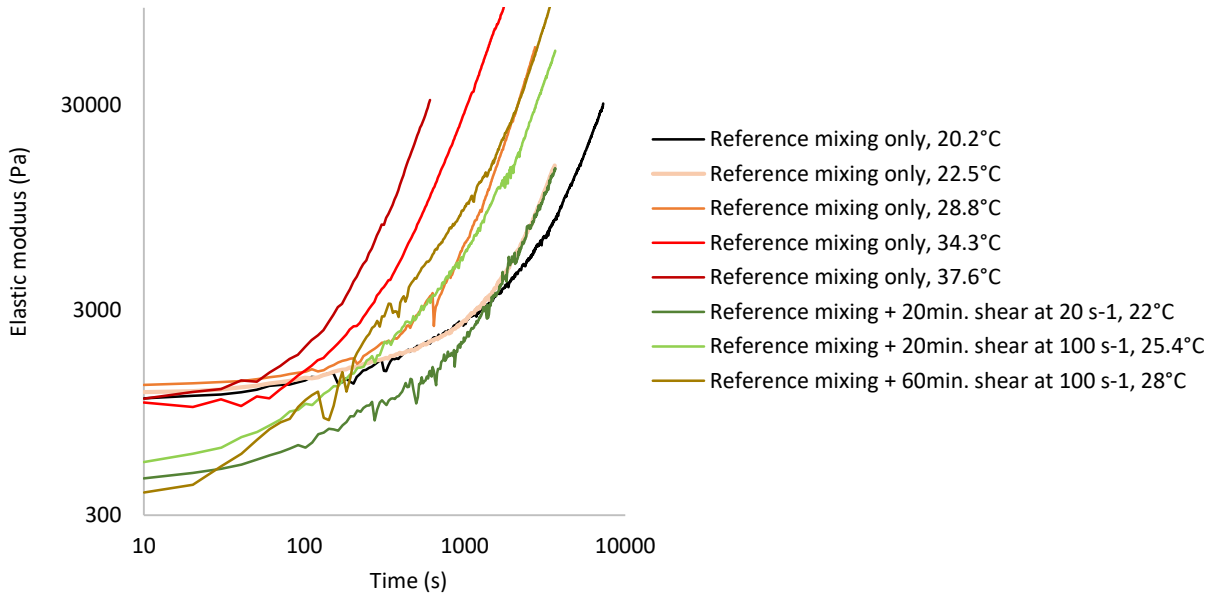

Figure 6.5: Evolution of elastic moduli over time (samples prepared using (S_1, μ_{0_1}), ϕ=26%)

As we observed in previous chapter, we also observe here two stages for the evolution of elastic modulus over time. At first stage, elastic moduli of samples that are prepared by heated or cooled sodium silicate solutions (i.e. Group 1) stay constant, while elastic moduli of samples that are sheared after reference mixing (i.e. Group 2 and Group 3) increase slightly. Initial values of elastic moduli are similar for samples belonging to Group 1, while for samples of Group 2 and Group 3, initial values of elastic moduli are lower than that of Group 1 and these values change with respect to applied shear protocol after reference mixing. At second stage, elastic moduli increase considerably with sharper increments, where increment trends are similar for all samples. Moreover, increased temperature of sodium silicate solution as well as the increased shear duration or shear rate accelerates the transition between first and second stages. We remark that independent from the history of preparation, evolution of elastic moduli of geopolymers having close temperature values (i.e. those having 22°C - 22.5°C and 28°C – 28.8°C) become identical later. This suggests that temperature is actually the key factor that pilots the development of mechanical properties. In this case, the increment of elastic modulus must be proportional to the increment of temperature. In order to show whether elastic moduli of samples are in correlation with their temperature values, first, we established a power law (Equation 6.1) showing the evolution of elastic modulus over time based on the second stage of measurement results:

$$G_t^i = G_0^i t^n \quad (6.1)$$

Where G_t^i is the elastic modulus through time, G_0^i is a constant representing the proportionality between the variation of temperature and the value of elastic modulus and n is a power law exponent that is found as 2 for all geopolymer samples. Secondly, we identified the values of proportionality constants (G_0^i) (Figure 6.6) in order to present the evolution of elastic modulus over time with respect to temperature.

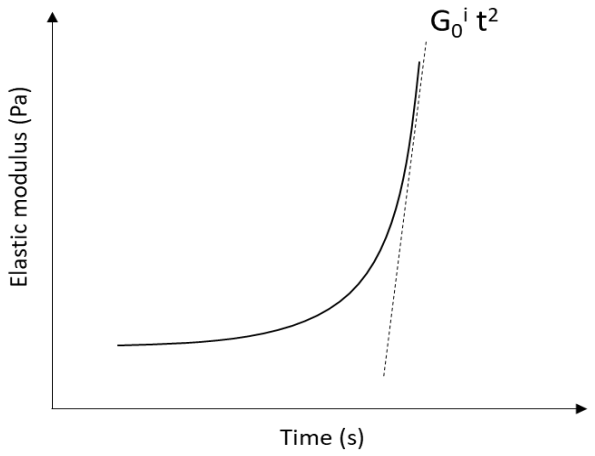

Figure 6.6: Diagram of identification the value of G_0^i

We present the values of proportionality constants (G_0^i) as a function of imposed temperature values in Figure 6.7. For a better analysis, we present obtained values in a logarithmic scale.

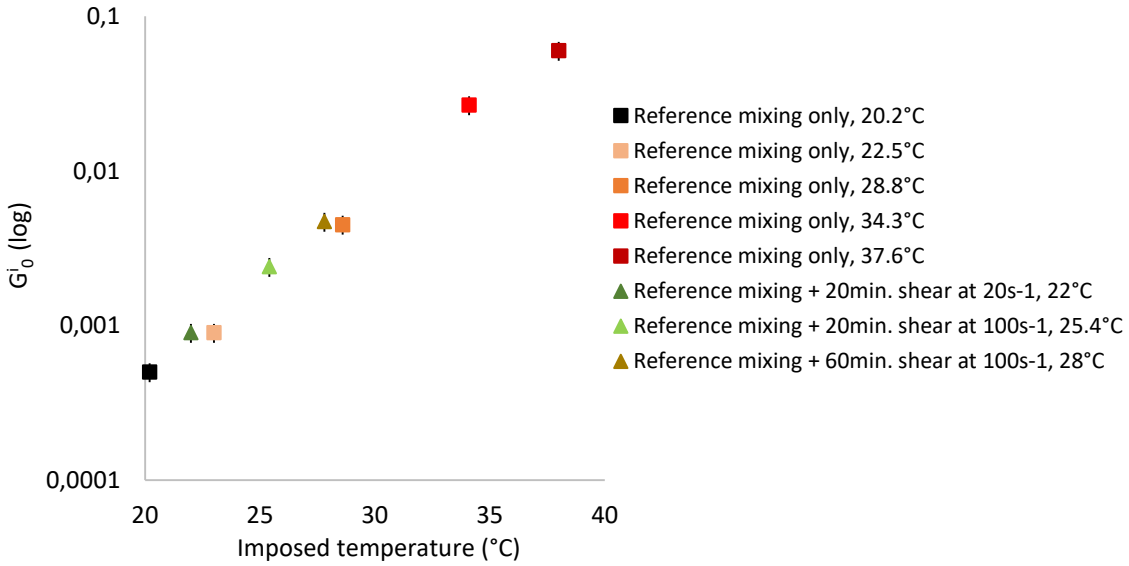

Figure 6.7: G_0^i values of geopolymer samples belonging to Group 1, Group 2 and Group 3 (samples prepared using (S_1, μ_{0_1}), ϕ=26%, standard error ≈ 14%)

Figure 6.7 shows that values of G_0^i increase linearly as a function of imposed temperatures regardless of the history of preparation or shear protocol of sample. Since the elastic moduli of geopolymers having close temperature values (i.e. those having 22°C - 22.5°C and 28°C – 28.8°C) become identical toward the end of rheological measurements, we obtained same values of G_0^i for these samples. These results demonstrate a strong correlation between development of mechanical properties and temperature. Moreover, since the development of mechanical properties accelerates with increased temperature, observed correlation implies also a shortening setting time with increased temperatures. Some of the studies in literature reported the observations supporting this hypothesis [3, 6, 7]. Poulesquen et al. [6] study the effect of temperature on the geopolymerisation kinetics by modifying the alkaline

activation solution and its temperature. Author mentioned that formation of a three-dimensional gel architecture is favored and accelerated as temperature rises and this phenomenon is more pronounced with KOH (i.e. Potassium hydroxide) and Aerosil 380 (i.e. Silica fume) system than NaOH and Aerosil 380 system. In fact, dissolution needs a thermal activation [3]. Therefore, when temperature of a geopolymer system increases, dissolution rate and dissolution speed increase and this triggers faster setting [3, 7]. Aupoil [7] referred that setting time of metakaolin-based geopolymers divided by 1.3 when dissolution speed increases by 50%. However, in order to show concretely a correlation between setting time and temperature, further information is necessary. In the following section, we present the evolution of setting time of a metakaolin-based geopolymer system with respect to variation of temperature.

Based on our results and the observations reported in literature, we can deduce that temperature is a key factor that pilots the development of mechanical properties during early geopolymerisation. In the following section, we present evolution of setting time with respect to temperature.

6.4. Evolution of setting time with respect to temperature

First, we recall that we monitored a temperature variation of ± 2.5 °C depending on the laboratory conditions during measurements. Since, this variation could manipulate analysis of results, we have decided to present temperature value of each geopolymer sample as a function of a mean value that is calculated from the temperature data (i.e. thermogram) monitored until its final setting time. We present initially the monitored thermogram of each geopolymer sample during one day by PicoLog TC-08 thermocouple instrument in Figure 6.8. Figure represents samples of Group 1 with respect to initial temperature values of their sodium silicate solutions before reference mixing while it represents samples of Group 2 and Group 3 with respect to applied mixing protocol after reference mixing. For a better analysis, we present obtained values in a logarithmic scale.

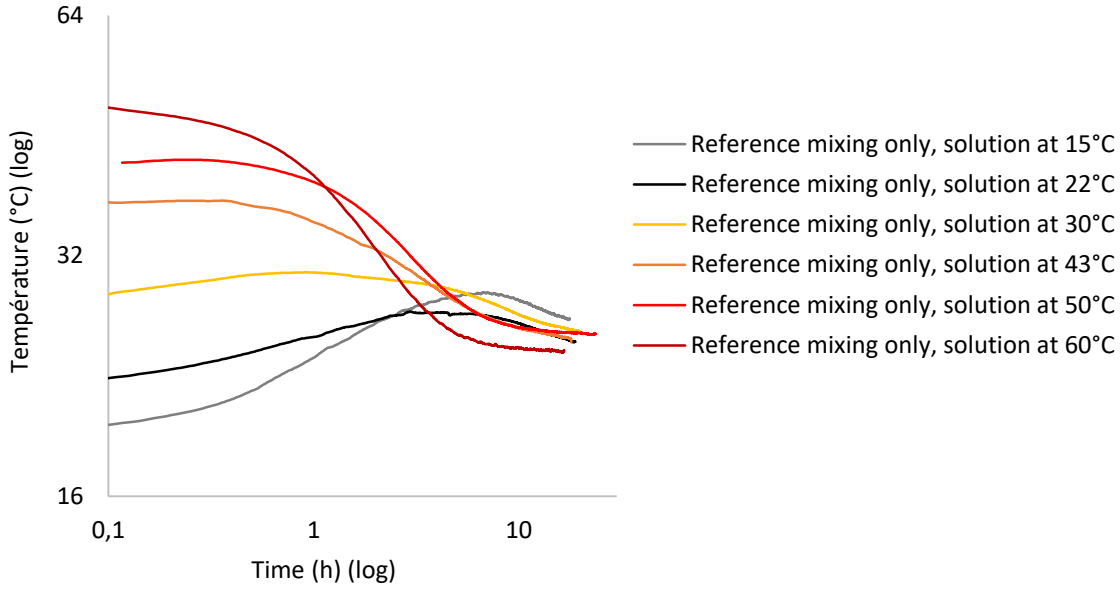

a

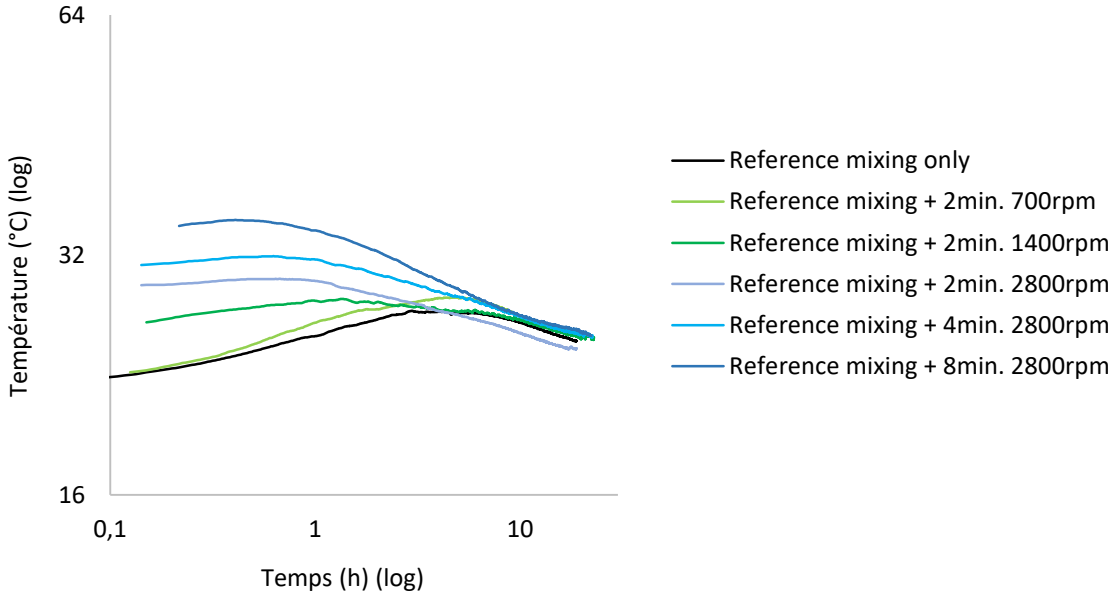

b

Figure 6.8: Evolutions of temperatures over time for samples of Group 1 (a), Group 2 and Group 3 (b). Time starts from the end of preparation.

Figure 6.8 shows first, a gradual increase of temperature when a geopolymer sample is prepared by a sodium silicate solution at lower temperature (i.e. geopolymers prepared by solutions at 15°C and 22°C in Figure 6.8-a) or by a mechanical mixing at slower speed/shorter duration (i.e. sample prepared by mixing at 700 rpm during 2 minutes in Figure 6.8-b). Temperature increases slightly until around 4 hours and then starts to decrease beyond 4 hours. Secondly, temperatures of geopolymers prepared by sodium silicate solutions below 60°C or by mechanical mixing speeds higher than 700 rpm or by mechanical mixing durations

more than 2 minutes stay constant for a while (i.e. around 40 minutes) and then starts to decrease for the rest of measurements. When a sodium silicate solution has a temperature value of 60°C (Figure 6.8-a), final geopolymer sample prepared using this solution has a decreasing temperature directly after preparation. The ultimate temperature values of all samples become around 25°C at the end of measurement. However, it seems that the longer measurement durations would demonstrate better the stability of final temperature values. Observed thermograms show that in addition to pure heating of a sodium silicate solution, rising the speed or duration of mechanical mixing applied after reference mixing induces also the increment of temperature of a geopolymer sample. This could result in the variation of setting time. In order to present whether setting time changes depending on the temperatures of geopolymers, we present their final setting times as a function of computed mean temperature values in Figure 6.9.

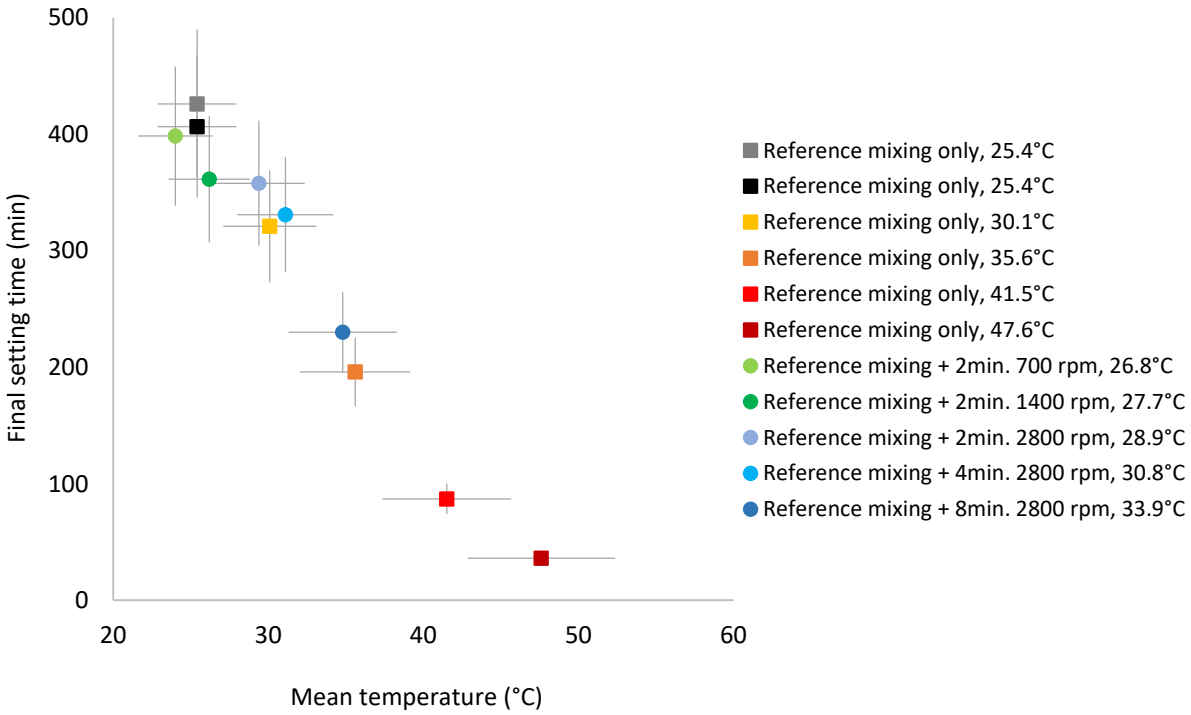

Figure 6.9: Setting time as a function of temperature (samples prepared using (S_1, μ_{0_1}), ϕ=26%, standard error ≈ 10%)

Figure 6.9 shows initially that setting time of a metakaolin-based geopolymer system decreases as a function of increasing mean temperature. In addition, decline of setting time is more remarkable when variation of temperature is applied by pure heating. We observe that setting time decreases from around 400 minutes toward 30 minutes when temperature increases from 22°C to 60°C. When temperature rises due to applied mechanical mixing, setting time decreases by half (i.e. from around 400 minutes toward 200 minutes). Moreover, geopolymer samples belonging to different groups, thus different history of preparation, but having similar mean temperature values (i.e. those having 30.1°C-30.8°C) have similar setting times.

These results show that although the method of temperature variation (i.e. heating/cooling or mixing) of a geopolymer suspension is different, its setting time is controlled mainly by temperature, where increase of temperature (i.e. by heating or mixing) induces a faster setting. Since dissolution is activated thermally [3]***, this observation could be explained by increased dissolution rate of metakaolin with increasing temperature, which is in correlation with the other observations in literature*** [3, 7]***.***

6.5. Evolution of mechanical strength with respect to applied mixing protocol

We have presented so far that the increase of temperature could modify reaction kinetics, development of mechanical properties and the setting time. Based on obtained results, it is highly probable that increment of temperature induces implicitly microstructural modifications (e.g. degree of porosity). Basically, when formation of a gel network accelerates with rising temperature (see NMR results), its final characteristic properties, thus mechanical performance of resulting geopolymeric material could vary with temperature. Since we observed that increasing duration or speed of mechanical mixing provokes the increase of temperature, applied mixing protocol could then induce modification of mechanical strength. In order to show the evolution of mechanical strength as a function of mixing protocol, we present compressive and flexural strength of geopolymers that are exposed to different mechanical mixing protocols (i.e. Group 2 and Group 3) in Figure 6.10. We recall that two geopolymer systems with different chemical formulations are identified for mechanical measurements and samples are mixed directly using a mechanical mixer (see Table 6.5). Samples of first and second geopolymers systems are indicated as S1 and S2 respectively in figure.

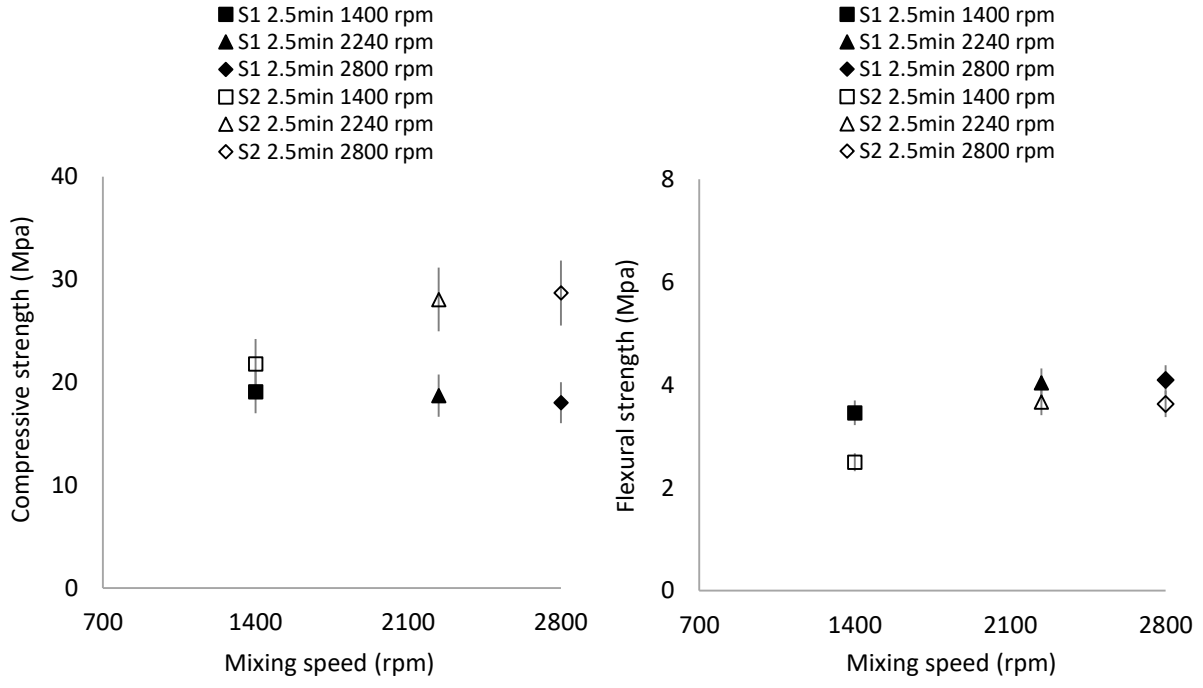

a₁ **a₂**

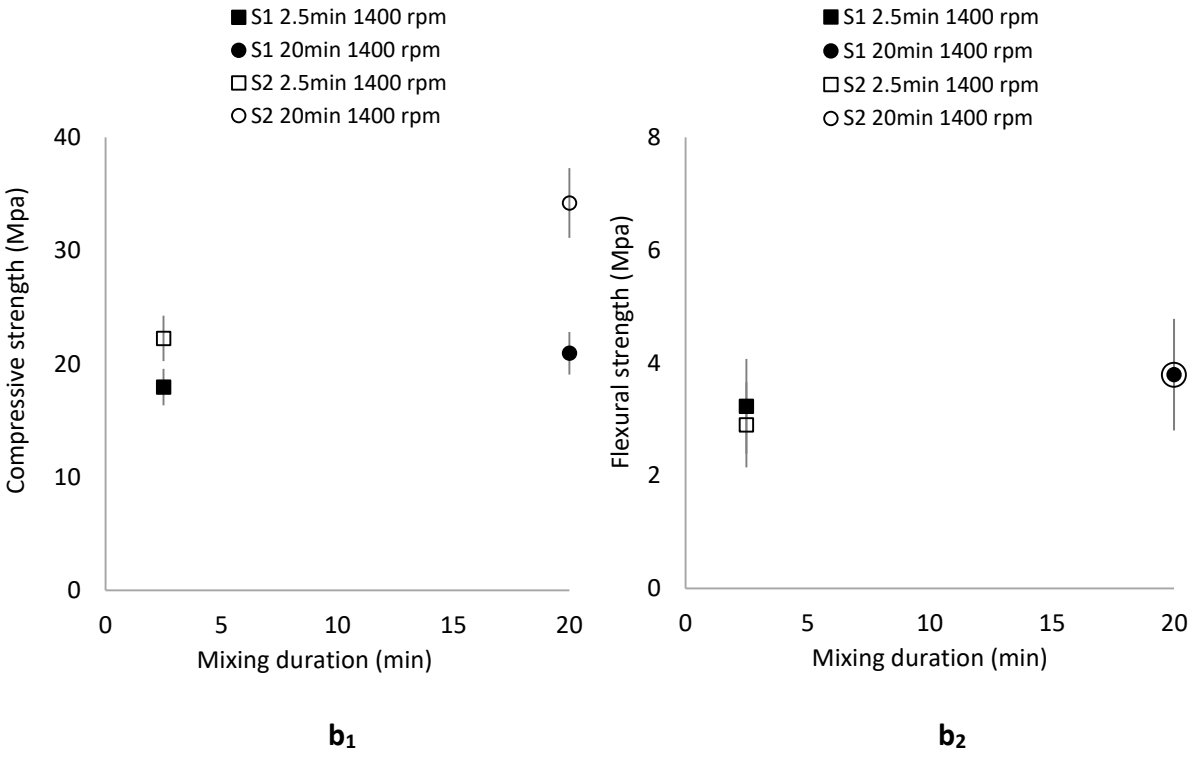

Figure 6.10: Compressive (a_1, b_1) and flexural (a_2, b_2) strength of geopolymers of Group 2 (a_1, a_2) and Group 3 (b_1, b_2) (standard errors of compressive and flexural strength are 11%-7% for first system (S^1), 9%-26% for second system (S^2) respectively)

Figure 6.10 shows initially that compressive strength values of samples belonging to S^2 (i.e. SiO_2/Al_2O_3 = 2.05; Na_2O/Al_2O_3 = 1.03; H_2O/Na_2O = 14.4) are higher than that of belonging to S^1 (i.e. SiO_2/Al_2O_3 = 1.84; Na_2O/Al_2O_3 = 0.77; H_2O/Na_2O = 19.4) in both case where mechanical mixing speed or duration changes. This could be explained especially by higher molar ratio of Si/Al of the first system. According to Loewenstein avoidance principle [11, 12], monosilicates and monoaluminates present in the medium form primarily Si-O-Al and Si-O-Si bonds during formation of a gel network, where formation of Al-O-Al bonds is not favored [11, 13]. Therefore, when Si content is lower, formed gel network has lower structural integrity with lower connections. However, geopolymers with high Si content are able to construct much larger and stronger gel networks [11], thus could present higher mechanical performance. Moreover, for geopolymer samples of S^2, we observe an increase of compressive strength with increasing mixing speed (i.e. from around 20 MPa to 30 MPa) or mixing duration (i.e. from around 20 MPa to 35 MPa). Compressive strength of samples belonging to S^1 stays constant around 20 MPa independent from variation of mixing speed or mixing duration (Figure 6.10, a_1 and b_1). The difference between mechanical behaviors of both system could still be explained by their chemical formulations. Since it is more likely to obtain a brittle and weaker structure with S^1, this system could be perturbed more by the applied mixing than S^2, where a part of its structure could be under breaking [3], thus system would need more time to restructure and strengthen its structure before setting. Moreover, flexural strength of both systems increases slightly with increasing mixing speed or mixing durations (Figure 6.10, a_2 and b_2).

Based on our results, we can deduce that applied mixing protocol influences also mechanical strength of geopolymers, especially for the systems having higher Si content.

6.6. Conclusion

In this chapter, we studied the interplay between parameters of mechanical mixing process, which are mainly mixing speed, mixing duration and temperature, and its influence on reaction kinetics, rheological as well as the setting time and mechanical properties of metakaolin-based geopolymers. In order to present whether the pure heating would modify a geopolymer system in the same way as the mechanical heating (i.e. originates from mixing), we simulated both types of heating on metakaolin-based geopolymers that are mixed by hand. In order to simulate pure heating/cooling, we heated or cooled sodium silicate solutions before mixing them with metakaolin, while in order to simulate mechanical heating, we mixed geopolymer samples additionally by mechanical mixers during different times or at different speeds. Afterwards, we performed measurements of NMR, oscillation rheology, Vicat and mechanical strength to observe the impact of temperature variation on reaction kinetics, development of elastic modulus, setting time and mechanical performance respectively.

Results of NMR measurements showed that dissolution rate and the dissolved quantity of aluminum increase with increasing temperature, while variation of temperature does not have a remarkable influence on polycondensation reaction. These results revealed that heating a geopolymer system accelerates mainly dissolution reaction.

Moreover, results of oscillation rheology measurements showed two stages for the evolution of elastic modulus over time. At first stage, elastic moduli of geopolymers that are prepared by heated or cooled sodium silicate solutions stay constant, while elastic moduli of samples that are sheared at different shear rates or shear durations increase slightly. At second stage, elastic moduli increase considerably with sharper linear increments, where increment trends are similar for all samples regardless of the method of temperature variation used to simulate pure or mechanical heating processes. In addition, increase of temperature accelerates development of mechanical properties. According to these results, we assumed that temperature would be the only parameter driving the development of mechanical properties. In order to show whether the development of elastic modulus of a geopolymer system is in correlation with its temperature, we computed a constant representing the proportionality between these two parameters and we showed that elastic modulus evolves as a function of the increase of temperature.

Results obtained from Vicat measurements revealed that setting time of a metakaolin-based geopolymer system decreases with increasing temperature and samples having similar temperature values have also similar setting times independent from their heating-cooling or mixing history.

Moreover, geopolymers that are exposed to different mixing protocols showed amelioration of mechanical strength as a function of mixing speed or mixing duration in case when their chemical formulations have higher Si content.

Results observed in this chapter demonstrated that no matter how the temperature of a metakaolin-based geopolymer system increases, its impact on ultimate rheological and mechanical properties would be the same. This means, a pure heating would influence characteristic properties of this system, thus rheological and mechanical performance in the same way as the mechanical heating (i.e. by mixing). Moreover, since the applied mixing protocol induces the increment of temperature, which triggers faster dissolution reaction, thus faster setting time, the overall mixing process of metakaolin-based geopolymeric materials must be under control to prevent undesirable consequences such as flash setting, strong viscosity etc. during their industrial applications. These materials must be mixed either slowly or at lower mixing durations.

References

[1] P. Duxson, A. Fernandez-Jimenez, J. L. Provis, G. C. Lukey, A. Palomo and J. S. J. v. Deveter, "Geopolymer technology: the current state of the art," *Journal of Materials Science,* vol. 42, pp. 2917-2933, 2007.

[2] N. Granizo, A. Palomo, A and Fernandez-Jimenez, "Effect of temperature and alkaline concentration on metakaolin leaching kinetics," *Ceramics International,* vol. 40, pp. 8975-8985, 2014.

[3] A. Bourlon, "Physico-chimie et rhéologie de géopolymères frais pour la cimentation des puits pétroliers. Chimie-Physique.," Université Pierre et Marie Curie - Paris VI, Paris, 2010.

[4] Sindhunata, J. S. J. v. Deventer, G. C. Lukey and H. Xu, "Effect of Curing Temperature and Silicate Concentration on Fly-Ash-Based Geopolymerization," *Industrial and Engineering Chemistry Research,* vol. 45, pp. 3559-3568, 2006.

[5] M. Palacios, M. M. Alonso, C. Varga and F. Puertas, "Influence of the alkaline solution and temperature on the rheology and reactivity of alkali-activated fly ash pastes," *Cement and Concrete Composites ,* vol. 95, pp. 277-284, 2019.

[6] A. Poulesquen, F. Frizon and D. Lambertin, "Rheological behavior of alkali-activated metakaolin during geopolymerization," *Journal of Non-Crystalline Solids,* vol. 357, pp. 3565-3571, 2011.

[7] J. Aupoil, "Etude des mécanismes de dissolution/polycondensation lors de la géopolymérisation: réactivité du métakaolin et influence de la solution d'activation. Matériaux.," Université Paris sciences et lettres, Paris, 2019.

[8] M. Palacios, P. F. G. Banfill and F. Puertas, "Rheology and Setting of Alkali-Activated Slag Pastes and Mortars: Effect of Organic Admixture," *ACI Materials Journal,* vol. 105, pp. 140-148, 2008.

[9] A. Favier, "Mécanisme de prise et rhéologie de liants géopolymères modèles. Materials.," Université Paris-Est, Champs-sur-Marne, 2013.

[10] P. Technology, *PicoLog TC-08 Temperature Logger User's Manual,* Pico Technology, 2005-2019.

[11] M. R. Rowles and B. O'Connor, "Chemical optimisation of the compressive strength of aluminosilicate geopolymers synthesised by sodium silicate activation of metakaolinite," *Journal of Materials Chemistry,* vol. 13, no. 29, pp. 1161-1165, 2003.

[12] W. Loewenstein, "The distribution of aluminum in the tetrahedra of silicates and aluminates," *American Mineralogist ,* vol. 39, pp. 92-96, 1954.

[13] A. Fernandez-Jimenez, A. Palomo, I. Sobrados and J. Sanz, "The role played by the reactive alumina content in the alkaline activation of fly ashes," *Microporous and Mesoporous Materials,* vol. 91, pp. 111-119, 2006.

Conclusions and Perspectives

We have showed in this thesis that the rheological, setting and mechanical properties of metakaolin-based geopolymers can be controlled by optimization of their particle packing and the variation of applied mixing protocol during their preparation.

In the first chapter, we presented a general information about geopolymeric materials including their synthesis and parameters affecting their final rheological and mechanical performance. We discussed the importance of controlling the rheological properties of these materials and we described the microstructural origins of their rheological behaviors. We mentioned that packing optimization and modifying the procedure of mixing could be beneficial to control particularly rheological and setting properties of geopolymeric materials. Therefore, we selected these methods in order to control rheological, mechanical and setting properties of studied geopolymers.

In the second chapter, we presented characterization of density, particle size distributions and maximum packing fractions of studied materials. We showed density values of solid and liquid materials are found using a gas pycnometer and a glass flask respectively. Moreover, we presented essential parameters influencing maximum packing densities of materials as well as the different methods to find the value of maximum packing. We showed the values of individual maximum packing densities of studied powder materials that are found using the Water Demand method, where these values increase from metakaolin powders toward limestone powders. Finally, we presented particle size distributions of studied powder materials that are measured using a laser granulometer. We showed that mean particle sizes of metakaolin and limestone powders vary from 5 µm to 16 µm and from 5 µm to 40 µm respectively while quartz powder has the lowest size around 3 µm. We also showed that grinding results in the increase of maximum packing, while its influence on particles size could not be captured clearly. We assumed that particles of studied metakaolin powder are sintered during grinding.

In the third chapter, we introduced initially different packing models and we selected Compressible Packing Model (CPM) due to its capacity of practical and repeatable prediction of particle packing. Later, we presented CPM in detail by giving basic mathematical background. Afterwards, we identified different binary powder couples between metakaolin-metakaolin, metakaolin-limestone and metakaolin-quartz powders. We measured maximum packing values of identified couples using Water Demand method and we computed also these values using CPM. We showed that both measured and computed values are in correlation, thus CPM predicts well the evolution of maximum packing as a function of optimization. Finally, we identified the promising binary couples between different powder materials revealing the best improvement of packing optimization.

In the fourth chapter, we presented the effect of particle packing optimization on rheological and mechanical properties of metakaolin-based geopolymers in two parts. At first part, we presented the effect of packing optimization on rheological properties. We verified initially

that limestone and quartz powders stay inert in the alkaline sodium silicate solution within the duration of rheological measurements. Later, we showed that viscosity of geopolymers decreases with the improvement of particle packing and this is valid in all conditions where nature of powder in binary mixture, solid volume fraction of geopolymer samples or molar ratio and viscosity of sodium silicate solution changes. Moreover, results obtained from rheological measurements correlated well with Krieger-Dougherty model, which means that this model predicts well the evolution of viscosity as a function of packing optimization. At second part, we presented the effect of packing optimization on mechanical properties of geopolymers. We showed initially that mechanical strength of geopolymers did not evolve considerably after 7 days, thus we used 7 days for mechanical measurements for the rest of the study. Afterwards, we presented that mechanical behavior of geopolymers based on different binary powder mixtures could not be related to the improvement of packing optimization alone due to the possibility of its combined impact with variation of chemical formulations. However, obtained results of geopolymers based on grinded metakaolin having a stable chemical formulation showed clearly the increase of mechanical strength as a function of packing optimization.

In the fifth chapter, we presented the evolution of reaction kinetics and the development of mechanical properties of metakaolin-based geopolymers. We introduced initially principles of nuclear magnetic resonance and oscillation rheology. Afterwards, we presented the evolution of an equivalent aluminum concentration, which demonstrated the kinetics of dissolution and polycondensation reactions. Later, we presented the development of mechanical properties by showing the evolution of elastic modulus over time. We observed that evolution of elastic modulus over time composed of two stages, where it has a smooth increment at first stage and a sharper increment at second stage.

In the sixth chapter, we presented the effect of applied mixing protocol on rheological, mechanical and setting properties of metakaolin-based geopolymers. Evolutions of equivalent aluminum concentrations obtained from ^{27}Al static NMR measurements showed that dissolution rate and the dissolved quantity of aluminum increased with increasing temperature that is arisen from heating of alkaline solution, longer or stronger mixing, while variation of temperature did not influenced considerably polycondensation reaction. Moreover, evolution of elastic modulus obtained from measurements of oscillation rheology showed two stages, where its increment was not remarkable at first stage but sharper and linear at second stage. We showed that development of elastic modulus, thus mechanical properties of geopolymers is controlled by temperature. Later, we presented the evolution of setting time as a function of temperature. Results obtained from Vicat measurements showed decreasing setting times with increasing temperature. Hence, we deduced that setting time was piloted by temperature. Finally, we presented the evolution of mechanical strength with respect to applied mixing protocol and we showed that compressive strength of geopolymers increased as a function of increased mixing durations or mixing speeds when the Si content of these geopolymers is higher.

As a perspective of this study, first, it would be interesting to investigate more about the influence of grinding solid precursors on rheological and mechanical properties. As grinding

contributes to improvement of packing optimization, its use could be beneficial to decrease viscosity while improving mechanical strength of geopolymers.

Secondly, it would be also interesting to observe shapes of different metakaolin powders and correlate this observation with the shape parameter of Compressible Packing Model in order to reinforce the obtained packing results. This could confirm that Compressible Packing Model predicts well the computed maximum packing density values of different types of powder mixtures.

Another perspective would be studying the rheological, mechanical and setting behavior of geopolymers that are based on different solid precursors. Since we observed that the development of mechanical properties as well as the setting time of metakaolin-based geopolymers are controlled mainly by temperature regardless of their mixing or preparation history, it would be interesting to observe whether the alternative geopolymer systems (i.e. including the binary mixtures developed based on more inert materials than limestone) would have similar behaviors.

Appendix A: Technical safety data sheets of materials

ARGICAL-M 1200S

ARGICAL-M 1200S est une pouzzolane artificielle (métakaolin), obtenue par broyage et calcination d'une argile kaolinique du bassin des Charentes.
ARGICAL–M 1200S is an artificial pozzolana (metakaolin). It is obtained by micronising and calcining a kaolinitic clay from the Charentes basin.

ARGICAL-M 1200S est un silicate d'alumine déshydroxylé de composition générale $Al_2O_3.2SiO_2$. C'est un matériau amorphe, non cristallisé, dont les particules présentent une forme lamellaire.
ARGICAL-M 1200S is a dehydroxylated aluminium silicate. Its general formula is $Al_2O_3.2SiO_2$. It is an amorphous non-crystallised material, constituted of lamellar particles.

DOMAINE D'UTILISATION : Additif pour bétons, mortiers, revêtements à base de ciment Portland ou de chaux.
PRODUCT USE: Additive for concretes, mortars and coatings made from Portland cement or lime.

ANALYSE CHIMIQUE
Chemical Analysis

SiO_2	**:**	**55 %**	**Fe_2O_3**	**:**	**1,8 %**
Al_2O_3	**:**	**39 %**	**TiO_2**	**:**	**1,5 %**
K_2O + Na_2O		**1,0 %**	**CaO + MgO**	**:**	**0,6 %**

PERTE AU FEU (1 050 °C)
Loss on ignition
1 %

CARACTÉRISTIQUES PHYSIQUES MOYENNES
Typical physical characteristics

pH	6
Indice pouzzolanique (essai Chapelle) *Pozzolanic index (Chapelle test)*	1 400 mg $Ca(OH)_2$ / g
Blancheur Photovolt filtre bleu *Brightness Photovolt blue filter*	74 %
Surface spécifique (BET) *Specific area (BET)*	19 m^2/g
Demande en eau (cône de Marsh) *Water demand (Marsh cone)*	1 650 g/kg
Masse spécifique *Specific gravity*	2,2 g/cm^3
Densité apparente *Bulk density*	
Non tassé / *Loose*	250 kg/m^3
Tassé / *Tamped*	400 kg/m^3

DISTRIBUTION GRANULOMÉTRIQUE
Particle size distribution

Inférieur à 2 µm : 55 %

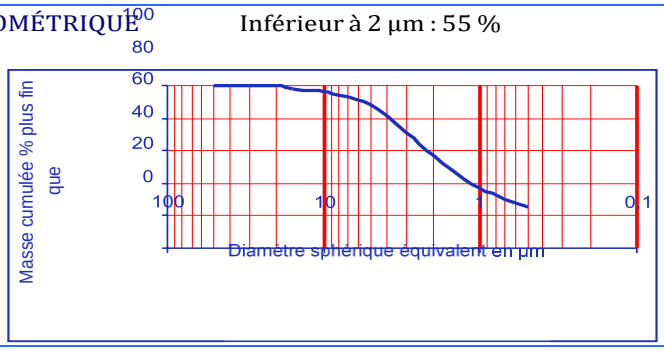

CONDITIONNEMENT / *Packaging*
Conteneur souple / *Bag* : 800 kg – Sacs 15 kg sur palette filmée / *Pallet* : 900 kg

Les informations contenues dans ce document sont données à titre purement indicatif. Les valeurs indiquées n'emportent pas obligation pour le fournisseur. Elles ne constituent en aucun cas une garantie sur le produit et sur ses spécifications.
Seule la fiche de spécification contractuelle dans le cadre de nos Conditions Générales de Vente engage notre société auprès de nos clients.
Révision 4 du 24/07/2008

ARGICAL-M 1000

ARGICAL-M 1000 est une pouzzolane artificielle (métakaolin), obtenue par calcination et broyage d'une argile kaolinique du bassin des Charentes.
ARGICAL-M 1000 is an artificial pozzolana (metakaolin). It is obtained by calcining and micronising a kaolinic clay from the Charentes basin.

ARGICAL-M 1000 est un silicate d'alumine déshydroxylé de composition générale : $Al_2O_3\ 2SiO_2$.
C'est un matériau amorphe, non cristallisé, dont les particules présentent une forme lamellaire.
ARGICAL-M 1000 is a dehydroxylated aluminium silicate. Its general formula is $Al_2O_3\ 2SiO_2$.
It is an amorphous non-crystallised material, whose particles are lamellar.

DOMAINE D'UTILISATION : Additif pour bétons, mortiers, revêtements à base de ciment Portland ou de chaux.
PRODUCT USE : Additive for concretes mortars and coatings made from Portland cement or lime.

ANALYSE CHIMIQUE
Chemical analysis

SiO_2	:	55 %	Fe_2O_3	:	1,4 %
Al_2O_3	:	40 %	TiO_2	:	1,5 %
K_2O+Na_2O	:	0,8 %	CaO+MgO	:	0,3 %

PERTE AU FEU (1050 °C) 1 %
Loss on ignition

CARACTERISTIQUES PHYSIQUES MOYENNES
Typical physical characteristics

pH	6
Indice pouzzolanique (essai Chapelle) *Pozzolanic index (Chapelle test)*	1000 mg $Ca(OH)_2$/g
Blancheur Photovolt filtre bleu *Photovolt brightness blue filter*	73
Surface spécifique BET *Specific area BET*	17 m^2/g
Demande en eau (Cône de Marsh) *Water demand (Marsh cone)*	900 g/kg
Masse spécifique *Specific gravity*	2,4 g/cm^3
Densité apparente *Bulk density*	
Non tassé / *Loose*	550 kg/m^3
Tassé / *Tamped*	850 kg/m^3

DISTRIBUTION GRANULOMETRIQUE Inférieur à 80 µm : 95 %
Paticle size distribution

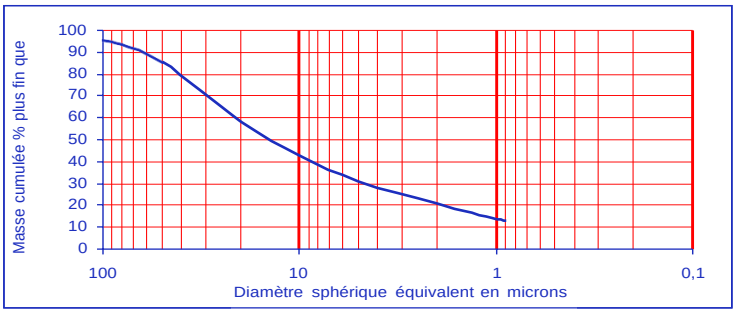

CONDITIONNEMENT / *Packaging*
Conteneur souple / *Bag* : 500, 1000 kg - Sacs 25 kg sur palette filmée / *Pallet* : 1250 kg

Les informations contenues dans ce document sont données à titre purement indicatif. Les valeurs indiquées n'emportent pasobligation pour le fournisseur.
Elles ne constituent en aucun cas une garantie sur le produit et sur ses spécifications.
Seule la fichede Spécification Contractuelle dans le cadre de nos Conditions Générales de Ventes engage notre société auprès des clients.
Révision 3 du 8/02/2007

Mike Wye & Associates Ltd.
Tel. : +44 (0)409-281644 - Fax : +44 (0)1409-281669 - http://www.mikewye.co.uk
e-mail : sales@mikewye.co.uk

Fiche technique

Omya International AG
P.O. Box
CH-4665 Oftringen

+41 62 789 29 29
+41 62 789 20 77

www.omya.com

Durcal® 5

SITE:	SALSES, France (certifié ISO 9001, ISO 14001 et OHSAS 18001)
DESCRIPTION DU PRODUIT:	Carbonate de calcium en poudre, naturel et fin, élaboré à partir d'un marbre blanc de grande pureté chimique.

COMPOSITION DU PRODUIT:

$CaCO_3$	98	%
$MgCO_3$	1.5	%
Fe_2O_3	0.05	%
Insolubles HCl	0.2	%

CARACTERISTIQUES TYPES DU PRODUIT:

Granulométrie:		
· Refus à 45 µm (ISO 787-7)	0.1	%
· Coupe granulométrique (d98%)	25	µm
· Diamètre moyen des particules (d50%)	5.5	µm
· Particules < 2 µm	23	%
Blancheur:		
· Blancheur Ry (C/2°, DIN 53163)	93	%
· CIE L*, a*, b* (ISO 11664-4)	96.9/0.9/3.6	
Taux d'humidité départ usine (ISO 787-2)	0.3	%

CARACTERISTIQUES GENERALES DU PRODUIT:

Densité apparente tassée (ISO 787-11)	1.3	g/ml
pH (ISO 787-9)	9	
Prise d'huile (ISO 787-5)	16	g/100g
Prise de VO (ISO 787-5)	26	g/100g

APPLICATIONS PRINCIPALES:

Peintures
- Peintures émulsion
- Peintures satinées
- Primaires
- Peintures routières

Finitions murales
- Enduits à base d'émulsion
- Plasters à base de résine synthétique

Plastiques
- PVC plastifié
  - Revêtements de sols
- Moulages de résine époxy/polyester insaturée

Adhésifs

REPARTITION GRANULOMETRIQUE (Malvern Mastersizer 2000):

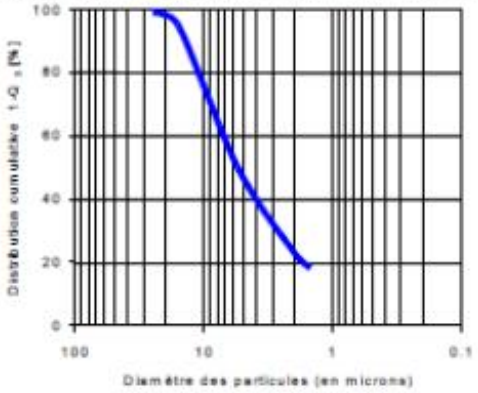

CONDITIONNEMENT STANDARD:
- VRAC
- SAC (papier) de 25 kg sur palette
- CONTENEUR SOUPLE sur palette

Fiche technique

Durcal® 65

SITE:	SALSES, France (certifié ISO 9001)		
DESCRIPTION DU PRODUIT:	Carbonate de calcium naturel et en poudre, élaboré à partir d'un marbre blanc de grande pureté chimique.		
COMPOSITION TYPE DE LA ROCHE:	$CaCO_3$	98	%
	$MgCO_3$	1.5	%
	Fe_2O_3	0.05	%
	Insolubles HCl	0.2	%
CARACTERISTIQUES TYPES DU PRODUIT:	Granulométrie:		
	· Refus à 355 µm (ISO 787/7)	0.2	%
	· Refus à 63 µm (ISO 787/7)	42	%
	· Coupe granulométrique (d98%)	180	µm
	· Diamètre moyen des particules (d50%)	45	µm
	Blancheur:		
	· Blancheur CIE L*, a*, b* (DIN 6174)	94/1.5/4.8	
	Taux d'humidité départ usine (ISO 787/2)	0.3	%
CARACTERISTIQUES GENERALES DU PRODUIT:	Densité apparente tassée (ISO 787/11)	1.7	g/ml
	pH (ISO 787/9)	8	

APPLICATIONS PRINCIPALES:

Finitions murales
- Enduits à base d'émulsion ou minéraux

Marbre reconstitué
Bétons de résine
Terrazzo

AUTRES APPLICATIONS:

Plastiques
- PVC plastifié / Plastisols PVC
  - Revêtements de sols

Mortier
Revêtements de surface
Enduits de rebouchage
Produits d'entretien
- Poudres à récurer

CONDITIONNEMENT STANDARD:

- VRAC
- SAC (papier) de 25 kg sur palette
- CONTENEUR SOUPLE sur palette

REPARTITION GRANULOMETRIQUE (Malvern Mastersizer 2000):

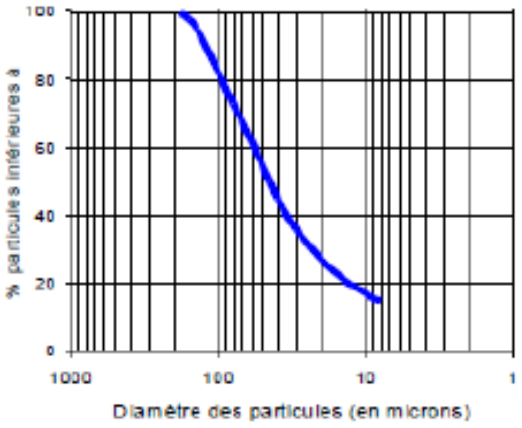

Quartz C800

Quartz (type A) - Compiègne (F)

Appellation	C4	C6	C10	C300	C400	C480	C500	C600	C800
315	99,00	100,00	100,00	100,00	100,00	100,00	100,00	100,00	100,00
200	92,00	99,90	100,00	100,00	100,00	100,00	100,00	100,00	100,00
160	88,00	98,00	100,00	100,00	100,00	100,00	100,00	100,00	100,00
125	80,00	95,00	99,90	100,00	100,00	100,00	100,00	100,00	100,00
100	69,10	90,00	98,50	100,00	99,90	99,90	100,00	100,00	100,00
80	60,00	82,00	95,00	99,00	99,50	99,70	100,00	100,00	100,00
63	50,00	73,00	90,00	97,00	98,50	99,30	100,00	100,00	100,00
40	36,00	54,00	75,00	86,00	94,50	97,00	100,00	99,90	100,00
32	28,80	43,20	67,00	79,00	90,00	95,00	100,00	99,00	100,00
24	21,60	32,40	53,00	66,00	80,00	91,00	99,90	98,00	100,00
16	14,40	21,60	35,33	44,00	60,00	78,00	95,00	97,00	99,90
12	10,80	16,20	26,50	33,00	50,00	62,00	88,00	91,00	99,00
8	7,20	10,80	17,67	22,00	33,33	46,00	70,00	82,00	96,00
4	3,60	5,40	8,83	11,00	16,67	20,00	31,00	56,00	72,00
2	1,80	2,70	4,42	5,50	8,33	7,00	15,50	21,00	36,00
1	0,90	1,35	2,21	2,75	4,17	0,70	7,75	3,00	9,00
d_{95}	**230,0**	**125,0**	**80,0**	**60,0**	**40,0**	**40,0**	**16,0**	**15,0**	**8,5**
d_{50}	**63,0**	**35,0**	**22,0**	**17,0**	**12,0**	**8,8**	**6,0**	**4,0**	**3,0**
Blaine	**207**	**297**	**386**	**478**	**642**	**872**	**1078**	**1750**	**2200**
Classe de finesse	**-**	**M**	**M**	**M**	**H**	**H**	**H**	**H**	**H**
i 28 jours	**0,780**	**0,785**	**0,792**	**0,802**	**0,820**	**0,820**	**0,830**	**0,862**	**0,895**
SiO_2	98,57	98,49	98,57	98,56	98,62	98,62	98,31	98,14	98,12
Fe_2O_3	0,04	0,04	0,05	0,03	0,04	0,04	0,06	0,09	0,08
Al_2O_3	0,58	0,64	0,63	0,61	0,54	0,54	0,76	0,83	0,84
TiO_2	0,03	0,02	0,03	0,03	0,03	0,03	0,04	0,04	0,04
CaO + MgO	0,02	0,03	0,03	0,03	0,03	0,03	0,03	0,04	0,05
$Na_2O + K_2O$	0,45	0,47	0,45	0,43	0,42	0,42	0,50	0,55	0,57
Perte au feu	0,20	0,20	0,13	0,20	0,20	0,20	0,20	0,20	0,20
Densité réelle	2,65	2,65	2,65	2,65	2,65	2,65	2,65	2,65	2,65
< 0,160 mm	88,00	98,00	100,00	100,00	100,00	100,00	100,00	100,00	100,00
< 0,063 mm	50,00	73,00	90,00	97,00	98,50	98,50	100,00	100,00	100,00
< 0,012 mm	10,80	16,20	26,50	33,00	50,00	50,00	88,00	91,00	99,00
Valeur/bleu	0,71	0,71	0,71	0,71	0,71	0,71	0,71	0,71	0,71
Chlorures	0,001	0,001	0,001	0,001	0,001	0,001	0,001	0,001	0,001
S total	0,01	0,01	0,01	0,01	0,01	0,01	0,01	0,01	0,01

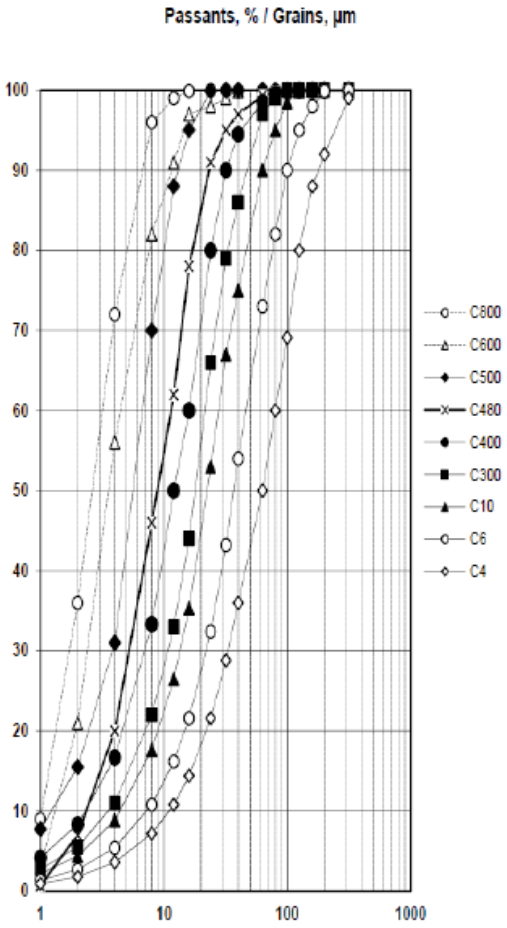

Sodium silicate

2.2 Éléments d'étiquetage

Étiquetage selon le règlement (CE) N° 1272/2008 [CLP]

Le produit n'est pas soumis à un étiquetage selon les directives CE ou les lois nationales respectives.

Autres dangers

non applicable

SECTION 3: Composition / informations sur les composants

3.1 Substances

non applicable

3.2 Mélanges

Composants dangereux Classification selon l'ordonnance (CE) N° 1272/2008 [CLP]

Nom de la substance	Concentration	Identificateur de produit	Classes et catégories de danger
Sodium silicate	20 - 60%	n°CAS: 1344-09-8 N°CE: 215-687-4 Numéro d'enregistrement REACH: Pas encore communiqué aux utilisateurs aval.	Eye Irrit. 2 - H319 Skin Irrit. 2 - H315 STOT SE 3 - H335

Appendix B: Flow curves and results of rheological and mechanical measurements of geopolymer suspensions

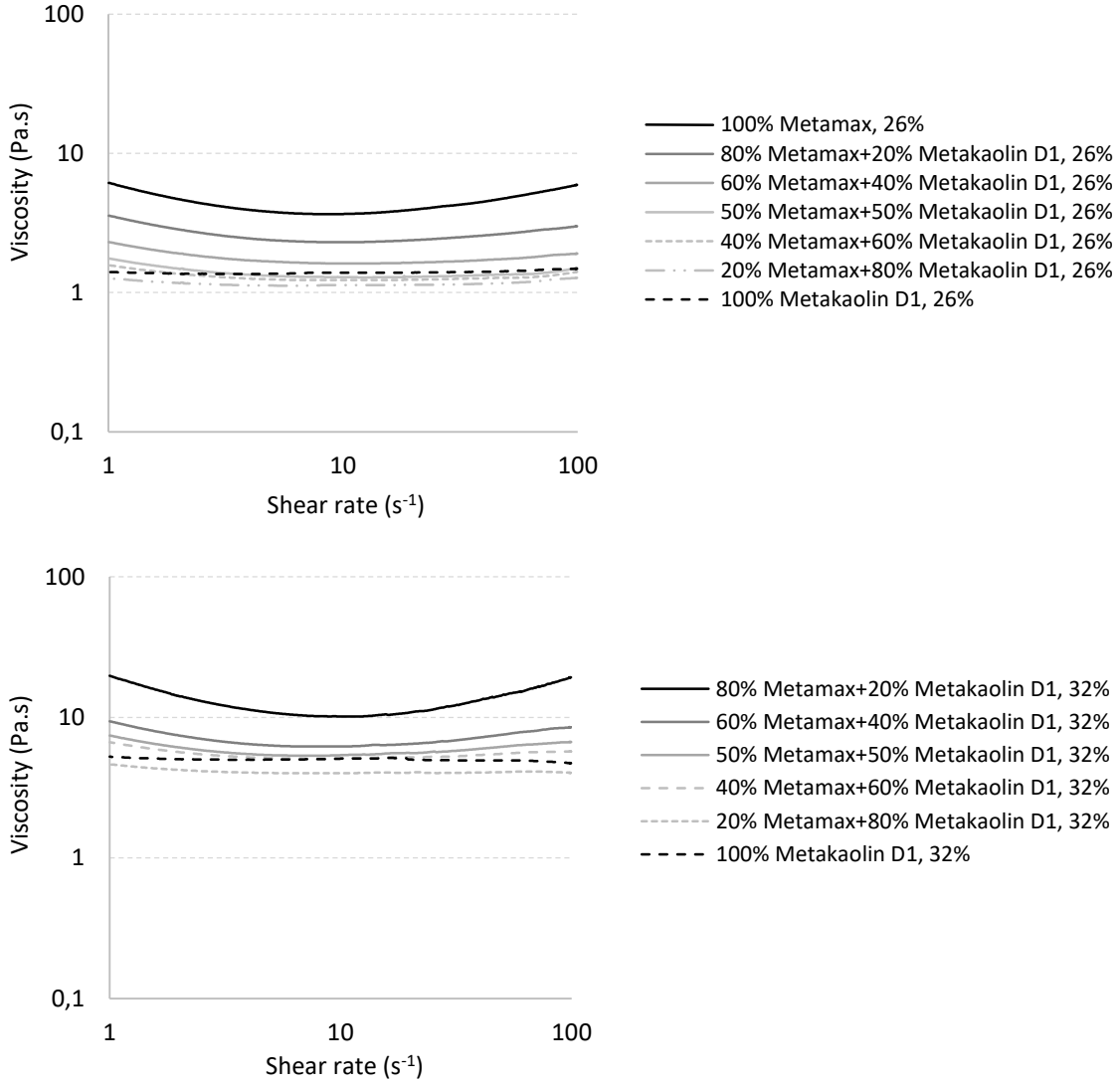

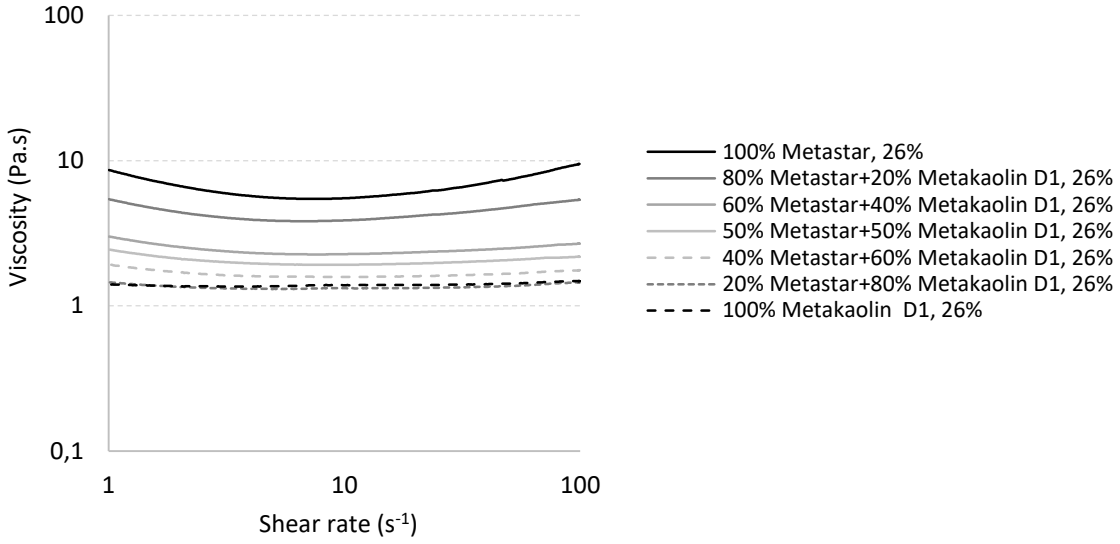
100
10
1
0,1
Viscosity (Pa.s)
1
10
100
Shear rate (s-1)
100% Metastar, 26%
80% Metastar+20% Metakaolin D1, 26%
60% Metastar+40% Metakaolin D1, 26%
50% Metastar+50% Metakaolin D1, 26%
40% Metastar+60% Metakaolin D1, 26%
20% Metastar+80% Metakaolin D1, 26%
100% Metakaolin D1, 26%

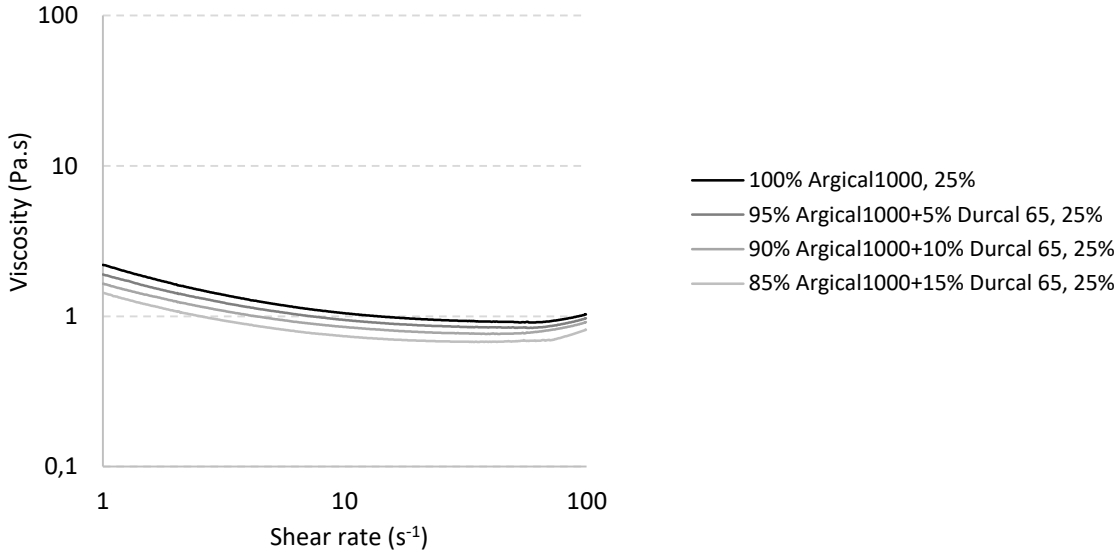
100
10
1
0,1
Viscosity (Pa.s)
1
10
100
Shear rate (s-1)
100% Argical1000, 25%
95% Argical1000+5% Durcal 65, 25%
90% Argical1000+10% Durcal 65, 25%
85% Argical1000+15% Durcal 65, 25%

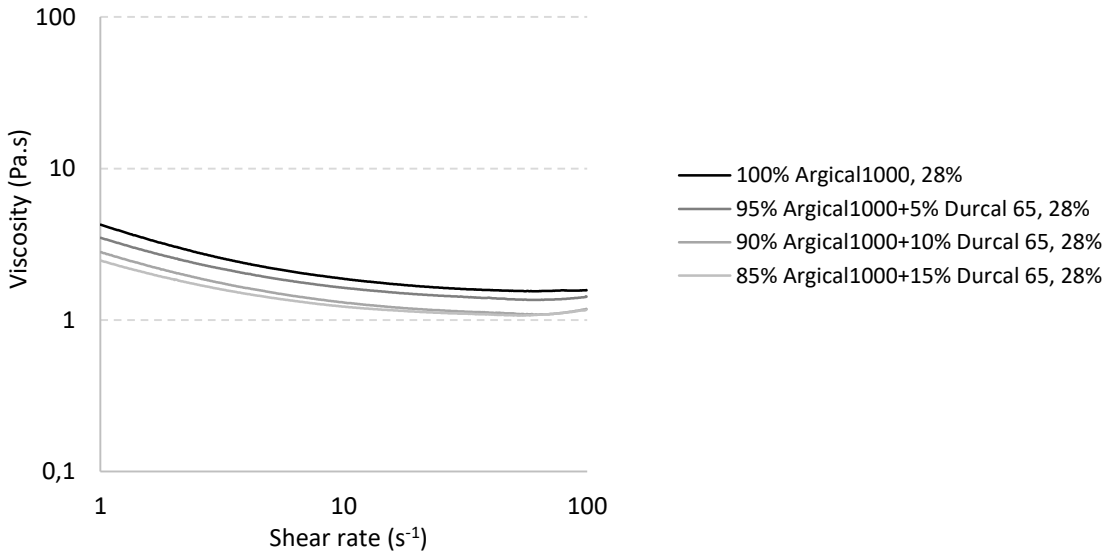
100
10
1
0,1
Viscosity (Pa.s)
1
10
100
Shear rate (s-1)
100% Argical1000, 28%
95% Argical1000+5% Durcal 65, 28%
90% Argical1000+10% Durcal 65, 28%
85% Argical1000+15% Durcal 65, 28%

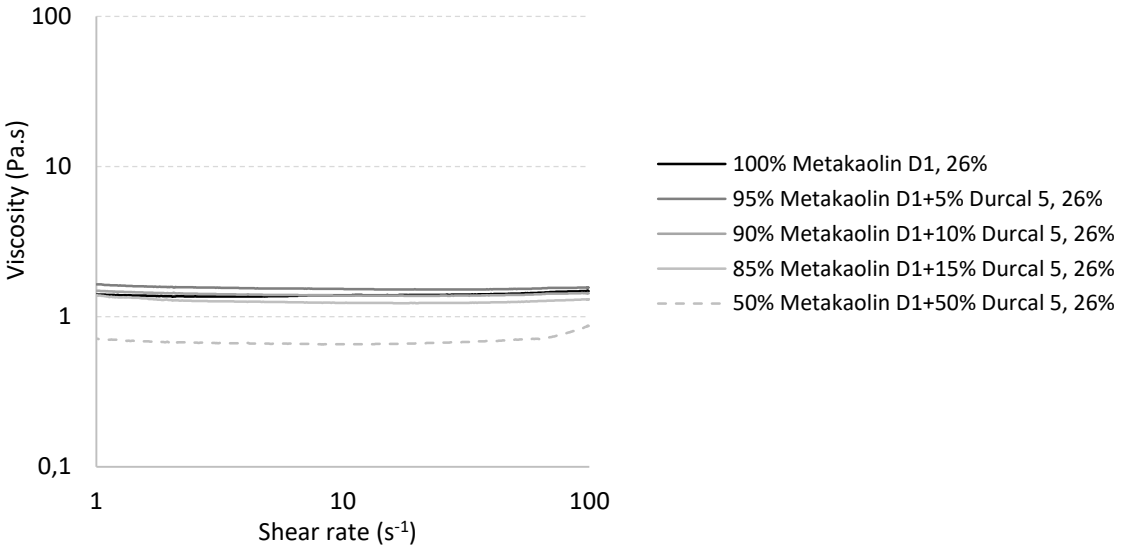
100
10
1
0,1
Viscosity (Pa.s)
1
10
100
Shear rate (s-1)
100% Metakaolin D1, 26%
95% Metakaolin D1+5% Durcal 5, 26%
90% Metakaolin D1+10% Durcal 5, 26%
85% Metakaolin D1+15% Durcal 5, 26%
50% Metakaolin D1+50% Durcal 5, 26%

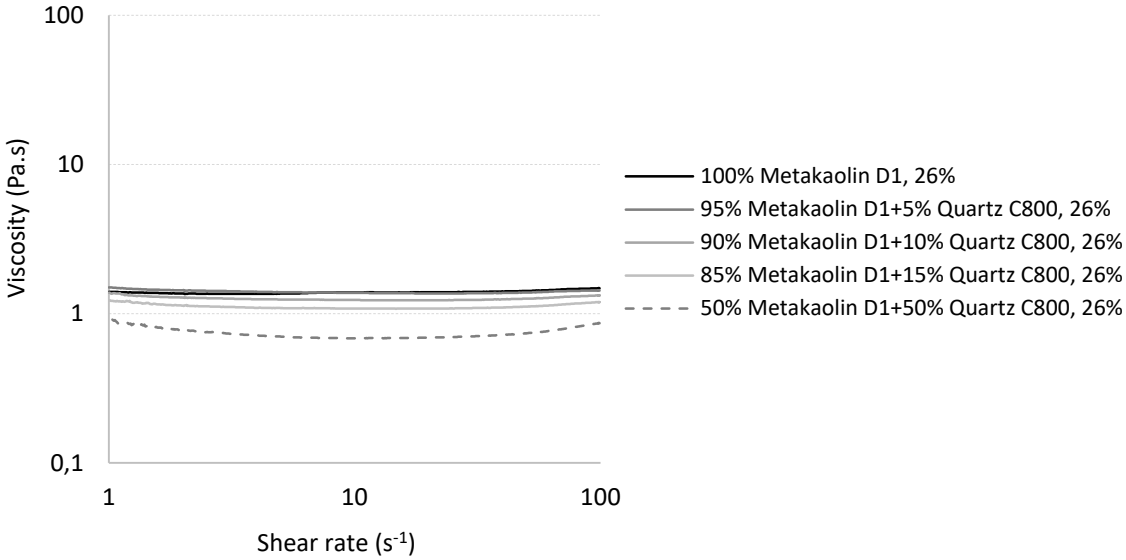
100
10
1
0,1
Viscosity (Pa.s)
1
10
100
Shear rate (s-1)
100% Metakaolin D1, 26%
95% Metakaolin D1+5% Quartz C800, 26%
90% Metakaolin D1+10% Quartz C800, 26%
85% Metakaolin D1+15% Quartz C800, 26%
50% Metakaolin D1+50% Quartz C800, 26%

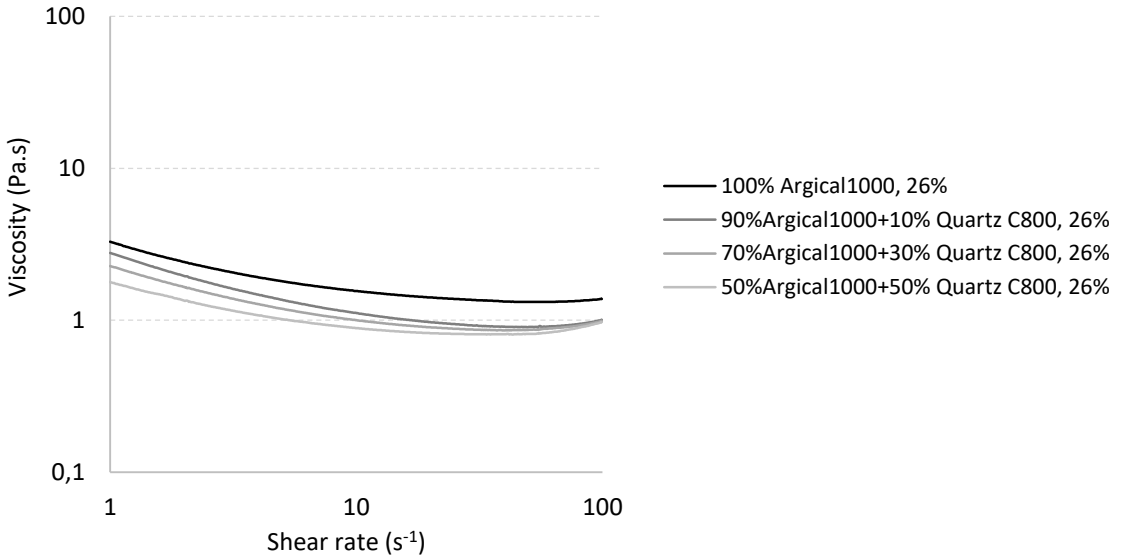
100
10
1
0,1
Viscosity (Pa.s)
1
10
100
Shear rate (s-1)
100% Argical1000, 26%
90%Argical1000+10% Quartz C800, 26%
70%Argical1000+30% Quartz C800, 26%
50%Argical1000+50% Quartz C800, 26%

Appendix B

(All geopolymers are prepared using sodium silicate solution (S_1), μ_{0_1})

Powder couple	Viscosity (Pa.s)	Maximum packing density Φ_{max}	Compressive strength (MPa)	Flexural strength (MPa)	Si/Al	Na/Al
100% Argical 1200S, 26%	2.25	0.31	10.77	2.92	1,84	0.77
80% Argical 1200S+20% Metakaolin D1, 26%	1.07	0.34	12.71	2.19	1.87	0.78
60% Argical 1200S+40% Metakaolin D1, 26%	0.52	0.37	9.88	2.39	1.90	0.79
50% Argical 1200S+50% Metakaolin D1, 26%	0.36	0.38	11.26	2.57	1.91	0.79
40% Argical 1200S+60% Metakaolin D1, 26%	0.28	0.40	12.80	2.98	1.93	0.79
20% Argical 1200S+80% Metakaolin D1, 26%	0.23	0.42	12.28	2.27	1.96	0.80
100% Metakaolin D1, 26%	0.24	0.42	6.61	1.24	1.99	0.81
50% Argical 1200S+50% Metakaolin D1, 32%	2.80	0.38	13.77	1.90	1.75	0.59
40% Argical 1200S+60% Metakaolin D1, 32%	1.88	0.40	15.98	3.61	1.77	0.59
20% Argical 1200S+80% Metakaolin D1, 32%	1.27	0.42	15.87	3.17	1.80	0.60
100% Metakaolin D1, 32%	1.22	0.42	6.82	3.32	1.83	0.60
100% Argical 1200S, 29%	16,2	0.31	36.66	4.62	1.91	0.86
80% Argical 1200S+20% Metakaolin D2, 29%	8.48	0.34	32.58	4.41	1.94	0.87
50% Argical 1200S+50% Metakaolin D2, 29%	3.70	0.38	27.95	3.82	1.99	0.88
20% Argical 1200S+80% Metakaolin D2, 29%	2.58	0.42	21.74	2.97	2.04	0.89
100% Metakaolin D2, 29%	3.23	0.42	15.39	2.37	2.07	0.90
100% Metamax, 26%	3.2	0.33	-	-	2.22	2.07
80% Metamax+20% Metakaolin D1, 26%	2.1	0.35	-	-	2.10	1.03
60% Metamax+40% Metakaolin D1, 26%	1.49	0.38	-	-	2.00	0.98
50% Metamax+50% Metakaolin D1, 26%	1.23	0.39	-	-	1.95	0.96
40% Metamax+60% Metakaolin D1, 26%	1.18	0.41	-	-	1.91	0.94
20% Metamax+80% Metakaolin D1, 26%	1.1	0.43	-	-	1.82	0.90
100% Metakaolin D1, 26%	1.34	0.42	-	-	1.74	0.87
80% Metamax+20% Metakaolin D1, 32%*	8.47	0.35	40.57	6.84	1.88	0.75
60% Metamax+40% Metakaolin D1, 32%	5.46	0.38	-	-	1.78	0.72
50% Metamax+50% Metakaolin D1, 32%	4.82	0.39	41.21	4.60	1.74	0.70
40% Metamax+60% Metakaolin D1, 32%	4.71	0.41	-	-	1.70	0.69
20% Metamax+80% Metakaolin D1, 32%	3.92	0.43	29.18	5.46	1.62	0.66
100% Metakaolin D1, 32%	4.96	0.42	17.50	3.25	1.54	0.64
100% Argical 1000, 29%	1.94	0.42	34.63	4.55	1.84	0.81
80% Argical 1000+20% Metakaolin D1, 29%	1.89	0.43	29.21	3.93	1.88	0.83
50% Argical 1000+50% Metakaolin D1, 29%	2.20	0.44	27.04	3.75	1.95	0.85
20% Argical 1000+80% Metakaolin D1, 29%	3.02	0.44	20.39	2.53	2.02	0.88

100% Metakaolin D1, 29%	3.43	0.42	15.39	2.37	2.07	0.90
100% Metastar, 26%	4.76	0.32	-	-	-	-
80% Metastar+20% Metakaolin D1, 26%	3.45	0.34	-	-	-	-
60% Metastar+40% Metakaolin D1, 26%	2.1	0.37	-	-	-	-
50% Metastar+50% Metakaolin D1, 26%	1.82	0.39	-	-	-	-
40% Metastar+60% Metakaolin D1, 26%	1.49	0.40	-	-	-	-
20% Metastar+80% Metakaolin D1, 26%	1.27	0.42	-	-	-	-
100% Metakaolin D1, 26%	1.34	0.42	-	-	-	-
100% Argical 1000, 25%	1.1	0.42	34.90	3.20	2.00	1.00
95% Argical 1000+5% Durcal 65, 25%	1	0.43	39.12	4.51	2.04	1.05
90% Argical 1000+10% Durcal 65, 25%	0.88	0.43	30.54	4.31	2.09	1.12
85% Argical 1000+15% Durcal 65, 25%	0.74	0.47	30.85	2.94	2.15	1.18
100% Argical 1000, 28%	1.89	0.42	-	-	1.89	0.87
95% Argical 1000+5% Durcal 65, 28%	1.64	0.43	-	-	1.92	0.91
90% Argical 1000+10% Durcal 65, 28%	1.35	0.43	-	-	1.97	0.97
85% Argical 1000+15% Durcal 65, 28%	1.24	0.47	-	-	2.02	1.03
100% Metakaolin D1, 26%	1.34	0.42	9.67	0.99	2.22	1.07
95% Metakaolin D1+5% Durcal 5, 26%	1.47	0.44	8.40	0.83	2.26	1.13
90% Metakaolin D1+10% Durcal 5, 26%	1.37	0.46	8.61	1.08	2.26	1.13
85% Metakaolin D1+15% Durcal 5, 26%	1.22	0.46	7.55	0.98	2.37	1.26
50% Metakaolin D1+50% Durcal 5, 26%	0.64	0.52	- **	- **	3.11	2.15
100% Metakaolin D1, 26%	1.34	0.42	9.67	0.99	2.22	1.07
95% Metakaolin D1+5% Quartz C800, 26%	1.35	0.43	8.39	0.95	2.26	1.13
90% Metakaolin D1+10% Quartz C800, 26%	1.19	0.44	7.63	1.00	2.32	1.19
85% Metakaolin D1+15% Quartz C800, 26%	1.04	0.45	6.54	0.76	2.37	1.26
50% Metakaolin D1+50% Quartz C800, 26%	0.66	0.49	- **	- **	3.11	2.15
100% Argical 1000, 26%	1.45	0.42	30.13	4.80	1.95	0.95
90% Argical 1000+10% Quartz C800, 26%	1.06	0.46	27.70	2.32	2.04	1.05
70% Argical 1000+30% Quartz C800, 26%	0.89	0.47	17.65	1.65	2.29	1.35
50% Argical 1000+50% Quartz C800, 26%	0.79	0.47	8.41	0.94	2.74	1.89
Argical 1200S, 26%	8.50	0.31	30.48	4.92	2.05	1.03
Argical 1200S (3h grinded), 26%	3.02	0.36	42.48	4.92	2.05	1.03
Argical 1200S (6h grinded), 26%	2.60	0.38	30.36	4.11	2.05	1.03
Argical 1200S (15h grinded), 26%	2.28	0.40	50.01	3.33	2.05	1.03

*: 100% Metamax, 32% was not performable due to very elevated viscosity
**: Measurements were not performable due to dough-like state of samples